



Iron-Catalysed Cross-Coupling of Secondary Alkyl Grignard Reagents

James Sanderson

Supervisors:

Dr. Andrew Dominey, Dr. David Nelson and Prof.
Jonathan Percy

December 2017

Acknowledgements

I would like to thank my supervisors, Dr. Andrew Dominey, Dr. David Nelson, and Professor Jonathan Percy, for their support and guidance throughout my PhD. I would also like to thank my colleagues and friends at GSK for their help.

I must thank my family and friends, both at home and in Scotland, for their kind words and motivation at difficult times throughout my studies.

Finally, I would like to thank Jelena for everything.

This thesis is the result of the author's original research. It has been composed by the author and has not been previously submitted for examination which has led to the award of a degree.

The copyright of this thesis belongs to the author under the terms of the United Kingdom Copyright Acts as qualified by University of Strathclyde Regulation 3.50. Due acknowledgement must always be made of the use of any material contained in, or derived from, this thesis.

Signed:

Date:

Abbreviations

acac	Acetylacetonate
ANOVA	Analysis of variance
API	Active pharmaceutical ingredient
aq.	Aqueous
ASAP-TOF	Atmospheric solid analysis probe with time-of-flight mass spectrometry
AT	Atom transfer
BDE	Bond dissociation enthalpy
BOX	Bisoxazoline
C18	Octadecyl carbon chain bonded silica
CAAC	Cyclic alkyl amino carbene
DABCO	1,4-Diazabicyclo[2.2.2]octane
dbm	Dibenzoylmethide
DBU	1,8-Diazabicyclo[5.4.0]undec-7-ene
dcpf	1,1'-bis(dicyclohexylphosphino)ferrocene
DFT	Density functional theory
DME	1,2-Dimethoxyethane
DMEU	1,3-Dimethyl-2-imidazolidinone
dmpe	1,2-Bis(dimethylphosphino)ethane
DoE	Design of experiments
dpbz	1,2-Bis(diphenylphosphino)benzene
dppe	1,2-Bis(diphenylphosphino)ethane
dppf	1,1'-Bis(diphenylphosphino)ferrocene
EA	Electron affinity
ECHA	European chemicals agency
EDG	Electron donating group
EDTA	Ethylenediaminetetraacetic acid
EPR	Electron paramagnetic resonance
Et	Ethyl
Et ₂ O	Diethyl ether
Equiv.	Equivalents
EWG	Electron withdrawing group
fac	Facial
FMO	Frontier molecular orbitals
GC	Gas chromatography
GLP	Good laboratory practice
HF	Hartree Fock
HOMO	Highest occupied molecular orbital
HPLC	High pressure liquid chromatography
HRMS	High resolution mass spectrometry
HTC	High throughput chemistry
IMes	1,3-Bis(2,4,6-trimethylphenyl)imidazol-2-ylidene
IP	Ionisation potential

IPr	1,3-Bis(2,6-diisopropylphenyl)imidazol-2-ylidene
LCMS	Liquid chromatography mass spectrometry
LKB	Ligand knowledge base
LUMO	Lowest unoccupied molecular orbital
MCD	Magnetic circular dichroism
Me	Methyl
mer	Meridinal
MI	Migratory insertion
NA	Not applicable
nacnac	β -Diketiminato
NBP	<i>N</i> -Butylpyrrolidinone
ND	Not detected
NDA	New drug application
NHC	<i>N</i> -Heterocyclic carbene
NMM	<i>N</i> -Nethylmorpholine
NMP	1-Methyl-2-pyrrolidinone
NMR	Nuclear magnetic resonance
NOP	<i>N</i> -Octylpyrrolidinone
OA	Oxidative addition
OFAT	One factor at a time
PCA	Principal component analysis
PCM	Polarisable continuum model
PD	Process development
PDI	Pyridine diimine
PEPPSI	Pyridine-enhanced precatalyst preparation stabilization and initiation
PMDETA	<i>N,N,N',N'',N'''</i> -Pentamethyldiethylenetriamine
PyBOX	Pyridine-bisoxazoline
QbD	Quality by design
RE	Reductive elimination
R _f	Retention factor
RI	Rapid injection
SciOPP	Spin-control-intended ortho-phenylene-bisphosphine
SET	Single electron transfer
SIPr	1,3-Bis(2,6-diisopropylphenyl)-4,5-dihydroimidazol-2-ylidene
TBME	<i>tert</i> -Butyl methyl ether
TD	Time dependent
THF	Tetrahydrofuran
TM	Transition metal
TMEDA	Tetramethylethylenediamine

Contents

Acknowledgements.....	i
Abbreviations	ii
Contents	iv
1. Abstract	1
2. Introduction: Cross-Coupling Reactions.....	2
2.1. History	2
2.2. Fundamental Processes in Transition-Metal Catalysed Cross-Coupling Reactions.....	5
2.2.1. Oxidative Addition.....	5
2.2.2. Transmetallation	6
2.2.3. Reductive Elimination	6
2.2.4. β -Hydride Elimination	7
2.2.5. Migratory Insertion	7
2.3. Modern Transition-Metal Catalysed Cross-Coupling Reactions.....	10
2.4. The Kumada Cross-Coupling Reaction.....	13
2.4.1. The Iron-Catalysed Kumada Cross-Coupling Reaction	16
2.4.2. 1998 Onwards – Some Mechanistic Considerations.....	17
2.4.3. Mechanistic Summary.....	28
2.5. Industrial/Pharmaceutical Applications of Iron-Catalysed Kumada Cross-Coupling Reactions.....	29
2.6. Principles of Green Chemistry	32
2.7. Design of Experiments – Toward Process Optimisation.....	34
2.7.1. A Typical 3-Factor Investigation	36
2.7.2. The Half Normal Plot.....	37
2.7.3. The ANOVA Table.....	38
2.7.4. The Model Graphs.....	39
2.8. Aim	40

3.	Iron-Catalysed iso-Propylation of Electron Deficient Aryl and Heteroaryl Chlorides	41
3.1.	Background.....	41
3.1.1.	Relevant Literature: Palladium and Nickel Catalysis.....	45
3.1.2.	Relevant Literature: Iron Catalysis	55
3.2.	Results and Discussion.....	64
3.3.	Conclusion	82
4.	The Application of DFT to Predict and Understand Trends in Reactivity.....	83
4.1.	Introduction.....	83
4.1.1.	Cross-Coupling of iso-Propylmagnesium Chloride with Aryl Chlorides.....	83
4.2.	Results and Discussion.....	90
4.2.1.	Cross-Coupling of iso-Propylmagnesium Chloride with Aryl Chlorides.....	90
4.3.	Conclusion	104
5.	Investigation of Alternative Additives for Secondary-Alkyl Cross-Coupling	105
5.1.	Introduction.....	105
5.1.1.	NMP Replacement	105
5.1.2.	Cross-Coupling of Cyclopropyl Nucleophiles.....	108
5.2.	Results and Discussion.....	113
5.2.1.	Investigation of Alternative Additives for the Cross-Coupling of iso-Propylmagnesium Chloride.....	113
5.2.2.	High-Throughput Chemistry for the Cross-Coupling of Cyclopropylmagnesium Bromide	116
5.3.	Conclusion	146
6.	Concluding Remarks.....	147
7.	Experimental	148
7.1.	General Information	148
7.2.	HPLC and GC Methods.....	149

7.2.1.	Preparation of Starting Materials/Ligands for the Iron-Catalysed Cross-Coupling Reactions	153
7.3.	iso-Propyl DoE Optimisation Studies	155
7.3.1.	Experimental Design 1	155
7.3.2.	Experimental Design 2	163
7.3.3.	Experimental Design 2: Augmented.....	169
7.3.4.	Confirmation of DoE Results	173
7.3.5.	Reproducibility Experiments	174
7.4.	Isolated iso-Propyl Substrates	176
7.5.	Additive Screening for iso-Propyl Cross-Coupling	180
7.5.1.	DoE Experiments for iso-Propyl Additives.....	183
7.6.	HTC Screens for Cyclopropyl Coupling	187
7.6.1.	Screen 1 – Cyclopropylmagnesium Bromide + (4-chlorophenyl)(morpholino)methanone	189
7.6.2.	Screen 2 - Cyclopropylmagnesium Bromide + 6-Chloroquinoline (2 catalysts, 24 ligands)	191
7.6.3.	Screen 3 – Cyclopropylmagnesium Bromide + 6-Chloroquinoline (1 catalyst, 12 ligands)	193
7.6.4.	Screen 4 – Cyclopropylmagnesium Bromide + 6-Chloroquinoline (4 catalyst, 8 ligands)	194
7.7.	DoE and Temperature Studies for Cyclopropyl Coupling.....	196
7.7.1.	DoE Investigation	196
7.7.2.	Low Temperature Investigation	203
7.7.3.	Elevated Temperature Investigation.....	204
7.7.4.	Controlled Addition Investigation	205
7.7.5.	6-Haloquinoline Test Reactions	206
7.8.	Isolated Cyclopropyl Substrates	207
7.9.	Computational Chemistry Data	208

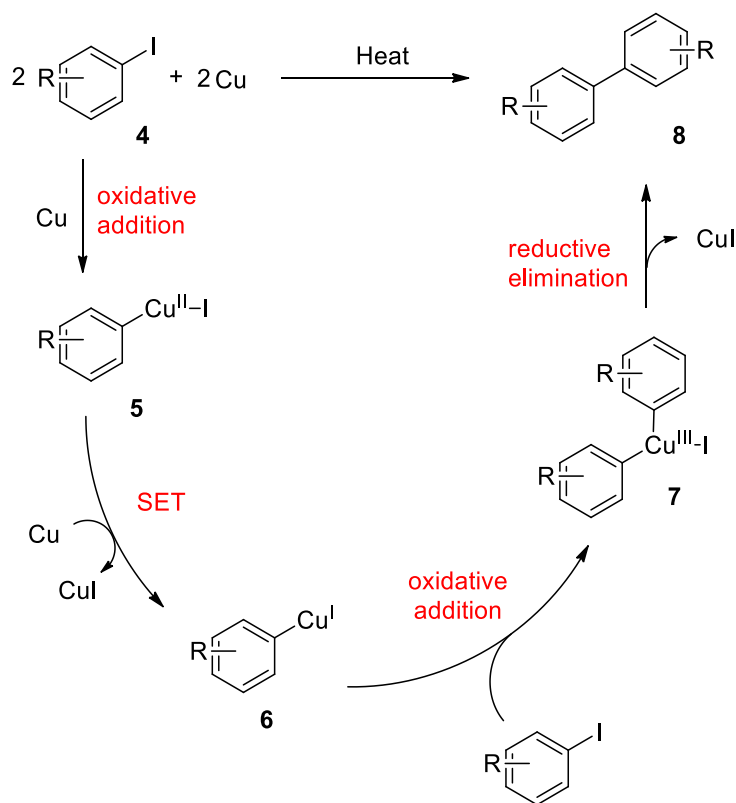
7.9.1.	Results from Method Screen	208
7.9.2.	Sample Input File.....	213
7.9.3.	JMP Analysis of Computational Results	214
7.9.4.	Bond Dissociation Energy Calculations	220
7.10.	Copies of NMR Spectra.....	221
8.	References.....	255

1. Abstract

Traditional methods for the preparation of secondary alkyl substituted aryl and heteroaryl chlorides are often poorly selective and have limited functional group tolerance. This thesis describes the use of process chemistry tools such as statistical design of experiments and high throughput chemistry to develop mild and sustainable methods to carry out sp^2 - sp^3 cross-coupling reactions using iron catalysis.

The early work is related to the discovery of an effective procedure for the preparation of *iso*-propyl substituted (hetero)arenes with minimal *iso*-propyl to *n*-propyl isomerisation. The reaction tolerates electronically diverse aryl chloride coupling partners, with excellent conversion observed for strongly electron deficient aromatic rings, such as esters and amides. Electron rich systems, including methyl and methoxy substituted aryl chlorides, were found to be less reactive. Furthermore, the reaction was found to be most successful when heteroaryl chlorides were submitted to the cross-coupling protocol. By mapping substituent effects on reaction selectivity, we were able to develop some mechanistic insight, helping to explain the requirement for electron-deficient aryl chlorides in these reactions. Through the estimation of the electron affinity of each aryl chloride, we were also able to develop a computational model which may be used to predict reactivity in the new cross-coupling procedure. Moderate isolated yields were achieved with selected aryl chlorides, and moderate to good isolated yields were obtained in all cases with heteroaryl chlorides.

The final chapter discusses the search for an alternative to 1-methyl-2-pyrrolidinone, the reprotoxic solvent/additive used in almost all iron-catalysed cross coupling reactions. A simple protocol for the preparation of cyclopropyl substituted heteroarenes was discovered through the combination of high throughput chemistry and statistical design of experiments.

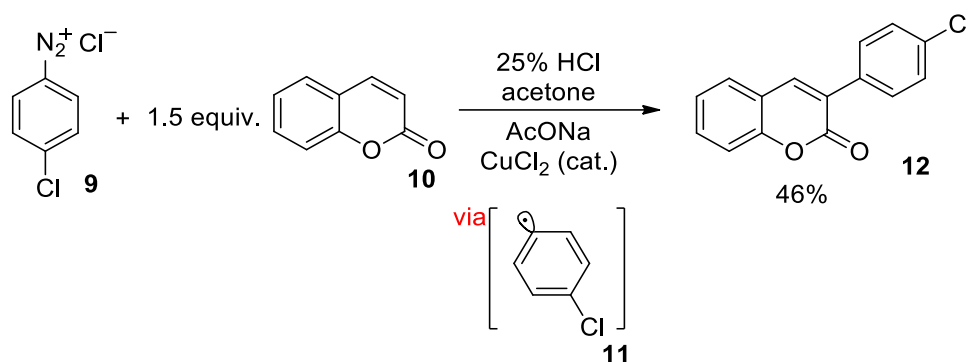


Scheme 2. Ullman coupling.

Both the Glaser and Ullman coupling reactions may be described as homocoupling reactions which proceed *via* organocopper intermediates. The Glaser coupling reaction forms a bisacetylene through a bimetallic RE between two of these intermediates. The Ullmann coupling reaction forms a biaryl through RE from a single organocopper intermediate. Both of these reactions utilise a ligand-free copper source, unlike modern TM-catalysed cross-coupling processes.

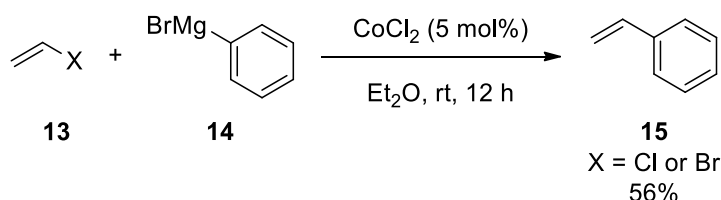
The early copper mediated coupling reactions suffer from numerous drawbacks, the most significant of which is that they are limited to homocoupling processes. Additionally, issues such as solvent toxicity, low selectivity and forcing conditions have been highlighted. These problems have been avoided in recent years through the development of cross-coupling reactions. The cross-coupling reaction is generally described as a reaction between a (pseudo)halide (organic electrophile) and an organometallic reagent (organic nucleophile), which may or may not be mediated by transition metal catalysis. The use of two fundamentally different reaction partners allows for much greater diversity in the final product, unlike the earlier methods described by Glaser and Ullman. The first examples of such reactions were reported in the mid-20th century by Meerwein⁵ and Kharasch.⁶

The Meerwein arylation involves the copper-catalysed reaction between an aryldiazonium salt (**9**) and a substituted alkene, such as coumarin (**10**, **Scheme 3**).⁵ Formally, the aryl diazonium adds across the double bond with loss of a molecule of nitrogen. Meerwein initially attributed this chemistry to the formation of aryl cations, but this proposal was rejected by Kochi who postulated the intermediacy of aryl radicals (**11**).⁷ In the proposed mechanism the aryl radical adds to the double bond, resulting in a new alkyl radical. This can then pick up a chlorine radical which is subsequently eliminated, reforming the double bond.



Scheme 3. Meerwein arylation.

The Grignard-based Kharasch coupling is a cobalt-catalysed cross-coupling reaction between an aryl Grignard reagent and an aryl or vinyl halide (**Scheme 4**).^{6, 8} Importantly, this reaction is an early analogue of the nickel or palladium-catalysed cross-coupling between Grignard reagent and (pseudo)halide, known as the Kumada cross coupling.



Scheme 4. The Kharasch cross-coupling.

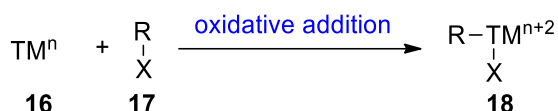
The early cross-coupling reactions, like the earlier coupling reactions, suffered from numerous drawbacks, such as poor selectivity, and limited functional group tolerance. The most significant issue was the selectivity of these reactions, with varying proportions of homocoupled impurities being formed. This is due to the radical nature of such processes. Significant advances were made in subsequent years due to increased understanding of the fundamental processes, and the advent of palladium and nickel catalysis.

2.2. Fundamental Processes in Transition-Metal Catalysed Cross-Coupling Reactions

TMs are now used in catalytic quantities, rather than the stoichiometric amounts used in the earlier coupling reactions. This greatly improves the atom economy of the reactions, as TMs generally have high molecular weights. It can also significantly reduce the cost of a process, as TMs can be expensive and the disposal of TM waste can be challenging. Many of the early reactions, as exemplified by the Glaser and Ullman coupling, utilised ligandless process and relied upon poorly selective (uncontrolled) SET processes to enable homocoupling of the reactants. The Meerwein arylation and Kharasch coupling reactions demonstrated a move towards TM-catalysis, but ligandless reaction conditions led to challenges with both selectivity and reactivity. Modern protocols generally use ligands, as they can promote certain steps in the catalytic cycle.

2.2.1. Oxidative Addition

The OA step in a cross-coupling reaction is the addition of a (pseudo)halide (**17**) to a TM (**16**, **Scheme 5**). This process results in the cleavage of the carbon-(pseudo)halide bond giving a TM centre with 2 additional ligands (**18**), which has been formally oxidised – donating 2-electrons to the (pseudo)halide in the process.



Scheme 5. The oxidative addition reaction.

The nature of the (pseudo)halide has been shown to strongly influence the mechanism of the OA reaction. Non-polar reagents, such as dihydrogen or C-H bonds, generally add to the TM *via* a concerted 3- or 4-centred transition state. Highly polar reagents, such as alkyl (pseudo)halides, often add to the TM through a 2-step S_N2 or radical based mechanism. Reactants of intermediate polarity, such as aryl (pseudo)halides have also been shown to add to the TM through a concerted pathway, similar to non-polar reagents.

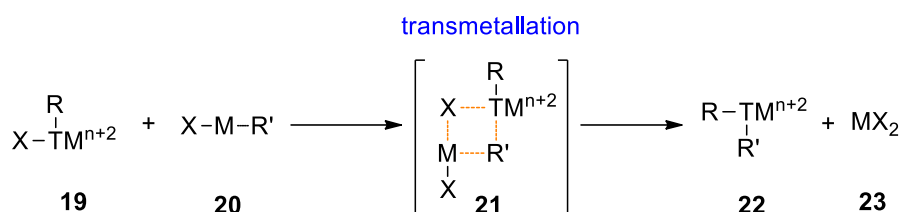
Some general trends have been observed in OA reactions:

- OA is typically more favourable when the TM centre is electron rich
- OA is preferred when the TM centre has minimal steric hindrance
- OA of non-polar substrates requires a site of unsaturation, and a d-electron count <18

These criteria can often be met through the choice of an appropriate ligand/TM combination.

2.2.2. Transmetallation

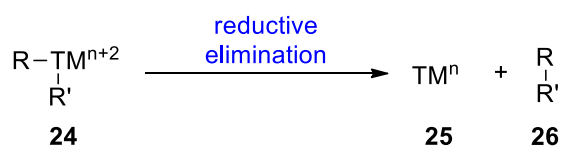
Transmetallation is often the second step in a cross-coupling reaction, following OA. Transmetallation generally involves the transfer of a carbon-based fragment from one metal, generally boron, silicon, tin or magnesium (**20**), to the TM centre (**19**, **Scheme 6**). The TM also transfers a non-carbon based fragment, generally the (pseudo)halogen, back to the metal centre. A plausible transition state is shown (**21**), although the nature of the organometallic species may lead to an alternative pathway. This reaction results in a stoichiometric amount of by-product (**23**) – an important consideration when using TM-catalysed cross-coupling in the preparation of active pharmaceutical ingredients (APIs). The identity of this stoichiometric waste can influence whether is feasible on an industrial scale.



Scheme 6. The transmetallation reaction.

2.2.3. Reductive Elimination

RE is the carbon-carbon (or carbon-heteroatom) bond forming step of the cross-coupling reaction, and is generally the last step (**Scheme 7**). RE is the reverse of OA – when the carbon-carbon/heteroatom bond is formed the TM centre is formally reduced, and its co-ordination number decreases by 2. It is generally unimolecular, with one TM centre forming the product from two covalently bound ligands, although dinuclear RE reactions have also been reported.⁹ The ligands must be *cis* for reductive elimination to occur, so *trans-cis* isomerisation may precede this reaction.



Scheme 7. The reductive elimination reaction.

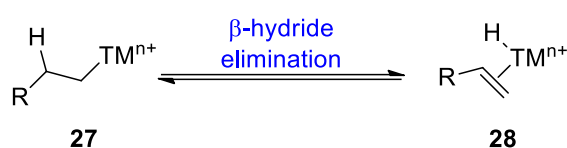
Like OA, some general trends have been observed in RE reactions:

- First row TMs reductively eliminate faster than second row TMs
- Electron poor TMs reductively eliminate faster than electron rich TMs
- Sterically hindered complexes reductively eliminate more quickly than unhindered ones

These criteria can often be met through the choice of an appropriate ligand/transition metal combination.

2.2.4. β -Hydride Elimination

In TM complexes where higher alkyl species are present (\geq ethyl), *syn* β -hydride elimination can lead to the formation of side products (**Scheme 8**). In the β -hydride elimination reaction, a hydrogen in the β -position to the TM centre (**27**) is transferred from the alkyl group to the TM (**28**). This forms a TM-hydride and an alkene, which may or may not remain bound to the TM centre. For β -hydride elimination to occur, the metal must have a vacant co-ordination site. This is due to the formation of 2 ligands for the TM in place of one. Co-ordinatively saturated TM centres are unable to undergo β -hydride elimination without the prior dissociation of a ligand.



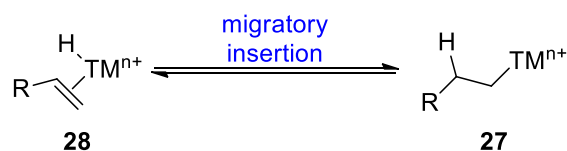
Scheme 8. The β -hydride elimination reaction.

Ligands bound to the TM centre can influence β -hydride elimination:

- A bulky ligand may promote RE over β -hydride elimination
- Increased electron donation can promote β -hydride elimination
- Chelating ligands can reduce the likelihood of β -hydride elimination

2.2.5. Migratory Insertion

Migratory insertion (MI) is the reverse of β -hydride elimination. In the MI reaction, an unsaturated ligand migrates from the TM centre into an adjacent TM-ligand bond (**Scheme 9**). This results in the formation of a new, single, TM-ligand bond (**30**) in place of the original 2 TM-ligand bonds (**29**), leaving an open co-ordination site at the TM centre.

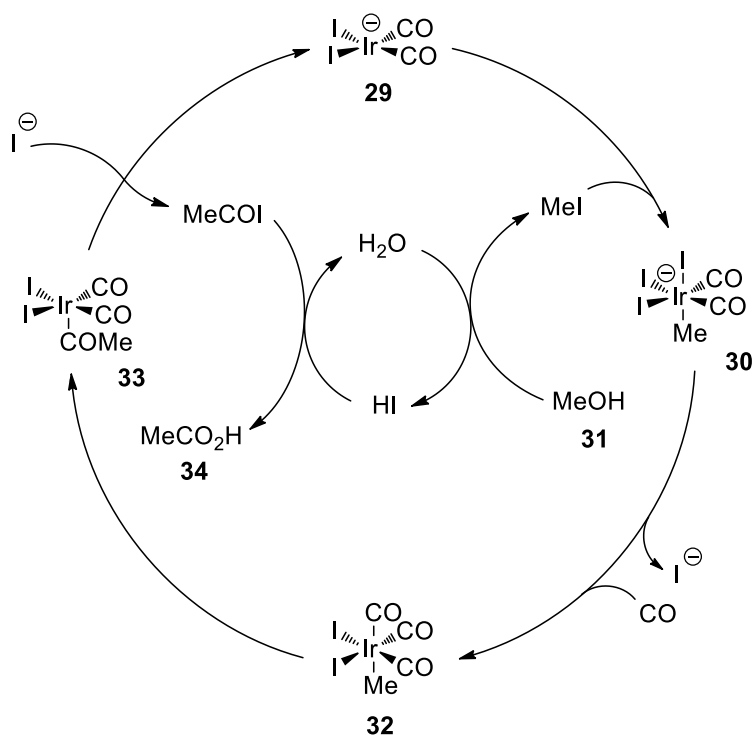


Scheme 9. The migratory insertion reaction.

The MI reaction is a key step in numerous TM-catalysed processes, including the Heck reaction (*vide infra*) and the Monsanto/Cativa acetic acid processes. The latter is responsible for the preparation of acetic acid (**34**) from methanol (**31**) on a \sim 12 Mt/a scale (**Scheme 10**).¹⁰ The Cativa

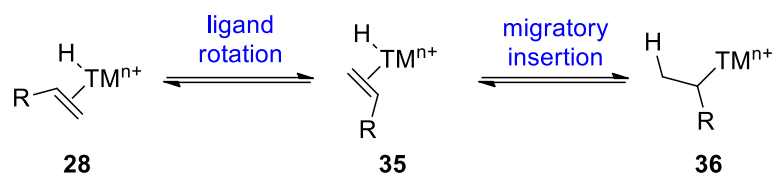
process utilises an iridium catalyst, and has largely replaced the Monsanto process which utilises a rhodium catalyst. This switch occurred because it was found that the iridium-catalysed acetic acid synthesis could be carried out with lower levels of water, expediting drying of the final product.¹¹

The reaction begins with iridium complex **29**, which undergoes OA with methyl iodide, giving Ir^{III} species **30**. Ligand exchange to form **32** is then followed by migratory insertion, and RE, yielding acetic acid **34** after hydrolysis of an intermediate acyl iodide.

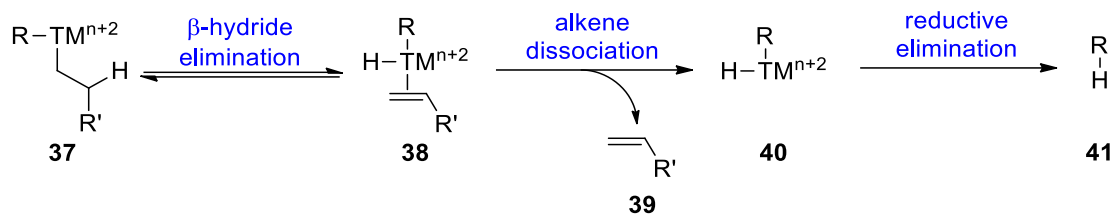


Scheme 10. The Cativa acetic acid process.

Although MI reaction is productive in the Heck and acetic acid processes, it can lead to the formation of undesired side-products during the formation of sp^2 - sp^3 bonds. If MI occurs following β -hydride elimination, the hydride can add to either side of the alkene, leading to isomerisation of a *sec*-alkyl group (**Scheme 11**). However, if the alkene dissociates, RE of the remaining carbon-based ligand and hydride would lead to reduction of the starting (pseudo)halide (**Scheme 12**).



Scheme 11. Isomerisation *via* β -hydride elimination.



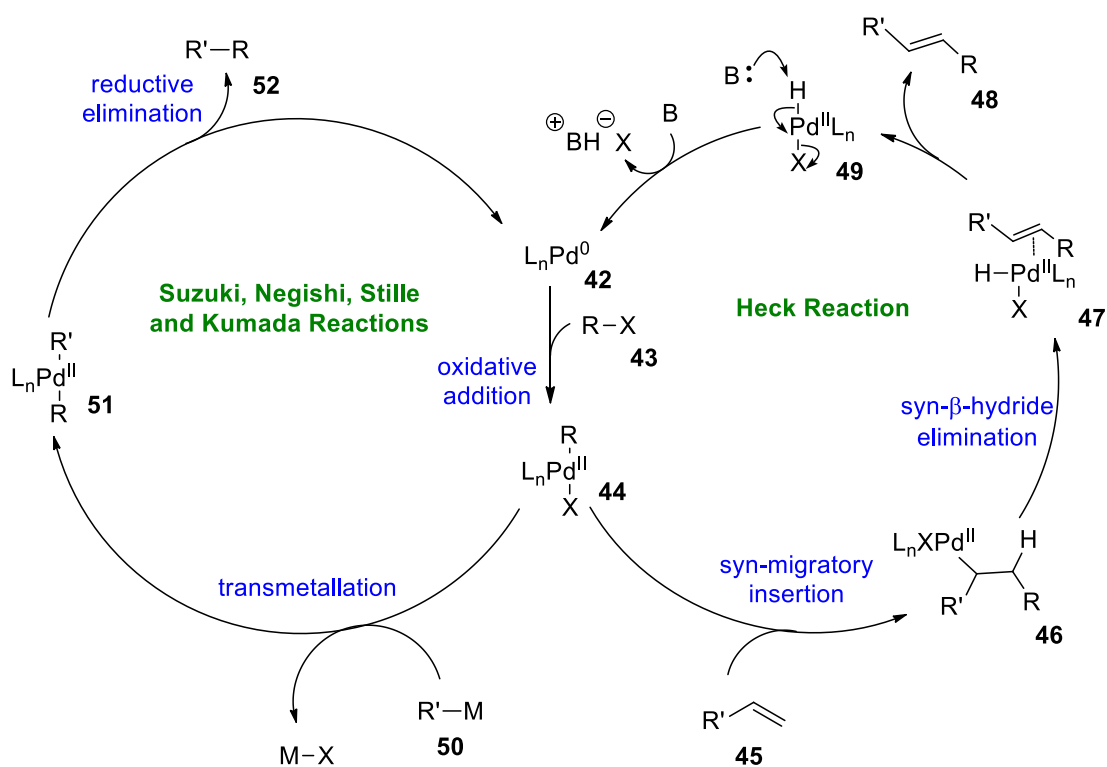
Scheme 12. Reduction of (pseudo)halide *via* β -hydride elimination.

Overcoming the problem of β -hydride elimination is crucial in achieving efficient, selective and robust cross-coupling of sp^3 species with sp^2 or sp^3 partners.

2.3. Modern Transition-Metal Catalysed Cross-Coupling Reactions

TM-catalysed cross-coupling reactions have received a huge amount of interest in the past 40 years, with these reactions becoming extremely powerful techniques in the synthetic organic chemist's toolbox. This methodology is widely used in industry and academia alike, lending itself to the preparation of complex aromatic compounds, such as natural products and APIs. The importance of the TM-catalysed cross-coupling reaction was highlighted by the award of the Nobel Prize in chemistry to Richard Heck, Ei-ichi Negishi and Akira Suzuki in 2010.¹

The Heck cross-coupling gives *E*-alkenes (**48**) from the reaction between an alkene (acting as the organic nucleophile) and a (pseudo)halide. The Negishi and Suzuki reactions generally create sp^2 - sp^2 or sp^2 - sp^3 linkages between (pseudo)halides and organozinc or organoboron species (respectively).



Scheme 13. Palladium-catalysed cross-coupling reactions.

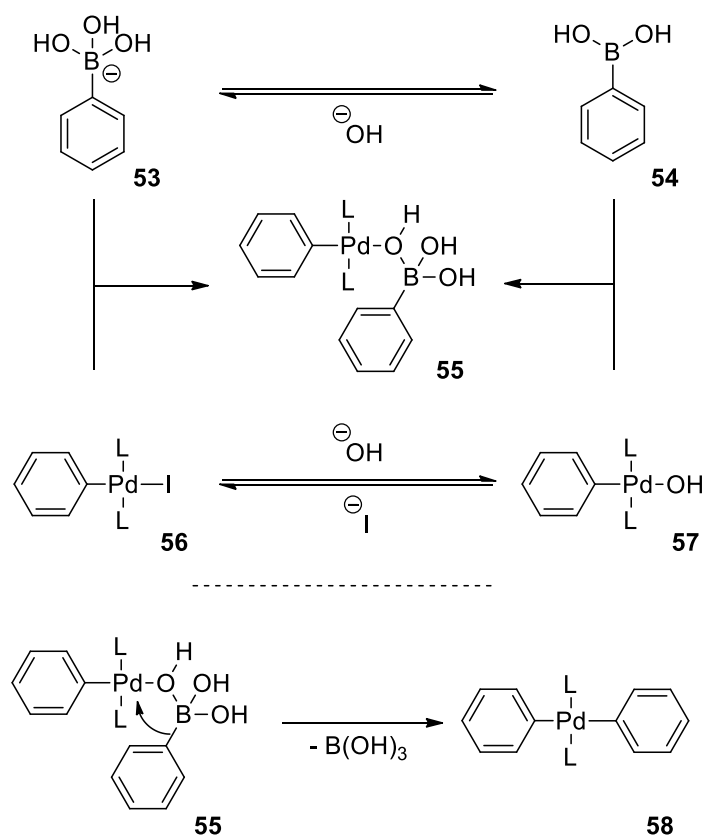
A general catalytic cycle for the prize-winning cross-coupling reactions is shown in **Scheme 13**.¹ Initially, when using a Pd^0 source, the palladium loses two of its four ligands giving a coordinatively unsaturated Pd^0 centre **42**. If Pd^{II} was used, the TM would require reduction to Pd^0 , this typically occurs through action of an organometallic reagent or phosphine ligand. The electrophilic coupling partner then undergoes an OA reaction, giving a coordinatively saturated Pd^{II} centre **44**,

in the presence of bisphosphine or less bulky monophosphine ligands. If a bulkier monophosphine ligand is used, the palladium centre may remain 3 co-ordinate.

At this point the catalytic cycle of the Heck reaction deviates from that of the Negishi and Suzuki reactions. In the Heck reaction, the nucleophilic coupling partner is an alkene, which co-ordinates to the Pd^{II} centre followed by migratory insertion of the electrophilic coupling partner and ligand rotation. *Syn*-β-hydride elimination then releases the reaction product allowing base to reduce the Pd^{II} to Pd⁰ to continue the catalytic cycle (**49**).

In the Negishi and Suzuki reactions we observe a transmetallation of the nucleophilic coupling partner **50**: organozinc and organoboron species respectively. This is followed by RE to give the product, and release Pd⁰ to re-enter the catalytic cycle. The mechanism for TM-catalysed cross-coupling reactions of the Stille and Kumada type can be generalised to that in **Scheme 13**. There is further subtlety however when considering the Suzuki reaction, as boron species are not nucleophilic. Thus, Pd-OH species are proposed to be the active nucleophile.¹²

In the last 3-4 years, Scott Denmark has used rapid injection nuclear magnetic resonance (RI-NMR) spectroscopy to observe the elusive transmetallation intermediates formed in the Suzuki reaction (**Scheme 14**).^{13, 14} Initially, through a series of detailed experiments, it was demonstrated that the Pd-OH species formed by ligand displacement **56** to **57**, may be responsible for the formation of a crucial Pd-O-B intermediate **55**. However, boron ate complex **53** may also lead to the Pd-O-B species in some cases. Aryl transfer from B to Pd in **55** leads to the formation of the final diarylpalladium species **58**, which can then undergo rapid RE to give the desired product.



Scheme 14. Denmark's Suzuki investigation, L = P(*i*-Pr)₃.

2.4. The Kumada Cross-Coupling Reaction

One of the earliest modern cross-coupling reactions was independently discovered by both Kumada and Corriu in 1972.^{15, 16} They reported an effective coupling reaction, forming a new carbon-carbon bond between a Grignard reagent and an alkenyl halide, catalysed by nickel-phosphine complexes. This discovery was observed at around the same time as the Mizoroki-Heck reaction, but it pre-dates the Suzuki-Miyaura cross-coupling reaction by 7 years.¹ A palladium-catalysed variant of the Kumada (Kumada-Corriu) cross-coupling reaction was demonstrated in 1975.

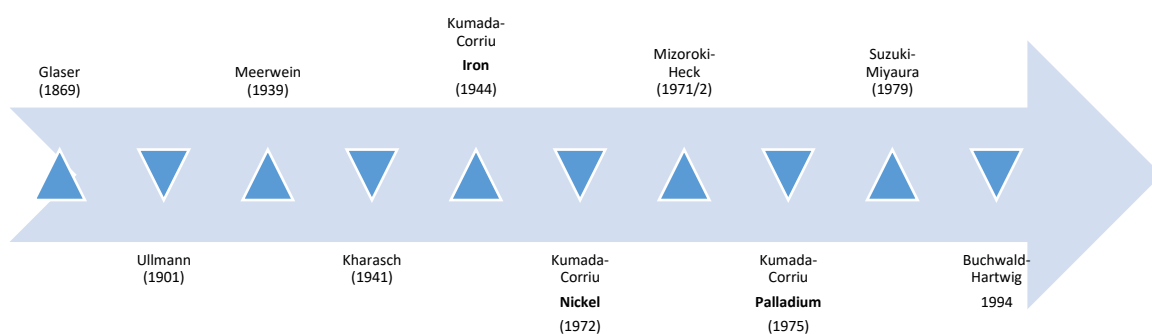
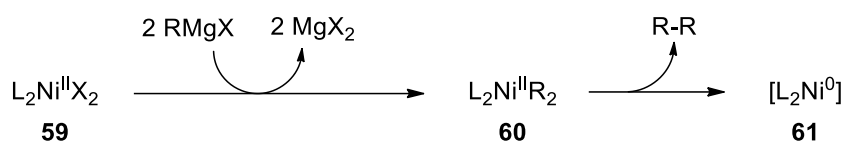


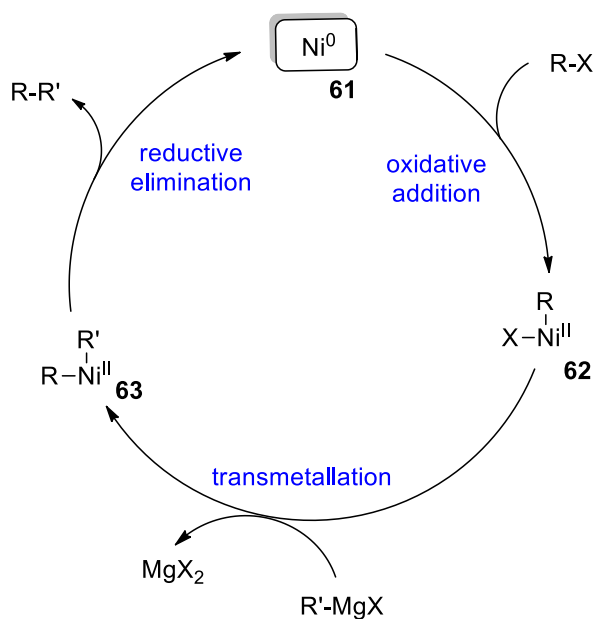
Figure 1. Timeline for TM-catalysed coupling and cross-coupling reactions.

The Kumada cross-coupling was proposed to proceed by the mechanism shown in **Scheme 16** (*cf.* **Scheme 13**) by Kumada in 1976.¹⁷ Initially, the nickel centre is reduced by Grignard reagent from Ni^{II} to Ni^0 (**Scheme 15**). Transmetalation with two molecules of Grignard reagent gives nickel complex **60** with two organic ligands. RE of the organic ligands (promoted by the approach of aryl halide) may give rise to a Ni^0 species **61**, which can then undergo OA to enter the catalytic cycle. This pathway represents a general route for the reduction of TMs by two electrons to enter a catalytic cycle (*vide infra*).



Scheme 15. Reduction of nickel *via* organomagnesium species.

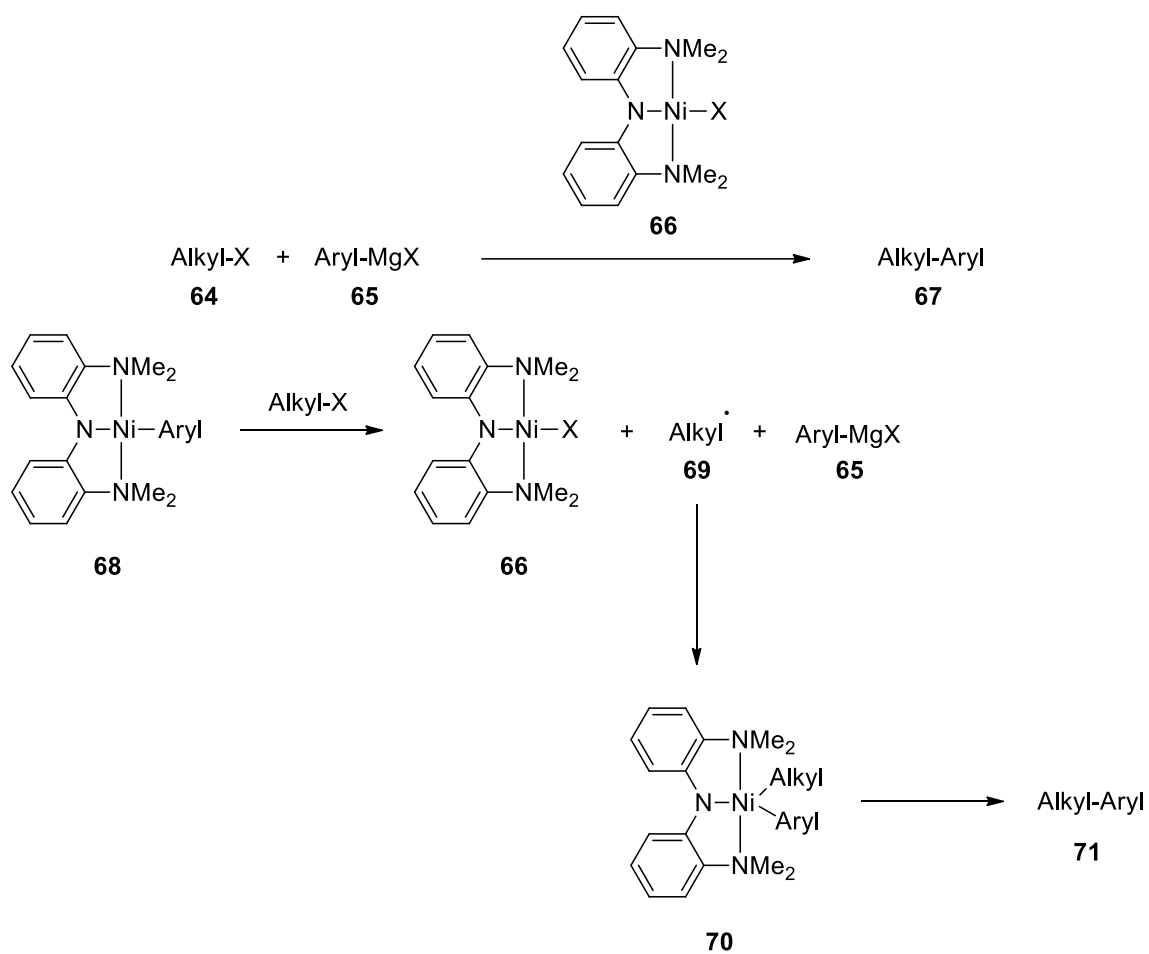
The active catalyst **61** can then undergo OA (**62**), followed by transmetallation with a molecule of Grignard reagent to give a new nickel species with two (different) organic ligands (**63**, **Scheme 16**). The approach of another molecule of aryl halide can then promote RE of the organic groups giving the product, regenerating Ni⁰. This pathway was based upon empirical observations that; 1) nickel species with two organic ligands readily undergo RE followed by OA in the presence of an aryl halide and, 2) the resulting nickel halide species can then undergo transmetallation with a Grignard reagent. This differs from the palladium-catalysed process, as approach of the aryl halide promotes RE.¹⁸⁻²⁰ Note that approach of the aryl chloride was proposed to form a σ -complex with nickel by the authors in 1976.¹⁷ Ni⁰ is now more widely accepted as the active species in solution.



Scheme 16. Nickel catalysed Kumada cross-coupling.

An alternative proposed mechanism has recently been reported in the literature, with the authors describing a bimetallic OA when *NNN*-pincer ligands are used (**Scheme 17**).^{21, 22} Arylnickel intermediate **68** was suggested to facilitate alkyl radical formation, which then added to a second arylnickel intermediate giving a Ni^{III} species (**70**). Ni^{III} is known to undergo rapid RE, thus forming the desired alkylbenzene species. In recent years, researchers such as MacMillan and Molander

have taken advantage of this rapid RE (from Ni^{III} over Ni^{II}) to carry out challenging cross-coupling reactions utilising nickel/photoredox dual catalysis.^{23, 24}



Scheme 17. Proposed bimetallic oxidative addition pathway.

2.4.1. The Iron-Catalysed Kumada Cross-Coupling Reaction

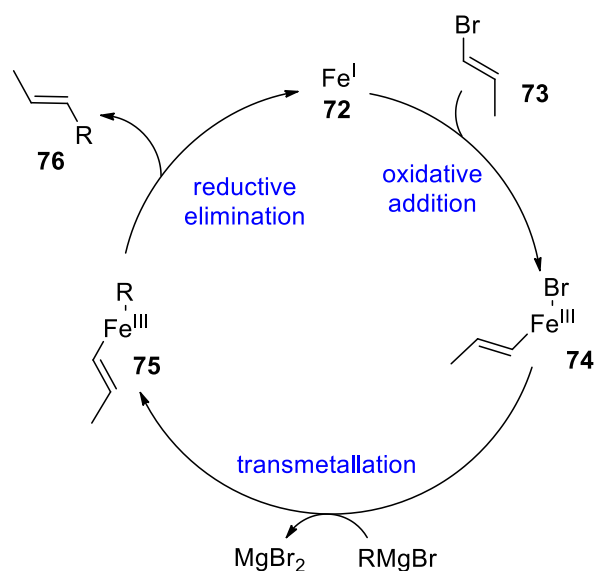
The discovery of TM-catalysed cross-coupling reactions and the subsequent increases in the understanding of such processes since has greatly advanced the field of synthetic organic chemistry (among others). It has allowed the preparation of increasingly complex structures; however, most processes use precious metals such as palladium, and require expensive, bulky, and often patented ligands to ensure selectivity. Thus, in recent years there has been a drive to improve the sustainability of these processes. There are numerous methods to reduce the environmental impact of chemical reactions, but this report will highlight the relatively recent field of iron-catalysed cross-coupling reactions and the Kumada cross-coupling in particular.

The Kumada cross-coupling reaction was chosen because there have been numerous reports of iron-catalysed processes in the literature.^{25, 26} Iron is cheap, earth abundant, and an essential element in the human body. Therefore, its use in the preparation of drug molecules is governed much less strictly than heavier/more toxic TMs such as palladium or nickel.

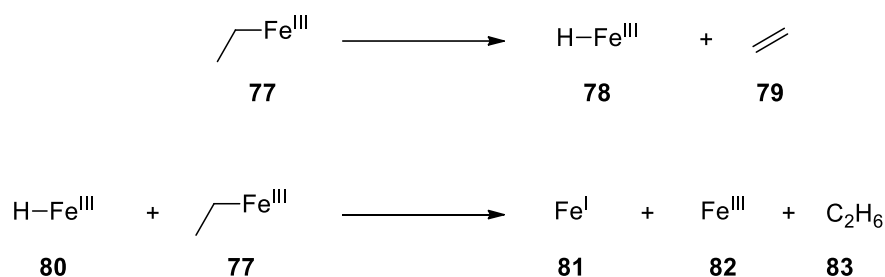
2.4.1.1. Early Discoveries

The ability of iron to catalyse cross-coupling reactions was demonstrated before the Kumada coupling itself, with successful experiments demonstrated as early as 1944.²⁷ Mottez was the first to report such a reaction, with a cross-coupling between aryl Grignard reagents and alkyl bromides.²⁷ The catalytic activity of iron was not investigated again until 1971, when Kochi reported the “alkenylation of Grignard reagents” with copper, silver and iron salts.²⁸ In this early article, Kochi highlighted the stereoselectivity of the process; the reaction of both *cis*- and *trans*-1-bromopropene with methylmagnesium bromide proceeded without isomerisation of the double bond.

A more detailed report in a later article proposed a mechanism involving an Fe^I-Fe^{III} redox cycle,²⁹ with initial reduction of the Fe^{III} precursor by the Grignard reagent giving the catalytically active Fe^I species (**73**, **Scheme 18**). A typical catalytic cycle then proceeds, with OA followed by transmetallation and finally RE. Kochi suggested the intermediacy of Fe^I following electron paramagnetic resonance (EPR) spectroscopy and analysis of the stoichiometry of gases evolved during the process (**79** and **83**, **Scheme 19**).^{29, 30} Later titration experiments by Norrby³¹ and Bedford³² also drew similar conclusions.



Scheme 18. Kochi's mechanism.



Scheme 19. Kochi's proposal for Fe^I formation.

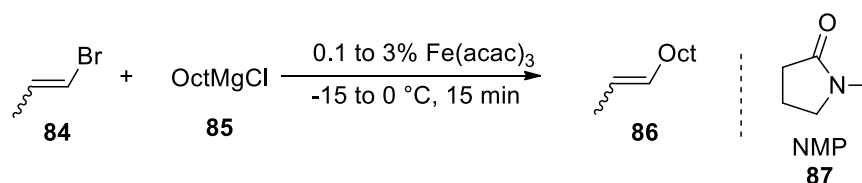
Following the early investigations by Kochi, there were few reports of iron-catalysed cross-coupling reactions, probably for two reasons. Firstly, the selectivity of the iron-catalysed processes was poor, and the mechanistic study of such reactions was challenging due to iron's propensity to undergo SET, along with associated paramagnetism. Secondly, the discovery of the palladium and nickel alternatives, which were much easier to study using standard techniques such as NMR spectroscopy, totally overshadowed the use of the cheaper, more earth abundant metal.

2.4.2. 1998 Onwards – Some Mechanistic Considerations

The field of iron-catalysed cross-coupling reactions underwent a major revival in the 1990s. This was motivated by several factors, including the scarcity of the mid-to-late transition metals such as palladium and platinum, the relative toxicity of these heavy transition metals, and the availability of other catalytically active metals. Driven by the early reports of the catalytic activity of iron toward the Kumada cross-coupling reaction by Kochi, and a recent report into the iron-catalysed cross-coupling of organomanganese reagents,³³ Cahiez chose to reinvestigate the

earlier chemistry. Cahiez noted the positive influence of 1-methyl-2-pyrrolidinone (NMP, **87**) as a cosolvent in the organomanganese cross-coupling reactions and chose to investigate its effect upon the iron-catalysed analogue.³⁴

Studies with a number of additives such as NMP (**87**), dimethylacetamide and 1,2-dimethoxyethane (DME, **390**) showed that a THF-NMP mixture increased the yield of the reaction between 1-bromopropene and octylmagnesium chloride to 87% compared to 48% with THF alone (**Scheme 20**). It was also found that the source of iron was unimportant; Fe(dbm)₃, Fe(acac)₃ and FeCl₃ all gave similar yields under the same conditions; only Fe₂SO₃ gave a reduced yield due to its insolubility in THF. Interestingly, varying the catalyst loading between 0.1 and 3% had little effect on the yield of the process, with a loading of 1 mol% being optimal. The additive, NMP, was suggested to act to stabilise iron in the catalytic cycle, promoting the reaction pathway and reducing off-cycle processes such as β-hydride elimination from the alkyl species.

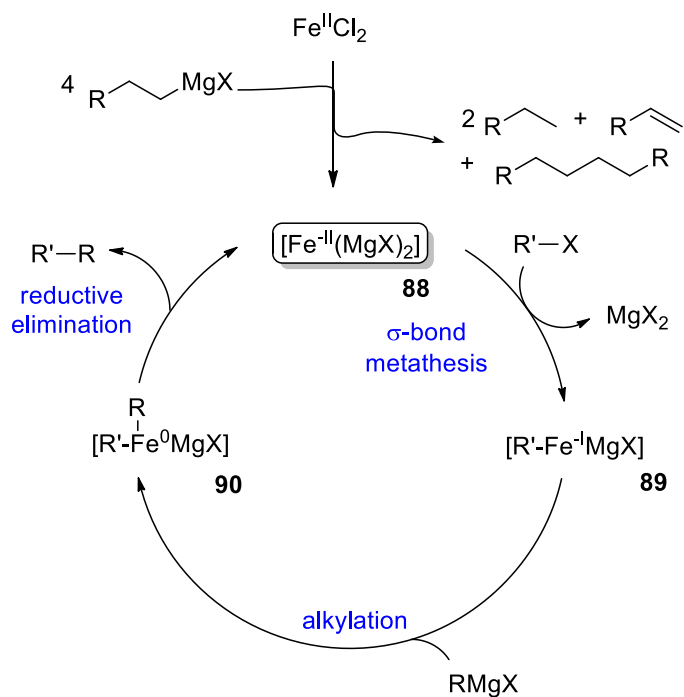


Scheme 20. Cahiez's cross-coupling.

Following this report the field of iron catalysis underwent a renaissance, with Cahiez producing a number of articles, and significant interests developing from other groups such as those of Bedford, Fürstner, Nakamura and Norrby.

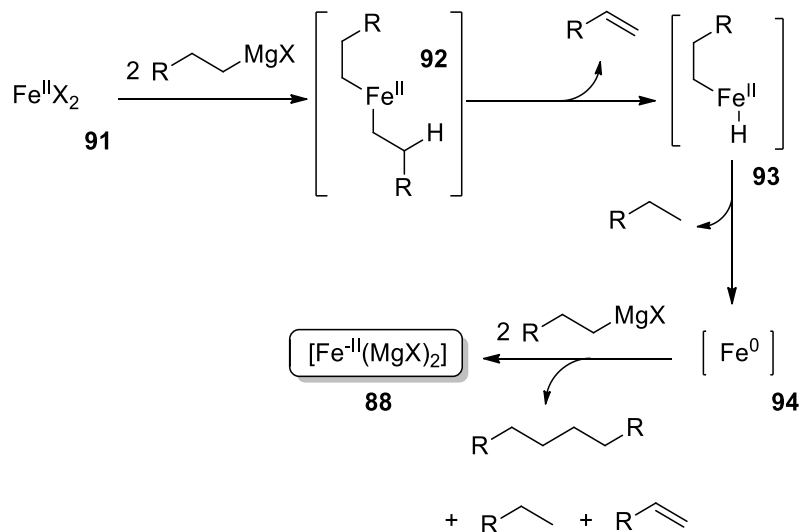
Fürstner investigated the reaction between (hetero)aryl halides and alkyl Grignard reagents and presented the first new insight into the mechanism of such reactions in 2002.³⁵ The report suggested the intermediacy of highly reduced Fe^{-II} 'inorganic Grignard reagents' (**88**, **Scheme 21**), initially proposed by Bogdanovic.^{36, 37} These interesting proposals were supported through a detailed investigation into the origin of such species and their role in the catalytic cycle. Importantly, Fürstner noted a significant difference in the reactivity of Grignard reagents with and without β-hydrogens,^{35, 38, 39} which led to further studies (*vide infra*).⁴⁰

Fürstner proposed the catalytic cycle shown in **Scheme 21**. Inorganic Grignard reagent **88** was suggested to undergo OA, *via* σ-bond metathesis (**89**), followed by alkylation from the organic Grignard reagent (**90**). This 2-electron process gave a Fe^{-II}/Fe⁰ catalytic cycle.



Scheme 21. Füstner's proposals.

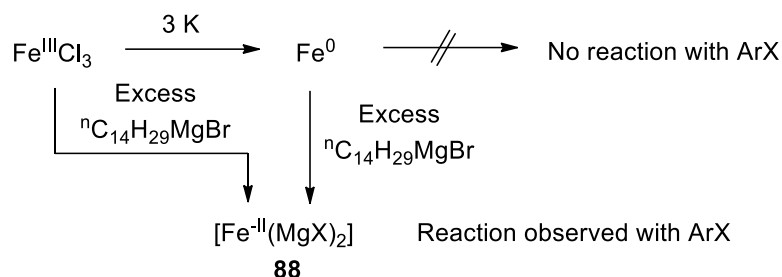
The Fe^{II} (or Fe^{III}) salt **91** was proposed to be the pre-catalyst which was then reduced *in situ* to form the catalytically active (formally) Fe^{II} species **88** through a series of transmetalations and β -hydride eliminations (**Scheme 22** cf. Nickel, **Scheme 15**).⁴¹



Scheme 22. Reduction of iron *via* β -hydride elimination.

Füstner used two experiments in an attempt to prove that the Fe^{II} species could be formed, and to demonstrate their catalytic ability (**Scheme 23**). The first reaction used the standard catalytic conditions to form the proposed Fe^{II} intermediate **88**. The product readily underwent an OA reaction with a molecule of aryl chloride. To rule out the possibility of Fe^{0} catalysis Füstner then

reduced Fe^{III} to Fe⁰ using potassium and found that this was unreactive with the aryl chloride. However, after adding excess Grignard reagent to the pre-formed Fe⁰, catalytic activity was observed. This certainly suggests that Fe species with oxidation states <0 can be formed in the presence of excess Grignard reagent, but does not prove their catalytic activity.



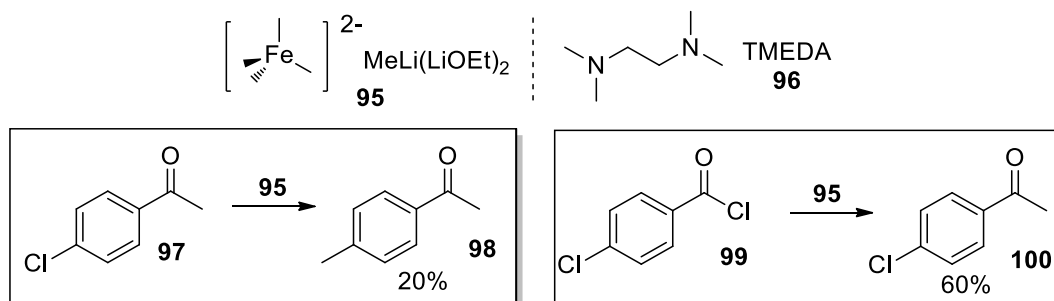
Scheme 23. Fürstner's observations.

Fürstner's proposals relating to the catalytic activity of Fe^{<0} were disputed by Norrby and Bedford. Norrby carried out computational studies using density functional theory (DFT), which suggested that RE from Fe⁰ to Fe^{-II} was prohibitively high in energy.³¹ Bedford furthered this discussion through the distinctions between *pre-catalyst/active catalyst* and *on-cycle/off-cycle species*.⁴² Furthermore, the formation of Fe^{-II} species by Bogdanović was observed in the presence of the strong reductant Mg⁰.^{36, 37} It is unlikely, based upon Norrby's findings, that Grignard reagents can promote the formation of Fe^{<0}.

During the investigation above⁴¹ Fürstner made some key observations: 1) the reaction between 4-chlorobenzoate and ethylmagnesium chloride proceeds in quantitative yield where the reaction with methylmagnesium chloride does not; 2) the reactions with different Grignard reagents have very different physical appearances: with methylmagnesium chloride a yellow colour persists but with ethylmagnesium chloride, the initial yellow colour darkens to black-violet as the reaction proceeds.⁴⁰ Fürstner attributed these differences to the presence of two different catalytically-active species; a new homoleptic Fe^{II} super-ate complex (**95**, **Scheme 24**) of the composition 'R₄Fe(MgX)₂' in the former case, and the low valent Fe^{-II} species **88** in the latter. Evidence was provided to support the presence of both species – the latter through substitution with structurally characterised Fe^{-II} complexes.

Fürstner used methyllithium under catalytically relevant conditions to investigate the formation of the Fe^{II} super-ate species. The addition of MeLi to FeCl₃ in the presence of tetramethyl ethylenediamine (TMEDA, **96**) led to the isolation of "an *exceptionally* sensitive red solid which vigorously ignites in air and rapidly decomposes when allowed to reach ~0 °C."⁴⁰ This complex

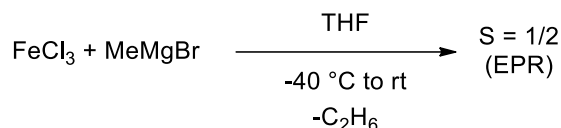
was found to be $[(\text{Me}_4\text{Fe})(\text{MeLi})][\text{Li}(\text{OEt})_2]_2$ (**95**). The compound, an organoferrate complex, was found to be poorly reactive towards aryl chlorides and iodides, but sufficiently reactive with activated compounds such as acyl chlorides (**Scheme 24**), enol triflates and electron deficient heteroaromatics to transfer the methyl groups.⁴³



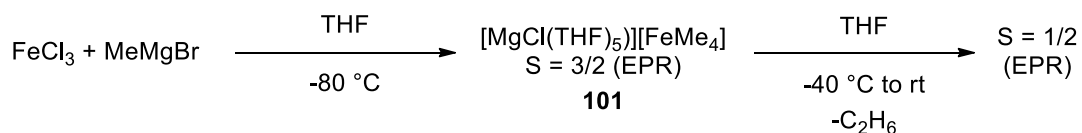
Scheme 24. Furstner's methyl-iron complex.

Neidig further investigated the reaction between FeCl_3 and methylmagnesium bromide.⁴⁴ The use of a Grignard reagent at higher temperatures meant it was possible to link this study to the earlier observations by Kochi.²⁹ At low temperature ($-80\text{ }^\circ\text{C}$) the authors observed a homoleptic tetramethyliron ferrate complex **101**, which was shown to have a spin $S = 3/2$, and exhibit a distorted square planar geometry. Upon heating, this Fe^{III} species underwent a chemical transformation resulting in a Fe^{I} species with spin $S = 1/2$.

Kochi



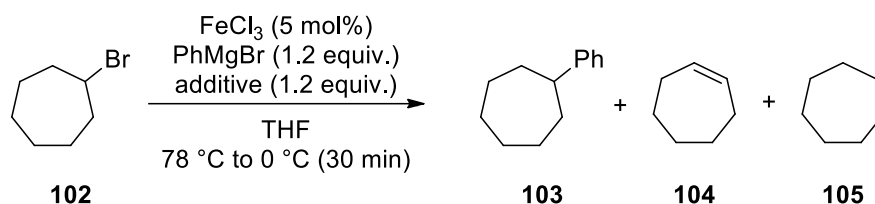
Neidig



Scheme 25. Neidig's observations.

Following this study, Neidig sought the identity of the elusive $S = 1/2$ species, observed in many Fe catalysed processes.⁴⁵ Careful manipulation of the unidentified compound resulted in the isolation of $[\text{MgCl}(\text{THF})_5][\text{Fe}_8\text{Me}_{12}]$ from reaction of FeCl_3 with MeMgBr in THF. These observations match Kochi's early mechanistic understanding, reported in 1976.^{29, 30} The differences between Furstner's and Neidig's observations were suggested to be related to both solvent and counterion (Et_2O vs. THF and Li vs. Mg).

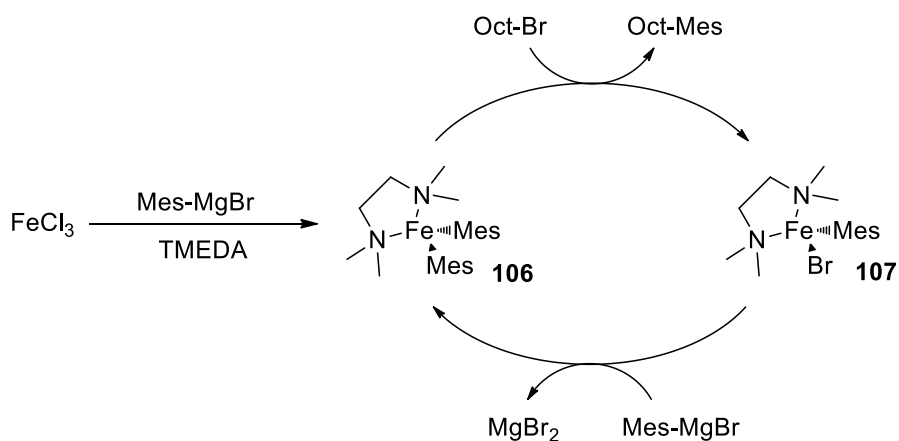
Nakamura began to investigate iron-catalysed cross-coupling in 2004, with his seminal publication relating to the coupling of cyclic primary and secondary alkyl halides with aryl Grignard reagents.⁴⁶ In this report, the use of a TMEDA (**96**) was shown to be beneficial in suppressing side reactions such as hydrodehalogenation (**104**), which gives olefin formation *via* β -hydride elimination followed by alkene dissociation and RE (**Figure 2**).



Entry	Additive	103	104	105	102	Ph-Ph
1	None	5	79	0	4	6
2	Et ₃ N	3	78	0	11	5
3	<i>N</i> -Methyl morpholine	8	72	0	4	5
4	DABCO	20	2	0	75	3
5	NMP	15	3	trace	79	4
6	TMEDA	71	19	3	trace	10

Figure 2. Nakamura's aryl-cycloheptane cross-coupling.

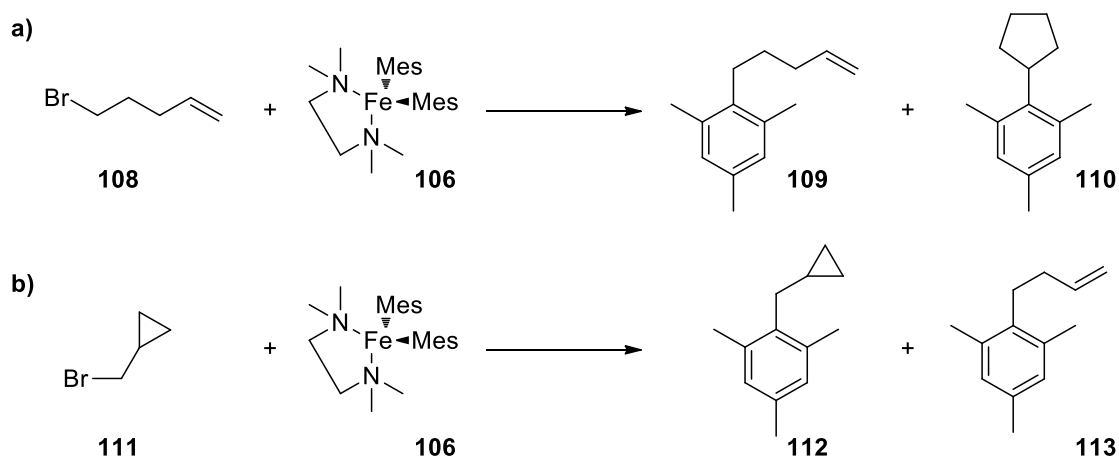
Nakamura further investigated the effect of TMEDA (**96**) on the reaction, firstly isolating and characterising what were thought to be catalytic intermediates following NMR experiments (**106** and **107**, **Scheme 26**), then using radical clock experiments to determine the nature of the mechanism.⁴⁷



Scheme 26. Nakamura's observations.

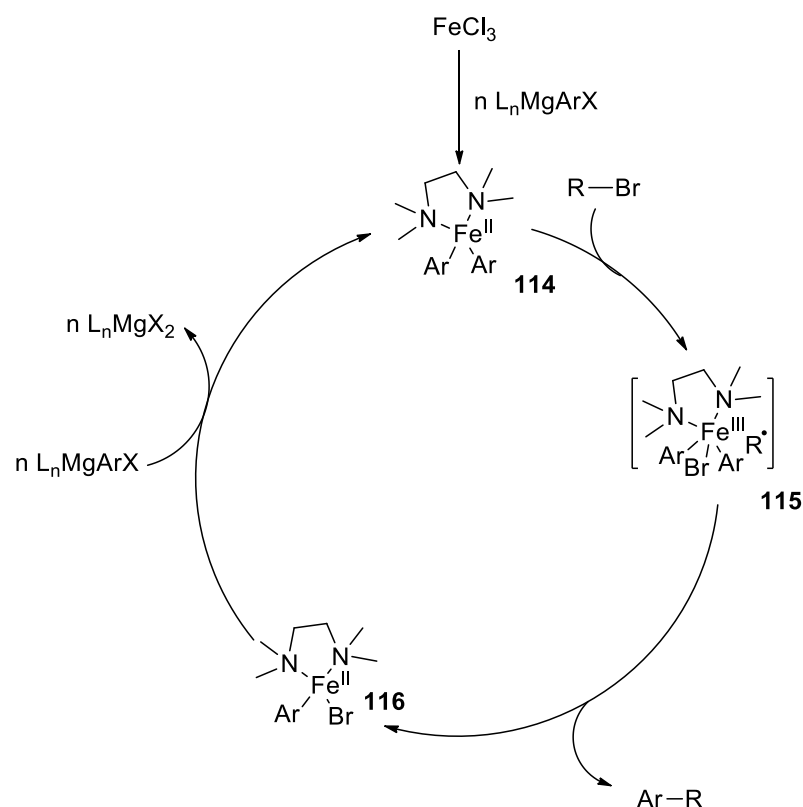
It was found that reaction of **106** with 1-bromo-5-hexene **108** gave no radical cyclisation product **110**, but treatment of **106** with (bromomethyl)cyclopropane **111** gave a mixture of both cyclopropanated and ring opened products (**112** and **113**). The rate of radical cyclisation of the

5-hexenyl radical is much slower than the rate of radical ring opening of the cyclopropylmethyl radical, by a factor of $10^3 \text{ M}^{-1} \text{ s}^{-1}$. Thus, Nakamura was able to propose the intermediacy of a short-lived radical species generated by the oxidation of Fe^{II} to Fe^{III} (**Scheme 28**). Interestingly, earlier experiments showed different results in the reaction of 1-bromo-5-hexene with phenylmagnesium bromide. Under conditions where all starting materials were mixed at $-78 \text{ }^\circ\text{C}$ then allowed to warm to room temperature, cyclised product was observed *exclusively*; controlled addition of phenylmagnesium bromide and TMEDA (**96**) to a solution of 1-bromo-5-hexene and FeCl_3 gave *no* radical cyclisation.



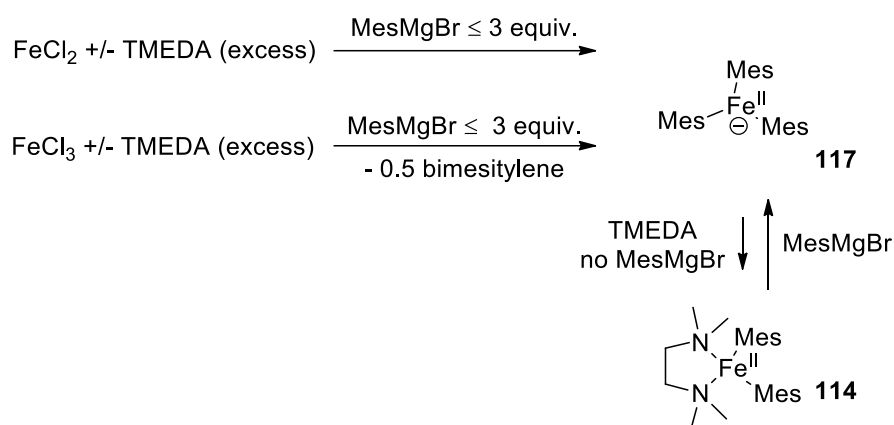
Scheme 27. Radical clock experiments.

The isolation of intermediates **106** and **107**, combined with radical clock experiments gave a possible catalytic cycle which involves Fe^{II} and Fe^{III} intermediates (**Scheme 28**). Initial reduction of FeCl_3 to Fe^{II} by the Grignard reagent gives intermediate **114**; heterolytic cleavage of the alkyl halide bond then allows addition to form intermediate **115** with associated alkyl radical. Fast radical coupling of the alkyl radical with an aryl group gives the product and a further Fe^{II} intermediate **116** which undergoes transmetallation with a molecule of Grignard reagent to reform **114**. It must be noted here that the work carried out by Fürstner involved the coupling of (*hetero*)aryl halides and *alkyl* Grignard reagents, where this work investigates the coupling of *alkyl* halides and *aryl* Grignard reagents. Thus, different mechanisms are likely to proceed, so a direct comparison is not possible.



Scheme 28. Nakamura's proposed catalytic cycle.

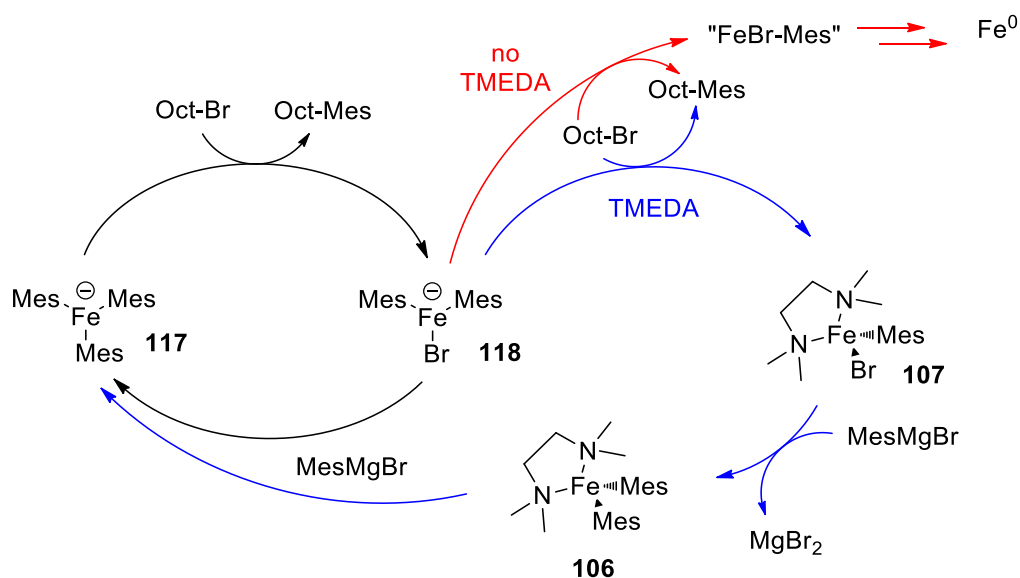
Bedford recently investigated the effect of TMEDA (**96**) upon the cross-coupling between mesitylmagnesium bromide (MesMgBr) and an alkyl halide (**Scheme 29**).⁴⁸ It was noted that in the earlier investigations by Nakamura a set ratio of iron/Grignard reagent/TMEDA (1:3:8) was used to determine the catalytically active species, and that under real reaction conditions the molar excess of Grignard reagent over Fe was likely to be much higher. Thus, Bedford chose to study the effect of an increased concentration of Grignard reagent upon the formation of iron species in the presence of TMEDA. Under the same conditions there were found to be at least 3 paramagnetic species, with *ate* complex **117** observed at the highest concentration. Adding a further 4 equivalents of Grignard reagent pushed the equilibrium strongly towards **117**, with no other paramagnetic species observable by NMR spectroscopy. The *ate* complex was found to react more rapidly with bromooctane than the TMEDA complex **114** and the reaction of the TMEDA (**96**) complex was also found to have an induction period. This data suggested that the *ate* complex was responsible for the catalytic activity in this case.



Scheme 29. Bedford's observations.

The use of benzylmagnesium chloride also resulted in the formation of an iron *ate* complex, suggesting the presence of such species in reactions with the bulkier Grignard reagents. When using smaller aryl Grignard reagents such as 4-tolylmagnesium chloride, Bedford noted a change in the appearance of the reaction mixture depending upon the reaction conditions. In reactions where controlled addition was used, the solution was generally yellow with transient red intermediates, whereas rapid addition of the Grignard reagent led to black suspensions of 'catalytically active zero-valent iron nanoparticles'.⁴⁹ This difference was attributed to the relative stability of the benzyl and mesityl iron species with respect to RE.⁴⁸

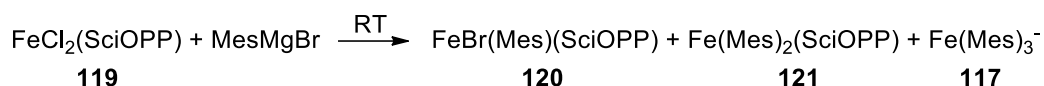
Bedford proposed a new catalytic cycle, based upon his observations; intermediates **106** and **107** were suggested to be resting states (**Scheme 30**). Instead, Bedford suggested that intermediates **117** and **118** were responsible for the formation of the desired cross-coupled product.



Scheme 30. Bedford's revised mechanism.

Nakamura invoked his earlier TMEDA mechanistic pathway in a cross-coupling reaction in the presence of the 3,5-di(*t*-butyl)-SciOPP ligand. Interestingly, a radical clock experiment using (iodomethyl)cyclopropane gave the ring opened product *exclusively* (**Scheme 27b**).⁵⁰ Again, this suggests the intermediacy of a short lived radical species generated by the oxidation of Fe^{II} to Fe^{III}.

More recently, Neidig used physical-inorganic methodology to probe the FeMes₂(SciOPP) mediated process, combining Mössbauer spectroscopy, magnetic circular dichroism (MCD) and DFT.⁵¹ In this report, the FeCl₂(SciOPP) pre-catalyst was exposed to varying amounts of mesitylmagnesium bromide, and the resulting solutions were freeze trapped for Mössbauer and MCD measurements. They observed species similar to those isolated by Bedford;⁴⁸ **Figure 3** shows some experimental results. With only 2 equivalents of Grignard reagent the majority of the Fe in the mixture was found to be Fe(Mes)₂(SciOPP) **121**; increasing the stoichiometry of Grignard reagent to 20 equivalents and beyond again pushed the equilibrium strongly towards the Fe(Mes)₃⁻ complex **117**.



Entry	MesMgBr Equivalents	120 / mole fraction	121 / mole fraction	122 / mole fraction
1	1	1	0	0
2	2	0.03	0.90	0.07
3	20	0	0.38	0.62
4	100	0	0.02	0.98

Figure 3. Neidig's observations.

Under the reaction conditions used, Neidig noted some significant findings using a sample enriched in ^{57}Fe . Firstly, it was observed that the $\text{Fe}(\text{Mes})_2(\text{SciOPP})$ species **121** was persistent at the higher concentrations of Grignard reagent, which may suggest that SciOPP can coordinate to $\text{Fe}(\text{Mes})_3^-$ **117**. Secondly, $\text{Fe}(\text{Mes})_2(\text{SciOPP})$ was found to give selective formation of mesityldecane in the reaction with 1-bromodecane, where $\text{Fe}(\text{Mes})_3^-$ formed a mixture of mesityldecane and decene. Both observations suggest that although $\text{Fe}(\text{Mes})_3^-$ may be formed, it is unlikely to be the catalytically active species under these reaction conditions. This was proposed to agree with Nakamura's earlier catalytic cycle, where TMEDA (**96**) was the ligand (Scheme 28).

2.4.3. Mechanistic Summary

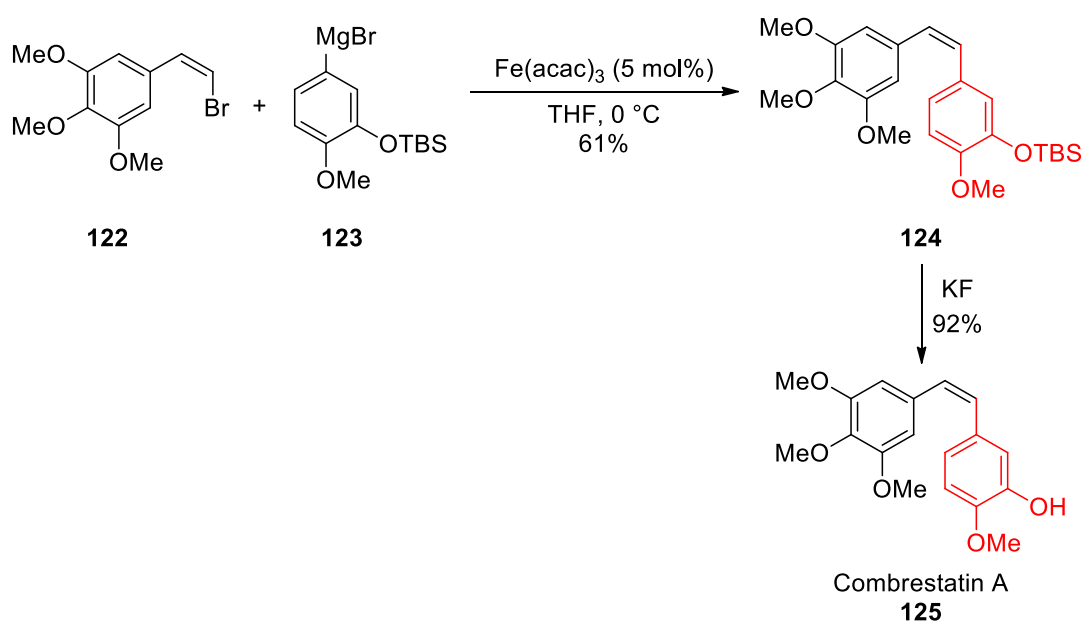
In summary, a great deal of work has been carried out on iron-catalysed Kumada cross-coupling reactions in recent years. It is thought that the catalytically active species, with alkyl Grignard reagents, have oxidation states $\text{Fe}^{<0>$. This is due to their powerful reducing nature. This has however been disputed in recent years, with others such as Norrby suggesting Fe^{I} to be the active catalyst.^{31, 52-54} An Fe^{II} intermediate is more widely accepted with aryl Grignard reagents, as they are less reducing than their alkyl counterparts.^{47, 51}

The overall mechanism for these processes is still not fully understood, but it is agreed that reduction of Fe^{III} is required to form the active catalyst. Following this it is thought that OA of a (pseudo)halide is followed by Grignard transmetallation and finally RE. This mechanism may be radical or ionic in nature, with both suggested in the literature.^{35, 47, 55} The most relevant insights were reported by Norrby in 2012.⁵³ Here it was suggested that the catalytic cycle proceeds through a standard TM-catalysed cross-coupling pathway; OA, transmetallation then RE. The article also noted that the redox cycle must occur *via* Fe^{I} - Fe^{III} intermediates, as any RE from Fe^{II} to Fe^0 was found to be prohibitively high in energy.

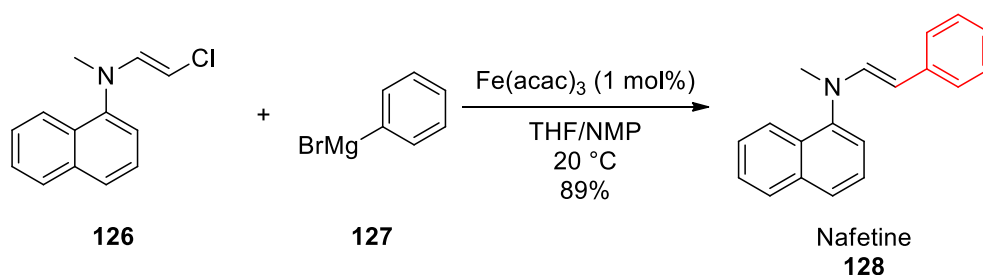
There is significant disagreement in the mechanistic proposals for the cross-coupling between mesitylmagnesium bromide and alkyl halides. Initially Nakamura proposed a catalytic cycle invoking Fe^{II} - Fe^{III} intermediates **106** and **107**.⁴⁷ This was based upon the isolation of intermediates which were thought to be upon the reaction pathway (**Scheme 28**). Bedford disputed this claim; it was proposed that excess Grignard reagent in the reaction mixture would form higher-order Fe-aryl species of the type $[\text{Fe}(\text{Mes})_3]$.⁴⁸ This Fe^{II} *ate* complex was found to react more quickly with electrophiles than the previous $[\text{FeR}_2(\text{TMEDA})]$ complexes. Neidig then investigated a related FeSciOPP complex using Mössbauer, MCD and DFT.⁵¹ These species were shown to form intermediates very similar to those reported by Nakamura. Kinetic investigations showed that $[\text{FeR}_2(\text{SciOPP})]$ intermediates were responsible for the catalytic activity in these reactions. Study of the Fe^{II} *ate* complexes suggested that they were responsible for the formation of β -hydride elimination products. Thus, the slow addition of Grignard reagents in the presence of electrophile promoted a catalytic cycle like that in **Scheme 28**.

2.5. Industrial/Pharmaceutical Applications of Iron-Catalysed Kumada Cross-Coupling Reactions

Despite significant challenges with mechanistic understanding, iron-catalysed Kumada cross-coupling reactions have been applied by researchers within the pharmaceutical industry. Some of the earliest cross-couplings reported with iron were between aryl or alkyl Grignard reagents and vinyl (pseudo)halides. This is apparent when studying the literature for iron-catalysed carbon-carbon bond formation in the preparation of APIs or natural products.⁵⁶ Numerous researchers have utilised conditions similar to those used by Kochi in 1971²⁸ and Cahiez in 1998³⁴ in the synthesis of natural products such as combrestatin A **125**⁵⁷ (Scheme 31) and APIs such as nafetine **128**⁵⁸ (Scheme 32).



Scheme 31. Camcho-Dávila's synthesis of combrestatin A.

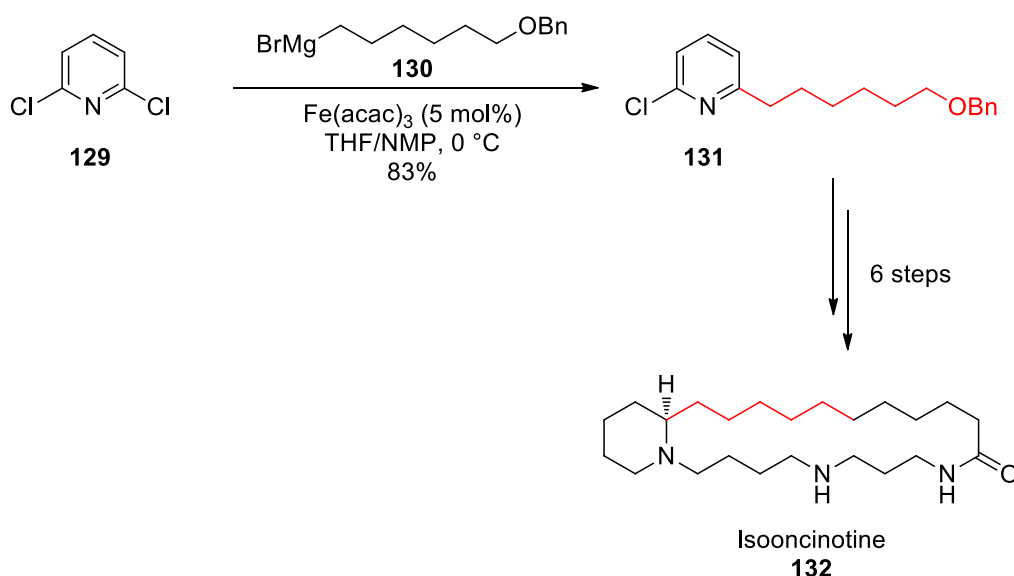


Scheme 32. Zorin's synthesis of nafetine.

Although aryl-vinyl cross-couplings have been demonstrated in the preparation of both natural products and APIs, (hetero)aryl-alkyl or (hetero)aryl-aryl cross-coupling reactions would offer greater synthetic utility. This is because many drug-like molecules contain sp^2 - sp^3 and/or aryl-aryl

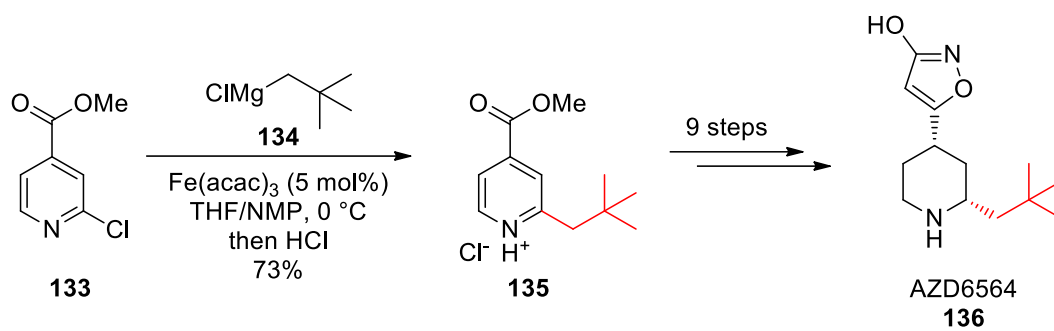
(sp^2-sp^2) linkages. Several researchers have demonstrated the use of iron in the preparation of APIs on both small scale, for medicinal chemistry, and large scale, for process chemistry applications. Olsson⁵⁹, Risatti⁶⁰ and Fürstner's⁶¹ reports are all discussed later in **Chapter 3** and **Chapter 5**.

Another interesting application of iron in the preparation of a natural product was disclosed by Fürstner in 2004.⁶² The authors were able to prepare (-)-isooncinotine **132** following an initial iron-catalysed cross-coupling of a primary alkyl Grignard reagent (**Scheme 33**). Simple slow addition of Grignard reagent **130** selectively gave the monoalkylation product **131**. 6 synthetic steps after the cross-coupling reaction gave the spermidine alkaloid **132**, which has proven challenging to isolate from natural sources.



Scheme 33. Fürstner's synthesis of isooncinotine.

Researchers at AstraZeneca also used an iron-catalysed cross-coupling of an alkyl Grignard reagent and heteroaryl chloride in the preparation of their drug candidate AZD6564 **136** (**Scheme 34**).⁶³ The authors demonstrated the synthesis of intermediate **135** on a 100 gram scale. Unfortunately, the formation of (presumed) iron hydroxide species led to challenges with the work-up and isolation. A combination of citric acid and ethylenediaminetetraacetic acid (EDTA) washes were used to counteract these issues, but the final good laboratory practice (GLP) route circumvented iron altogether, opting for a palladium catalysed Negishi reaction.



Scheme 34. Synthesis of AZD6564.

2.6. Principles of Green Chemistry

A key consideration for synthetic chemists of all disciplines should be the environmental impact and sustainability of their procedures and processes. In 1998 Paul Anastas and John Warner coined the “12 principles of green chemistry” as a series of factors likely to produce a greener chemical process.⁶⁴ They are listed below, with descriptions taken from the American Chemical Society (ACS).⁶⁵

1. Prevention

It is better to prevent waste than to treat or clean up waste after it has been created.

2. Atom Economy

Synthetic methods should be designed to maximise the incorporation of all materials used in the process into the final product.

3. Less Hazardous Chemical Syntheses

Wherever practicable, synthetic methods should be designed to use and generate substances that possess little or no toxicity to human health and the environment.

4. Designing Safer Chemicals

Chemical products should be designed to affect their desired function while minimising their toxicity.

5. Safer Solvents and Auxiliaries

The use of auxiliary substances (e.g., solvents, separation agents, etc.) should be made unnecessary wherever possible and innocuous when used.

6. Design for Energy Efficiency

Energy requirements of chemical processes should be recognised for their environmental and economic impacts and should be minimised. If possible, synthetic methods should be conducted at ambient temperature and pressure.

7. Use of Renewable Feedstocks

A raw material or feedstock should be renewable rather than depleting whenever technically and economically practicable.

8. Reduce Derivatives

Unnecessary derivatisation (use of blocking groups, protection/ deprotection, temporary modification of physical/chemical processes) should be minimised or avoided if possible, because such steps require additional reagents and can generate waste.

9. Catalysis

Catalytic reagents (as selective as possible) are superior to stoichiometric reagents.

10. Design for Degradation

Chemical products should be designed so that at the end of their function they break down into innocuous degradation products and do not persist in the environment.

11. Real-time analysis for Pollution Prevention

Analytical methodologies need to be further developed to allow for real-time, in-process monitoring and control prior to the formation of hazardous substances.

12. Inherently Safer Chemistry for Accident Prevention

Substances and the form of a substance used in a chemical process should be chosen to minimise the potential for chemical accidents, including releases, explosions, and fires.

Catalysis is very important in modern synthetic chemistry, and is therefore included as one of the 12 principles. The use of catalytic, rather than stoichiometric, reagents also has relevance to a number of the other 12 principles, including; prevention and atom economy. Using iron in place of heavier TMs such as palladium can further reduce the environmental impact of cross-coupling reactions. Iron is less toxic than palladium (principles 3 to 5), often requires lower reaction temperatures (principle 6) and is earth abundant (principle 7). Significant attention must however be paid to the use of solvents, additives and ligands in iron-catalysed cross-coupling reactions (principle 3 to 5).

2.7. Design of Experiments – Toward Process Optimisation

Chemists working in pharmaceutical process research and development (PD) require robust and scalable synthetic steps and routes for the preparation of drugs and synthetic intermediates on a (multi)kilogramme scale. Following the selection of a suitable chemical step, researchers generally use multivariate approaches to carry out reaction optimisation; one of these methods is statistical design of experiments (DoE).

There have been two main drivers for the application of DoE in PD. There is an increased motivation from regulatory authorities towards quality by design (QbD), in which companies are required to demonstrate significant process understanding. This means DoE is now expected as part of a new drug application (NDA) submission.⁶⁶ Also, there is a changing economic environment, in which pharmaceutical chemists are expected to use their time in a much more efficient manner. In DoE, the number of experiments that are necessary is defined at the outset, meaning it is possible to manage time more effectively.

Primarily, DoE aims to address a given question through a series of well-considered experiments. One approach to this may be to define an interesting starting point, possibly current reaction conditions, and prepare an experimental design around it. To do this chemists often use programs such as Stat-Ease's Design Expert or Umetrics' MODDE. The software gives the user a simple interface through which an appropriately structured investigation can be prepared. DoE employs statistical analysis, along with a symmetrical design space allow the maximum amount of data to be extracted from a minimal number of experiments. A DoE investigation studies multiple parameters at once, allowing links between them to be observed and understood.

The symmetry of a DoE means the investigator is able cover chemical space more efficiently. This becomes apparent when considering the traditional one factor at a time (OFAT) approach. When looking to optimise a transformation with three variables (V_1 , V_2 and V_3) the OFAT method would sequentially change each of them, moving towards the desired response with each iteration (blue arrows, **Figure 4**). The conditions giving the greatest response (e.g. conversion to product) at the end of the investigation are considered to be optimal. Unfortunately, due to the linearity of these changes, it is possible to completely miss the ideal solution (green section, **Figure 4**). In a full factorial DoE investigation, the researcher would carry out 2^3 experiments to understand responses from the chosen variables, within the chosen ranges (**Figure 4**). Selecting reactions at the corners of a cube means it is possible to predict the combination of V_1 , V_2 , and V_3 leading to the greatest response.

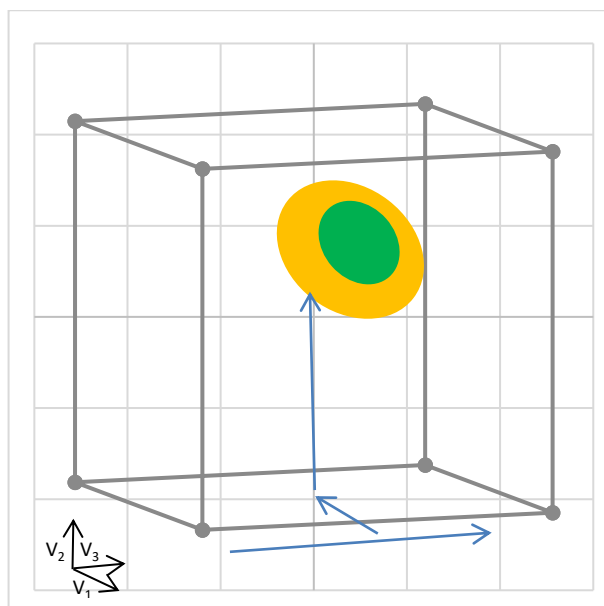


Figure 4. One factor at a time optimisation.

Along with an improved understanding of chemical space, DoE is also able to address other shortfalls associated with the OFAT approach. These include variability, noise, and two factor interactions. *Variability* occurs on a day-to-day basis; an experiment may be run several times with a different percentage yield each time. This deviation is due to *experimental noise*; slight changes in temperature, for example, may affect the process. DoE is able to estimate this in two ways. Firstly, by using centre-point reactions, which are repeated throughout the experimental design; any scatter in these data points gives a real (measurable) value for the experimental error under the centre-point conditions. In addition, the use of averaging allows the software to evaluate noise via standard deviation. *Two factor interactions (vide infra)* are observed when these variables work together to produce a positive or negative effect. Furthermore, with the cubic design shown below, it is possible to investigate the change in response of variable V_1 at high and low levels of V_2 and V_3 respectively. The effect of V_1 can then be averaged across the four values, giving a sharpened estimate (blue arrows, **Figure 5**).

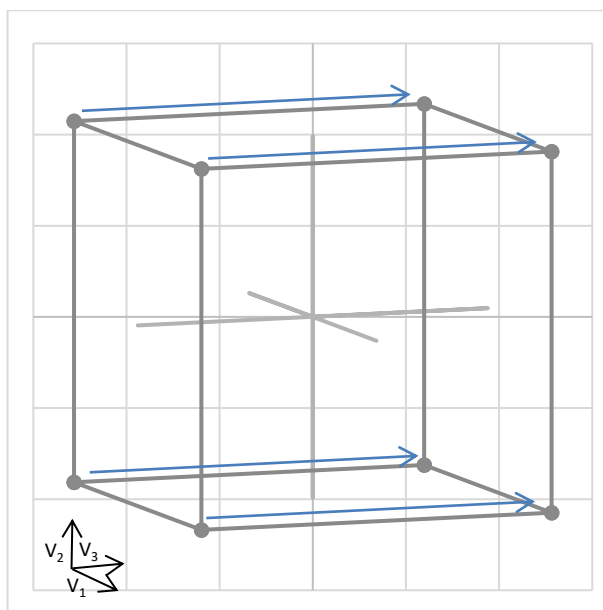
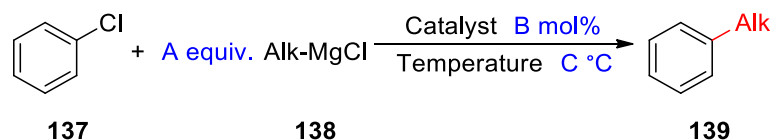


Figure 5. Optimisation using statistical design of experiments.

The sub-sections below serve to introduce the key output from the DoE investigation, and how to interpret the data.

2.7.1. A Typical 3-Factor Investigation

A typical DoE investigation would consider 3 or more variables for a chosen reaction. For example; temperature, reactant equivalents (**138**) and catalyst loading (**Scheme 35**).



Entry	Factor / units	Low	Centrepoint	High
1	A / equiv.	1	2	3
2	B / mol%	1	5.5	10
3	C / °C	0	20	40

Scheme 35. A typical 3-factor DoE investigation.

A full factorial DoE would require ($2^3 =$) 8 experiments to understand the effect of each variable upon the outcome of the reaction, in this case conversion to alkylated product **139**. The researcher would also carry out a number of reactions at the centrepoint conditions. These would be repeated at least once, allowing the DoE software to assess the variability in the experimental data. After running the investigation, the reaction outcome would be entered to the software, which would carry out a statistical analysis of the results. Some random data is included in the following sections to exemplify the method of data analysis.

2.7.2. The Half Normal Plot

The DoE software would produce a half-normal plot (**Figure 6**) from the experimental output. This plot can be read by looking for points furthest to the right – those with the highest ‘standardised effect’. A model for the data can then be built selecting the factors with the greatest influence over the reaction outcome. The point furthest to the right is a *two-factor interaction*. This is where two factors combine to have an effect, which is often greater than the individual factors themselves. The plot suggests that a combination of equivalents of Grignard reagent *and* catalyst loading has a large positive effect on the reaction (orange = positive effect).

Design-Expert® Software
Product

▲ Error estimates

Shapiro-Wilk test

W-value = 0.900

p-value = 0.432

A: Grignard reagent

B: Catalyst

C: Temperature

■ Positive Effects

■ Negative Effects

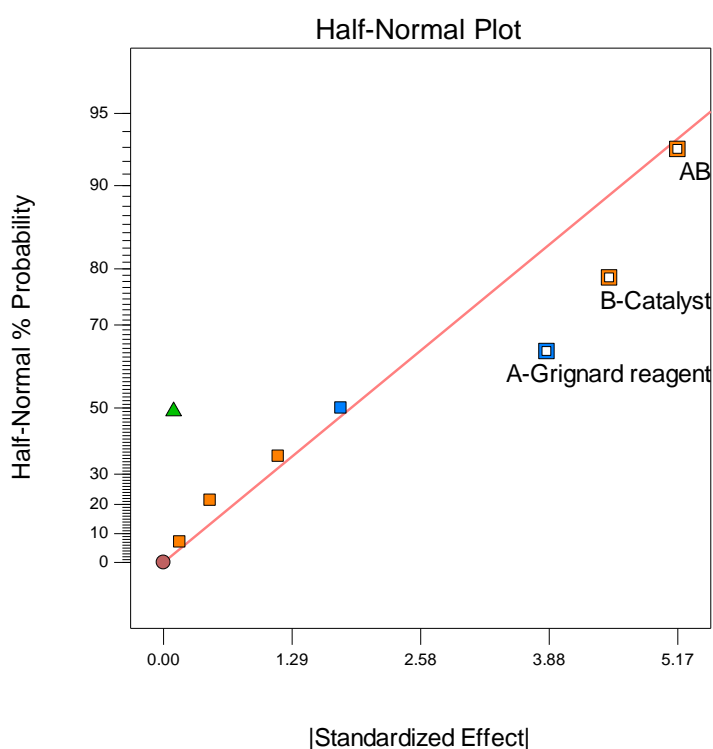


Figure 6. Example of a half-normal plot.

2.7.3. The ANOVA Table

From the selected data, the DoE software would carry out some statistical analysis. This would then result in an analysis of variance (ANOVA) table (**Table 1**). Within this table, we are generally looking at two columns - 'p-value', and 'statistical significance'. The p-value represents a 95% confidence interval for the model. Any p-value <0.05 suggests that the data is 'statistically significant' and that the chosen factor has an influence on the outcome of the reaction. The data in **Table 1** is random, which leads to no effect being observed. Only the 'lack of fit' column has a p-value <0.05. This suggests that the experimental data does not fit the model predicted by the DoE software.

Table 1. Example of an ANOVA table.

	Sum of Squares	df	Mean Square	F Value	p-value	Statistical significance
Model	123.28	3	41.09	0.32	0.8137	not significant
A-Grignard reagent	29.68	1	29.68	0.23	0.6496	
B-Catalyst	40.19	1	40.19	0.31	0.5983	
AB	53.41	1	53.41	0.41	0.5452	
Residual	779.82	6	129.97			
Lack of Fit	779.77	5	155.95	3465.65	0.0129	significant
Pure Error	0.045	1	0.045			
Cor Total	903.09	9				

2.7.4. The Model Graphs

After analysing the ANOVA table, the researcher would view the 'model graphs' (**Figure 7**). They show the effect that each factor has on the outcome of the reaction. The model graph shown in **Figure 7** shows the two-factor interaction between equivalents of Grignard reagent *and* catalyst loading. Low levels of catalyst are plotted in black, and high levels of catalyst are plotted in red. The chart suggests that a large negative effect is observed at low catalyst loading when increasing the equivalents of Grignard reagent. The chart also suggests that a small positive effect is observed at high catalyst loading when increasing the levels of Grignard reagent. If this was real data, this may represent significant catalyst deactivation with a combination of low catalyst and high Grignard reagent.

Design-Expert® Software
Factor Coding: Actual
Product (%)
(adjusted for curvature)
● Design Points

X1 = A: Grignard reagent
X2 = B: Catalyst

Actual Factor
C: Temperature = 20

■ B- 1
▲ B+ 10

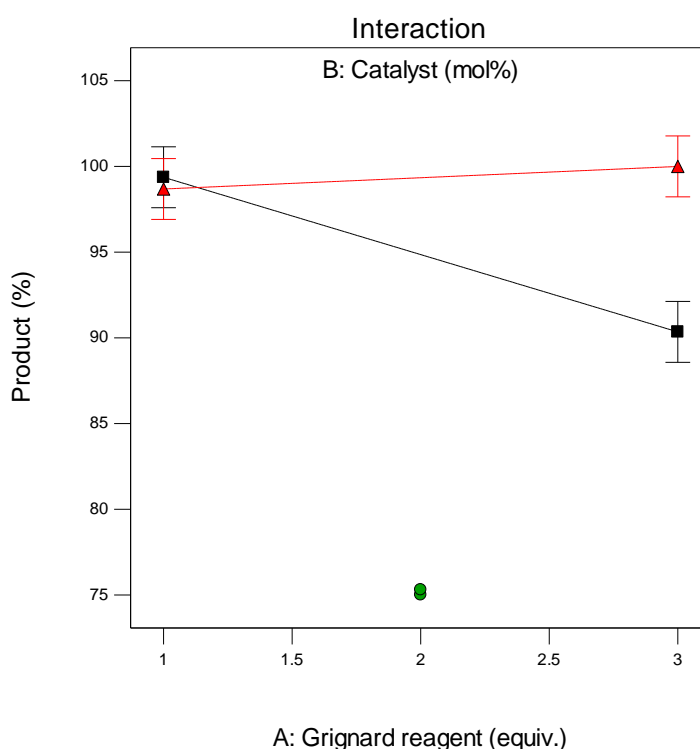


Figure 7. A sample model graph.

2.8. Aim

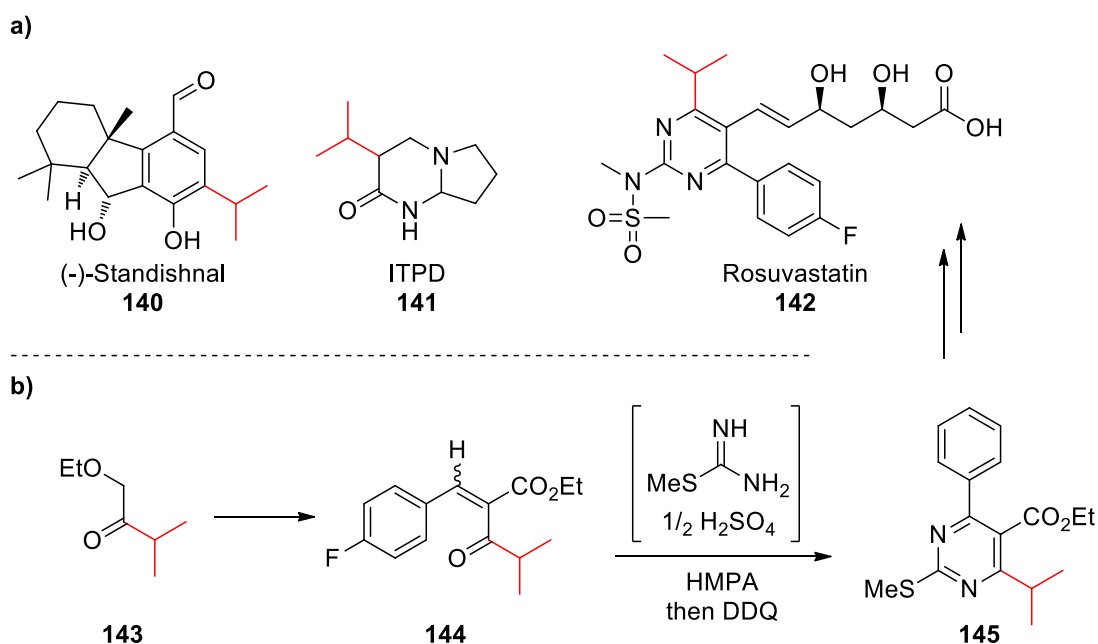
The mechanistic studies discussed throughout **Chapter 2** serve to demonstrate the significant challenges in further understanding such process. As is apparent from **Section 2.5**, many researchers have utilised iron-catalysed cross-coupling reactions in the preparation of alkyl-substituted heteroaromatics of relevance to the pharmaceutical industry. Thus, with consideration the principles of green chemistry (**Section 2.6**) the aim of this thesis is to investigate the application of iron-catalysed cross-coupling reactions to the coupling of secondary alkyl Grignard reagents with aryl and heteroaryl chlorides.

Attention will be paid to the scale-up potential during the investigations. Being located within a PD department within a pharmaceutical company allows the use of standard process chemical applications such as DoE (**Section 2.7**), and high throughput chemistry. These tools will be utilised frequently in the search for robust and scalable processes, which may be amenable to the preparation of APIs.

3. Iron-Catalysed *iso*-Propylation of Electron Deficient Aryl and Heteroaryl Chlorides

3.1. Background

The *iso*-propyl group is an important structural motif in both natural products including (–)-Standishnal **140** and APIs such as Rosuvastatin **142** (Scheme 36a).^{67, 68} The introduction of this group can require harsh and forcing conditions including those employed in the Friedel-Crafts alkylation (Scheme 37);⁶⁹ this leads to problems of both selectivity and functional group tolerance. To avoid these difficulties, it is often introduced early in a synthetic process, as demonstrated in the preparation of **142** (Scheme 36b).⁶⁷ The addition of an *iso*-propyl group *via* late stage functionalisation is less practical; introducing an *iso*-propyl group to a scaffold in a medicinal chemistry programme, for example, to explore the effects of size and hydrophobicity within a binding pocket, can therefore be challenging.

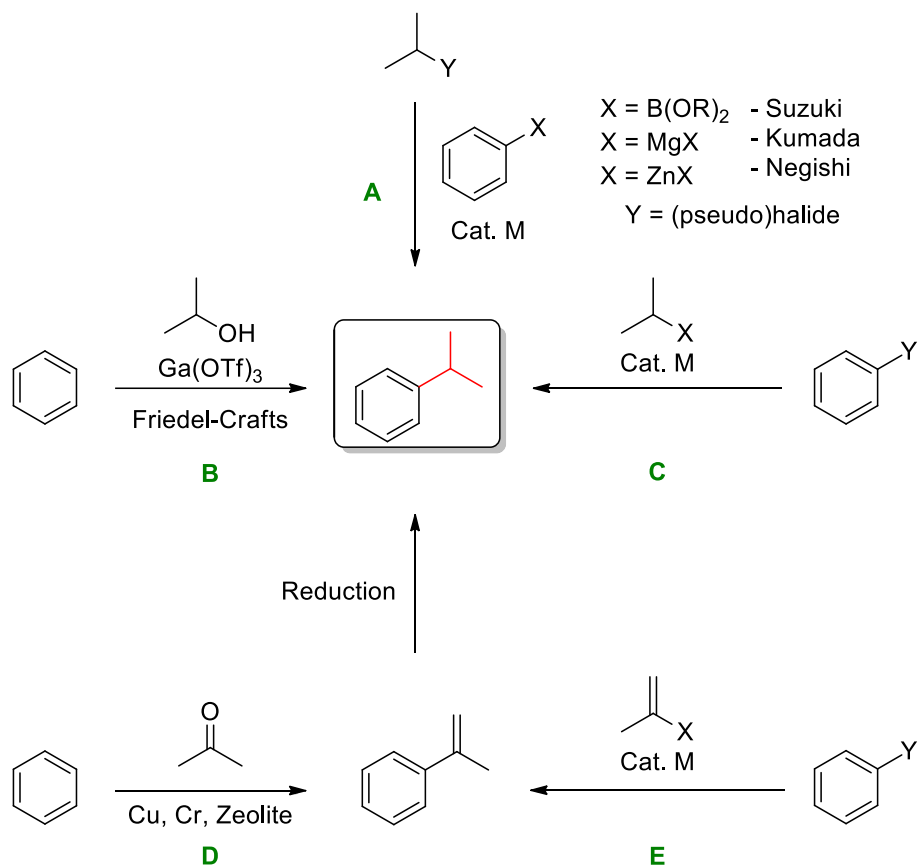


Scheme 36. a) Some APIs and natural products containing the *iso*-propyl group. b) Rosuvastatin synthesis.

As discussed in **Chapter 2**, over the last 40 years the use of TM-catalysed cross-coupling reactions as simple, mild and reliable reaction chemistries has burgeoned. The rapid expansion of this area of research has provided the synthetic chemist with a palette of new techniques to create some bonds, especially sp^2 - sp^2 linkages, with superb levels of control and selectivity.

Despite the ubiquity and flexibility of palladium-catalysed C-C bond forming reactions, certain substrates remain challenging. The installation of secondary alkyl groups *via* cross-coupling methodology often leads to undesired by-products resulting from β -hydride elimination pathways.⁷⁰ Significant efforts have been made in recent years to address these problems through the application of palladium catalysis with sterically hindered phosphine and *N*-heterocyclic carbene (NHC) ligands;^{71, 72} most of the progress in this area has been made with Suzuki-Miyaura transformations.^{73, 74} Secondary alkyl organoboron species are generally less available than their aryl counterparts. They have been shown to be competent cross-coupling partners in certain applications, but they are generally prepared in a wasteful and step-inefficient manner, often *via* transmetallation from a Grignard or organolithium reagent.⁷⁵ A Kumada (RMgX)¹⁶ type cross-coupling reaction of secondary organometallics, directly using the more reactive reagent, would therefore offer significant advantages in relation to efficiency and atom economy (**Scheme 37**). Furthermore, magnesium is of higher abundance in the Earth's crust than boron, meaning its use may be considered less environmentally deleterious. Recent studies have also shown organoboron species to be carcinogenic, thus their use in pharmaceutical manufacture requires careful analysis to limit residual organoboron intermediates in APIs. Organomagnesium species are generally highly reactive, and can be removed from waste streams through the careful addition of aqueous medium. Magnesium salts are prevalent in nature and broad applications, thus their presence in waste streams may be less concerning than organoboron species.

Some general methods for the introduction of an *iso*-propyl group are shown in **Scheme 37**.



Scheme 37. Some methods for the introduction of an *iso*-propyl group. A: Aryl organometallic in a cross-coupling process. B: Friedel-Crafts alkylation. C: Alkyl organometallic in a cross-coupling process. D: Catalytic petrochemical preparation. E: Alkenyl organometallic in a cross-coupling process followed by hydrogenation.

Route A represents the reaction between an alkyl (pseudo)halide and aryl organometallic species. This methodology has been demonstrated on numerous occasions, generally under palladium- or nickel-catalysis.^{76, 77} There have also been several reports of iron-catalysed alternatives, which are discussed in **Chapter 2**, **Chapter 3** and **Chapter 5**. Alkyl halides are generally a cause for concern when proposed as part of a synthetic route for a pharmaceutical compound. Their ability to readily form reactive species such as cations or radicals means that they can easily react with biological molecules in the body. This is especially worrying, as they could plausibly alkylate DNA, and are therefore classed as mutagenic.⁷⁸ This is more common for the heavier bromides and iodides, due to the lower carbon-halogen bond strength. Alkyl chlorides are therefore suitable alternatives, but their low boiling point can be challenging, especially in large scale synthesis.

Route B represents a typical Friedel-Crafts process, which may be carried out on an industrial scale in the petrochemical industry.⁷⁹ Friedel-Crafts alkylations are typically poorly selective, with

challenges of both functional group tolerance and regioselectivity. They are generally avoided in pharmaceutical synthesis for these reasons.

Route C represents the reaction between an alkyl organometallic species and aryl (pseudo)halide, and shows a switch in polarity of the reagents from **Route A**. There are again numerous examples of this type of process, especially palladium-catalysed Suzuki reactions and palladium- or nickel-catalysed Kumada cross-couplings.^{71, 72} This also represents one of the most reported reactions under iron catalysis, with numerous researchers reporting the cross-coupling of primary alkyl Grignard reagents with aryl (pseudo)halides.^{25, 26} Alkyl organometallics, such as organolithium and Grignard reagents, are generally highly reactive. This reduces the likelihood of alkylating agents (from alkyl halides) being present in reaction mixtures during pharmaceutical manufacture; aryl (pseudo)halides generally don't pose such a significant hazard as alkyl species.

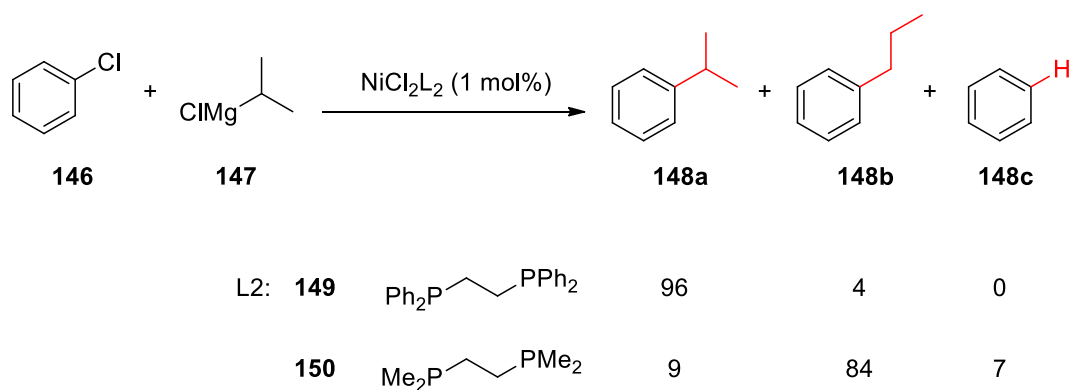
Route D represents another Friedel-Crafts type process, which may be carried out on an industrial scale in the petrochemical industry. This produces a vinyl species which can be reduced to the alkyl species using hydrogenation.⁸⁰ Much like **Route B**, challenges may be expected with both chemo- and regioselectivity of such a process. **Route E** represents another cross-coupling process, between an aryl (pseudo)halide and vinyl organometallic. The reverse, as with **Route A/ Route C** may also be a plausible synthetic route. Again, this produces a vinyl species which can be reduced to the alkyl species using hydrogenation.⁸¹⁻⁸⁴

3.1.1. Relevant Literature: Palladium and Nickel Catalysis

The cross-coupling of alkyl species bearing β -hydrogens with aryl halides remains a challenge in TM catalysis. In recent years, numerous systems have been developed to carry out these more testing processes. The modified catalysts are generally based upon palladium or nickel, with bulky *N*-heterocyclic carbene (NHC) or phosphine ligands. β -Hydride elimination in these reactions can have three significant effects:

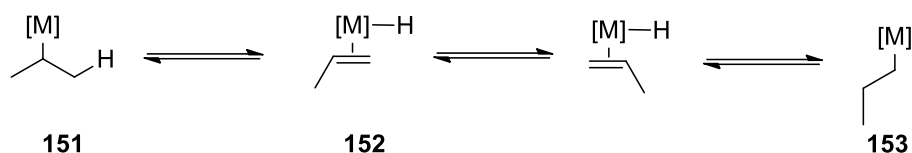
1. Loss of starting material resulting in lower yield, or hydrodehalogenation
2. Isomerisation of catalytic intermediates resulting in the formation of unwanted side products *via* β -hydride elimination
3. Reduction of the catalyst to catalytically inactive species

An early report on the isomerisation of alkyl groups in TM-catalysed cross-coupling reactions was made by Kumada in 1972.⁸⁵ This article highlighted a nickel-phosphine catalysed procedure which resulted in varying amounts of isomerisation depending upon the steric and electronic nature of the ligand (**Scheme 38**). The bulkier, less electron releasing, 1,2-bis(diphenylphosphino)ethane (dppe) **149** gave the highest conversion to the desired *iso*-propyl cross-coupled product. Significantly more isomerised side product was observed with the less bulky, more electron releasing 1,2-bis(dimethylphosphino)ethane (dmpe) **150**. This could be related to accelerated RE, promoted by the bulky **149**.



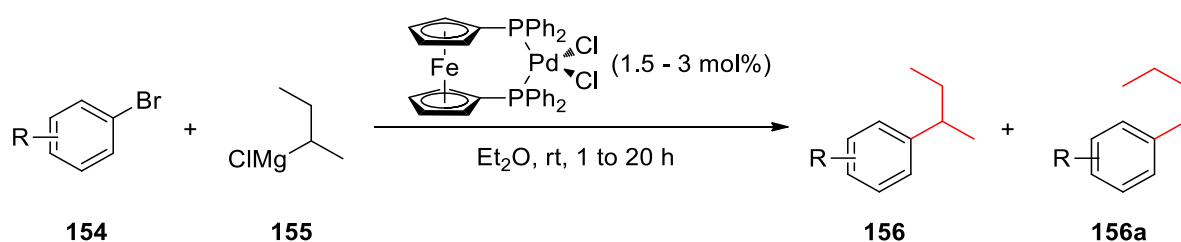
Scheme 38. Kumada's observations.

The mechanism Kumada proposed is now widely accepted within TM-catalysis; it involves β -hydride elimination followed by migratory insertion (**Scheme 39**). Kumada suggested that strong electron donation from the ligand could facilitate β -hydride elimination. The second step may proceed to give the branched or linear isomer, with the linear isomer being more favourable upon reinsertion due to steric effects. Such processes have been described previously by Reger, with both iron⁷⁰ and palladium TM-alkyl species.^{86, 87}



Scheme 39. β -Hydride elimination mediated isomerisation.

An efficient catalytic system for the cross-coupling of secondary alkyl nucleophiles with sp^2 bromides was demonstrated in 1984 (**Scheme 40**).⁸⁸ Hayashi was able to perform the cross-coupling of *sec*-butyl nucleophiles with a range of aryl/alkenyl electrophiles, with little or no isomerisation, using a $\text{PdCl}_2(\text{dppf})$ pre-catalyst. Excellent yields were reported for both Grignard and zinc reagents, although the zinc reagents required much longer reaction times. The authors offered significant insight for such an early article. They suggested that the rate of RE must be faster than that of β -hydride elimination to reduce isomerisation and hydrodehalogenation. The fast RE in this case was attributed to a large P-Pd-P angle, and a small Cl-Pd-Cl angle at the palladium centre. This should lead to a small Ar-Pd-R bond angle upon OA and transmetalation, with the close proximity of Ar and R groups leading to rapid RE.



Scheme 40. Hayashi's reaction conditions.

Hayashi observed excellent branched to linear ratio in a number of substrates (**Table 2**). The authors were able to couple *sec*-butylmagnesium chloride with electron neutral (**157**), electron deficient (**160**) and electron rich (**158**) substrates. Moreover, no isomerisation was observed in the reaction with sterically hindered 2-methylbromobenzene **159**.

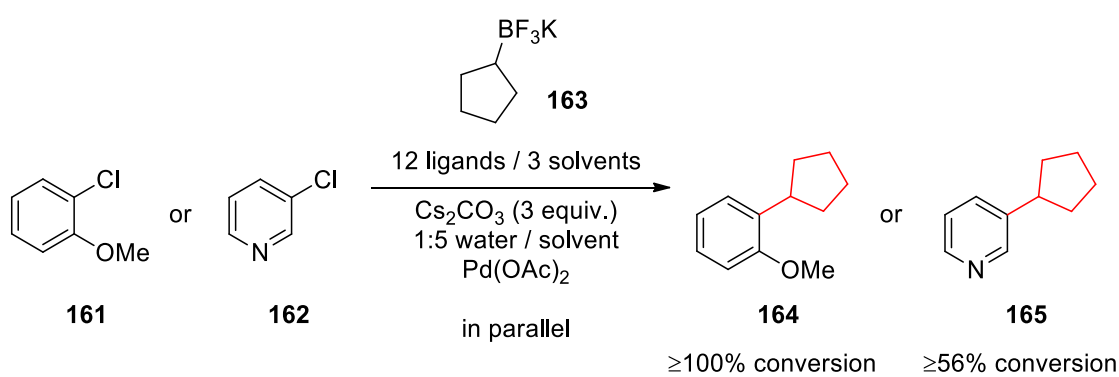
Table 2. A small selection of Hayashi's reported substrate scope.

Entry	Product	R	<i>s</i> -Bu (a) / %	<i>n</i> -Bu (b) / %
1	157a / 157b	H	95	0
2	158a / 158b	4-OMe	75	1
3	159a / 159b	2-CH ₃	58	0
4	160a / 160b	3-CF ₃	72	0

More recently, TM-catalysis has moved toward the use of more stable/less reactive organic nucleophiles such as organoboron reagents. The Suzuki cross-coupling reaction represents one of the most widely used carbon-carbon bond forming reactions in both industry and academia.¹

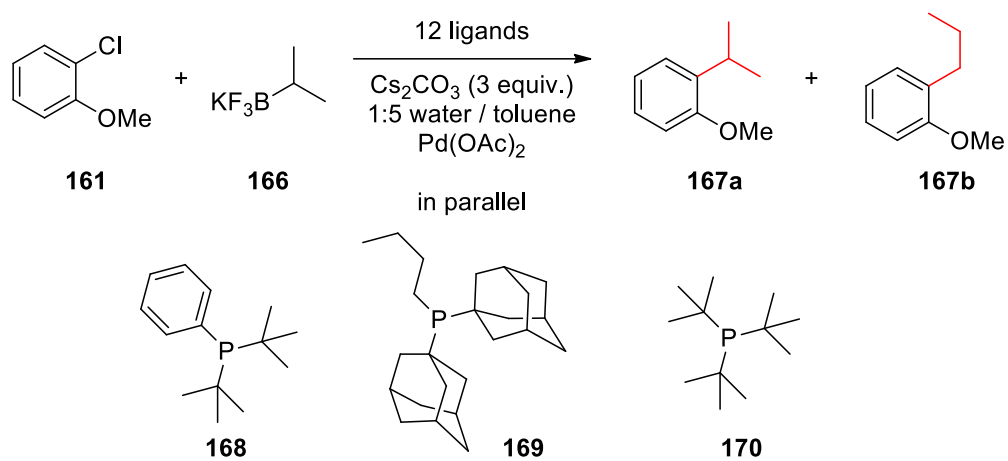
⁷² This is due to the relative stability and availability of organoboron species. Problems associated with β -hydride elimination are still prominent in the Suzuki reaction, but it has received much greater attention than the Negishi and Kumada counterparts as a whole.

Molander and Dreher were amongst the first to publish couplings of alkyl species in Suzuki reactions.⁸⁹ Their article presented the cross-coupling of secondary alkyl trifluoroborates with electron rich and electron poor aryl chlorides. The authors chose potassium alkyl trifluoroborates in order to suppress unwanted competitive protodeboronation.⁸⁹ Then, using parallel experimentation, they investigated the reaction between potassium cyclopentyl nucleophiles and two (hetero)aryl chlorides (**Scheme 41**). This screen used 12 ligands and three solvents to determine the ideal reaction conditions. It was found that ligand **169** (**Scheme 42**) with Cs_2CO_3 in toluene gave the greatest reactivity.



Scheme 41. Parallel experimentation protocol for cyclopentyl cross-coupling.

The cyclopentyl nucleophile represents a simple secondary alkyl cross-coupling partner; β -hydride elimination, isomerisation and reinsertion would result in the same product. This is true for all racemic cycloalkyl nucleophiles. Unfortunately, the conditions discovered by Molander and Dreher were unsuitable for the coupling of *iso*-propyl trifluoroborate without isomerisation. After repeating the earlier ligand screen di-*tert*-butyl(phenyl)phosphine **168** and tri-*tert*-butylphosphine **170** were highlighted as the best ligands to suppress the undesired β -hydride elimination pathway. This example serves to highlight the difficulty in balancing steric and electronic effects upon the palladium centre. The *n*-butyldiadamantylphosphine ligand **169** gave the greatest reactivity due to the electron releasing nature of the tertiary alkyl ligands. However, the steric bulk of this ligand also gave poor selectivity with more challenging substrates such as 2-chloroanisole and methyl 2-chlorobenzoate.



Scheme 42. Further parallel experimentation for *iso*-propyl cross-coupling.

Molander and Dreher further tested the three monophosphine ligands **168**, **169**, and **170** with a small selection of aryl chlorides (**Figure 8**). The authors found highly variable results across the series. Di-*tert*-butyl(phenyl)phosphine **168** and tri-*tert*-butylphosphine **170** continued to show the highest *iso*-propyl to *n*-propyl ratio, although this was significantly diminished when methyl-2-chlorobenzoate (**174**) was coupled.

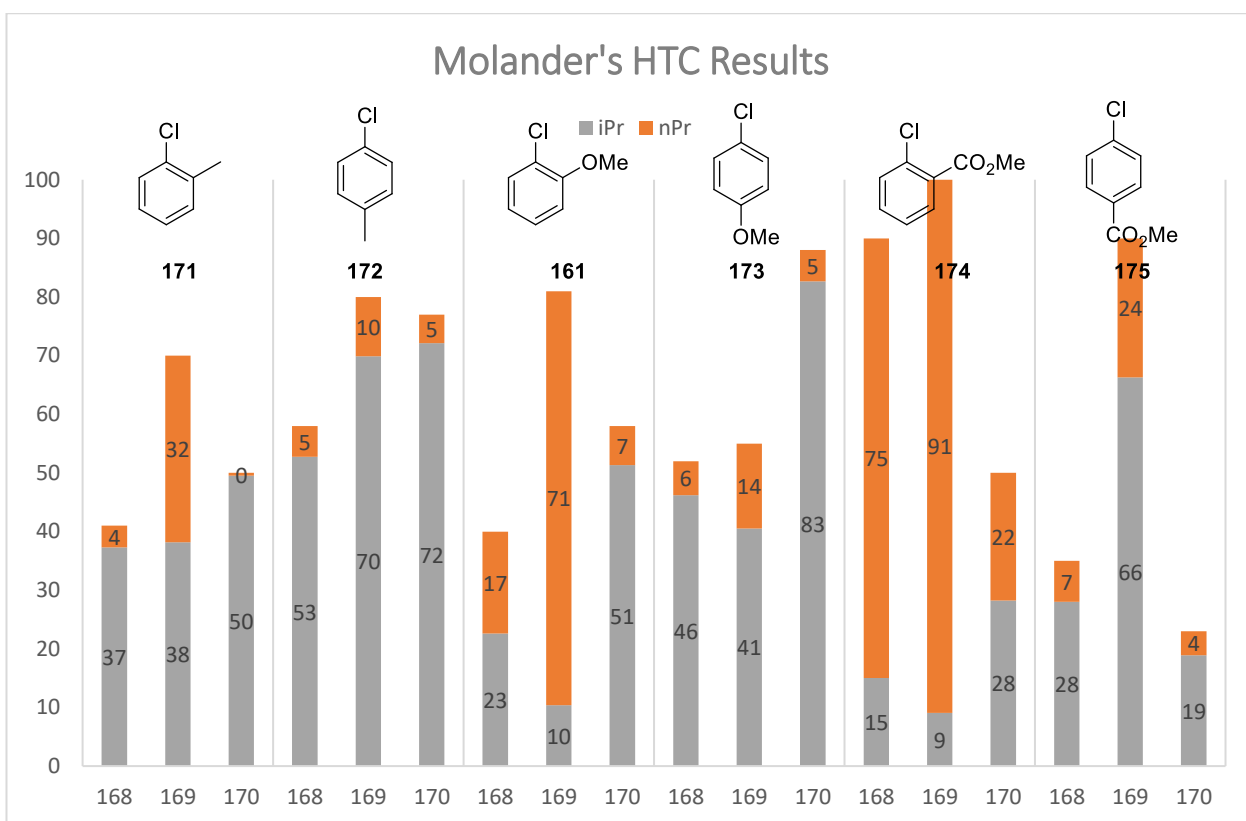


Figure 8. Molander and Dreher's results from the *iso*-propyl cross-coupling ligand screen. Grey bar = *iso*-propyl (**a**), orange bar = *n*-propyl (**b**).

At a similar time to Molander's study, van den Hoogenband reported the cross-coupling of alkyl trifluoroborates and aryl bromides using a number of bulky biaryl monophosphine ligands.⁹⁰ Such Pd(P) species were previously shown to effectively promote the cross-coupling of primary alkylboronic acids.⁹¹ Poor yields were observed when employing the original reaction conditions (3 mol% Pd(OAc)₂, 6 mol% SPhos, 3 equiv. K₂CO₃, 1 equiv. ArBr and 1.5 equiv. cyclopentyl trifluoroborate in MeOH at reflux), so an alternative solvent and ligand were sought. Interestingly, the application of RuPhos **178** in a toluene/water solvent system gave increased product formation (**Figure 9**). The authors optimised these conditions for the cross-coupling of cyclopentyl nucleophiles leading to synthetically useful isolated yields in a number of cases.

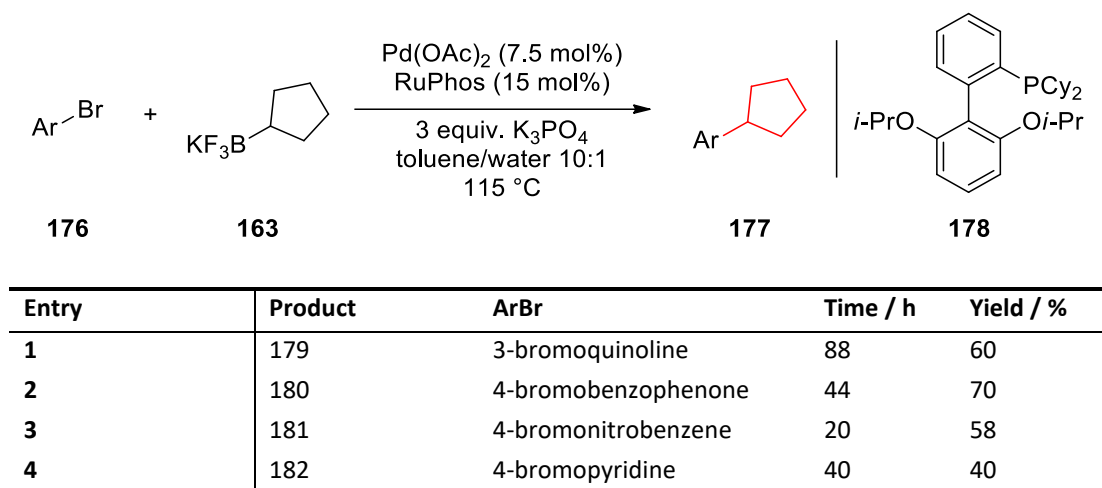


Figure 9. van den Hoogenband's cyclopentyl cross-coupling.

Again, when applying the optimised reaction conditions to the coupling of acyclic *sec*-butyltrifluoroborate reduced yields were observed, further demonstrating the difficulty with such substrates (**Figure 10**). The authors suggested that this was due to a more competitive β -hydride elimination pathway, probably arising from the increased flexibility of the *sec*-butyl ligand upon Pd. Although the yields were relatively low, the reaction was found to be selective for the formation of the *sec*-butyl isomer. This may be due to a poor π -interaction between Pd and 2-butene after β -hydride elimination, leading to preferential alkene dissociation followed by RE of the hydrodehalogenated material. For example, the $[Ag(\text{olefin})]^+$ complex of *iso*-butene is found to be less stable than that of propene.⁹²

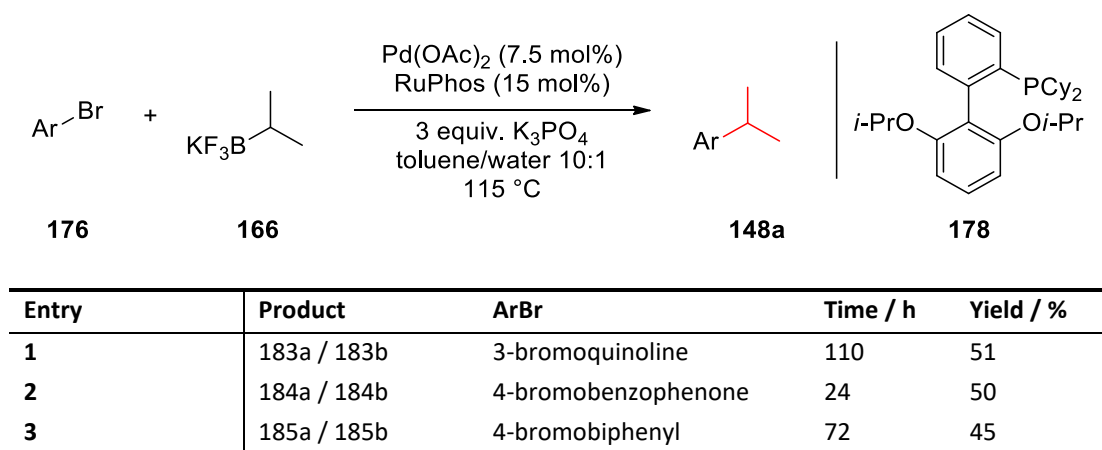
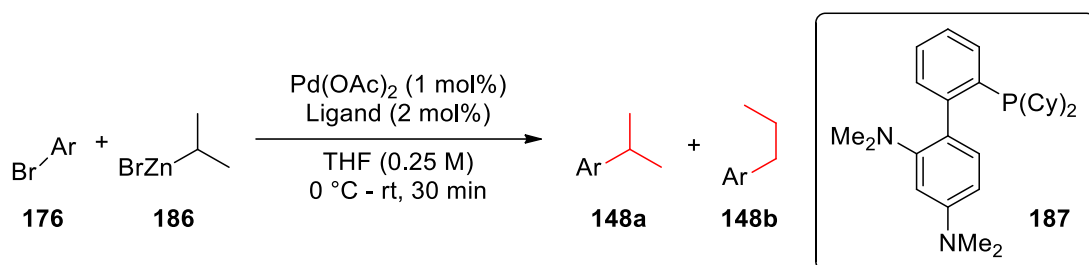


Figure 10. van den Hoogenband's *iso*-propyl cross-coupling.

Buchwald further demonstrated the use of bulky biaryl monophosphine ligands in the Negishi cross-coupling reaction in 2009.⁹³ The branched:linear ratio of reactions between *iso*-propylzinc bromide and aryl bromides was reported for seven ligand systems. This work established the superiority of a new ligand, CPhos (**187**, **Figure 11**), in this reaction. Buchwald was then able to

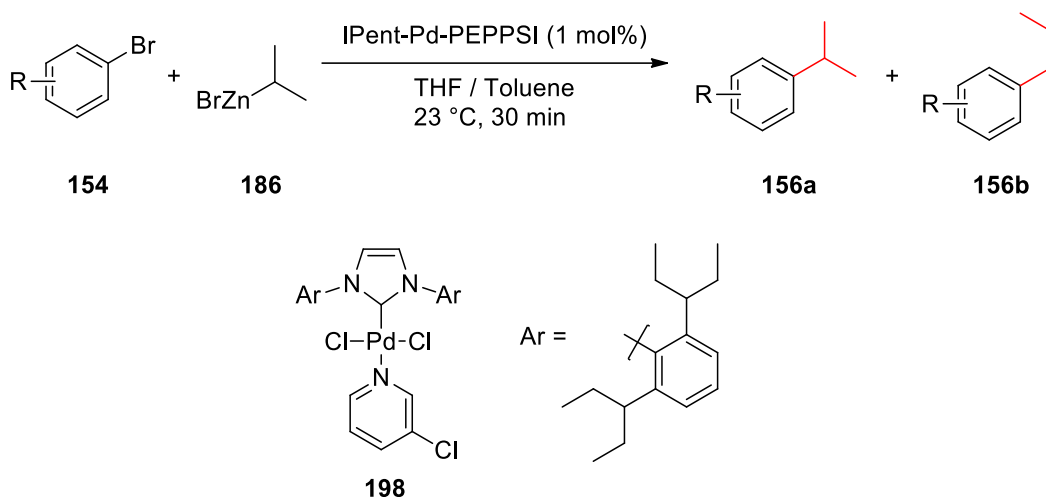
couple a range of aryl and heteroaryl halides with a number of alkylzinc species successfully. All preparations gave high yields, and good ratios of the desired branched product. Interestingly, this preparation allowed the cross-coupling of typically more challenging substrates, including cyclopentyl and *sec*-butyl zinc nucleophiles and electrophiles containing a benzyl alcohol substituent. The authors reported further studies related to this in 2014, where other acyclic secondary alkyl nucleophiles were coupled with high yield and selectivity.⁹⁴



Entry	Product	(Het)ArBr	Yield / %	<i>i</i> -Pr: <i>n</i> -Pr
1	188a / 188b	4-OMeC ₆ H ₄	92	37:1
2	185a / 185b	4-PhC ₆ H ₄	95	39:1
3	189a / 189b	4-CO ₂ MeC ₆ H ₄	94	46:1
4	190a / 190b	4-CNC ₆ H ₄	87	59:1
5	191a / 191b	4-CHOC ₆ H ₄	89	43:1
6	192a / 192b	4-NO ₂ C ₆ H ₄	50	28:1
7	167a / 167b	2-OMeC ₆ H ₄	97	27:1
8	193a / 193b	2-PhC ₆ H ₄	97	22:1
9	194a / 194b	2-CO ₂ MeC ₆ H ₄	91	37:1
10	195a / 195b	2-CNC ₆ H ₄	89	20:1
11	196a / 196b	2-SMeC ₆ H ₄	95	30:1
12	197a / 197b	5-bromoindole	96	58:1

Figure 11. Buchwald's catalytic system and substrate scope, highest *iso*-propyl to *n*-propyl selectivity highlighted in **bold**.

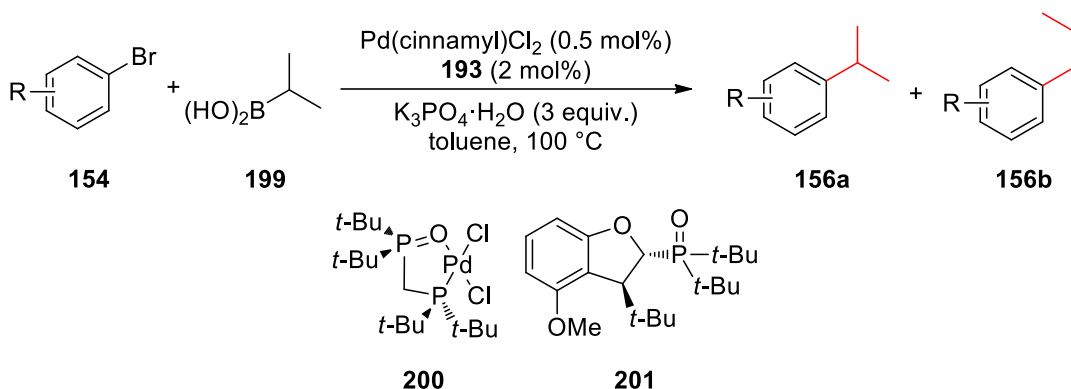
An interesting addition to the Negishi portfolio was made by Organ.⁹⁵ NMR and computational studies suggested that NHC ligands with increased steric bulk enhanced the electropositivity of the palladium centre (**Figure 12**).⁹⁶⁻⁹⁹ This should promote RE, reducing the observed β -hydride elimination, and leading to successful coupling. The authors proposed that through space interactions between the *N*-aryl *iso*-propyl groups of the NHC ligand help to stabilise any buildup of positive charge following OA. The selected Pd-PEPPSI-IPent catalyst **198** was efficient when cross-coupling secondary alkyl zinc species, with moderate to excellent yields across a range of aryl chlorides. Unfortunately, isomerisation was still observed with *sec*-butyl and *iso*-propyl nucleophiles.



Entry	Product	ArBr	Yield	<i>i</i> -Pr: <i>n</i> -Pr
1	189a / 189b	4-CO ₂ Me	94	56:1
2	192a / 192b	4-CHO	92	59:1
3	196a / 196b	2-CN	76	28:1
4	167a / 167b	2-OCH ₃	54	23:1

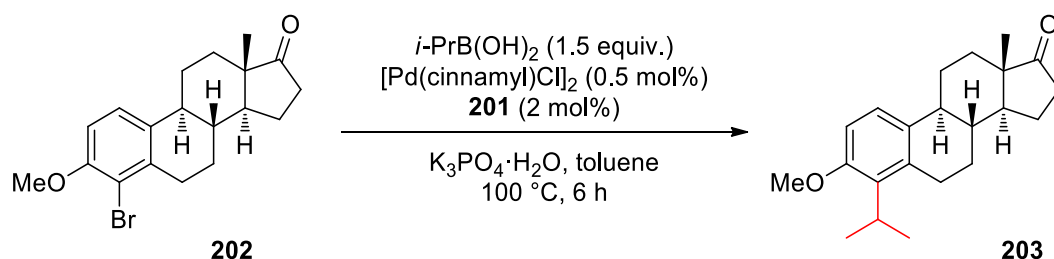
Figure 12. Organ's Pd(PEPPSI)IPent catalytic system and substrate scope, highest *iso*-propyl to *n*-propyl selectivity highlighted in **bold**.

More recently Tang reported an efficient Suzuki cross-coupling reaction between sterically hindered aryl bromides and secondary alkyl boronic acids.¹⁰⁰ The authors showed significant mechanistic insight, and were able to use bulky P,P=O ligand (**200** and **201**, **Scheme 43**) to gain very high branched:linear ratios. The new ligand class was demonstrated to have a hemilabile coordination with the Pd centre, offering the stability of a 5-membered palladacycle combined with the flexibility of a monophosphine ligand. The hemilabile nature of the P,P=O ligand allows it to block any vacant coordination sites, which could lead to β -hydride elimination. The *tert*-butyl substituents on each phosphine were also suggested to increase steric bulk at both the front and rear of the pre-catalyst, reducing the space available for β -hydride elimination.



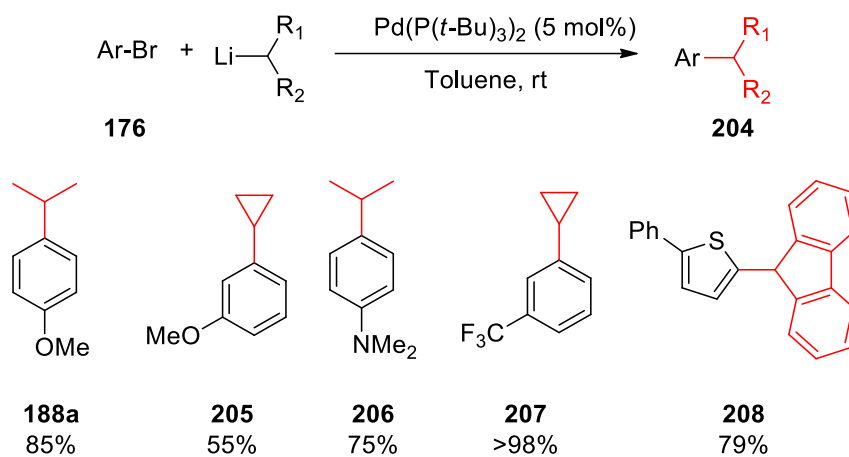
Scheme 43. Tang's reaction conditions. Palladacycle (**200**, lower left), optimal ligand (**201**, lower right).

The synthetic utility of Pd(P,P=O) catalytic system was exemplified in the synthesis of 4-*iso*-propyl substituted estrone **203** in **Scheme 44**. Here, the starting bromide **202** had two *ortho* substituents, and the product was isolated in 86% yield after 6 hours at 100 °C. The branched:linear ratio was reported to be 9.6:1.



Scheme 44. Tang's synthesis of estrone.

Some authors have demonstrated the direct cross-coupling of more reactive organolithium reagents. Feringa showed that it was possible to couple a number of secondary alkyl lithium species with a wide range of aryl bromides using a simple palladium pre-catalyst (**Scheme 45**).¹⁰¹ Although this procedure demonstrated a broad substrate scope, its synthetic utility may be limited by the high reactivity of the organolithium reagents with common functional groups. Organoboron or organozinc species are preferable in this respect, as they have excellent functional group tolerance.



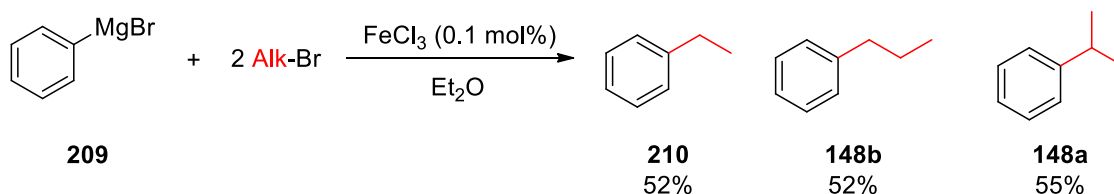
Scheme 45. Feringa's organolithium cross-coupling.

In summary, a number of groups have investigated the reaction between secondary alkyl nucleophiles and aryl halides under TM catalysis. These studies have focussed upon the use of bulky mono- and bisphosphine ligands, NHCs, and the recently developed P,P=O ligands. The overall aim in all cases was to promote RE over unwanted β -hydride elimination to reduce/eliminate unwanted byproducts. The most successful ligands were shown to be of the P,P=O type,¹⁰⁰ closely followed the Pd-PEPPSI-IPent catalyst of Organ.⁹⁵ In the P,P=O case the high selectivity was suggested to be due to a hemilabile ligand, which preferentially formed a 5-membered palladacycle, reducing the likelihood of an open coordination site. The success of the Pd-PEPPSI-IPent system was proposed to be due to the relatively high electrophilicity of Pd, promoting rapid RE.

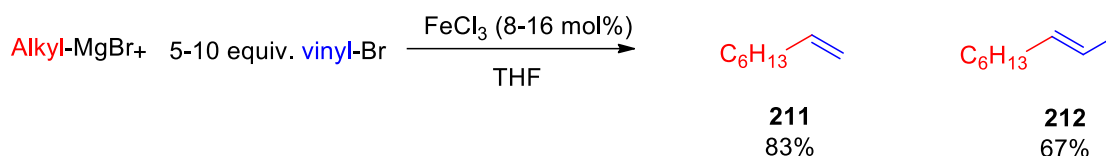
3.1.2. Relevant Literature: Iron Catalysis

The use of precious metal catalysts is often challenged in a pharmaceutical process research and development environment, due not only to cost of goods and questionable sustainability of supply, but also because of the toxicity arising from the presence of trace residues in APIs.¹⁰² In recent years, there has been a significant resurgence of interest in the application of earth abundant metals in cross-coupling reactions;¹⁰³ iron has been pre-eminent due to its abundance, low toxicity, low cost and high versatility.^{26, 104} Pioneering research by Vavon and Mottez in 1944²⁷ was advanced by Kochi in his seminal publication in 1971 (**Scheme 46**).¹⁰⁵

Vavon and Mottez



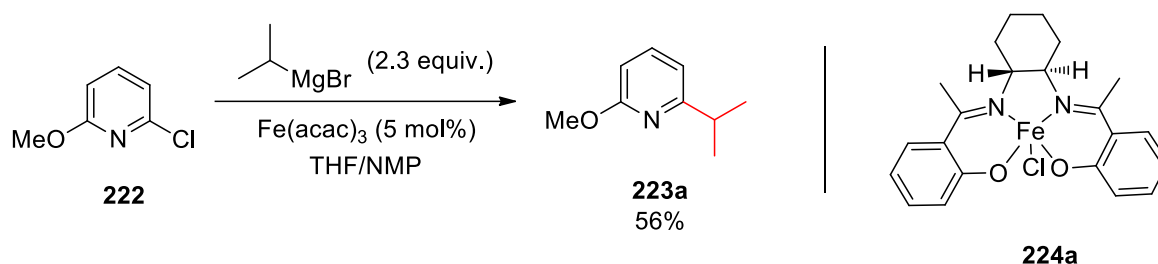
Kochi



Scheme 46. Early reports of iron-catalysed cross-coupling reactions.

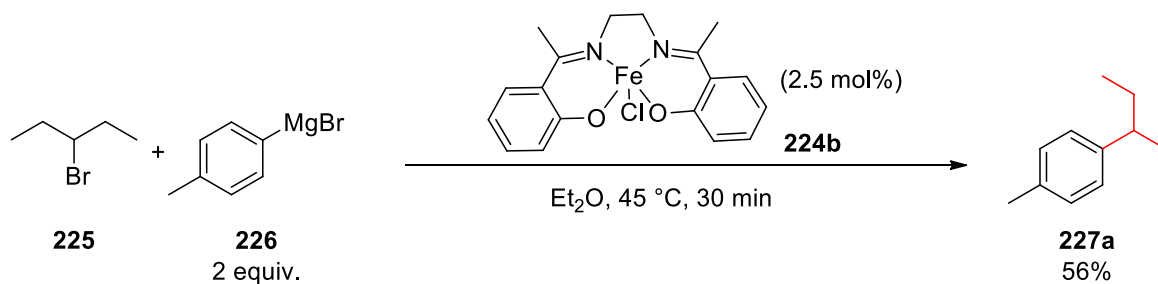
Most early reports focussed on the reaction of primary alkyl Grignard reagents with aryl or vinyl halides; there are very few reports of the iron-catalysed cross-coupling of secondary alkyl nucleophiles with aryl halides in the literature. One of the early reports by Kochi suggested that it was possible to couple *iso*-propylmagnesium bromide and *cis/trans* 1-bromopropene without isomerisation of the *iso*-propyl group.¹⁰⁶ Further examples of such reactions were reported by Cahiez in 1998.³⁴ Moderate yields were observed from the reactions of both *iso*-propyl and *tert*-butyl Grignard reagents (**Scheme 47**).

be used with secondary alkyl Grignard reagents, but this was not supported with experimental evidence.



Scheme 49. Fürstner's iron-catalysed cross-coupling of *iso*-propylmagnesium bromide.

Bedford investigated a number of $\text{Fe}(\text{salen})\text{Cl}$ complexes the same year, choosing to study the reaction between aryl Grignard reagents and alkyl bromides.¹⁰⁷ The reaction was successful in most cases, but numerous by-products were observed. Interestingly, the cross-coupling of 3-bromopentane with *p*-tolylmagnesium bromide proceeded without isomerisation (**Scheme 50**). The authors demonstrated the successful cross-coupling of electron rich Grignard reagents with a number of alkyl halides; cyclohexyl halides were shown to give the highest conversion to desired product (**Figure 13**).



Scheme 50. Bedford's *sec*-alkyl cross-coupling.

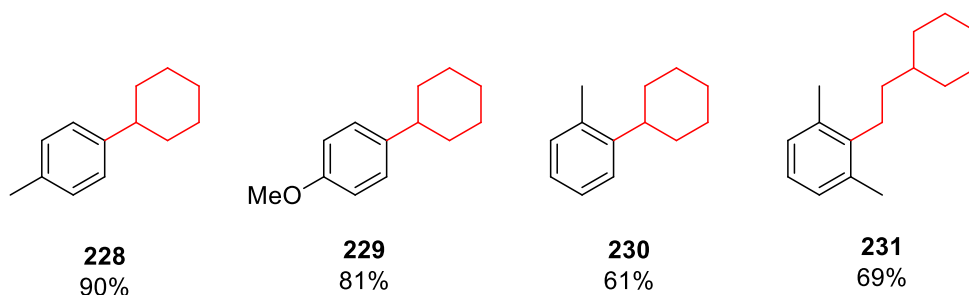
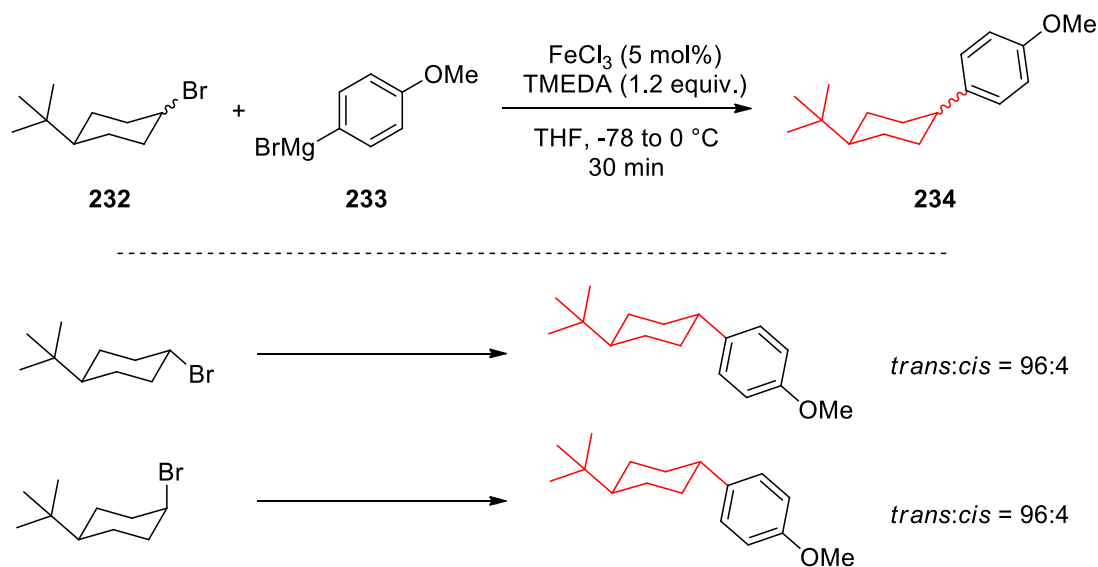


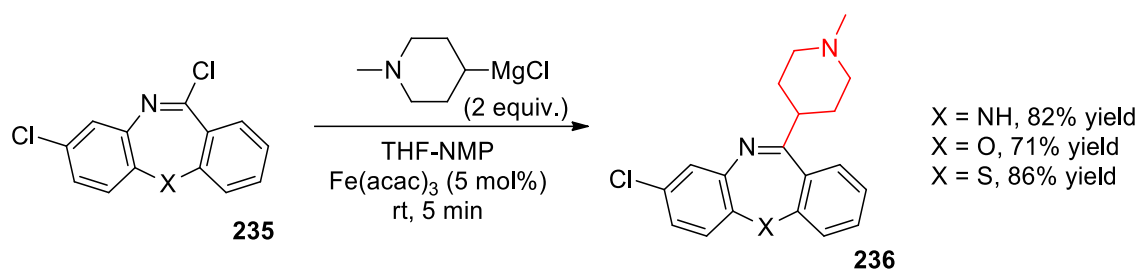
Figure 13. Examples of Bedford's primary/secondary alkylation.

Nakamura reported a similar process in 2004, utilising the simple diamine TMEDA as a ligand/additive in the reaction.⁴⁶ Cyclohexyl bromide was coupled with a number of aryl and heteroaryl Grignard reagents in excellent isolated yields. The authors reported an interesting finding: isomeric sterically locked *tert*-butylcyclohexyl bromides led to the same product ratio (**Scheme 51**). The authors proposed the intermediacy of an iron-bound radical to explain their findings.



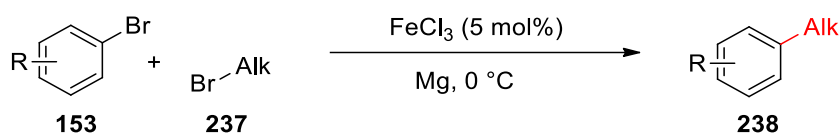
Scheme 51. Nakamura's stereochemical observations.

Olsson reported the cross-coupling of imidoyl chlorides such as **235** with alkyl Grignard reagents using an $\text{Fe}(\text{acac})_3$ pre-catalyst.⁵⁹ Several secondary nucleophiles were used, forming coupled products in good to excellent yields. This methodology was then utilised to prepare analogues of Clozapine (**Scheme 52**) in one step from relatively simple starting materials. The reaction was chemoselective, with the Grignard reagent reacting only at the imidoyl chloride while the aryl chloride remained untouched.



Scheme 52. Olsson's clozapine synthesis.

Another successful cross-coupling between aryl and secondary alkyl fragments was achieved by von Wangelin.¹⁰⁸ Instead of a pre-formed Grignard reagent this investigation used two halides with magnesium in a domino process (**153** and **237**, **Figure 14**). The reaction with cyclohexyl bromide was successful with a range of aryl halides, and one example of *sec*-butyl bromide was reported in 62% yield. Coupling of *sec*-butyl bromide was also suggested to proceed without isomerisation. Additionally, this preparation appeared to be applicable to a range of electron rich and electron deficient aryl chlorides and bromides. Most other methods are limited to electron deficient aryl chlorides as coupling partners.

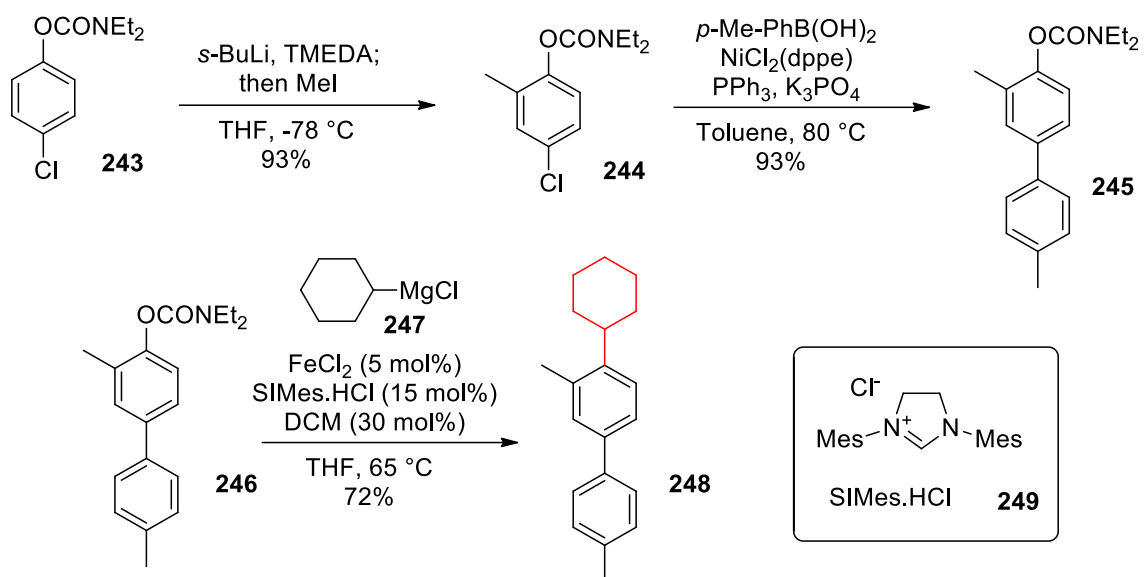


Entry	Product	R	Alk	Yield / %
1	239	4-MeC ₆ H ₄	<i>c</i> -hex	70
2	240	4- <i>t</i> -BuC ₆ H ₄	<i>i</i> -Bu	67
3	228	4-MeC ₆ H ₄	<i>s</i> -Bu	62
4	229	2-OMeC ₆ H ₄	<i>c</i> -hex	66
5	241	4-FC ₆ H ₄	<i>c</i> -hex	48
6	242	4-NMe ₂ C ₆ H ₄	<i>c</i> -hex	72

Figure 14. von Wangelin's reductive cross-coupling.

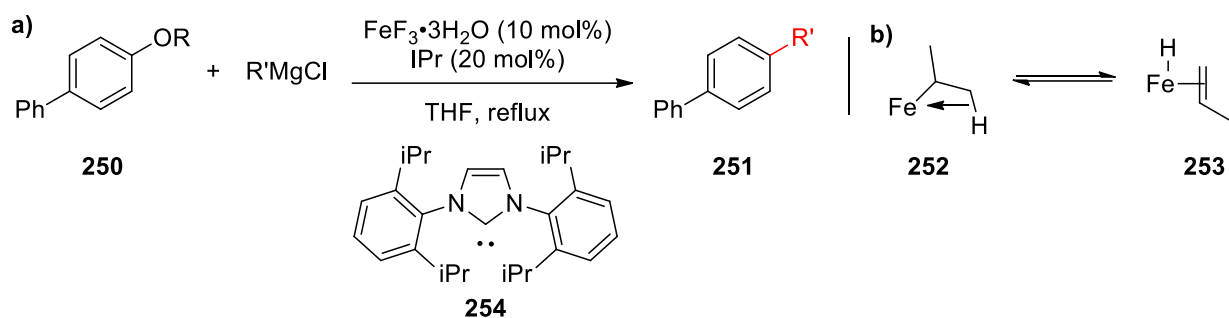
Species which usually react slowly under palladium or nickel catalysis can often be reactive in iron-catalysed reactions. For example, electron deficient aryl chlorides, sulfamates and carbamates can all be used. An interesting application of the iron-catalysed cross-coupling of the latter was described by Garg in 2012.¹⁰⁹ The ease of preparation of aryl carbamates from the phenols was highlighted as the major reason for studying them. The authors were able to cross-couple numerous aryl groups with hexylmagnesium chloride using an FeCl₂ pre-catalyst in combination with an NHC ligand; SIMes, **249**. Garg's approach worked well for bulky and secondary Grignard reagents with no reduction in yield. This was demonstrated in the synthesis of **248** (**Scheme 53**). The electronic nature of the carbamate group could also be used to direct

ortho-lithiation upon the aromatic group, and to promote a nickel-catalysed Suzuki cross-coupling reaction at the *para*-position.



Scheme 53. Garg's iron-catalysed cross-coupling.

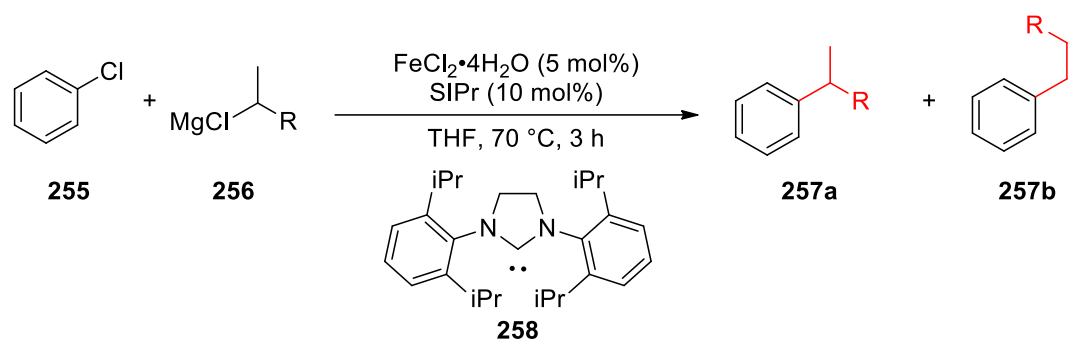
Cook also demonstrated the use of aryl sulfamates, along with tosylates, in an iron-catalysed cross-coupling reaction.¹¹⁰ A number of iron sources and associated ligands were investigated, and it was found that $\text{FeF}_3 \cdot 3\text{H}_2\text{O}$ and IPr (**25a**, **Figure 15a**) were the best combination. Variable yields were reported for the cross-coupling with *n*-butylmagnesium chloride. The biggest differences in yield were observed in the reactions with bulky electrophilic coupling partners. Expanding the substrate scope to include secondary alkyl Grignard reagents resulted in a small reduction in yield, although the sulfamates were less affected. A branched:linear selectivity of 6.5:1 was achieved in the cross-coupling of *iso*-propylmagnesium chloride. The authors suggested that this high selectivity, compared to that obtained with other iron salts, was due to the strong coordination of the fluoride ligand.¹¹¹ This was proposed to prevent open coordination at the metal centre, suppressing β -agostic interactions, which can lead to β -hydride elimination (**Figure 15b**).



Entry	Product	R	R'MgCl	Yield / %	<i>i</i> -Pr: <i>n</i> -Pr
1	255	SO ₂ NMe ₂	<i>n</i> -BuMgCl	90	
2	256	SO ₂ NMe ₂	<i>c</i> -HexMgCl	77	
3	185a / 185b	SO ₂ NMe ₂	<i>i</i> -PrMgCl	65	6.5:1
4	255	Ts	<i>n</i> -BuMgCl	74	
5	256	Ts	<i>c</i> -HexMgCl	39	
6	185a /185b	Ts	<i>i</i> -PrMgCl	50	1:10

Figure 15. Cook's iron-catalysed cross-coupling of aryl pseudohalides.

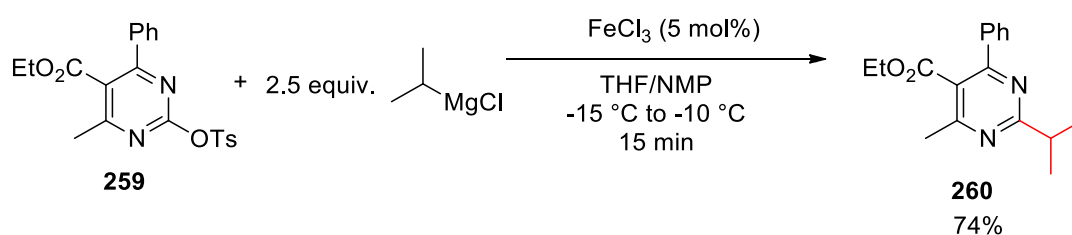
Perry used FeCl₂•4H₂O in combination with SIPr (**258**) to effect the cross coupling of Grignard reagents with non-activated aryl chlorides.⁵⁵ The authors optimised the reaction conditions, and found that adding four equivalents of Grignard reagent in two aliquots gave the highest conversion. Introduction of the more challenging *iso*-propyl and cyclohexyl nucleophiles led to a reduced overall yield. Higher branched:linear ratios were observed when 6 equivalents of Grignard reagent were added, but this was at the expense of yield. It was proposed that the reaction may proceed via an ionic (*versus* radical) mechanism, owing to this high level of isomerisation – secondary radicals would be preferred to primary radicals due to stabilisation *via* hyperconjugation.^{31, 53, 104} The use of 4 to 6 equivalents of organometallic reagent is highly wasteful, and significantly reduces the atom economy of the process. Aqueous effluent containing high levels of magnesium halide may also pose challenges if used in large scale manufacture due to the requirement for specialist disposal.



Entry	Product	Grignard Eq.	R	Yield / %	<i>i</i> -Pr: <i>n</i> -Pr
1	148a / 148b	4	CH ₃	69	1.2:1
2	148a / 148b	6	CH ₃	31	3.1:1
3	157a / 157b	4	C ₂ H ₅	67	2.4:1
4	157a / 157b	6	C ₂ H ₅	48	10.4:1

Figure 16. Perry's acyclic *sec*-alkylation.

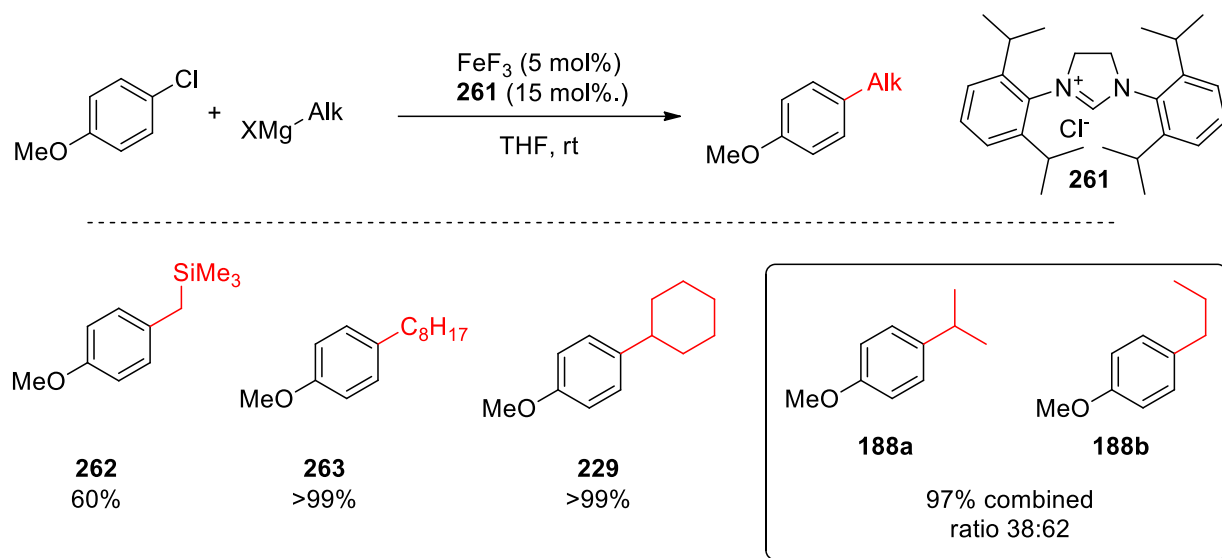
Wang and Quan recently reported the cross-coupling of heteroaromatic tosylates with alkyl and aryl Grignard reagents under iron catalysis.¹¹² The authors showed that Fe^{III} salts such as Fe(acac)₃ and FeCl₃ were competent pre-catalysts for the reaction between primary or secondary alkyl Grignard reagents and pyrimidin-2-yl tosylates (e.g. **259**, **Scheme 54**) when used in combination with a THF/NMP solvent system. They also demonstrated that, by switching from NMP to TMEDA, it was possible to react the same electrophiles with aryl Grignard reagents. Interestingly, *iso*-propylmagnesium chloride was found to react without isomerisation giving **260** in 74% isolated yield. Other secondary alkyl Grignard reagents were also tolerated, including the challenging cyclopropylmagnesium chloride. The use of NMP in iron catalysed processes is notable; many cross-coupling procedures utilise it as a cosolvent although no researchers have yet determined its effect upon the reaction mechanism.



Scheme 54. Furstner's *iso*-propyl cross-coupling.

Nakamura reported a further investigation into the iron-catalysed Kumada cross-coupling in 2015.¹¹³ In this investigation the authors returned to a FeF₃/NHC catalytic system they had previously reported for the reaction between *sp*² Grignard reagents and *sp*² electrophiles.¹¹¹ In earlier examples of cross-coupling catalysed by iron, high reactivity and/or selectivity was

obtained when using activated, electron deficient (hetero)aryl (pseudo)halides (*vide supra*). Nakamura found that the FeF₃/NHC catalysed protocol was able to couple deactivated, electron rich, aryl chlorides with alkyl Grignard reagents (**Scheme 55**). Primary and secondary nucleophiles were coupled in good to excellent isolated yields, but significant isomerisation was observed when *iso*-propylmagnesium chloride was used.



Scheme 55. Nakamura's Fe/NHC catalysed alkylation.

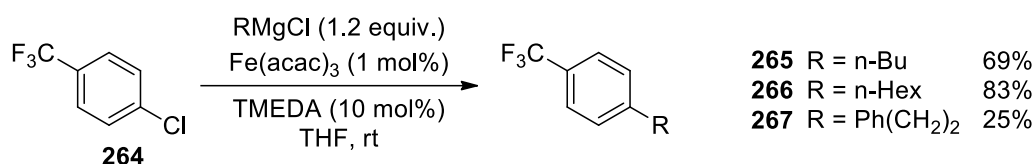
In summary, a number of methods have been used to cross-couple secondary alkyl nucleophiles with aryl halides. Initially, simple metal/ligand systems were used, such as nickel or palladium with phosphine ligands, or Fe(acac)₃ with no added ligands. As the investigators strove to achieve generality in yield, the complexity of the catalytic systems increased. The advent of NHC ligands greatly influenced this development; most recent publications on nickel, palladium or iron catalysis demonstrate the synthetic utility of those ligands. Unfortunately, there are still significant barriers to the cross coupling of secondary nucleophiles due to β -hydride elimination processes. This can be overcome by promoting fast RE.¹⁰⁰ In order to address this problem it may be possible to optimise previous reaction conditions, or to develop entirely new reaction conditions. Both may lead to a greater understanding of the fundamental processes.

In most cases, the iron-catalysed cross-coupling of secondary alkyl Grignard reagents used less reactive chloride coupling partners, instead of the more expensive and less readily available bromides or iodides. Though aryl nucleophile/alkyl halide coupling is well-known,⁷⁷ the use of alkyl organometallics also circumvents the handling of volatile alkyl chlorides which are potentially toxic alkylating agents. Through the strategic use of DoE, we hoped to develop an

effective, more general and straightforward preparation of *iso*-propyl arenes and heteroarenes from the corresponding chlorides *via* an iron-catalysed reaction.

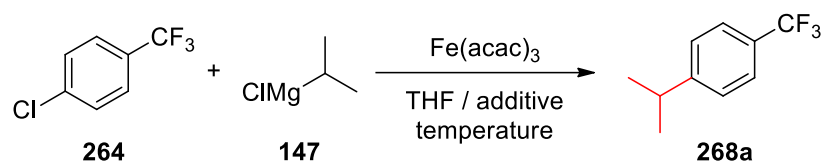
3.2. Results and Discussion

The literature examples introduced in the previous section serve to demonstrate the synthetic utility of iron-catalysed processes. Unfortunately, the use of secondary alkyl cross-coupling partners continues to represent a significant hurdle. Many researchers have reported efficient reactions of cycloalkanes, but acyclic, non-linear *sp*³ substrates remain under-represented. In 2013 Fox *et al.* demonstrated an operationally simple reaction between primary alkyl Grignard reagents, such as *n*-butylmagnesium chloride, and electron-deficient aryl chlorides.¹¹⁴ However, the reaction was less successful when phenethylmagnesium chloride was used (**267**); only 48% conversion was reported in the reaction with 1-chloro-4-(trifluoromethyl)benzene (**Scheme 56**). No examples of cross-coupling processes of secondary alkyl Grignard reagents were reported.



Scheme 56. Fox's alkylation of electron deficient aryl chlorides – isolated yields.

With operational simplicity and synthetic utility in mind the reaction between *iso*-propylmagnesium chloride and 1-chloro-4-(trifluoromethyl)benzene **264** was chosen to carry out a preliminary investigation (**Scheme 57**). DoE was utilised for this study, rather than carrying out a traditional OFAT optimisation. DoE can offer many advantages over the classical OFAT approach.^{115, 116} Due to its multivariate nature it is possible to optimise several components at once, leading to a significant reduction in the overall amount of experimentation. The statistical analysis used in an experimental design also means that it is possible to reveal interactions between components, a distinct benefit over OFAT studies (see **Section 2.7**).



Scheme 57. Model reaction chosen for the DoE investigation.

Stat-Ease's Design-Expert 7 (DX7) was used to prepare a preliminary screening DoE with 6 factors (**Table 3**). These factors were chosen based upon literature precedent, in order to answer a number of questions:

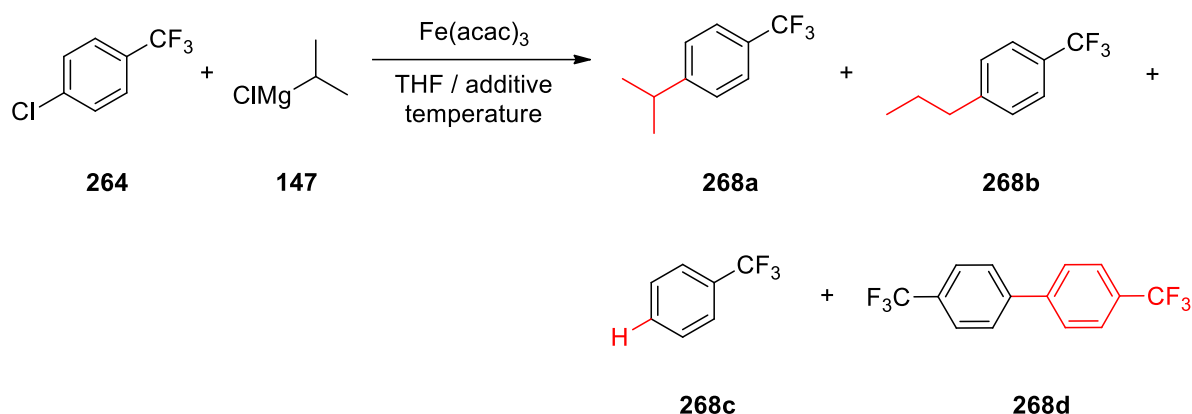
- What is the effect of reaction temperature?
 - Temperatures between -78 and +77 °C used previously.
- What is the effect of catalyst loading?
 - Catalyst loadings between 0.1 and 10 mol% used previously.
- What is the effect of concentration?
 - Dilute processes give more waste, can the volume of solvent be reduced?
- Does addition time influence reactivity?
- Can added primary alkyl Grignard reagent promote the reaction with *iso*-propylmagnesium chloride?
 - Is reduction of the active catalyst challenging with *iso*-propylmagnesium chloride, does this explain the lack of previous examples.
- Is it possible to use TMEDA or NMP as an additive?
 - TMEDA and NMP have been used widely, could conditions be optimised using DoE to discover optimal conditions for this reaction.

Table 3. Factors chosen for the preliminary DoE investigation. Volumes – 1 L kg⁻¹ limiting reagent.

	Factor	Ranges
A	Reaction temperature	-20 to 20 °C
B	Catalyst loading	0.1 to 5 mol%
C	Concentration	20 to 60 volumes
D	Addition time (Grignard reagent)	0 to 10 minutes
E	Added <i>n</i> -butylmagnesium chloride	Yes or no
F	Ligand	NMP or TMEDA

Scoping experiments, carried out at the higher and lower ranges in **Table 3**, showed that a number of side-products could be formed in the reaction between *iso*-propylmagnesium chloride and 1-chloro-4-(trifluoromethyl)benzene (**Scheme 58**). Both linear **268b** and branched **268a** isomers were observed, along with homocoupled aryl chloride **268d**. Hydrodehalogenated material **268c**

was not observed, but has been discussed in many reports of the iron-catalysed cross-coupling of alkyl Grignard reagents.

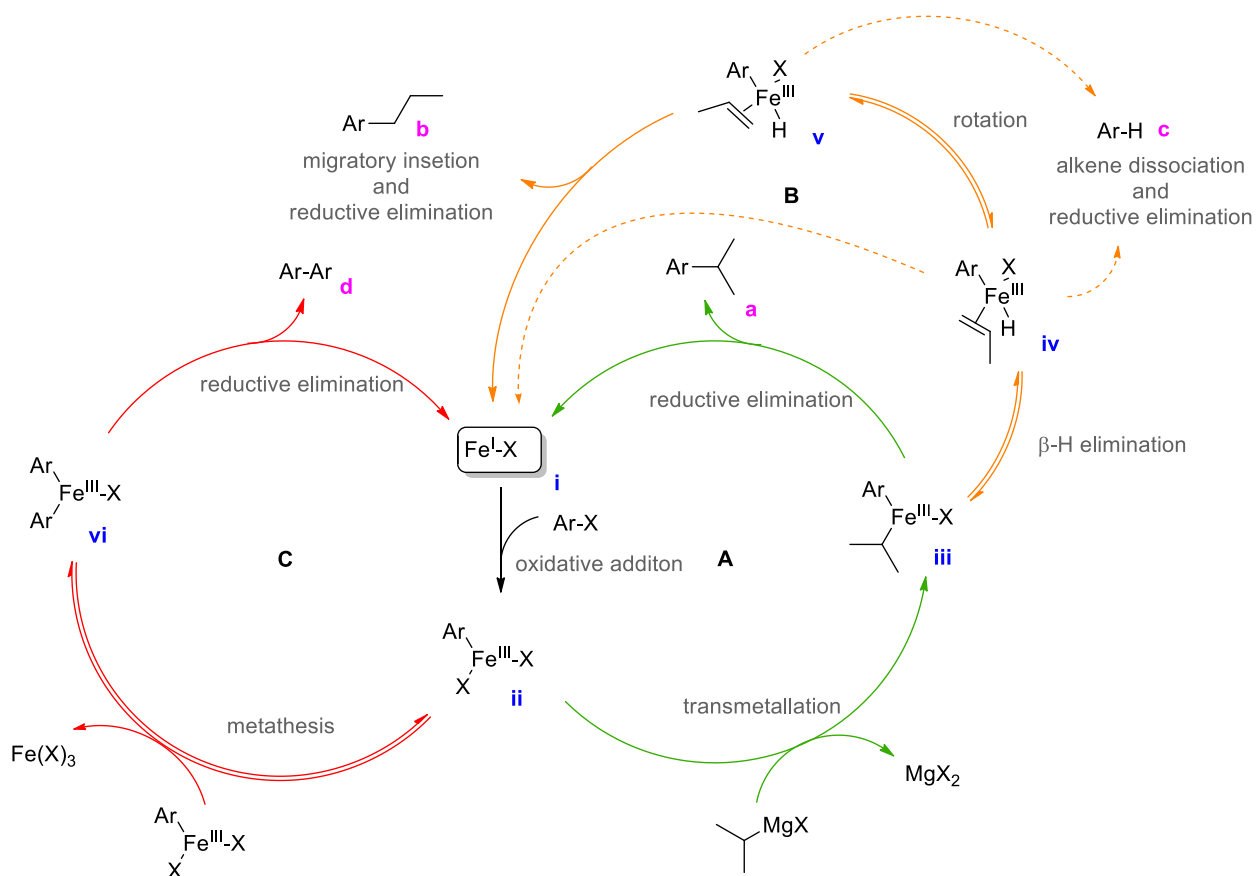


Scheme 58. Reaction chosen for DoE investigation along with proposed side-products.

A plausible mechanism for the formation of all side-products is shown in **Scheme 59**. Starting from a Fe^{I} species (**i**), formed from the initial reduction of the Fe^{III} pre-catalyst, OA could give a FeX_2Ar species (**ii**). Transmetalation, to give $\text{FeXAr}(\textit{iso}\text{-propyl})$ intermediate **iii**, followed by direct RE would lead to the desired *iso*-propyl coupled product **a**.

Slow RE from **iii** may result in undesirable β -hydride elimination, giving vinyl-iron intermediate **iv**. Alkene rotation from could give a second vinyl iron intermediate **v**. MI of the hydride species, followed by RE would then give *n*-propyl side product **b**. Alkene dissociation from either vinyl-iron intermediate **iv** or **v**, followed by RE of the remaining aryl- and hydride-ligands, could result in the formation of the reduced side-product **c**.

Slow transmetalation from **ii** could also lead to a metathesis between 2 FeX_2Ar species (**ii**). This would result in a new FeXAr_2 intermediate (**vi**) which, upon RE, would result in the formation of the final undesired side-product **d**.



Scheme 59. Plausible catalytic cycle, demonstrating pathways for side-product formation.

Within the chosen factors were four continuous (numerical) and two categorical (X or Y) variables. This gave a series of 16 experiments with eight centre-point reactions. The reactions were carried out using an Electrothermal Integrity 10[®] system in four sets, with eight experiments per run. The centre-point reactions, carried out at the centre of the design space (e.g. 0 °C, 2.55 mol% catalyst...), were repeated to assess the experimental variability between runs. Examination of experiments 4 and 17, 5 and 18, and 7 and 17 showed reasonable agreement (**Table 4**). The only centre-points which did not agree completely were 12 and 16, but the comparison was sufficient to derive good models.

Table 4. Centre-point reactions for the evaluation of experimental error.

Experiment	Factor 5	Factor 6	Response 1	Response 2	Response 3	Response 4
	E: <i>n</i> -BuMgCl	F:Ligand	SM / %	Product / %	Isomer / %	Biaryl / %
4	no	TMEDA	68	24	1	8
5	Yes	TMEDA	63	27	1	9
7	No	NMP	0	94	1	5
12	Yes	NMP	1	91	1	6
15	Yes	NMP	0	92	1	6
16	no	NMP	0	93	1	6
17	no	TMEDA	68	23	1	8
18	yes	TMEDA	62	28	1	9

Statistical analysis of the full data-set using DX7 suggested that the important factors were catalyst loading, ligand and a two-factor interaction between them. This is exemplified in the half-normal plot (**Figure 17**). Catalyst loading and ligand, shown furthest to the right, were found to have the greatest effect upon conversion to desired product.

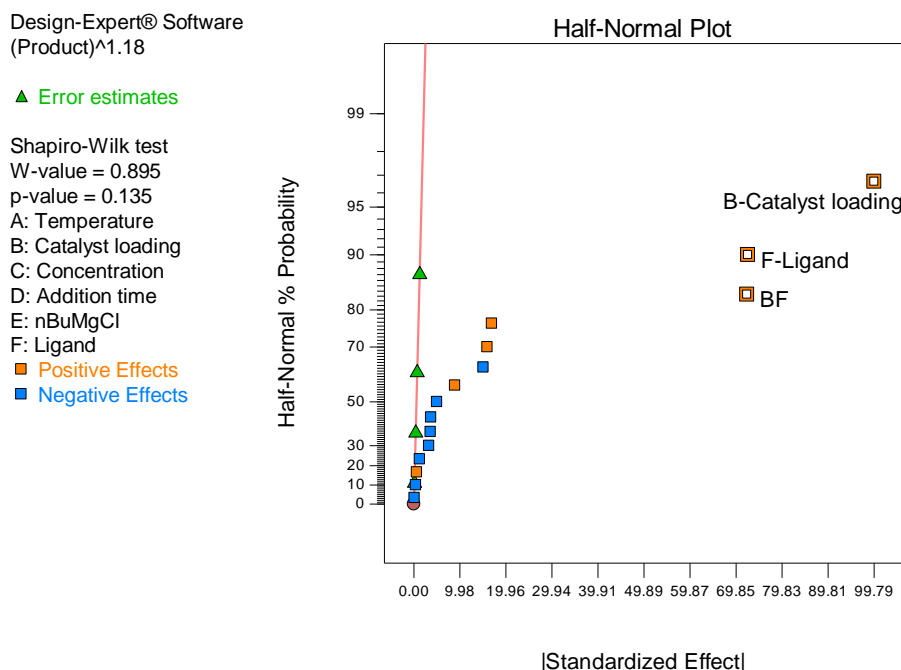


Figure 17. Half-normal plot for preliminary DoE investigation.

The statistical significance of both catalyst loading and ligand choice is demonstrated in the ANOVA table (**Table 5**). The p-value is a direct measure of a 95% confidence interval; any p-values less than 0.05 suggest that the model is significant, and that this factor has an effect. The ANOVA table suggests that the model is statistically significant, as the associated p-value is <0.05. It also demonstrates very low p-values for both curvature and lack of fit. These responses are unlikely to be mutually exclusive (*vide infra*).

Table 5. Analysis of variance table (abridged).

Source	p-value	Statistically Significant?
Model	< 0.0001	significant
B-Catalyst loading	< 0.0001	significant
F-Ligand	< 0.0001	significant
BF	< 0.0001	significant
Curvature	< 0.0001	significant
Lack of Fit	0.0002	significant

The observed two-factor interaction showed that with TMEDA (red line, **Figure 18**) increasing the catalyst loading from 0.1 mol% to 10 mol% had a moderate effect upon product formation.

However, with NMP, the same increase in catalyst loading showed a much more significant effect (green line, **Figure 18**). Interestingly, this diagram highlights a recurring theme throughout the series of DoE investigations. The centre-point conditions marked as circles lie above the predicted linear response.

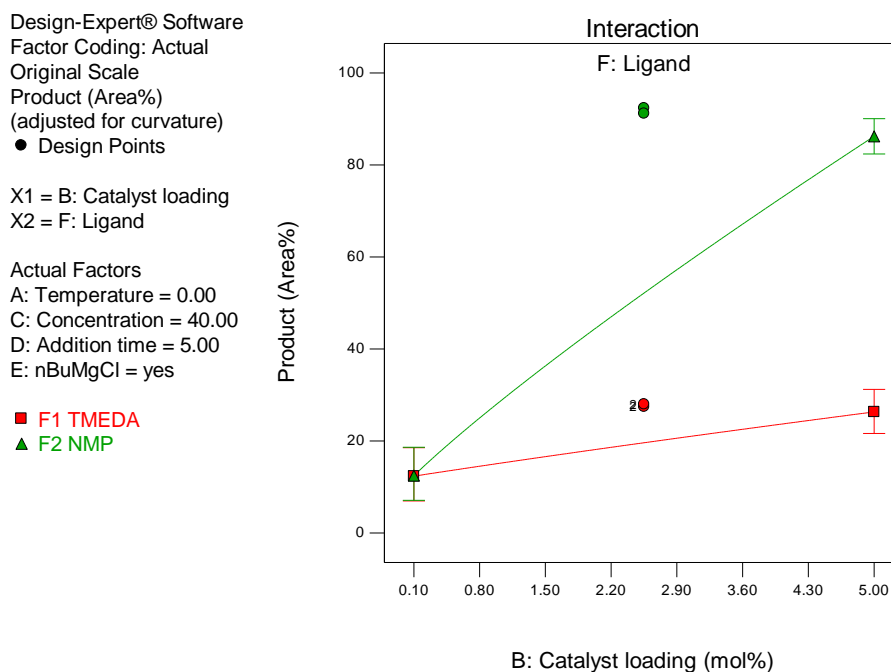
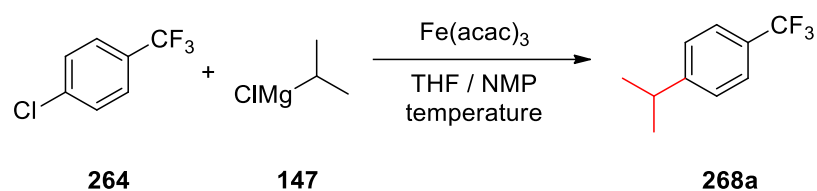


Figure 18. Interaction plot for the effect of catalyst loading and TMEDA or NMP.

The curvature exhibited with the interaction between catalyst and ligand cannot be modelled by the fractional-factorial design employed here, which would represent a linear model, this also explains the significant lack of fit observed in the ANOVA table. It is possible to augment the design, by adding face-centred experiments, to allow a quadratic response to be built to address the curvature observed in **Figure 18**. However, as only two of the six factors selected for investigation were shown to influence the reaction, it was possible to eliminate several variables for a follow-up study.

DX7 was then used to prepare a smaller DoE with four factors (**Figure 19**), requiring an initial set of only 12 experiments. Reaction mixtures were analysed using GC area (uncorrected), and the results were then imported directly into DX7 and the response to changes in the chosen factors was analysed. Duplicate reactions were performed throughout the investigation to demonstrate good reproducibility and give confidence in the subsequent statistical analysis.



Label	Factor	Range
A	Temperature	-20 to 40 °C
B	Grignard addition time	0 to 30 minutes
C	Ligand loading	10 to 300 × catalyst mol%
D	Catalyst loading	0.1 to 10 mol%

Figure 19. Chosen factors and responses for the preliminary experimental design.

The results from this second series of experiments showed again that efficient conversion was achieved with the higher catalyst loadings. A number of two-factor interactions were observed: the most significant of these was between catalyst loading and NMP. By increasing the level of NMP a higher level of the desired product was observed; this effect was more pronounced when a catalyst loading of 10 mol% was used (red line, **Figure 20**). A similar (but inverse) relationship was observed with temperature; the lower temperatures used gave the best reaction profiles (**Figure 21**). As with NMP, the response to temperature was increased when more catalyst was present.

Design-Expert® Software
 Factor Coding: Actual
 Product
 (adjusted for curvature)
 ● Design Points

X1 = C: Ligand
 X2 = D: Catalyst Loading

Actual Factors
 A: Temperature = 10.00
 B: Addition Time = 15.00

■ D- 0.10
 ▲ D+ 10.00

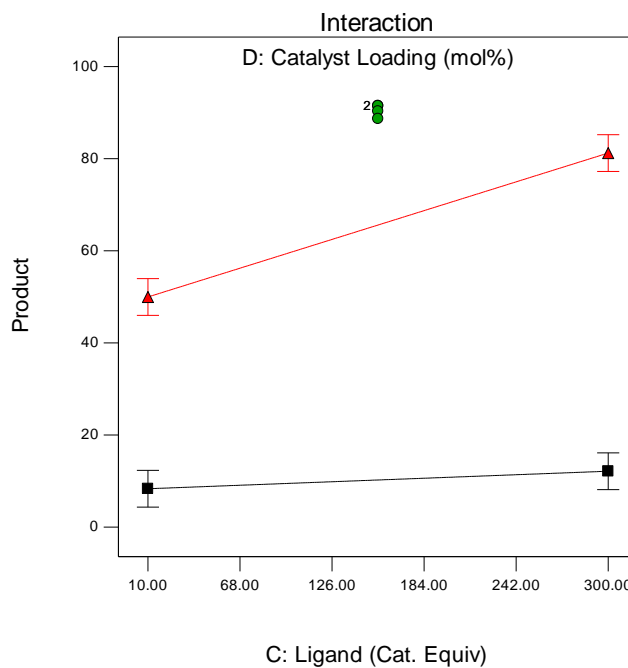


Figure 20. Interaction plot for catalyst and ligand loading.

Design-Expert® Software
 Factor Coding: Actual
 Product
 (adjusted for curvature)
 ● Design Points

X1 = A: Temperature
 X2 = D: Catalyst Loading

Actual Factors
 B: Addition Time = 15.00
 C: Ligand = 155.00

■ D- 0.10
 ▲ D+ 10.00

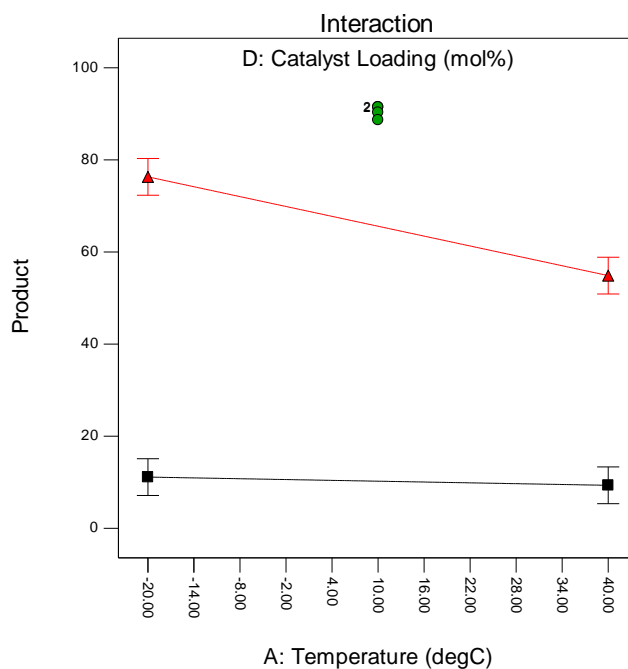


Figure 21. Interaction plot for temperature and catalyst loading.

During data analysis, it became apparent from reactions carried out at the centre of the design-space that the chosen experimental design (2^{4-1}) was not optimal. The experiments at the centre

of the design space (5.05 mol% Fe(acac)₃, 783 mol% NMP) gave the highest levels of product; this behaviour cannot be represented by a linear model. A further 10 experiments were therefore carried out to expand the previous investigation and allow greater definition of non-linear effects. Following the addition of this data, statistical analysis suggested that a curved response surface would best fit the data obtained during the investigation (**Table 6**).

Table 6. ANOVA table for second DoE investigation.

Source	p value	Statistically Significant?
Model	< 0.0001	significant
A-Temperature	0.0340	significant
C-Ligand	0.0002	significant
D-Catalyst Loading	< 0.0001	significant
CD	0.0885	not significant

The most significant factor was an interaction observed between the loadings of catalyst and NMP, as suggested by the first investigation. The improved model was used to generate a 3-dimensional plot of this interaction (**Figure 22**); the optimal region for product formation is highlighted in red. Higher levels of both Fe(acac)₃ and NMP gave increased conversion to the desired product; further changes to catalyst/ligand loading only resulted in the formation of side products.

The DoE results were then used to study the formation of isomer **268b**, hydrodehalogenated¹¹⁷ compound **268c** and biaryl **268d** (**Scheme 58**). Unfortunately, we were unable to generate a statistically significant model for the formation of the undesired side-products, which may be related to the very low levels observed throughout the DoE. However, it was clear that higher catalyst loading gave more of both the isomerised product, and the biaryl **268d** formed from reductive homocoupling of two aryl chloride species.³¹ Any optimal conditions must therefore balance the productive and non-productive pathways – too little catalyst/NMP gave poor conversion, and too much catalyst/NMP led to higher levels of side products.

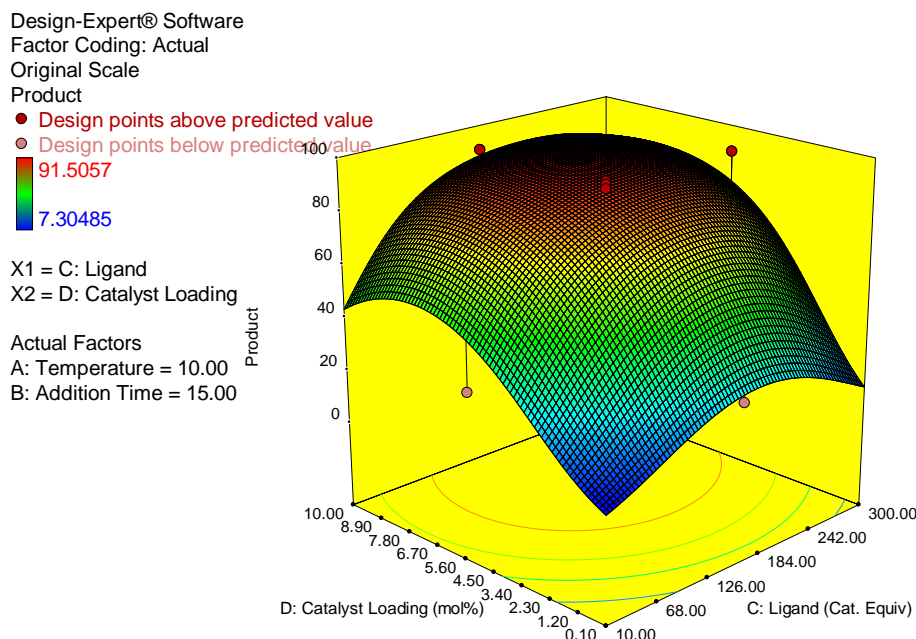


Figure 22. Three-dimensional response surface for catalyst and ligand loading.

Upon completion of the experimental design DX7 was used to predict a set of optimal conditions to achieve the highest level of *iso*-propylated product (**Table 7**), together with a 95% confidence interval. Pleasingly, when implementing these conditions a conversion of 90% was observed; only 4% of the *n*-propyl isomer was formed in this reaction, which is a branched:linear ratio of almost 23:1. This is a higher ratio than those reported under iron/NHC catalysed conditions in the literature.³⁵ The remaining material was found to be the reductive homocoupling product **268d**, at 6%.

Table 7. Predicted optimal conditions (P) and experimental results (E) with a 95% confidence interval of 91-96%.

	Temperature / °C	Ligand Loading / multiple of catalyst mol%	Catalyst Loading / mol%	Product / %
P	-20	199	7.8	95
E	-20	200	7.8	90

The experiments throughout the DoE used 97% purity Fe(acac)₃; recent reports have shown marked catalytic activity related to trace impurities in iron salts.¹¹⁸⁻¹²⁰ It was possible to use 99.9% trace metals basis Fe(acac)₃ and reduce the catalyst loading to 7.5 mol%. Control experiments showed no reaction with Cu(acac)₂ or Pd(acac)₂, and minimal reactivity with Ni(acac)₂; Fe(acac)₂ displayed a similar product distribution to Fe(acac)₃, analogous to earlier reactions with iron chlorides (**Table 8**).³⁵ A series of experiments were also conducted at this point to test both

experimental reproducibility and confirm the selection of both temperature and addition time for the Grignard reagent (**Table 9**).

Table 8. Control experiments with other transition metals.

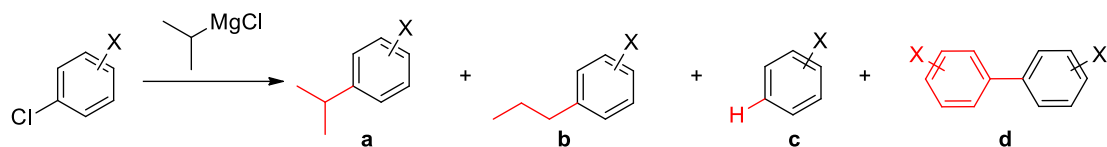
Entry	Catalyst	Hydrodehalogenated	Starting Material	Product	Isomer	Biaryl
1	Fe(acac) ₂ (7.5 mol%)	4	0	90	1	4
2	Cu(acac) ₂ (0.075 mol%)	1	99	0	0	0
3	Ni(acac) ₂ (0.075 mol%)	11	81	7	1	1
4	Pd(acac) ₂ (0.075 mol%)	60	26	0	0	14
5	No TM	1	99	0	0	0

Table 9. Control experiments related to temperature Fe(acac)₃ purity.

Entry	Temp. / °C	Addition Time / min	Iron / % purity	Cat. Loading / mol%	Starting Material	Product	Isomer	Biaryl
1	(-20)	0	97.0	7.77	0	94.2	1.6	4.1
2	20	0	97.0	7.77	0	88.0	5.1	7.0
3	(-20)	0	99.9	7.50	0.2	93.5	1.3	5.0
4	20	0	99.9	7.50	0.0	89.8	4.5	5.7

A series of aryl chlorides were tested in the iron-catalysed cross-coupling with *iso*-propylmagnesium chloride using higher purity Fe(acac)₃ at 7.5 mol% catalyst loading (**Figure 23**). The reaction gave the highest level of the desired coupling product when strongly inductively electron withdrawing substituents were present on the aryl chloride. The best substrates were the 3- and 4-substituted trifluoromethyl benzenes **268** and **269** (**Entries 1** and **2**); conversion to the desired product was higher for the *meta*-species, consistent with the inductively electron withdrawing (-I) effect of the trifluoromethyl group. The alkoxycarbonyl groups of **189** and **270** (**Entries 4** and **5**) were tolerated with good conversion to product in both *meta*- and *para*-cases. Moreover, no reaction was observed between the ester and *iso*-propylmagnesium chloride. Dichlorobenzenes **272** and **273** (**Entries 7** and **8**) gave moderate conversion to the *iso*-propylated product, but were found to form high levels of both hydrodehalogenated and homocoupled species. Interestingly, both biphenyl and terphenyl were observed by GCMS, suggesting that OA was still competitive after the first substitution. Aryl chlorides containing fluorine atoms **275** and **276** (**Entries 10** and **11**) and cyano groups **190** and **277** (**Entries 12** and **13**) were also reactive, though they produced higher amounts of undesired by-products. Difluoromethyl and difluoromethoxy benzenes **278** and **279** (**Entries 14** and **15**) also gave moderate levels of *iso*-propyl addition. Despite methyl substituted starting materials **284** and **285** (**Entries 35** and **36**) failing to give the desired products, possibly because they were too electron rich, they have been

included for completeness (*vide infra*). The *meta*-methoxy substituted starting material **286** (Entry 23) gave a higher conversion than the *para*-analogue **188** (Entry 22) – suggesting that the reaction was aided by a *-I* effect.



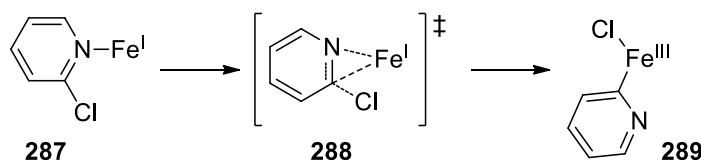
Entry	Product	X	Ar-Cl	Ar- <i>i</i> -Pr (a)	Ar- <i>n</i> -Pr (b)	Ar-H (c)	Ar-Ar (d)
1	268	4-CF ₃	ND	90 (45)	4	ND	6
2	269	3-CF ₃	ND	97	<1	ND	3
3	270	4-CO ₂ MOR ⁱ⁾	ND	84 (46)	ND	16	ND
4	189	4-CO ₂ Me	5	80 (23)	<1	15	ND
5	270	3-CO ₂ Me	ND	88	2	10	ND
6	271	4-Pyridyl ⁱⁱ⁾	<1	76 (48)	ND	24	ND
7	272	4-Cl	ND	71	1	12	16 ⁱⁱⁱ⁾
8	273	3-Cl	ND	64	2	14	20 ⁱⁱⁱ⁾
9	274	4-SO ₂ NEt ₂	5	70	7	11	7
10	275	4-F	ND	69	1	1	30
11	276	3-F	ND	59	1	32	9
12	190	4-CN	ND	69	ND	31	ND
13	277	3-CN	23	54	ND	22	2
14	278	4-CHF ₂	5	62	2	22	10
15	279	4-OCHF ₂	2	60	1	28	9
16	280	4-SMe	19	57	1	18	7 ^{iv)}
17	281	4-OCF ₃	2	53	2	35	9
18	282	3-OCF ₃	17	40	ND	37	6
19	283	4-CH ₂ F	83	13	ND	4	ND
20	284	4-Me	54	7	ND	38	2
21	285	3-Me	54	6	ND	38	2
22	188	4-OMe	66	3	ND	31	ND
23	286	3-OMe	27	22	1	42	8

Figure 23. Aryl chlorides tested in the iron-catalysed cross coupling reaction. GC conversion (isolated yields in parentheses). ⁱ⁾ MOR = morpholine; ⁱⁱ⁾ 2-(4-chlorophenyl)pyridine; ⁱⁱⁱ⁾ terphenyl also observed (see Supporting Information); ^{iv)} biaryl also observed (see Supporting Information). ND – not detected. Volumes – 1 l kg⁻¹ of limiting reagent.

Although necessary to form the desired *iso*-propylated product, the presence of relatively large amounts of NMP made the isolation of the simple substituted cumenes **268a** and **189a** quite

difficult. Quenching reactions with either sulfuric or citric acid enabled efficient removal of NMP from the organic phase in most cases. Unfortunately, the 4-trifluoromethyl product **268a** also formed a robust azeotrope with THF, making product isolation even more problematic. A pre-packed reverse phase (C18) column was used in an attempt to trap the organic product due to its low polarity (R_f of 0.69 in neat hexane), allowing the polar solvents to be washed away. The process was successful, removing all traces of both THF and NMP prior to further purification. Subsequent distillation of the reaction mixture from **268a** gave a 45% isolated yield of the desired compound. It was possible to apply this procedure to 4-methoxycarbonyl product **189a**, giving an isolated yield of 23% from a challenging product mixture. These very small and volatile molecules represent worst case scenarios for product isolation; similar retention times and boiling points led to difficulty in separating hydrodehalogenated material from the desired product with the aryl chlorides.

To expand the substrate scope of the iron-catalysed Kumada cross-coupling further, we chose to investigate a number of heteroaryl chlorides. Excellent conversion was observed in all cases, with some substrates demonstrating quantitative formation of the *iso*-propylated material (**Figure 24**). An alternative mechanism has previously been proposed by Jutand *et al.*, which may explain the improved reactivity of pyridyl substrates (**Scheme 60**).¹²¹ A similar mechanism was presented by von Wangelin for chlorostyrenes – where pre-coordination of the substrate was found to accelerate the OA reaction, similar to **287** → **289**.¹²²



Scheme 60. Jutand's proposal for oxidative addition of chloropyridines.

Chloro-pyridines gave good to excellent conversion to the desired *iso*-propyl analogues (**223a**, **290** to **297**). Purification of these substrates using either normal phase or reverse phase column chromatography resulted in moderate to good isolated yields. Methoxy substituted pyridine **223a** was isolated in 79% yield, a significant improvement over the previous report.³⁵ Alkoxy carbonyl substituted pyridines **292** and **293** gave very good conversion; the *tert*-butyl ester **292** displayed lower conversion than the ethyl analogue **293**, possibly due to steric effects. Cyanopyridine **294** demonstrated reduced selectivity, much like the carbocyclic substrates **190** and **277** (**Entries 10** and **11**, **Figure 23**). Normal phase chromatography, used in the purification of **292** and **293**, gave a reduced yield due to close running impurities; reverse phase chromatography used in the purification of **290** and **291** also led to challenges related to volatility and aqueous solubility.

Fused ring heterocycles such as isoquinoline (**295**) and biaryl pyridazine (**296**) also displayed excellent conversion and high selectivity for *iso*-propylation. Additionally, it was possible to isolate 6-chloro-2-*iso*-propylpyridine (**297**) following the iron-catalysed cross-coupling process although a slight modification of the reaction conditions was required.

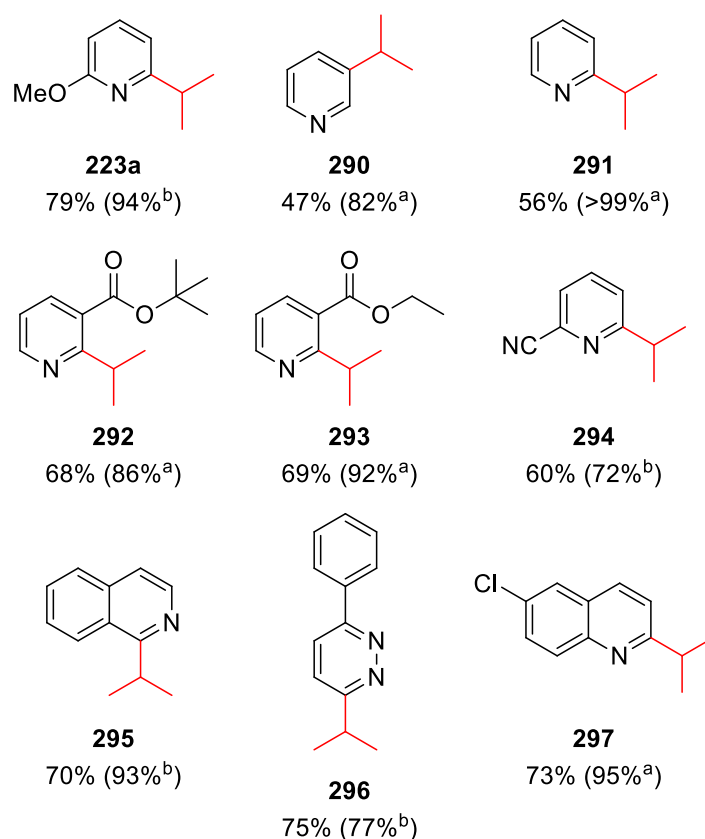


Figure 24. Heteroaryl chlorides prepared using the iron-catalysed Kumada cross-coupling. Isolated yields (conversion in parentheses). ^a) Conversion by GC area ^b) Conversion by HPLC area.

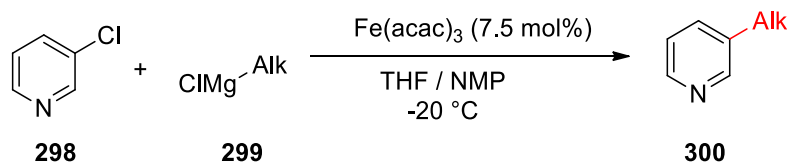
The selectivity demonstrated in this reaction may be relevant to medicinal chemistry programmes, especially when considering the recent patent literature around such motifs.¹²³⁻¹²⁶

This methodology may offer a new pathway for the selective introduction of an alkyl group to the pyridyl ring of a fused heteroaromatic, such as quinoline, giving access to new analogues in a simple and scalable manner. Fürstner previously reported the mono-alkylation of aryl and heteroaryl dichlorides with primary alkyl Grignard reagents; the highly activated pyrazine and pyrimidine electrophiles required temperatures of -78 °C to temper the reactivity of the second halide.⁴³

After application of this new *iso*-propylation methodology to the heteroaryl chlorides, we chose to explore the use of other Grignard reagents. 3-Chloropyridine was chosen as a model substrate for this investigation due to the successful cross-coupling with *iso*-propylmagnesium chloride

(292, Figure 24). Cyclohexylmagnesium chloride gave a very similar result to *iso*-propylmagnesium chloride (Entries 1 and 6, Table 10). The selectivity for the desired product was eroded with cyclopentylmagnesium chloride (Entry 5) and further changes to the Grignard reagent gave poorer results. The cyclohexyl and *iso*-propylmagnesium halides are the closest analogues, and the DoE was optimised for the application of the latter. Because the cyclopentyl and acyclic magnesium halides are less structurally similar to cyclohexyl and *iso*-propylmagnesium halides, it is likely that the optimised reaction conditions are now unsuitable. Further DoE could be undertaken to reoptimise the conditions to be more effective for other Grignard reagents or aryl chlorides. The high dependence of the performance of the reaction on Grignard reagent structure contrasts sharply with the observations of Lamaty *et al.*, who demonstrated the cross coupling of a variety of Grignard reagents, including *iso*-propylmagnesium chloride, with a single pyrrolo-[3,2-*c*]quinoline.¹²⁷

Table 10. Product distributions for the reaction between 3-chloropyridine and a selection of other Grignard reagents. Conversion by GC.



Entry	Product	RMgCl	Ar-Cl	Ar-R	Ar-R'	Ar-H	Ar-Ar	Product
1	290	<i>iso</i> -propyl	ND	82	ND	18	ND	
2	301	methyl	92.9	ND	NA	ND	7.1	
3	302	<i>sec</i> -butyl	33.4	66.6	ND	ND	ND	
4	303	<i>cyclo</i> -pentyl	ND	52.4	NA	30.0	17.6	
5	304	<i>iso</i> -butyl	76.7	23.3	ND	ND	ND	
6	305	<i>cyclo</i> -hexyl	15.8	81.7	NA	ND	2.5	

R' – isomerised; ND – not detected; NA – not applicable.

We have already commented on an apparent relationship between the inductive effects of substituents and conversion; in an attempt to quantify this relationship, we tested a series of substituted 4-tolyl chlorides (**Figure 25**). Increasing the number of fluorine atoms, and therefore the $-I$ effect, gave a higher conversion to the *iso*-propylated product. A modest trend ($R^2 = 0.93$, 4 points) was observed between $\log_{10}(k_X/k_H)$ and σ_p ; however, the results for the three methoxy substituents did not fit this trend.

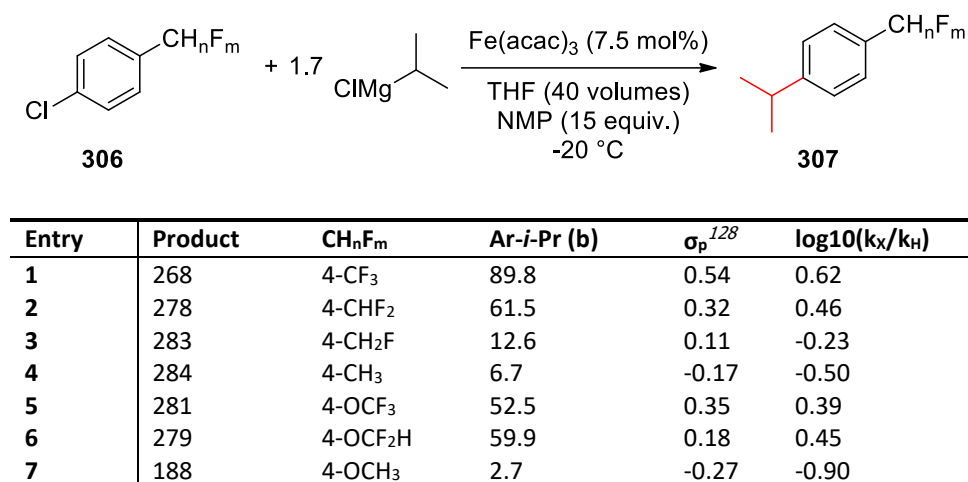


Figure 25. (Fluoro)methyl and (fluoro)methoxy substituted aryl chlorides.

The Hammett plot (**Chart 1**) shows a small positive reaction constant ($\rho = 1.72$) which suggests a very limited build-up of negative charge in the transition state of the rate determining step; this would be consistent with electron-donation from the catalytic metal centre to the arene in an OA reaction. A step like this could be accommodated within a cycle carried by Fe(I)³¹, Fe(0) or Fe(-II)³⁵ species.⁵³

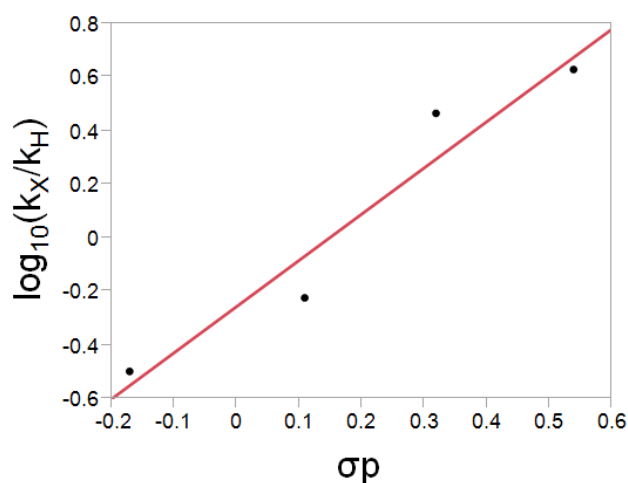


Chart 1. Hammett plot for 4-methyl analogues.

Unfortunately, investigating the remaining aryl chlorides using Hammett studies yielded a much weaker correlation (**Chart 2**). A moderate trend was observed between conversion and σ_m (blue circles – $R^2 = 0.76$), suggesting that the electronic nature of the *meta*-substituent could influence the reaction. A poor trend was observed between conversion and σ_p (orange squares – $R^2 = 0.52$), suggesting that the electronic nature of the *para*-substituent had less influence on the reaction. This could be related to inductive effects, which are more pronounced with *meta*- over *para*-substituents. However, the data for σ_m may be skewed by the large grouping at $\sigma_m \approx 0.4$.

The σ_p data may be better represented by the dashed lines shown in **Chart 2**. There appears to be a linear correlation between the electron rich substrates, with $\sigma_p < 0$, shown as a dashed grey line. There also appears to be a second linear relationship between the more electron deficient substrates, with $\sigma_p > 0$, shown as a dashed yellow line. The new representation suggests that there could be a change in the rate determining step. This could be OA, transmetalation, or RE; OA may be more challenging with the electron rich substrates, so this might explain the change in slope.

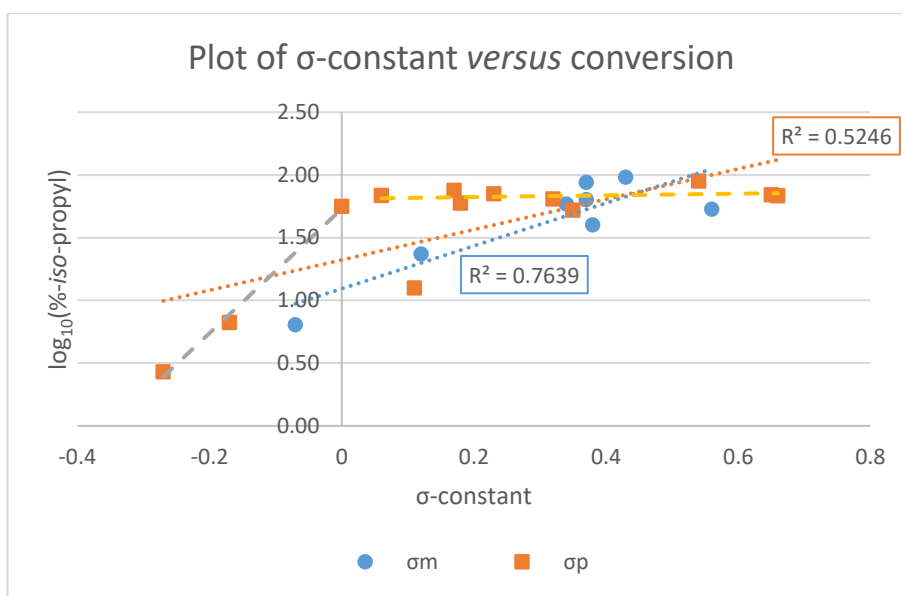


Chart 2. Wider Hammett study including all substrates. Best linear fit of all σ_m data – blue dotted line. Best linear fit of all σ_p data – orange dotted line. Modified linear fits representing change in RDS – grey and yellow dashed lines.

The iron-catalysed cross-coupling reactions were found to be incredibly fast, with reaction times of less than 30 minutes for most substrates. Thus, a simple triage approach was sought (**Figure 26**), rather than investigating mechanistic pathways, which have proven challenging in the past. This was hoped to increase the speed of the prediction, meaning that a researcher could easily determine the reaction outcome in a shorter timescale than carrying out the reaction itself. We sought to determine whether a simple property of the starting aryl chloride be used to predict the outcome of the iron-catalysed cross-coupling reaction. It was anticipated that computational chemistry, specifically DFT, could be used to predict and understand the observed differences in reactivity.

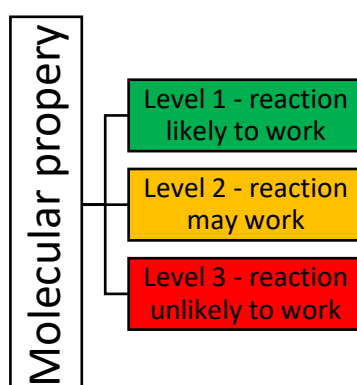


Figure 26. DFT triage approach.

3.3. Conclusion

Following a simple DoE optimisation it was possible to couple *iso*-propylmagnesium chloride with electron deficient aryl chlorides, in very high conversion. These reactions gave excellent selectivity for the branched isomer, with minimal isomerisation to the *n*-propyl side-product. It was easy to apply the newly developed reaction conditions to heteroaryl chlorides, with excellent conversions and good isolated yields in many cases. Isomerisation, known to present a significant problem for secondary alkyl species, was minimal. The conditions developed were mild and highly selective, offering significant advantages over classical Friedel-Crafts alkylation, and other TM-catalysed processes. The use of iron, rather than heavier transition metals such as palladium, meant the chemistry was more suited to the preparation of APIs, as it is known to have much lower toxicity. Furthermore, the coupling of (hetero)aryl chlorides allowed the use of the cheapest and most widely available starting materials.

It was also possible to deploy cyclohexylmagnesium chloride in the reaction due to its similarity to *iso*-propylmagnesium chloride although other Grignard reagents were less effective. However, through the use of a simple DoE optimisation it may be possible to expand the scope and selectivity with a wider set of Grignard reagents and aryl chlorides, particularly if the desired application is the introduction of a primary or secondary alkyl group on a large-scale.

The productivity of reactions with aryl chlorides was found to be highly substrate specific. A Hammett study was carried out to understand the effect of substituents on the reactivity of the substrates. A strong correlation was observed for some substrates, such as α -fluorotoluenes. This did not hold for different substituents. Therefore, alternative methods will be sought to investigate the differences in reactivity in **Chapter 4**.

4. The Application of DFT to Predict and Understand Trends in Reactivity

4.1. Introduction

4.1.1. Cross-Coupling of *iso*-Propylmagnesium Chloride with Aryl Chlorides

Following reaction optimisation using DoE, a number of differentially substituted aryl chlorides were tested in the cross-coupling procedure (**Figure 27**). Substrates with electron-withdrawing substituents were found to give the highest conversion to desired product; substrates with electron-donating substituents were found to give the lowest conversion to the desired product. Conversion varied from 3% ($\log_{10} = 0.43$) with electron rich substrates such as *para*-methoxychlorobenzene (**Entry 18**) to 97% ($\log_{10} = 1.98$) with electron deficient substrates such as *meta*-trifluoromethylchlorobenzene (**Entry 1**). Conversion is reported as $\log_{10}(\% \text{-}i\text{-propyl})$ following the use of Hammett studies in **Chapter 3**, it was also considered to represent the rate of entry to the productive pathway of the catalytic cycle. The large variation observed led to the questions: can these trends be predicted and understood and will this give any insight into the reaction mechanism?

Mechanistic investigations of catalytic processes using iron have been shown to be especially challenging due to the sensitive nature of the organoiron intermediates, and the potential for the formation of paramagnetic species.^{129, 130} Experts in physical inorganic chemistry use highly specialised techniques such as Mössbauer spectroscopy, EPR and MCD.¹³¹

Mössbauer spectroscopy allows the study of solid or frozen samples from a cross-coupling reaction. The observed spectra can give information on electron density around the iron centre, allowing insight into both oxidation and spin state. Each iron species in a cross-coupling reaction would lead to a different Mössbauer spectra, therefore allowing their identification. EPR can also give information on the spin state of iron species in a reaction, but only if this has a non-integer value ($S = 1/2, 3/2, 5/2$ etc.). This is very useful for the identification of Fe^{I} and Fe^{III} species, which have been proposed by numerous researchers (*vide supra*). MCD is a very powerful technique for the analysis of both isolated and freeze-trapped samples. It allows the investigation of electronic structure and transitions within paramagnetic molecules. When combined with TD-DFT it can also give significant insight into specific transitions and their nature with respect to structure and bonding. All of these techniques require specialist equipment, expert knowledge and inert

atmospheres, none of which are available for use within a pharmaceutical company, such as GSK. Therefore, alternative methods were sought to investigate the observed differences in reactivity.

The results from **Chapter 3** are shown in **Figure 27**. They are compared to Hammett's σ -constant following the earlier Hammett study, which is briefly reviewed below.

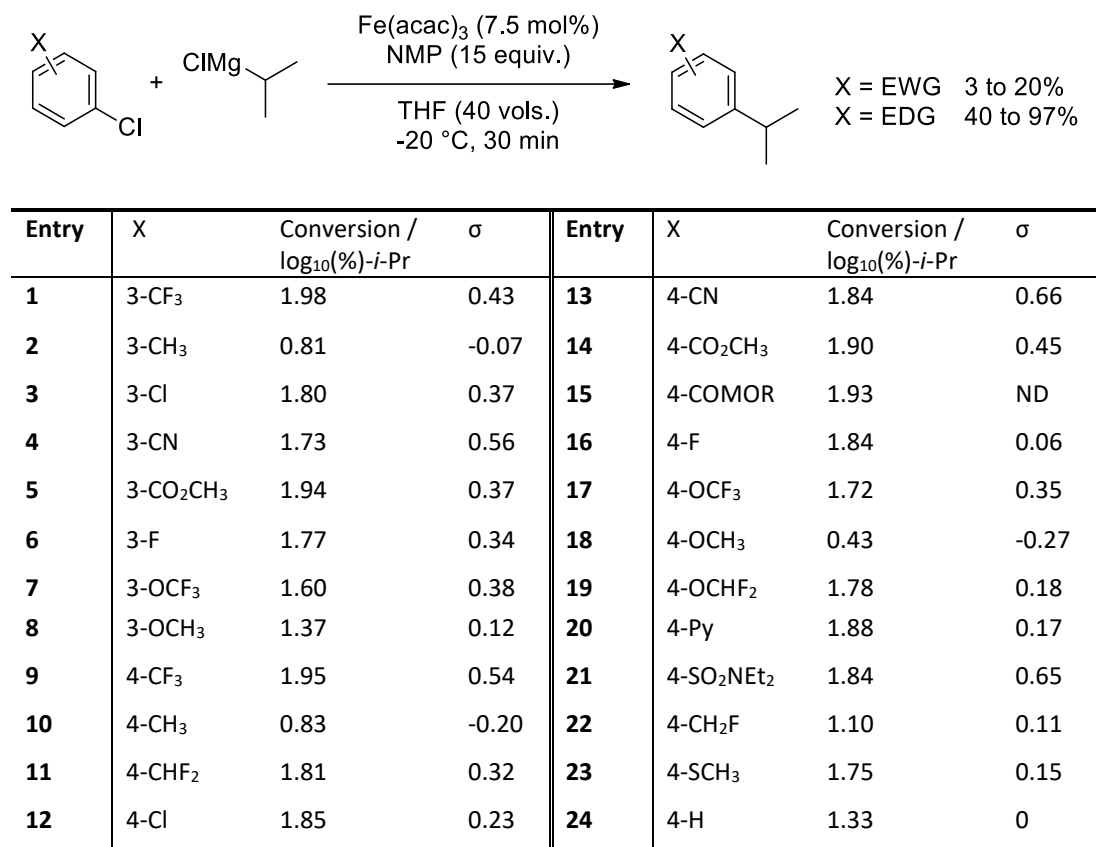


Figure 27. Results from **Chapter 3** substrate scope investigations (GC area). MOR = morpholine. Hammett's σ -constant is derived from the difference between the ionisation constant of substituted and unsubstituted benzoic acids (**Figure 28**). The σ -constant is represented as the difference between K and K_0 i.e. the difference in pK_a (ΔpK_a , **Equation 1**) between the substituted and unsubstituted benzoic acids.

Equation 1.

$$\sigma = \log \frac{K}{K_0} = \Delta pK_a$$

K = acid dissociation constant for the ionisation of substituted benzoic acid

K_0 = acid dissociation constant for the ionisation of benzoic acid

Substituents which stabilise the anion formed during the ionisation of the benzoic acid (**308**) – those which are electronegative – promote the forward reaction, therefore increasing the value

of K versus K_0 . This results in a positive σ -constant. Substituents which destabilise the anion formed during the ionisation of the benzoic acid (**308**) – those which are electropositive – promote the reverse reaction, therefore decreasing the value of K versus K_0 .

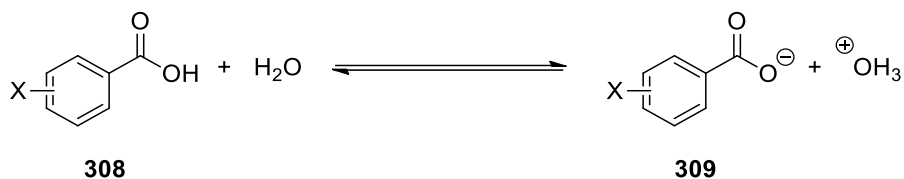


Figure 28. The derivation of Hammett's σ -constant.

During a Hammett study, the substrate's σ -constant is plotted against the relative rate of reaction of the *para*- or *meta*-substituted substrate, and the unsubstituted ($X = \text{H}$) analogue (**Equation 2**, **Figure 28**). The nature of substituent X either stabilises or destabilises the transition state of the rate determining step, and leads to a positive or negative correlation between σ -constant and $\log_{10}(k_X/k_H)$ – this is the ρ -value. If the transition state of the rate determining step is stabilised by an electron withdrawing substituent, this results in a positive ρ -value. If the reaction is accelerated by an electron donating substituent, this results in a negative ρ -value. The magnitude of ρ can be used to understand the extent of charge build up in the rate determining step. A large positive ρ -value, for example, would suggest that a significant negative charge was present.

Equation 2.

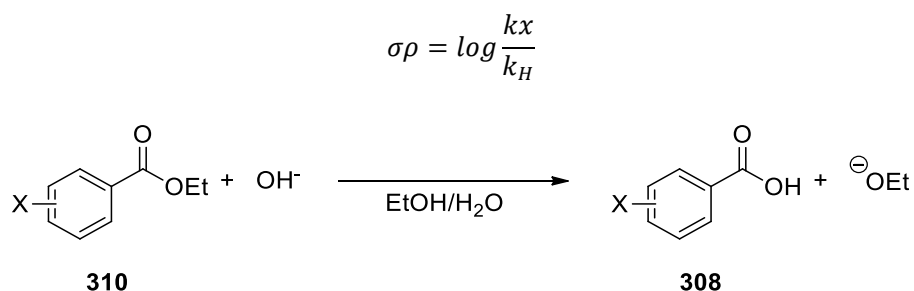


Figure 29. The identity of Hammett's ρ -value.

Initially, a small Hammett study was carried out with 4-chloro- α -fluorotolyl substrates (**Figure 30**). This gave a positive ρ -value of 1.72 (**Chart 3** – $R^2 = 0.93$), suggesting that OA may be the selectivity determining step. Norrby previously reported a Hammett study with the iron-catalysed cross-coupling of primary alkyl Grignard reagents.³¹ In this investigation a positive ρ -value was also observed, suggesting a rate limiting, and irreversible OA. Norrby observed a much higher ρ -value of 3.8, but aryl triflates were used in place of aryl chlorides for the more electron rich aromatics. This was proposed to accelerate OA for the less reactive electron rich substrates.

Norrby also discussed some general trends related to ρ -values observed in palladium-catalysed cross-coupling reactions. Other researchers reported ρ -values of between 1 and 1.5 for rate-limiting OA in a Heck reaction,¹³² and 2.3 for OA of an aryl iodide to Pd⁰ directly.¹³³

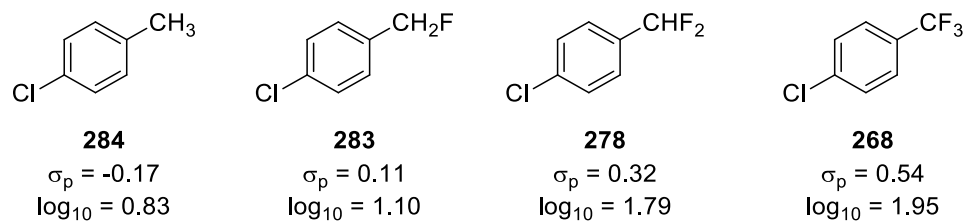


Figure 30. α -Fluorotolyl derivatives investigated using Hammett plot.

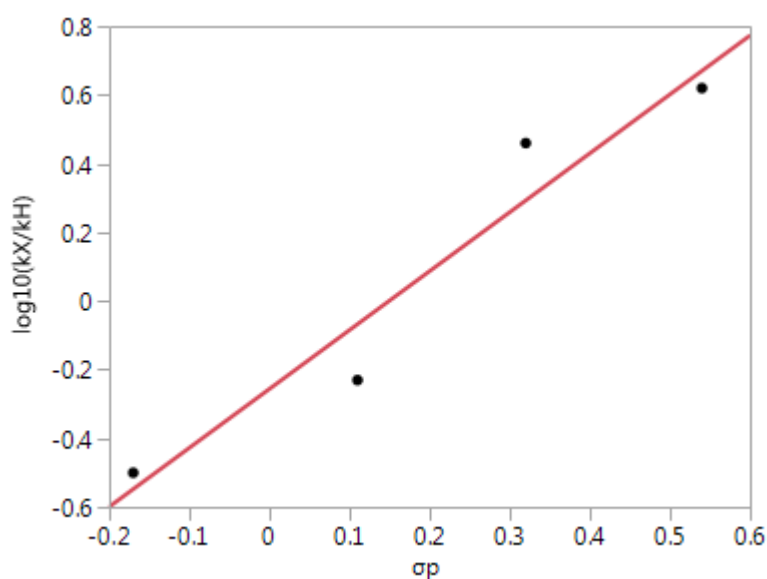


Chart 3. Hammett Plot for α -fluorotolyl derivatives.

Researchers have previously used molecular properties, such as bond dissociation enthalpy (BDE) or ligand bite angle, as descriptors for reactivity in transition metal catalysed processes.^{134, 135} For example, Houk and Merlic demonstrated the application of DFT to determine the C-X bond BDEs of a number of mono- and di-halogenated heterocycles in an attempt to explain selectivity in palladium-catalysed cross-coupling reactions (**Figure 31**).¹³⁶ The authors found that it was possible to determine theoretical BDEs using B3LYP or G3B3; B3LYP was found to give faster results but G3B3 was shown to be more accurate. This is directly related to the complexity of the method used; G3B3 begins with a B3LYP structural optimisation but then carries out further calculations at higher levels of theory to reduce the error associated with the earlier DFT approximations.¹³⁷ The authors carried out the investigation above following a combined experimental/theoretical investigation, although this suggested that BDE was not the only selectivity determining factor.¹³⁴

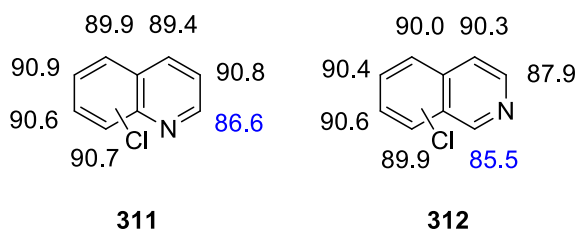
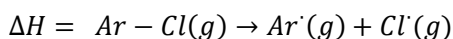


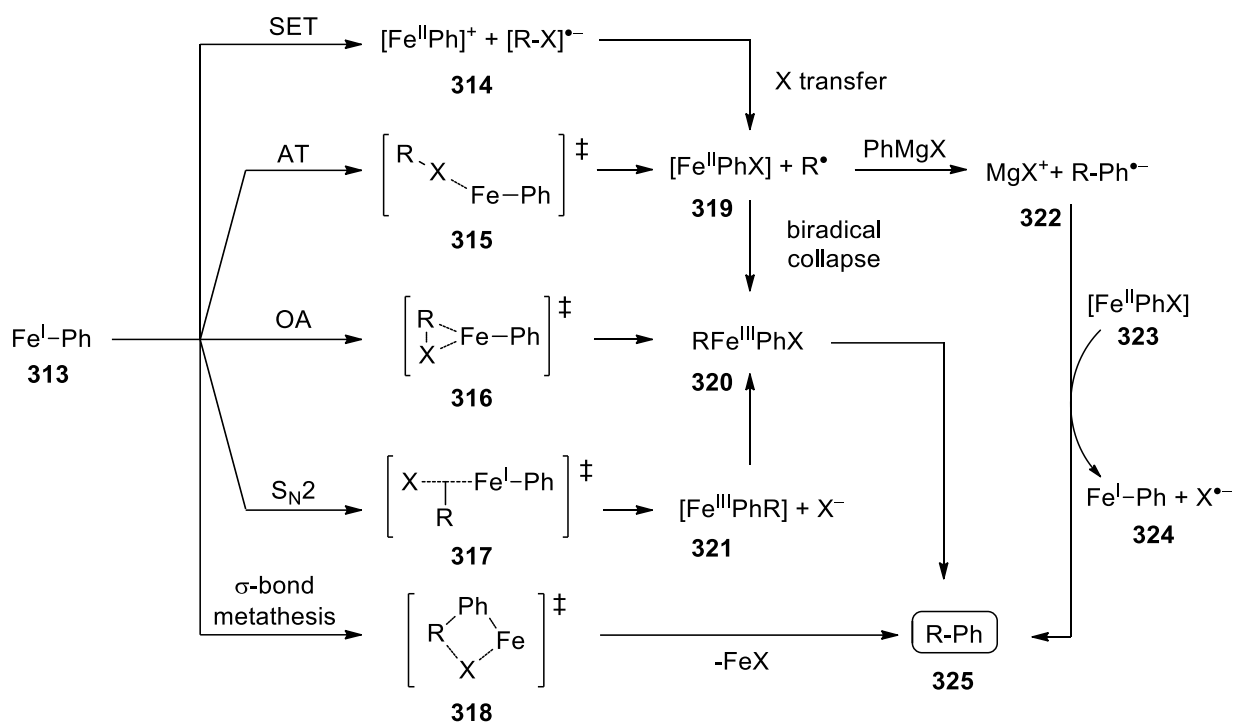
Figure 31. Houk and Merlic's BDEs of chloro-quinoline and -isoquinoline isomers, preferred site of reaction highlighted (kcal mol⁻¹).

The BDE was determined by calculating the energy difference between heteroaryl chloride, and the heteroaryl and chlorine radicals individually (**Equation 3**). This modelled the heterolytic cleavage of the carbon-chlorine bond, which may be expected to occur during an OA reaction within a catalytic cycle. As demonstrated in **Figure 31**, there is generally a very small difference between the BDE of the carbon-chlorine bond at different positions within the heteroaryl halide. Experimental error with DFT can be around 1 kcal mol⁻¹, so differences smaller than those observed above may fall within this range.

Equation 3.



Several mechanisms have been proposed for OA to iron (**Scheme 61**). Norrby included a detailed description of such reactions in a study of "the radical nature of iron-catalysed cross-coupling reactions".¹³⁸ The first suggested mechanism was SET between the Fe^I species **313** and an alkyl (or aryl) halide, forming the ion pair **314**. X transfer from the substrate (R-X) could then lead to radical pair **319** which, followed by biradical collapse, leads to the common OA intermediate **320**. The radical stability of R would be expected to influence this reaction significantly. The second mechanism was proposed to be an atom transfer (AT) between Fe^I species **313** and an alkyl halide *via* transition state **315**. This alternative process would lead directly to radical pair **319**. Again, the radical stability of R would be expected to influence this reaction. A third proposal was the classical direct 3-centred transition state **316**, giving OA intermediate **320** directly. As discussed in **Section 2.2.1**, this is a common OA pathway for low- or intermediate polarity reagents, such as C-H bonds or aryl (pseudo)halides. The fourth OA mechanism was suggested to be an S_N2 type reaction, *via* transition state **317**. This is most likely for highly polar reagents such as alkyl (pseudo)halides, and would be unlikely with an aryl chloride. The final mechanistic proposal was a σ-bond metathesis *via* transition state **318**, proposed by Fürstner and demonstrated in Scheme 21, but is generally limited to d⁰ metal complexes with H-H or C-H bonds.



Scheme 61. Norrby's mechanisms for the oxidative addition of an alkyl halide to a $\text{Fe}^{\text{I}}\text{Ph}$ species. Frontier molecular orbital (FMO) energies may also be used to describe selectivity in chemical processes. The characteristics of the highest occupied molecular orbital (HOMO) and lowest unoccupied molecular orbital (LUMO) of compounds are often used to understand their chemical and physical behaviour. Dixon *et al.* carried out a thorough investigation into a number of properties which can be directly associated with either HOMO energy, LUMO energy or the HOMO-LUMO gap.¹³⁹ The authors found a linear correlation between calculations with standard [6-31G(d)] and larger (aug-cc-pVTZ+1) basis sets for a number of molecular properties, including:

- HOMO energy: ϵ_{HOMO}
- LUMO energy: ϵ_{LUMO}
- Ionisation potential: $IP_{\text{calc}} \approx -\epsilon_{\text{HOMO}}$
 - The energy necessary to remove an electron from a neutral atom or molecule
- Electron affinity: $EA_{\text{calc}} \approx -\epsilon_{\text{LUMO}}$
 - The energy released when an electron is added to a neutral atom or molecule
- Electronegativity: $\chi_{\text{HL}} = \left(\frac{IP+EA}{2}\right)$
 - The ability of an atom or molecule to attract electrons

Again, during an OA process the transition metal and aryl chloride would be expected to undergo a HOMO-LUMO interaction. Therefore, like BDE, one of the molecular properties above may serve as a useful descriptor for selectivity in the iron-catalysed cross-coupling reaction. DFT HOMO and

LUMO energies are determined simply by carrying out a structural optimisation of the desired aryl chloride. The computational chemistry software then gives values for the FMOs of the molecule, and can be used to describe the shape of these orbitals, and their atomic coefficients.

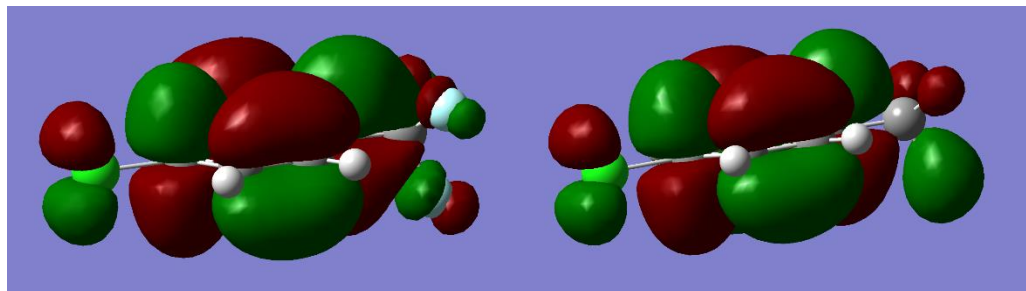
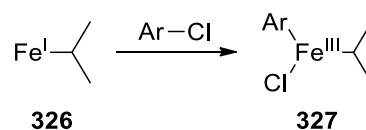


Figure 32. LUMO plots for *para*-CF₃ and *para*-CH₃ substrates. *para*-CF₃ LUMO LHS, *para*-CF₃ LUMO+1 RHS.

The electron affinity (EA) of a molecule is defined as the amount of energy taken in or given out when a neutral atom or molecule accepts an electron, giving the corresponding radical anion. This describes the atom or molecules ability/desire to accept an additional electron. EA may also be used to investigate reactivity in an OA reaction. The OA process could be thought as electron donation from the transition metal to the aryl halide substrate (**Scheme 62**). The greater a molecule's EA, the more likely it could be to undergo OA.



Scheme 62. Possible oxidative addition to iron-alkyl species.

Following the studies above, DFT was employed to understand differences in reactivity, and produce a model capable of predicting the outcome using a series of new substrates.

4.2. Results and Discussion

4.2.1. Cross-Coupling of iso-Propylmagnesium Chloride with Aryl Chlorides

4.2.1.1. Computational Investigation of Bond Dissociation Enthalpy

During the investigation reported in **Chapter 3** the observed differences in reactivity seemed to strongly correlate with the electronic nature of the starting material. Electron deficient substrates gave successful cross-coupling reactions, where electron rich substrates gave poor reactivity. It was envisaged that a highly electronegative substituent, such as a CF₃ group, could influence the BDE of a carbon-chlorine bond in the same molecule (**Figure 33a**). The BDE of a molecule may be represented by its homolytic cleavage into a biradical pair (**Figure 33b**).

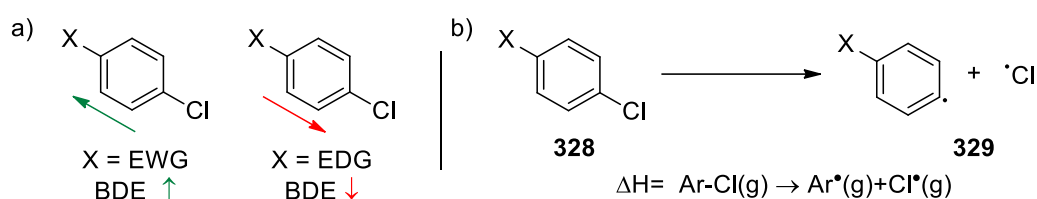


Figure 33. The proposed substituent effect on BDE.

Following Houk and Merlic's success with the B3LYP basis set for BDE calculations, this method was used for a preliminary investigation. Initially, gas phase calculations were compared to Hammett σ -constants to test for a correlation between BDE and other molecular properties. This gave a good linear trend with σ_m , and a moderate trend with σ_p . A single outlier, 4-CO₂CH₃ (**189**) was removed during this and further investigations (*vide infra*). This data suggests that molecular properties such as BDE can be influenced by the electronic nature of substituents upon the

aromatic ring. However, this effect appears to be greatest when the functional group is closest to the C-Cl bond.

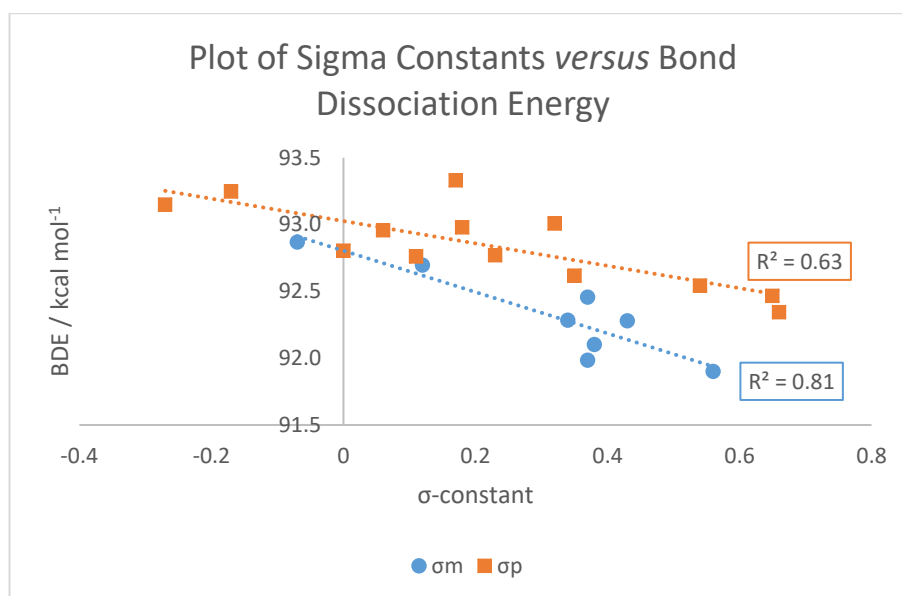


Chart 4. Plot of Hammett σ -constants versus BDE for *meta*- and *para*-substituted aryl chlorides. Houk and Merlic also demonstrated the requirement for a proximal functional group to influence the C-Cl BDE in their calculations (**Figure 31**).¹³⁶ The theoretical BDE of the C-Cl bond was only significantly reduced in the 2-position of chloroquinoline, or the 1- or 3-position of chloroisoquinoline. This effect was pronounced for all other heterocycles studied.

The calculated BDE values were then compared to conversion, described as $\log_{10}(\% \text{-iso-propyl})$ (**Chart 5**). The outlier – 4-CO₂CH₃ (**189**) with a BDE of 89.6 kcal mol⁻¹, was included in this plot for completeness, but was removed from further BDE studies.

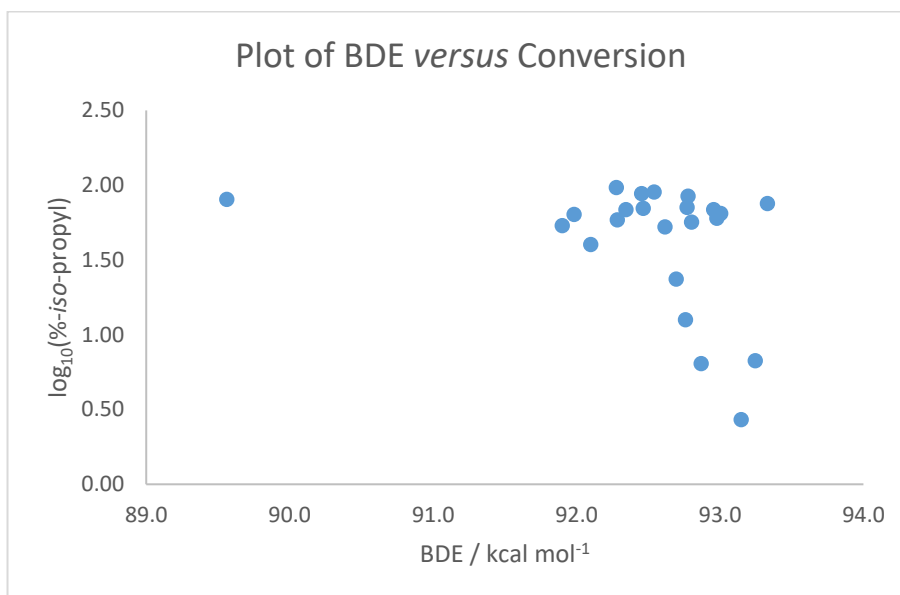


Chart 5. Plot of BDE *versus* conversion, all substrates included.

Even after excluding the single outlier above a linear correlation still was not observed, but a scattering of points (**Chart 6**). The α -fluorotolyl substituted aryl chlorides used in the preliminary Hammett study (**Figure 30**) did, however, display a very weak trend ($R^2 = 0.39$ – orange squares, **Chart 6**). This suggests that BDE, as with the Hammett studies earlier (**Chart 3**), may be used to predict trends within similar series of compounds. Unfortunately, this predictive capacity does not translate to aryl chlorides with significantly different substituents.

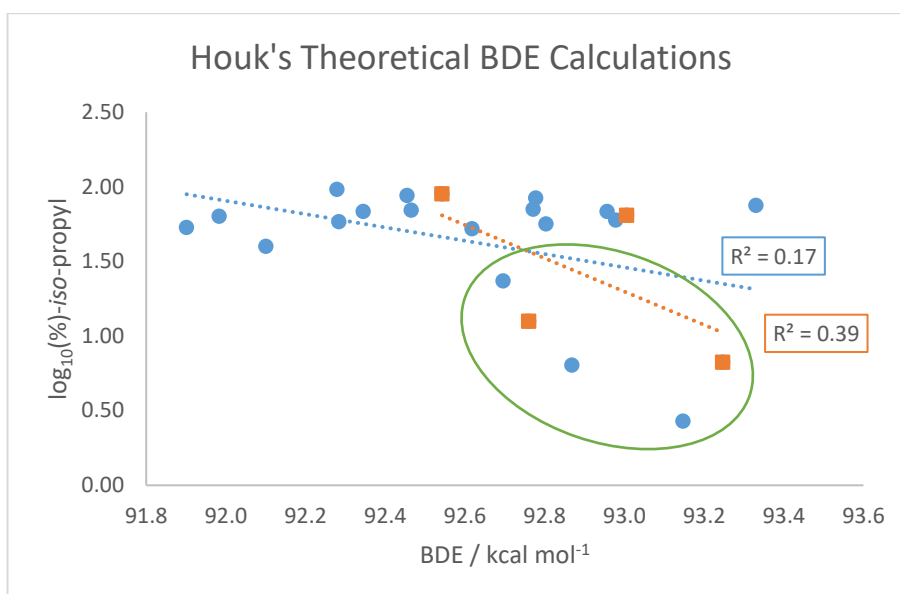


Chart 6. Plot of BDE *versus* conversion, outlier removed. Electron rich substrates (highlighted) demonstrate lower conversion, but similar BDE to other aryl chlorides.

These results suggest that BDE has little influence on the reactivity of aryl chlorides in this iron-catalysed cross-coupling procedure. This may be due to the small variation observed in BDE across the series of substrates tested. The calculated BDE values displayed very little spread across the series of aryl chlorides. Switching from an electron donating group (EDG), such as *para*-methoxy **188** to an electron withdrawing group (EWG), such as *para*-trifluoromethyl **269**, only increased the BDE by 0.7 kcal mol⁻¹. This could explain the challenges observed when attempting to correlate BDE values with conversion, especially when the error with DFT calculations can be around 1 kcal mol⁻¹. The varied characteristics of the aryl chlorides tested could also limit the usefulness of a property such as BDE to predict/understand reactivity.

BDE has been used to understand barriers to OA in cross-coupling reactions (**Scheme 63**). However, most investigations have compared different halides and/or pseudohalides, rather than different substituents upon the reactant (**Figure 34**).¹³⁶ The BDE difference observed by changing leaving group was shown to be within the 0.1-1 kcal mol⁻¹ range discussed above.

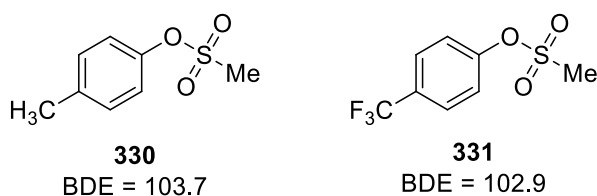
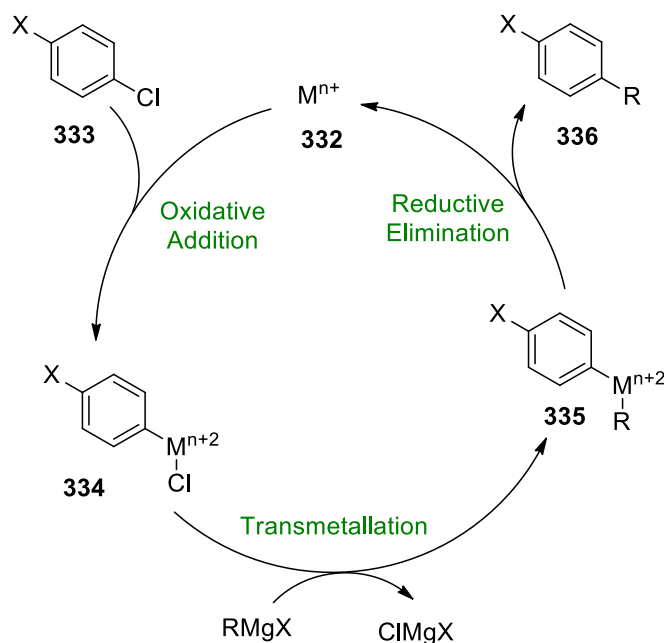


Figure 34. Zheng's investigation of the BDE of sulfonate leaving groups (wb97XD, kcal mol⁻¹).

4.2.1.2. Computational Investigation of LUMO Energies

Although the previous investigation demonstrated that BDE had no significant effect upon reactivity, the observed trend between BDE and Hammett's σ_m (**Chart 4**) suggested that other molecular properties may be used to investigate differences in reactivity. The electronic nature of the aromatic group appeared to have a major effect upon the efficiency of the cross-coupling reaction. Electronegative and electropositive substituents on the aryl chloride should influence the energy of the FMOs. This could cause a variation in the potential for OA, transmetalation or RE in a catalytic cycle (**Scheme 63**).



Scheme 63. Typical catalytic cycle in a Kumada cross-coupling reaction.

It was possible to determine the theoretical LUMO energies of all coupled aryl chlorides using the methodology applied by Dixon *et al.*¹³⁹ Gas phase calculations demonstrated moderate correlations between $-E_{\text{LUMO}}$ and Hammett σ -constants, with both σ_m (blue circles, **Chart 7**) and σ_p (orange squares, **Chart 7**) giving R^2 values of around 0.6 to 0.7.¹²⁸ The trend observed here displayed an improved correlation compared to the previous BDE/ σ -constant comparison in

Chart 4; a higher R^2 value was given for σ_m in the earlier analysis but this could be related to a large grouping of data at low BDE/high σ -constant.

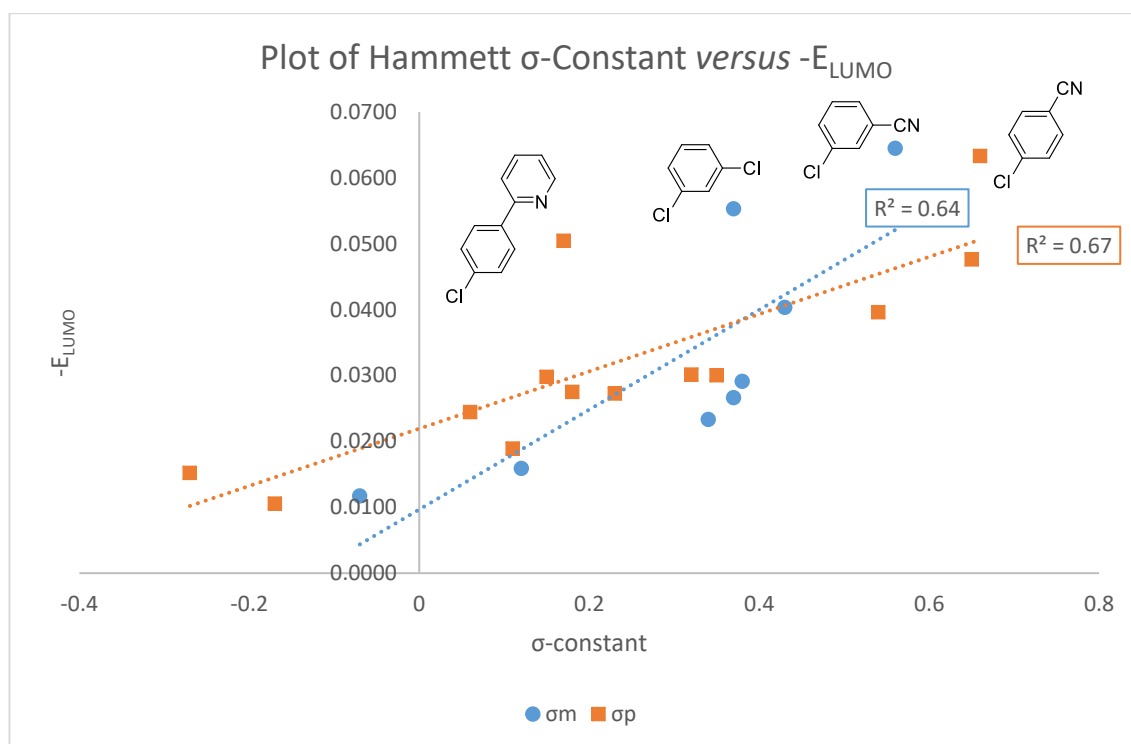


Chart 7. Plot of Hammett σ -Constants versus $-E_{LUMO}$. Outliers marked on the plot close to their respective points.

With the correlation between E_{LUMO} and σ -constants both σ_m and σ_p appeared to fall on a similar linear trajectory. This was unlike earlier Hammett-type studies, or BDE/ σ -constant comparisons, where the separation of σ_m and σ_p was required as *meta*-substituents appeared to behave differently to their *para*-analogues. This suggested that it may be possible to recombine the data for further E_{LUMO} investigations.

When plotting $-E_{LUMO}$ against $\log_{10}(\%)-iso$ -propyl a trend began to emerge; lower $-E_{LUMO}$ values gave reduced conversion to the desired product (**Chart 8**). This trend could be fitted by a second-order polynomial, giving an R^2 value of 0.8. Some significant data grouping was observed, especially where $-E_{LUMO} \approx 0.025$ eV, probably because many the substrates tested fell within this region. Notable is the apparent drop-off at higher $-E_{LUMO}$, the curve appears to fit well, but the data may be better represented through a linear relationship beyond $-E_{LUMO} = 0.04$ eV. The data falls into 3 regions:

- $-E_{LUMO} \leq 0.02$ eV: where all reactions gave low productivity
- 0.02 eV $>$ $-E_{LUMO} \leq 0.03$ eV: where most reactions gave high productivity
- $-E_{LUMO} \geq 0.04$ eV: where all reactions gave high productivity

This appears to be the foundation of a triage method. Unfortunately, the data does not fit well with several the substrates displaying $-E_{LUMO} \approx 0.025$ eV.

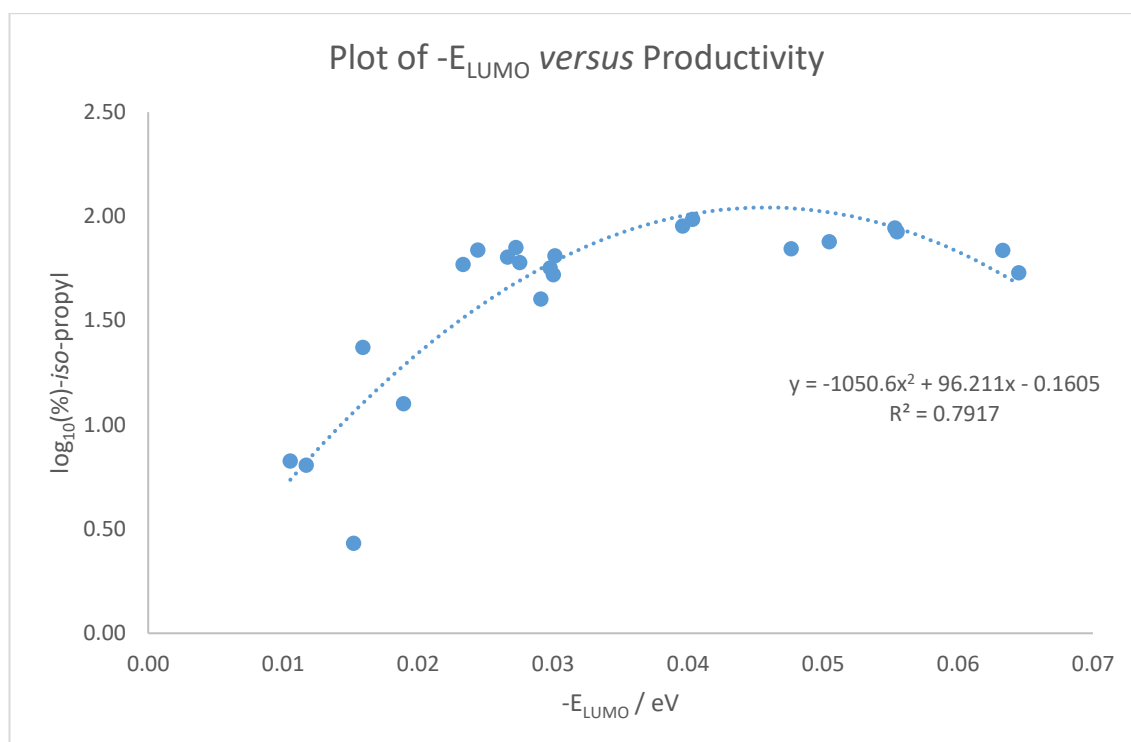


Chart 8. Plot of Hammett σ -Constants versus LUMO Energy for *meta*- and *para*-Substituted Aryl Chlorides.

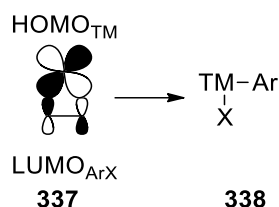
Dixon earlier noted the ability to correlate E_{LUMO} with EA through the relationship in **Equation 4**. This could mean that the EA of a molecule, rather than its E_{LUMO} , could be used to investigate the observed trends in reactivity.

Equation 4.

$$EA_{calc} \approx -\epsilon_{LUMO}$$

4.2.1.3. Computational Investigation of Electron Affinity

Although BDE failed to give a meaningful correlation, the LUMO investigation did appear to be more promising. The OA step in a cross-coupling reaction involves a HOMO_{TM}-LUMO_{ArX} interaction between the active TM catalyst and aryl halide.¹⁴⁰⁻¹⁴³ The TM effectively donates electron(s) to the LUMO of the halide cross-coupling partner (**Scheme 64**, as described in **Scheme 61**).



Scheme 64. A possible HOMO-LUMO interaction between TM and ArX.

The FMOs of the aryl chlorides may be used to determine other fundamental molecular properties, as discussed by Dixon *et al.*. A molecule's E_{LUMO} has been shown to be linked to EA or reduction potential (RP), which are inversely correlated.¹⁴⁴ DFT orbital energy calculations often result in large errors, which depend strongly upon the employed approximations,^{145, 146} thus determining the energy of ground and excited state molecules separately may offer an advantage. The relationship described does begin to explain the improved trend when comparing E_{LUMO} with conversion (**Chart 8**).

EA can be determined in two ways using computational analysis:

1. Through the correlation:

$$EA_{calc} \approx -E_{LUMO}$$

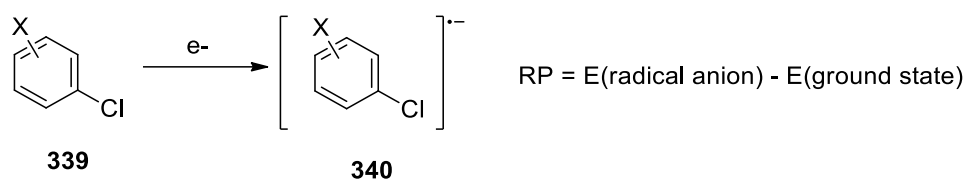
2. By investigating following energy difference:

$$RP_{calc} = E_{radical\ anion} - E_{ground\ state}$$

$$RP \propto -EA$$

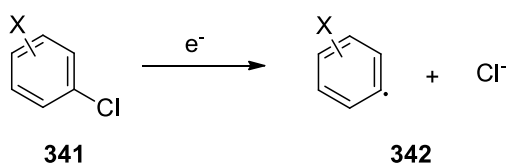
$$RP(V\ vs.\ SCE) = -(0.295 \pm 0.06) + EA$$

To avoid challenges related to DFT orbital energies Gillmore *et al.* carried out investigations where they calculated the RP of a number of organic molecules, including (hetero)aryl chlorides (**Scheme 65**).¹⁴⁷⁻¹⁴⁹ Through the use of a polarisable continuum model (PCM), which applies a dielectric constant to the calculation to model a solvent, they were able to obtain an excellent correlation between experimental and theoretical RP values.



Scheme 65. The method of determining a molecule's RP (or EA).

Application of Gillmore *et al.*'s methodology (B3LYP/6-31G(d)) led to challenges with structural optimisation; the aryl chloride radical anions were found to dissociate in both gas phase and PCM calculations (**Scheme 66**). Discussion with Dr. Greg Anderson (formerly University of Strathclyde) led to the selection of an alternative functional and basis set (M06-2X/6-311++G(2d,2p)), giving much higher success with the optimisations which failed before. It has previously been suggested that the Minnesota functionals (especially M06-2X) perform better with organic molecules than B3LYP, particularly when investigating excited states.¹⁵⁰⁻¹⁵² This could be related to the high proportion of Hartree-Fock (HF) exchange (54%) expressed within the functional. This lack of HF exchange in DFT calculations containing radical species has been shown to give spurious results, including non-linear alkynyl radicals.¹⁵³ The presence of HF exchange is thought to stabilise localised radical species, avoiding undesired orbital re-hybridisation, which led to the alkynyl radical bending observed by Carter.



Scheme 66. The observed chloride anion dissociation.

Comparing the uncorrected theoretical EA values with σ -constants gave a similar trend to LUMO comparison (**Chart 9**). A positive correlation was observed between both σ -constants and EA; systems with higher values of σ_p or σ_m have a larger EA. This observation relates directly to the derivation of Hammett's σ -constants – substrates which have a greater ability to stabilise a negative charge generally have a larger, more positive σ -value.

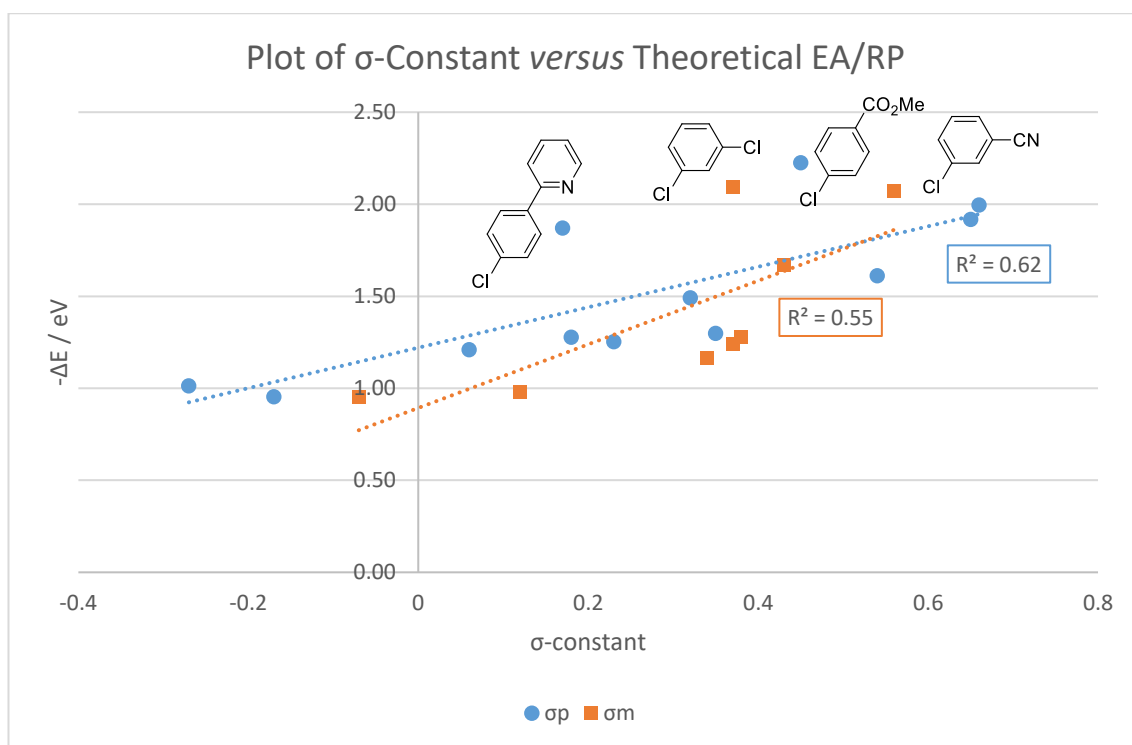


Chart 9. Plot of Hammett's σ -constant versus calculated RA, outliers shown.

The theoretical EA values were compared to conversion [$\log_{10}(\%)\text{-iso-propyl}$], giving a correlation which demonstrated significant curvature (**Chart 10**). Statistical analysis using JMP¹⁵⁴ suggested that an exponential 3-parameter model (**Equation 5**) could be used to fit the data, giving an R^2 value of 0.78. As with the $-E_{\text{LUMO}}$ correlation in **Chart 8** the data fell into 3 distinct regions (*vide infra*).

Equation 5.

$$y = a + b \times \text{Exp}(cx) \quad a = \text{asymptote}; b = \text{scale}; c = \text{growth rate}; x = (-)\Delta E/eV$$

$$a = 1.90; b = -482; c = -6.37$$

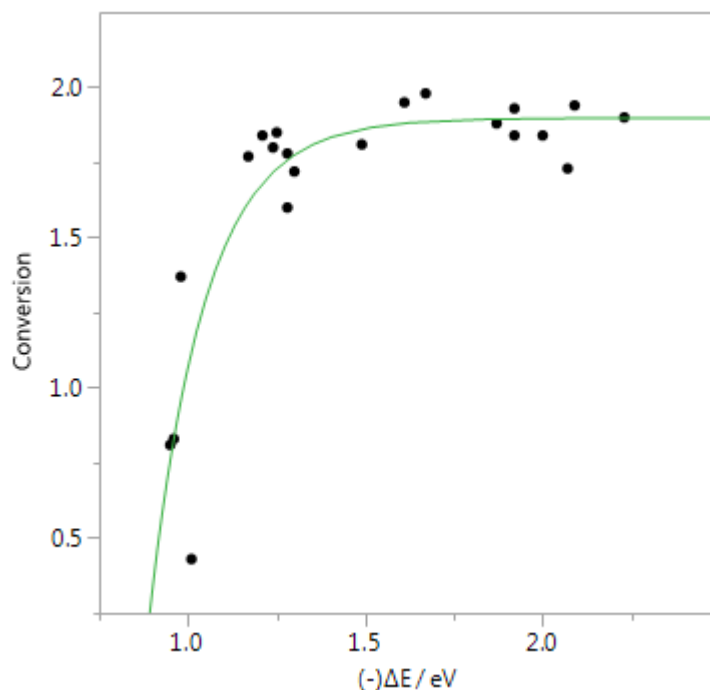
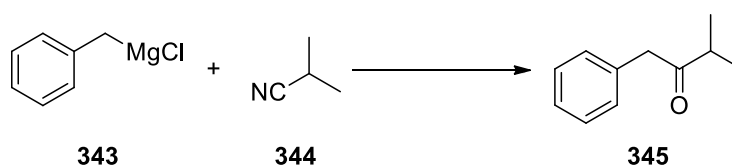


Chart 10. JMP plot for EA ($-\Delta E$) versus conversion ($\log_{10}(\% \text{-iso-propyl})$).

The coupled products are shown in **Figure 35**, with their conversion compared directly to calculated EA values. Highly electron deficient substrates were found to have EAs of around 1.8 to 2.1 eV; they also led to conversion of 70 to 90%. Highly electron rich substrates were found to have EAs of around 1.0 eV; they also gave conversions of 2 to 25%. Reactants with intermediate values of EA, between 1.2 and 1.7 eV gave conversion of 40 to 70%. The most significant outliers in this analysis were the nitrile substituted chlorobenzenes, which gave much lower conversion than expected. This may be related to undesired reactivity at the nitrile group, possibly leading to ketone formation (**Scheme 67**).¹⁵⁵



Scheme 67. Ketone formation from Grignard reagent and nitrile.

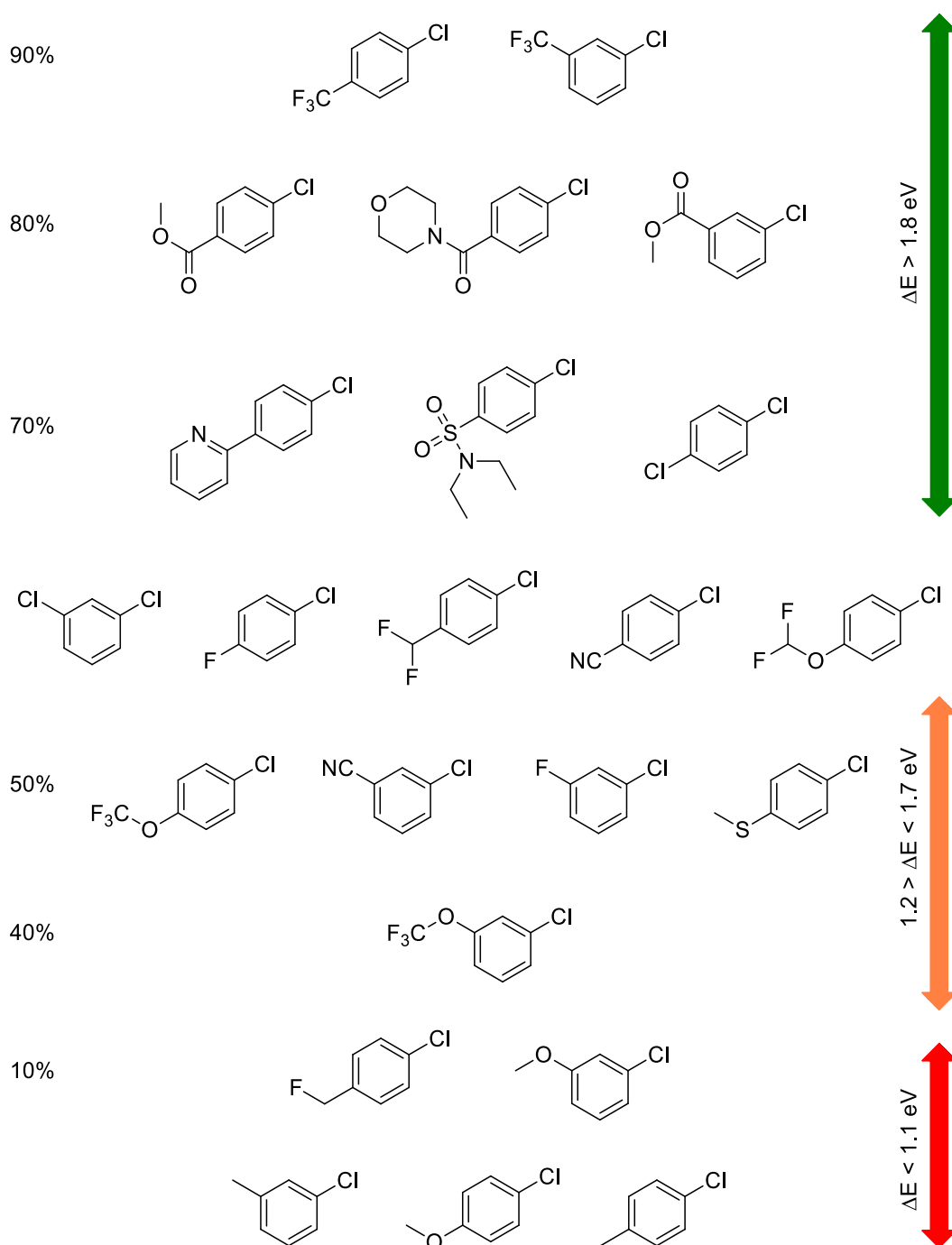


Figure 35. Conversion by GC (LHS), theoretical BDE (RHS).

A number of disubstituted chlorobenzenes were used to further test the correlation between EA and conversion. These substrates, and their associated EA/ $\log_{10}(\%)$ -*iso*-propyl values are shown in **Figure 36**. The new substrates were chosen to have varied electronic characteristics, with two EWGs in **346** and **349**, two electron rich groups in **347** and **348**, and a combination of both an EDG and an EWG in **350** and **351**. The combined effect of two strongly electron withdrawing trifluoromethyl groups in **346** promoted the reaction over a single trifluoromethyl group **268** and

269 (Figure 23). Having two inductively electron donating methyl groups also led to an additive effect, giving slightly poorer performance with **347** over **284** and **285**. Interestingly, the *meta*-fluoro substituent in **349** and **351** displayed relatively little effect on the outcome of the reaction compared to the non-fluorinated analogues **270** and **268**.

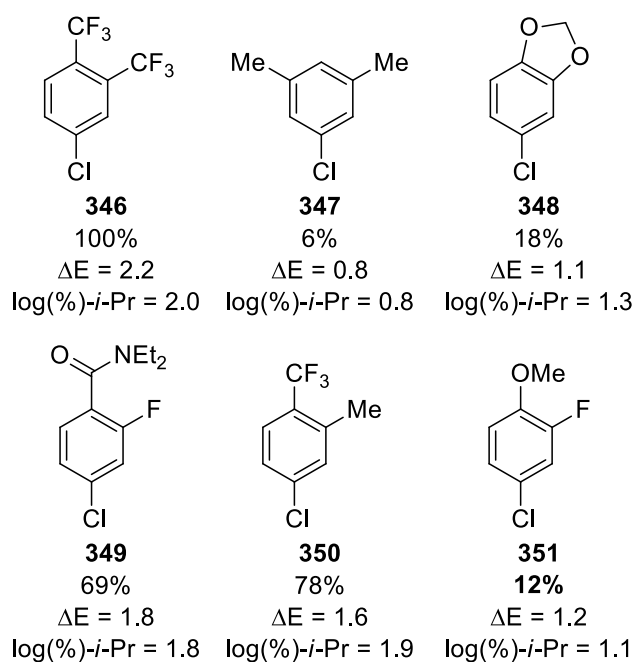


Figure 36. Substrates used to test the computational model's predictivity.

The new substrates were added to the exponential three-parameter fit (purple stars, **Chart 11**). The electron deficient substrates **346**, **349** and **350** displayed relatively good fit within the previous data. All gave high conversion to the desired product. Adding a second electron withdrawing trifluoromethyl group, in the case of **346**, further increased the conversion, with only one component observed by GC. The electron rich substrates also showed relatively good fit within the previous data. Electron rich substrate **347**, with the lowest calculated ΔE value, gave the poorest conversion to *iso*-propyl coupled product. The intermediate compounds **348** and **351** demonstrated the effect of an additional *meta*-substituent upon the parent alkoxybenzene. This observed *meta*-effect may be related to the increasing influence of the substituent as it moves towards the C-Cl bond.

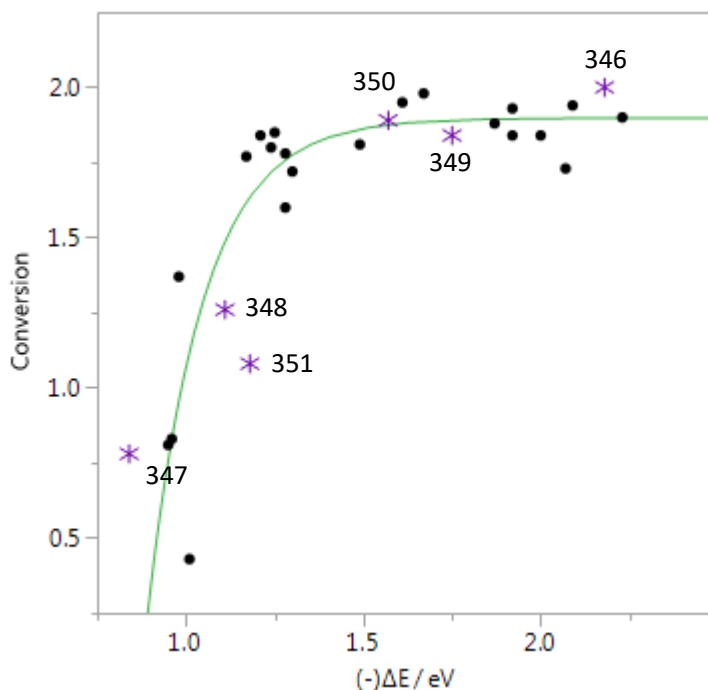
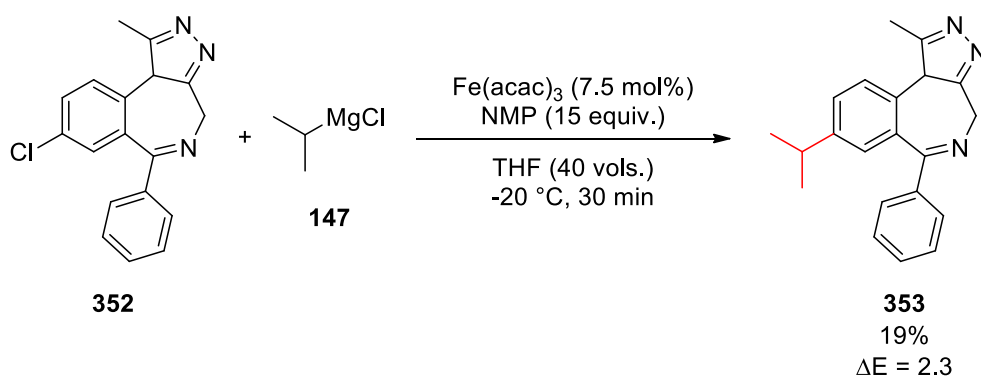


Chart 11. JMP plot with new substrates.

To further test the application of the EA correlation, a drug-like molecule was sought, and its EA was calculated before carrying out a cross-coupling reaction. Alprazolam **352** (**Scheme 68**) was found to have an EA of 2.3 eV. This should have resulted in high conversion to the desired *iso*-propyl product. However, the reaction led to a complex mixture of components, with only 19% product observed by LCMS. The major side-product in this reaction was hydrodehalogenated starting material. These results demonstrated a significant limitation for the use of EA to predict and understand reactivity. A simple property such as EA is unable to separate the desired cross-coupling from other modes of reactivity, much like the nitrile substrates.



Scheme 68. Alprazolam for a test of computational predictivity.

4.3. Conclusion

Several molecular characteristics were investigated as predictors for the iron-catalysed Kumada cross-coupling of *iso*-propylmagnesium chloride with aryl chlorides. Initially, BDE was tested, but the second functional group upon the substrate was found to have very little influence on this. The FMOs of the aryl chlorides were then investigated, and a weak non-linear correlation was observed between $-E_{\text{LUMO}}$ and $\log_{10}(\% \textit{iso}\text{-propyl})$, suggesting that this could be used to predict and understand reactivity. A relationship was found between $-E_{\text{LUMO}}$ and EA. A higher EA could lead to a more successful OA reaction. This relationship was further tested using Gillmore's method of calculating a RP, which is inversely correlated with EA. An improved relationship was observed, following the investigation of both ground state and excited state molecules according to the relationship:

$$RP_{\text{calc}} = E_{\text{radical anion}} - E_{\text{ground state}}$$
$$RP \propto -EA$$

It has been noted that DFT has some difficulty in calculating the E_{LUMO} of molecules due to the large number of approximations used. Therefore, calculating the energy of both molecules separately was considered to offer greater accuracy.

The correlation between EA and conversion was also found to hold for disubstituted aryl chlorides, and some predictivity was observed. However, when applying this method to the API alprazolam, the EA value obtained did not correlate with the conversion. This is probably related to side reactions with the substrate, which cannot be represented by such a simple computational model.

5. Investigation of Alternative Additives for Secondary-Alkyl Cross-Coupling

5.1. Introduction

5.1.1. NMP Replacement

Many iron-catalysed Kumada cross-coupling reactions use NMP to promote reactivity. This was first reported by Cahiez in 1998³⁴ following similar investigations with organomanganese reagents.^{33, 156} The 'NMP effect' is not well understood, but authors have proposed that it may act to solvate low-valent iron species and magnesium counter-ions or deagglomerate Fe⁰ nanoparticles.¹⁵⁷

There are sporadic reports of TMⁿ⁺(NMP)_{X_n} complexes, mostly formed by the dehydration of TM-chloride or perchlorate salts.¹⁵⁸⁻¹⁶¹ Researchers have also investigated adduct formation between FeCl₂ and NMP, demonstrating the formation of Fe₃Cl₆(NMP)₈ (**354**, **Figure 37**).¹⁶² The synthesis of this adduct required the preparation of a solution of FeCl₂.THF_{1.5} in NMP, thus the formation of the complex in the specified ratio is unlikely in a dilute ether solution, such as those used in cross-coupling reactions. The NMP has been shown co-ordinate *via* the carbonyl oxygen in all cases, giving a weakly co-ordinating ligand. Unfortunately, NMP has known reprotoxic effects on repeated exposure,¹⁶³ and its use is generally avoided in large scale pharmaceutical manufacture. The high boiling point of NMP, and its aqueous miscibility can also lead to significant challenges with purification of the product from an NMP-rich reaction mixture.¹⁶⁴

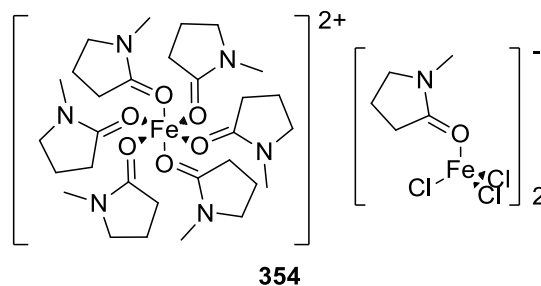


Figure 37. A Fe(NMP) adduct.

TM-catalysed cross-coupling reactions generally use well-defined ligands. These ligands are selected and developed following the vast amount of research carried out in the field of palladium catalysis in the last 50 years. Although iron-catalysed cross-coupling reactions predate their precious metal analogues, the field is much less advanced.^{129, 130, 165} Very little is understood about the active catalytic species, the oxidation state required for catalysis, or the effect of associated ligands have upon these factors. This is due to the complex redox behaviour of iron,

with oxidation states reported between Fe^{-2} and Fe^{+6} (**Figure 38**), and its propensity to undergo SET processes (*vide infra*).¹³¹

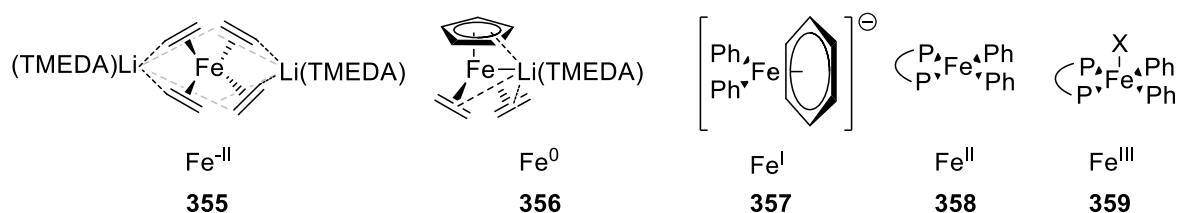
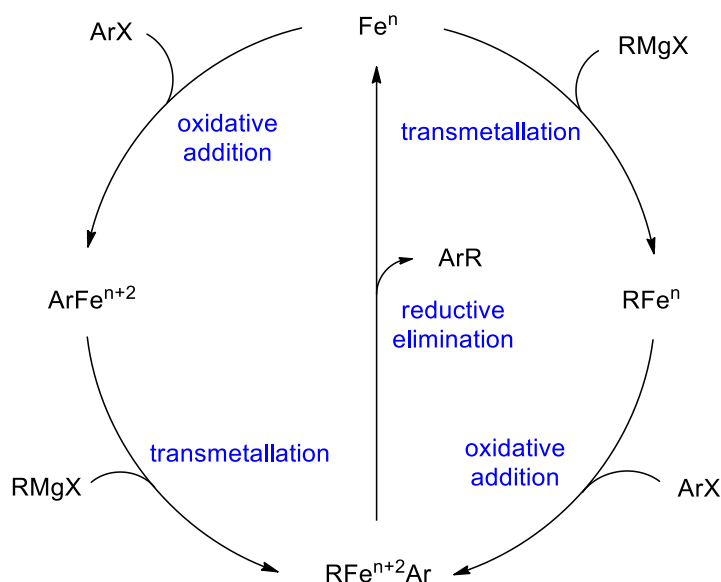


Figure 38. Some iron complexes displaying the variety of accessible oxidation states.

Many researchers have made mechanistic observations since the early discoveries, dating back to the 1940s. The first of these was J. Kochi, who proposed a catalytic cycle very similar to that of the canonical palladium-catalysed cross-coupling process. Two-electron OA, transmetallation and RE were discussed,¹⁶⁶ although the order of OA is still debated by Norrby and others (**Scheme 69**).^{129, 165}



Scheme 69. Norrby's discussion.

More recently, leading academics such as Fürstner, Bedford and Nakamura have demonstrated that a range of catalytic cycles can operate, depending strongly upon the nucleophile, electrophile and the presence of additional ligands. Detailed mechanistic investigations have been carried out by Neidig and co-workers, aiming to understand the nature of the sensitive catalytic intermediates formed in the reaction between iron pre-catalysts and organometallic species, such as Grignard reagents. However, to date this work has primarily discussed the formation of organoiron species from aryl or methyl Grignard reagents. These species are unable to undergo β -hydride elimination, which has been proposed to lead to the formation of the catalytically

active species with higher alkyl Grignard reagents. Several researchers have reported the formation of iron ate complexes in the presence of aryl, benzyl and methyl Grignard reagents; these species may be catalytically active, or resting states of the catalytic cycle (**Figure 39**).^{44, 45, 48, 167, 168}

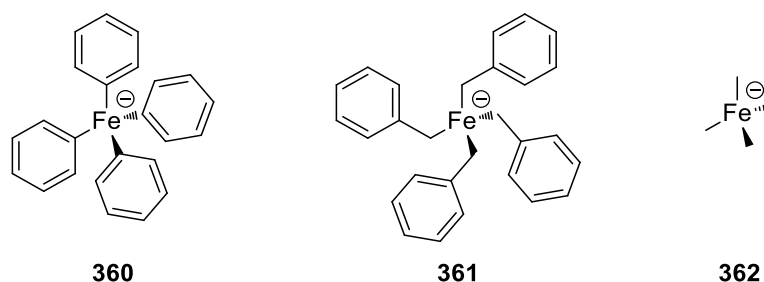


Figure 39. Some iron ate complexes.

In some early mechanistic investigations, Fürstner discussed the formation of an “inorganic Grignard reagent” **352** from the reaction between an alkyl Grignard reagent and FeCl_2 , as proposed by Bogdanović (**Scheme 21**).^{36, 37} These highly reduced organoiron intermediates were suggested to be the catalytically active species in a Fe^{-2} - Fe^0 catalytic cycle. Fürstner’s proposals relating to the catalytic activity of Fe^{-0} were disputed by Norrby, as discussed in **Chapter 2**. Norrby carried out computational studies using DFT, which suggested that RE from Fe^0 to Fe^{-II} was prohibitively high in energy.³¹ It is unlikely, based upon Norrby’s findings, that Grignard reagents can promote the formation of Fe^{-0} .

In the presence of ligands, such as phosphines or NHCs, and absence of Mg^0 , oxidation states <0 have not been observed.^{129, 130, 165} Instead, authors prefer a Fe^{II} - Fe^{III} or Fe^I - Fe^{III} catalytic cycle. Nakamura has invoked radical pathways for the coupling of aryl Grignard reagents with alkyl halides (**Scheme 27**).^{46, 47} With higher alkyl Grignard reagents, however, such as ethylmagnesium chloride the reaction may proceed via a 2-electron process, as described in **Scheme 69**.^{53, 54}

Many of the reports related to iron-catalysed cross-coupling describe the reaction between primary alkyl and aryl species. The focus of **Chapter 3** was the discovery of mild and scalable conditions for the secondary alkylation of aryl and heteroaryl chlorides. Unfortunately, this protocol was limited to the preparation of *iso*-propyl substituted (hetero)aromatics. Another interesting pharmaceutically relevant alkyl substituent is the cyclopropyl group. The focus of **Chapter 5** is to investigate the replacement of NMP for the formation of *iso*-propyl substituted (hetero)aromatics, and to explore the expansion of this methodology to cyclopropyl substituted (hetero)aromatics.

5.1.2. Cross-Coupling of Cyclopropyl Nucleophiles

Numerous natural products contain the cyclopropyl group; it is a privileged motif, used by researchers in the discovery of pharmaceutical and agricultural products.^{169, 170} Traditional methods for the introduction of a cyclopropyl group have generally limited its use in drug discovery, as carbene chemistry was often required.¹⁷¹

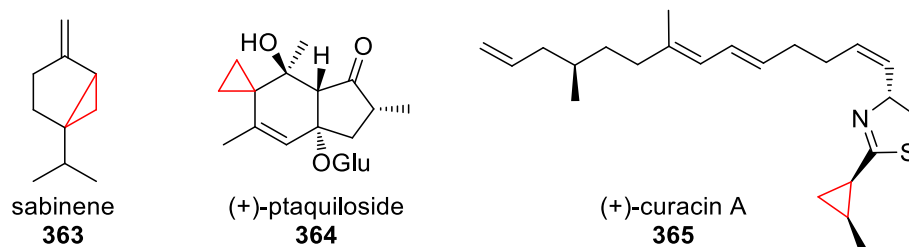


Figure 40. Some cyclopropyl containing natural products.

In recent years, the cyclopropyl ring has often been used as an alkyl bioisostere in pharmaceutical research due to improved metabolic stability owing to increased C-H bond strength.¹⁶⁹ Much like the *iso*-propyl group, the synthesis of drugs containing (hetero)aryl-cyclopropyl linkages generally utilises out-dated protocols, where the cyclopropyl motif is installed during ring formation (**Figure 41**).^{172, 173} This leads to lengthy linear synthetic routes for the preparation of cyclopropyl drug analogues. This is an unfavourable process in medicinal chemistry laboratories, where divergent methods are preferred. Medicinal chemists may wish to investigate numerous secondary alkyl motifs at a specific position on a heteroaryl substrate. The introduction of such a group at an early stage of the synthesis would limit throughput – a method for late stage functionalisation would be more time efficient, and enable higher throughput.

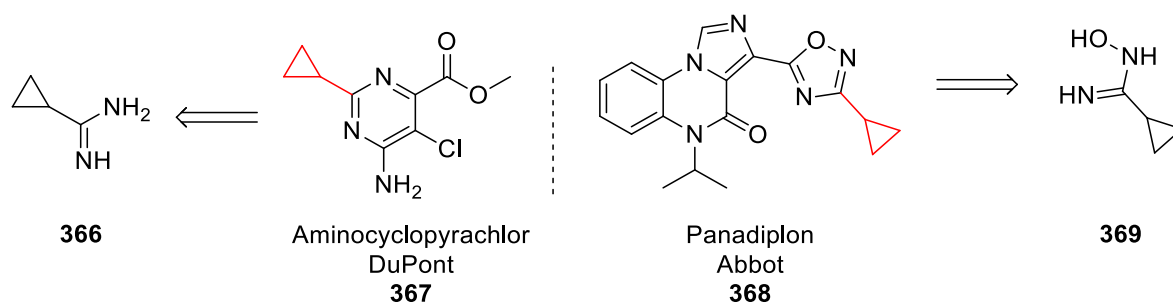


Figure 41. Synthesis of cyclopropyl containing drugs.

The installation of a cyclopropyl group using TM-catalysed cross-coupling would offer a significant advantage over the traditional alternatives. In fact, cyclopropyl containing drug candidates have increased in prevalence since the discovery of the Suzuki reaction (**Figure 42**).¹⁷⁰ The use of a simple, bench stable cross-coupling partner such as cyclopropylboronic acid or cyclopropyl

tetrafluoroborate has facilitated this. However, the cyclopropyl group continues to represent a significant challenge in cross-coupling reactions. This is due to a difficult and protracted syntheses of the coupling partner and undesirable reaction pathways such as protodemetalation of the organometallic reagent.¹⁷⁴ Cyclopropyl boronic acid can be prepared from a Grignard or organolithium reagent *via* transmetalation;^{175, 176} it would therefore be more economical to use this directly in synthesis.

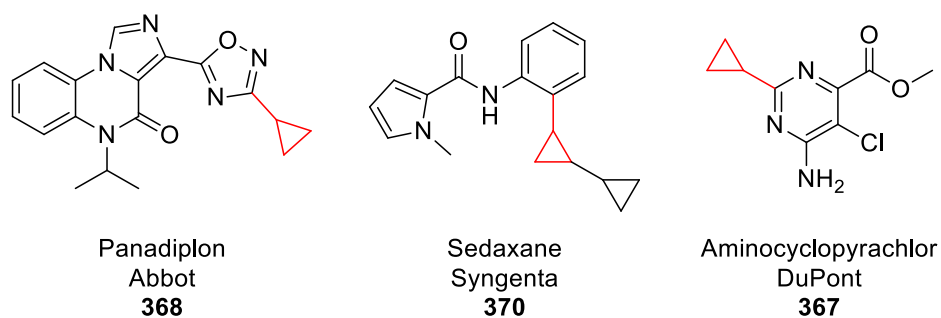
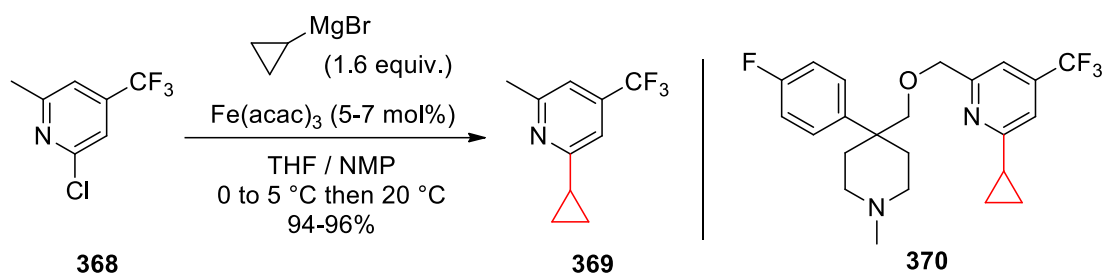


Figure 42. Some cyclopropyl containing drug candidates.

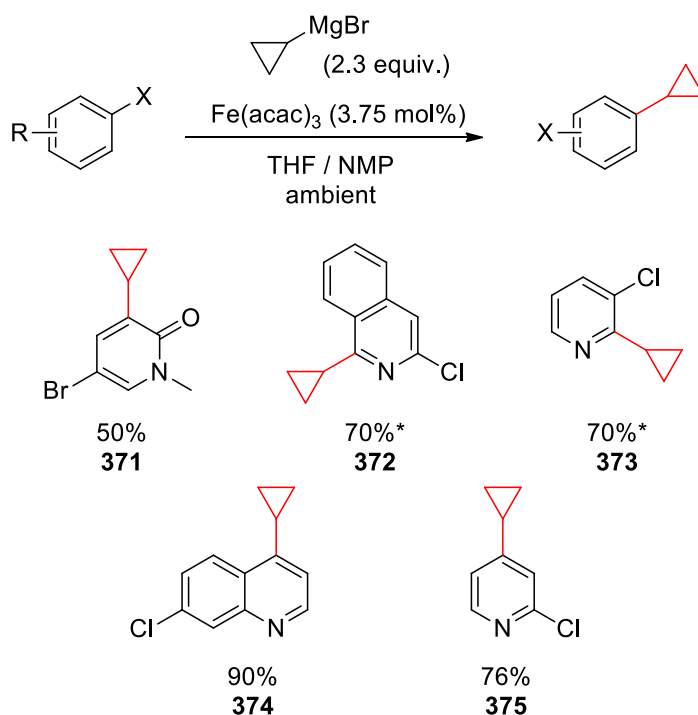
Many recent (hetero)aryl-cyclopropyl drugs have been prepared using palladium catalysis, again due to the synthetic utility of organoboron coupling partners. As discussed in the earlier chapters, there has been a drive to replace precious metal catalysts with earth abundant ones. There are many reasons for this, the most significant of which are the cost and toxicity associated with heavier TMs. There are very few examples of iron-catalysed (hetero)aryl-cyclopropyl cross-coupling in the literature. Only 3 research groups have reported such a reaction; 1 of these was directly related to the large-scale synthesis of pharmaceutically relevant compounds.

Risatti of Bristol-Myers Squibb reported a lengthy investigation into the development of a scalable route to a dual NK-1/serotonin receptor **370 (Scheme 70)**.⁶⁰ A major aim of this study was to replace a Suzuki reaction with an iron-catalysed Kumada cross-coupling. The new protocol utilised 5 mol% $\text{Fe}(\text{acac})_3$ in a THF/NMP solvent mixture at room temperature, rather than 10 mol% $\text{Pd}(\text{OAc})_2$ in combination with 20 mol% PCy_3 at 110 °C, to prepare advanced intermediate **369** from chloropyridine **368**.



Scheme 70. Risatti's cyclopropyl cross-coupling.

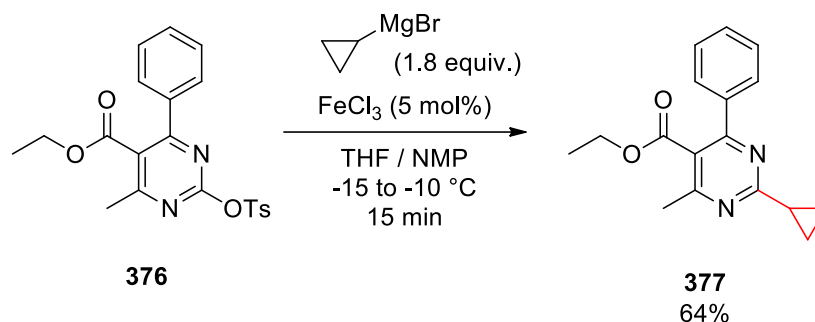
Malhotra, of Genentech, disclosed a chemoselective sp^2 - sp^3 cross-coupling protocol in the same year.¹⁷⁷ In this paper, methyl and cyclopropyl Grignard reagents were reacted with a number of dihalogenated (hetero)aromatics (**Scheme 71**). Like Risatti's report, the authors utilised $\text{Fe}(\text{acac})_3$ in a THF/NMP solvent system; some reactions proceeded in THF alone. Many of the cross-coupling reactions displayed similar chemoselectivity to alternative protocols, as described in the supporting information. With iron, the selectivity was found to be governed by electronic effects in most cases. Steric effects, however, became important with higher alkyl species, such as cyclopropylmagnesium bromide. Interestingly, the chemoselectivity could be switched with some coupling partners using either THF or a THF/NMP solvent system.



Scheme 71. Malhotra's cyclopropyl transfer (* no NMP).

Wang reported a further iron-catalysed cross-coupling procedure in THF/NMP following these early discoveries (**Scheme 72**).¹¹² The authors used FeCl_3 rather than $\text{Fe}(\text{acac})_3$ for the reaction of sp^2 electrophiles and sp^3 nucleophiles, but reverted to $\text{Fe}(\text{acac})_3$ when coupling sp^2 nucleophiles.

As mentioned in **Chapter 2**, this investigation focussed on the reaction between various Grignard reagents and several pyrimidinyl tosylates. Only one example of the reaction with cyclopropylmagnesium bromide was reported.



Scheme 72. Wang's FeCl_3 catalysed cross-coupling.

Although there are very few examples of iron-catalysed cyclopropylation in the chemical literature, several patents have demonstrated the use of $\text{Fe}(\text{acac})_3/\text{THF}/\text{NMP}$ to facilitate cyclopropyl addition (**Figure 43**).¹⁷⁸⁻¹⁸³ The chosen examples demonstrate the application of Kumada cross-coupling at numerous stages throughout the synthesis of drugs. Installation of the cyclopropyl group early in the process generally resulted in higher yields. Late stage functionalisation gave lower isolated yields, probably due to challenges with chemoselectivity.

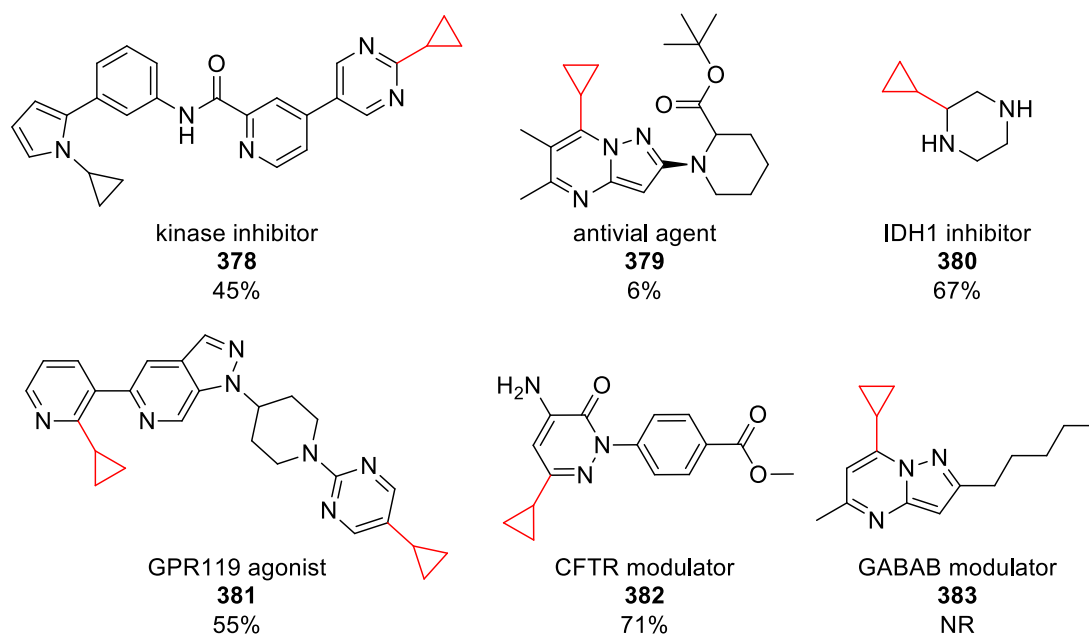


Figure 43. Recent patent literature demonstrating iron-catalysed cyclopropyl cross-coupling. Isolated yield in cross-coupling step displayed, NR = not reported.

As discussed earlier, NMP has known reproductive toxicity and is classed within the category 1 hazard class. GSK's solvent selection guide scores NMP with 4/10 for life cycle analysis overall;

the main contributors to this low score are high boiling point resulting in challenges with incineration (3/10), low availability of biotreatment (3/10) and NMP's reprotoxicity (1/10).¹⁸⁴ NMP is also listed by the European Chemicals Agency (ECHA) as a substance of very high concern, meaning alternatives must be sought for all applications.

It is notable that in all iron-catalysed processes utilising NMP, it is used as a co-solvent;^{25, 26} it is therefore present in stoichiometric or super-stoichiometric amounts. This leads to additional challenges with isolation and purification, as water is generally used to wash the NMP from the organic phase. This then results in further concerns with waste disposal, as the aqueous effluent is contaminated with high levels of NMP.

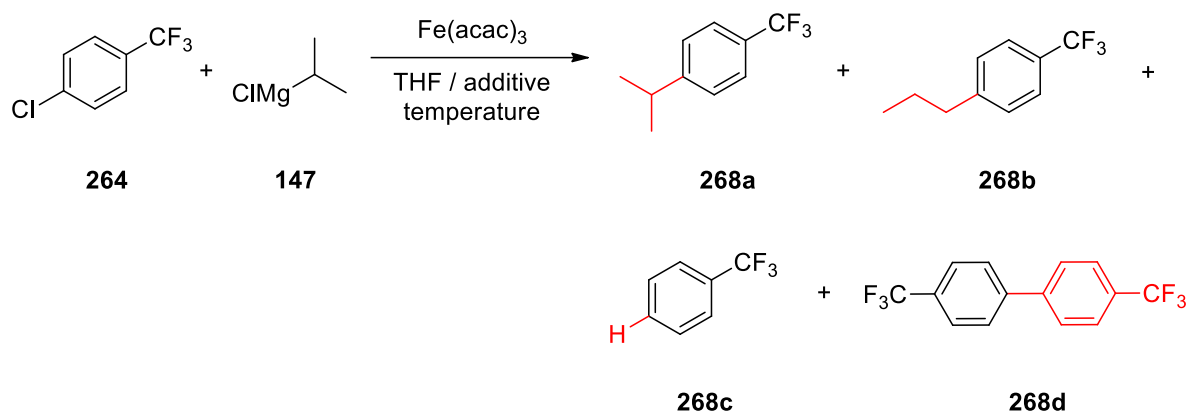
Two protocols were envisaged to avoid the use of NMP in iron-catalysed cross-coupling:

1. Search for an alternative co-solvent/additive using GSK's solvent selection guide (Section 5.2.1)
2. Search for a ligand, used in catalytic amounts, capable of facilitating cross-coupling (Section 5.2.2)

5.2. Results and Discussion

5.2.1. Investigation of Alternative Additives for the Cross-Coupling of iso-Propylmagnesium Chloride

A short investigation was carried out to explore the replacement of NMP with alternative additives. A series of reagents previously used in iron-catalysed cross-coupling procedures were tested to understand their effect upon the reaction between iso-propylmagnesium chloride and 1-chloro-4-(trifluoromethyl)benzene (**264**, Scheme 73).



Scheme 73. Products observed in the earlier DoE investigation.

15 additives were selected using either the GSK solvent selection guide, or following previous literature precedent (**Figure 44**).

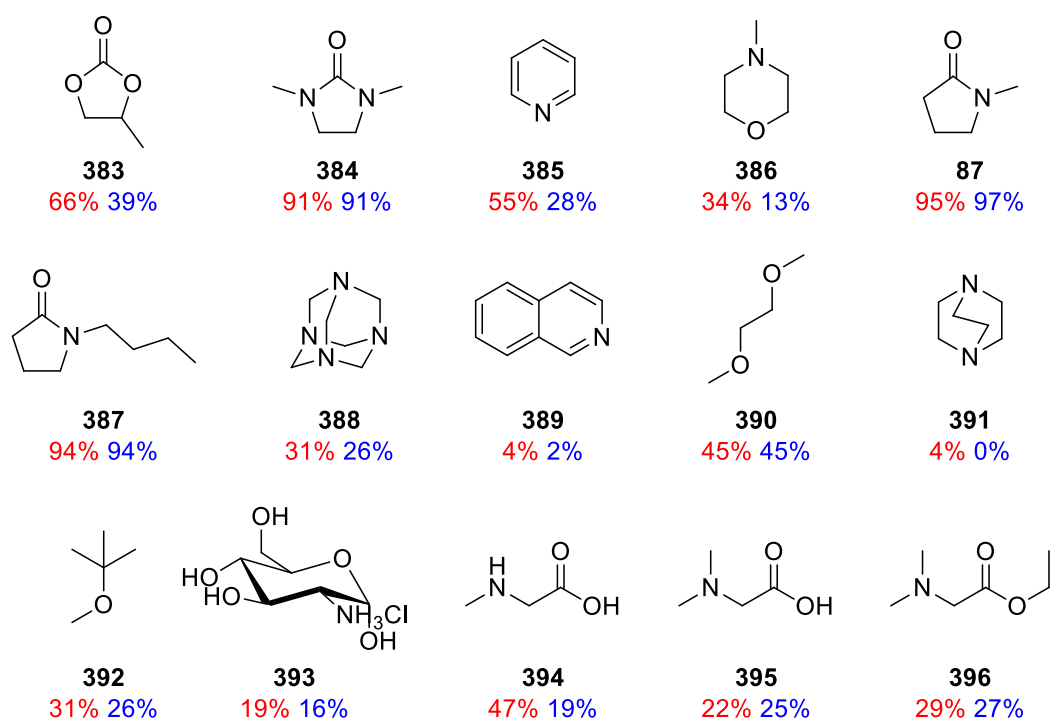
Propylene carbonate (**383**) is a highly desirable alternative to other dipolar aprotics. Its use has not been demonstrated in iron catalysis before, but a score of 10/10 in most factors on GSK's solvent selection guide meant it was chosen for this investigation.¹⁸⁴ 1,3-Dimethyl-2-imidazolidinone (DMEU, **384**) has also not been used in iron catalysis before, but it scores slightly lower on the health hazard scale of the solvent selection guide (4/10 *versus* 1/10 for NMP), so was also selected. Pyridine (**385**) has been used in combination with iron on numerous occasions, although not as an additive in a Kumada cross-coupling.²⁶ It was included due to the high activity of halo-pyridines in cross coupling. Could the co-ordination of pyridine to the Fe centre facilitate cross-coupling of other electrophiles? *N*-Methylmorpholine (NMM, **386**) was again selected to investigate the effect of nitrogen donor ligands to Fe.

NMP (**87**) was included as a comparison for the other solvents in this investigation. *N*-Octylpyrrolidinone (NOP, **387**) was added as an alternative to NMP. It has been proposed that alkyl chains longer than hexyl have no reproductive toxicity.¹⁸⁵ This has led to chemical company Eastman Chemicals marketing *N*-butylpyrrolidinone (NBP). NOP is significantly cheaper than NBP,

therefore was chosen for this investigation. 1,8-Diazabicyclo[5.4.0]undec-7-ene (DBU, **388**) and (DABCO, **391**) have been used in a number of reactions using iron, although generally as a base.²⁶ Like pyridine (**385**) and NMM (**386**) they were chosen to understand the effect of nitrogen donor additives on the cross-coupling reaction.

Isoquinoline¹⁸⁶ (**389**) has been used in iron-catalysed cross-coupling before, as have DME^{34, 187} (**390**) and *tert*-butyl methyl ether¹⁸⁸ (TBME, **392**). The remaining additives – glucosamine (**393**), methyl glycine (**394**), *N,N*-dimethyl glycine (**395**) and *N,N*-dimethyl glycine (**396**) – were all used by Časar in both cobalt- and iron-catalysed Kumada cross-coupling reactions.^{189, 190} If successful in promoting the reaction of *iso*-propylmagnesium chloride, they would offer a significant advantage over the other alternatives.

Additives with similar properties to NMP (**87**) gave the highest level of conversion to desired product, DMEU (**384**) and NOP (**387**) promoted efficient reactivity in both THF and 2-methyl THF. All other additives gave poor reactivity, excluding propylene carbonate (**383**), which gave moderate conversion in THF.



THF 2-MethylTHF

Figure 44. Additives tested in the iron-catalysed cross-coupling reaction. GC conversion.

Propylene carbonate is promoted within the GSK solvent selection guide due to its high boiling point and low toxicity.¹⁸⁴ The solvent was therefore selected for a simple DoE investigation; hydrodehalogenated material (**268c**) was the major product. The most productive reaction (**Table**

11) gave only 28% product (**Table 12**). The low catalyst and ligand loading compared to the earlier Fe(acac)₃/NMP reaction conditions is notable. Higher levels of catalyst or propylene carbonate only led to increased hydrodehalogenation.

Table 11. Reaction conditions giving the highest conversion for propylene carbonate.

Expt.	Run	Temp.	Cat. Mol%	Ligand eq.	Grignard eq.	Time	Conc.
9	29	-20	2.5	10	2	0	60

Table 12. Results from the reaction in **Table 11**.

Identity	Dehalogenated	SM	Product	Biaryl
GC Area %	53	11	28	8

Interestingly, all NMP-like solvents could promote the iron-catalysed cross-coupling reaction in both THF and 2-methylTHF, with very similar productivity. This is another preferred solvent, considered as a replacement for THF due to its low water miscibility and the ability to prepare it from renewable sources (furfural). DMEU was selected for a short DoE investigation, which showed that the combination of 2-methyl THF with DMEU gave less efficient cross-coupling than the previously optimised THF/NMP conditions.

The highest conversion in the DoE investigation was observed in a reaction at room temperature with high catalyst loading, and low concentration of substrate. This reaction also required significant levels of DMEU and 2 equivalents of Grignard reagent added over 30 minutes. Controlled addition may be preferred for large scale manufacture, but the required levels of the other variables precluded further investigation.

Table 13. Reaction conditions giving the highest conversion for DMEU.

Expt.	Run	Temp.	Cat. Mol%	Ligand eq.	Grignard eq.	Time	Conc.
32	14	20	10	300	2	30	60

Table 14. Results from the reaction in **Table 13**.

Identity	Dehalogenated	SM	Product	Biaryl
GC Area %	20	0	79	1

Following this series of experiments, it became apparent that a simple NMP replacement would be difficult to find. NOP or DMEU may be suitable replacements, but their similarity to NMP, and DMEUs reprotoxic risk phrase meant a more appropriate additive should be sought.

5.2.2. High-Throughput Chemistry for the Cross-Coupling of Cyclopropylmagnesium Bromide

Reactions catalysed by transition metals generally use well-designed ligands born from a vast wealth of knowledge in the field. The research carried out in the area of palladium-catalysed Suzuki-Miyaura cross-coupling reactions, for example, has driven the development of specialist ligands suited to a wide variety of cross-coupling partners (**Figure 45**). Unfortunately, the study of iron catalysis has only seen a significant resurgence in the last decade. This means that much less is known about the desirable characteristics of ligands.^{129, 130, 165}

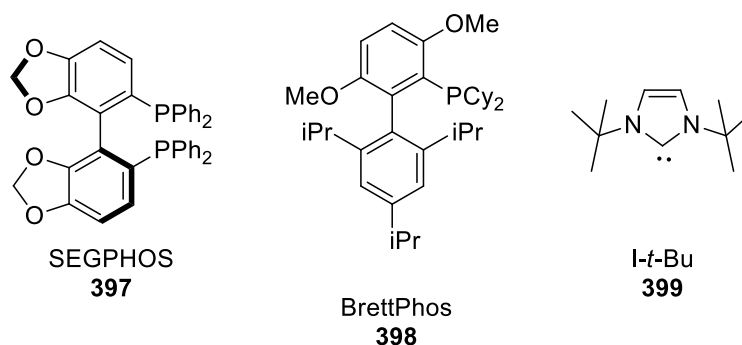


Figure 45. Some modern ligands for transition metals.

High-throughput chemistry (HTC) has been shown to give rapid results when investigating both bio- and chemo-catalytic processes.¹⁹¹⁻¹⁹⁴ By selecting a wide range of conditions, driven by prior knowledge, it is often possible to build up an understanding of the desirable properties related to catalyst/ligand combinations. An example of this was given in **Chapter 3**, where Molander and Dreher investigated the reaction between *iso*-propyl/cyclopropyl tetrafluoroborates and electronically varied aryl chlorides.¹⁹⁵ The authors found that the ideal ligand depended strongly upon the nucleophile. With cyclopropyl trifluoroborate, where isomerisation was not an issue, the ideal ligand was shown to be the sterically hindered, electron rich *n*-butyldiadamantylphosphine. However, with cyclopropyl trifluoroborate, where isomerisation was a major issue, the ideal ligands were shown to be the less sterically hindered, electron rich di-*tert*-butyl(phenyl)phosphine and tri-*tert*-butylphosphine (**Scheme 42**).

GlaxoSmithKline recently invested in high-throughput capability, introducing systems such as Mettler Toledo's QB5/QX96 weighing robot which is capable of weighing solid reactants and reagents into 30 vials or 48/96 well plates overnight.



Figure 46. Mettler Toledo Quantos QB5 instrument.

After reviewing the chemical literature, a series of 24 ligands were selected (**Figure 47**). They were chosen based upon previous reactivity, with a number of new systems added to investigate specific properties. Previous investigations have shown that redox active ligands can play a crucial part in the formation of an active catalytic species. This property gives the ligand the ability to stabilise catalytic intermediates which may otherwise be inaccessible.¹⁹⁶⁻¹⁹⁸

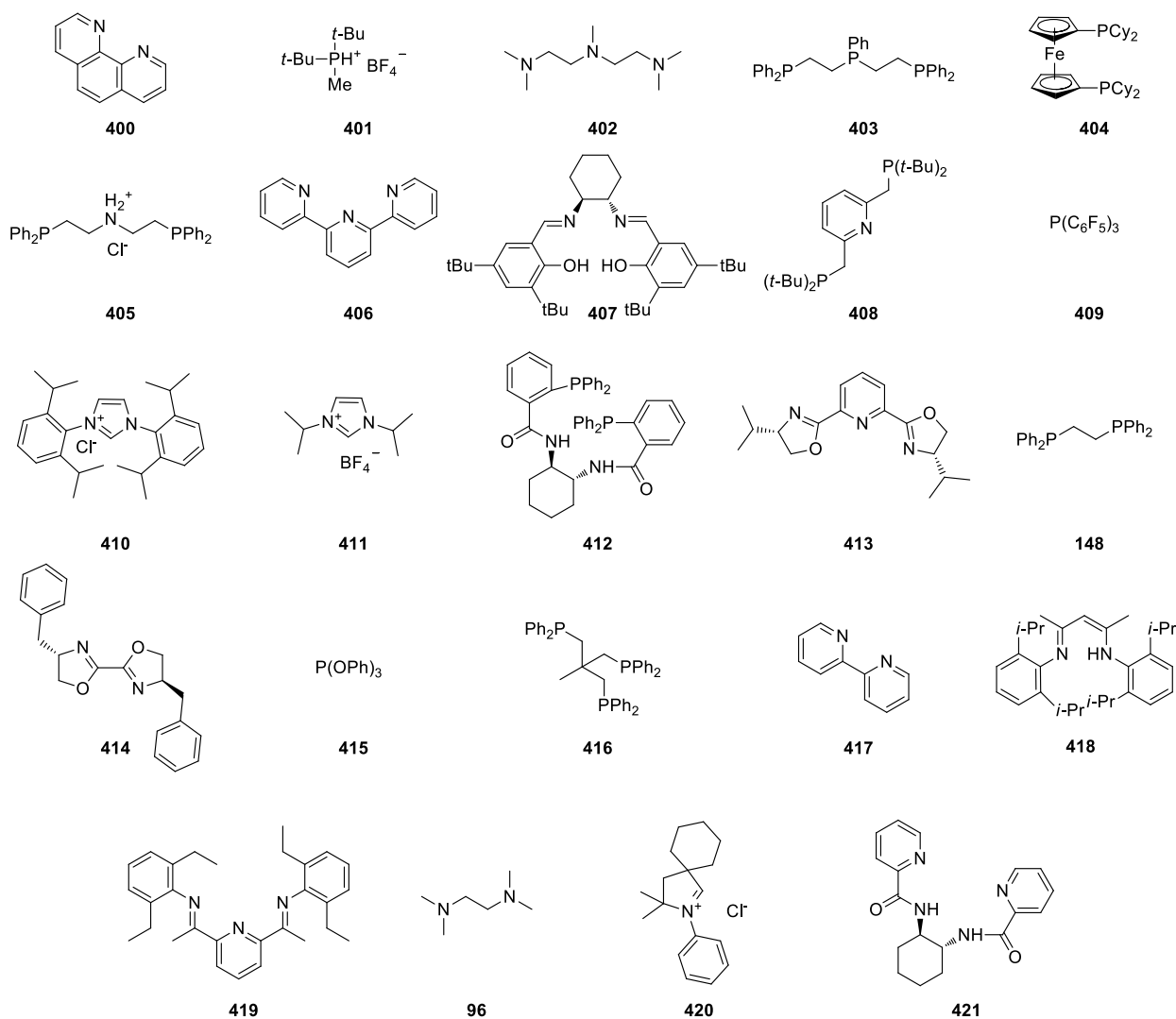


Figure 47. Ligands selected for high throughput screen.

Phenanthroline **400**, terpyridine **406** and bipyridine **417** have all been used in numerous iron-catalysed processes by other researchers.^{25, 26} They have not necessarily been used in cross-coupling reactions, but have been shown to facilitate C-H arylation using boronic acids¹⁹⁹ or aryl halides²⁰⁰ **400**, hydrosilylation^{201, 202} **406** and C-S cross-coupling²⁰³ **417**.

Monophosphines **401**, **409** were chosen as electron rich and electron deficient examples of standard phosphine ligands. The simple monophosphine PCy₃ was shown to promote the efficient cross-coupling of a homobenzylic ether by Shi.²⁰⁴ Phosphine ligands have been demonstrated to be efficient in numerous catalytic processes, especially with palladium in Suzuki reactions. Phosphite **415** was selected as a simple, cheap and bench stable alternative; they have been used successfully in several iron-catalysed reactions.²⁶ Phosphites, like phosphines, are σ -donors and π -acceptors. The presence of electronegative oxygen atoms, however, increases their π -acidity over σ -donor ability.

TMEDA **96** has been used on numerous occasions in the past,^{25, 26} with researchers suggesting that it coordinates to magnesium counterions in solution, rather than to the transition metal itself.⁴⁸ PMDETA **402** was therefore selected due to its similarity to TMEDA, but the ability to form 3 bonds with iron. The chelate effect may also mean that PMDETA is bound more strongly to Fe than TMEDA. PMDETA has been tested previously, in the reaction between aryl Grignard reagents and thioethers by Denmark.²⁰⁵ Triphosphine **403** and aminobisphosphine **405** were also used due to their similarity to TMEDA/PMDETA.

BOX **414** and PyBOX **413** have both been applied to iron-catalysed processes in recent years. BOX ligands have been shown to facilitate enantioselective radical couplings by Petrovic.²⁰⁶ PyBOX ligands have been used much more widely with iron, they have promoted Mukiyama Aldol reactions²⁰⁷ and aziridine formation,²⁰⁸ amongst others.

NHCs such as **409** and **410** have shown significant synthetic utility in iron-catalysed cross-coupling reactions.^{25, 26} This is due to their strong σ -donation,²⁰⁹ and therefore high affinity for iron.²¹⁰ cyclic alkyl amino carbene (CAAC) **420** was added to the screen as CAACs have been shown to be stronger σ -donors and π -acceptors than NHCs.²¹¹

Bisphosphines such as **404** and **148** have been demonstrated to be particularly useful – especially those with a wide bite angles (*vide infra*). Several authors have reported the synthetic utility of SciOPP ligand **422** (Figure 48) in cross-coupling reactions.^{50, 51, 212, 213} Trisphosphine **416**, may form a facial (fac) complex,²¹⁴ rather than the meridinal (mer) complexes that could be observed with PMDETA **402**,²¹⁵ trisphosphine **403** and aminobisphosphine **405** (Figure 48). Could this influence reactivity?

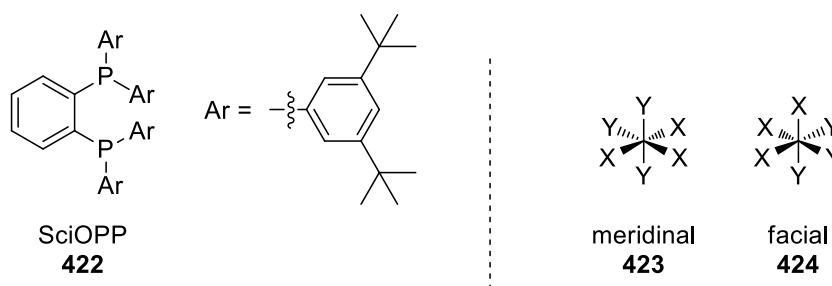


Figure 48. LHS: SciOPP ligand. RHS: meridinal and facial complexes.

PNP pincer complex **408**, nacnac **418** and pyridine diimine (PDI) **419** have all been used widely in non-precious metal-catalysis. They were chosen to determine their ability to promote this challenging cross-coupling. Pincer complexes have been championed by Milstein; early reports were focussed upon Ru-catalysed processes.²¹⁶ Fe(nacnac) complexes have been used widely in iron catalysis, most recently by Webster for hydrophosphination²¹⁷ and dehydrocoupling.²¹⁸ PDI

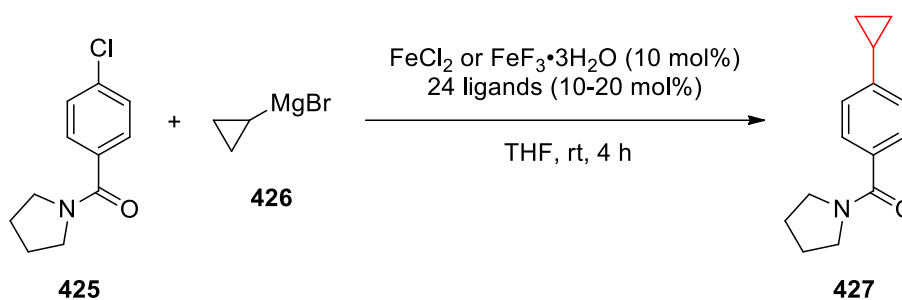
ligands have been exploited by Chirik for numerous processes including hydrosilylation, ammonia activation and ethylene dimerisation.²¹⁹⁻²²¹

Salen ligands such as **407** have also been shown to facilitate cross-coupling reactions with iron.^{35, 107} Trost ligands **412** and **421** are structurally similar to **407** and commercially available, unlike many of the salen ligands.

The ligands were combined with FeCl₂ and FeF₃·3H₂O, which are iron pre-catalysts known to be productive in iron-catalysed processes.^{25, 26} Iron halides were chosen in place of ligands such as acetylacetonate, as they were assumed to be less strongly bound to the Fe centre. Bidentate ligands generally have a stronger binding affinity due to the chelate effect;²²² Fe-O bonds also tend to be stronger than Fe-Cl bonds. Skinner and Connor showed that the enthalpy of formation of a M-Cl bond is around +120 kJ mol⁻¹, where the enthalpy of formation of a M-(acac) bond is around -200 kJ mol⁻¹.²²³ Gas phase Fe-O bond dissociation enthalpy of Fe(acac)₃ is reported to be 150 kJ mol⁻¹.²²⁴ Due to the octahedral coordination structure of Fe(acac)₃ ligand dissociation would be required to enable the binding of an incoming ligand. FeCl₂ and FeCl₃ also exhibit an octahedral structure in the solid state, formed through bridging chloride ligands. They may dissociate to monomeric FeCl₂ and FeCl₃ in solution phase, solvated by 4 or 3 THF molecules, respectively (for example). These solvent molecules should be more readily displaced by a strong donor ligand such as phosphines, carbenes or amines.

5.2.2.1. Screen 1 – Coupling of Cyclopropyl Grignard with Amide Substituted Aryl Chloride

The reaction between **425** and **426** (Scheme 74) was chosen for a preliminary investigation using the ligands introduced in Figure 47. Substrate **425** was selected for a number of reasons including challenges in monitoring side-product formation due to the volatility of the hydrodehalogenated side-product with 1-chloro-4-(trifluoromethyl)benzene **264**, and the low synthetic utility of alkyl-substituted α,α,α -trifluorotoluenes. Excellent chemoselectivity had also been observed previously in the reaction between primary- and secondary-alkyl Grignard reagents and aryl chlorides containing amide or ester substituents. Many APIs contain amide substituents, therefore any cross-coupling carried out in their presence may offer significant synthetic utility.

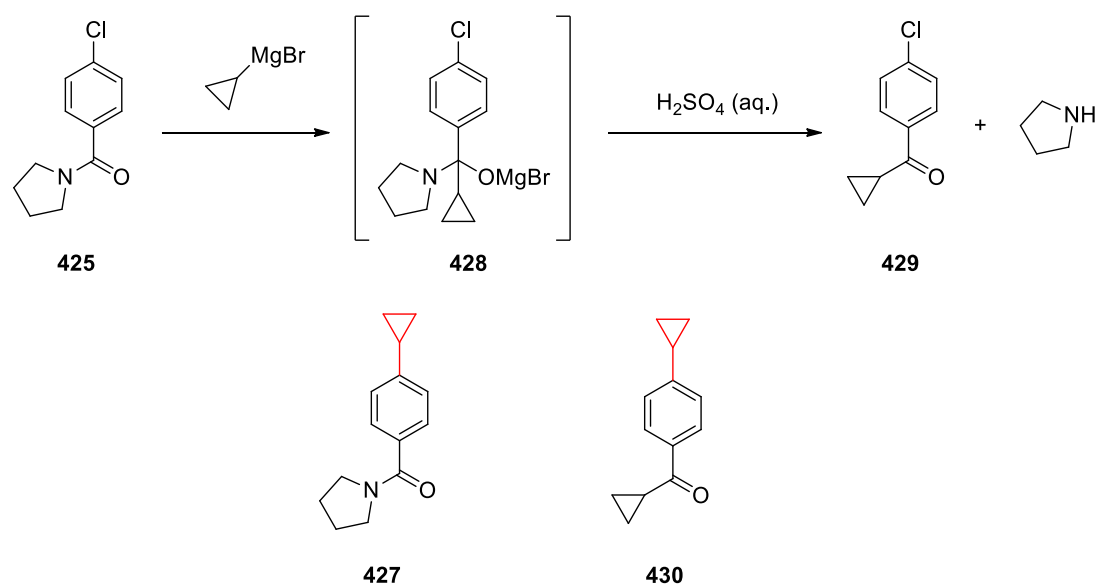


Scheme 74. Proposed reaction for the first high throughput screen.

The reactions were carried out using 10 mol% FeCl_2 or $\text{FeF}_3 \cdot 3\text{H}_2\text{O}$, combined with 10-20 mol% ligand. Bidentate, tridentate and tetradentate ligands were used at 10 mol% loading, in an attempt to promote the formation of a 1:1 FeX_n :ligand adduct. Monodentate ligands were used at 20 mol% loading to allow a 1:2 FeX_n :ligand ratio. All solids, including substrate, were weighed into HPLC vials using Mettler Toledo's QX96 robot. These HPLC vials were purged under nitrogen in a glove bag overnight. Liquid ligands were added to their respective vials using a Gilson positive displacement pipette. Anhydrous THF was then added using a multi-channel pipette. The catalyst/ligand/substrate mixture was stirred in solvent for 20 minutes before Grignard reagent was added using a multi-channel pipette. The reactions were stirred for 4 hours, then quenched with a pH 2 sulfate buffer, and sampled for HPLC and LCMS.

The major product observed in all 48 reactions was found to be cyclopropyl ketone (**429**, Scheme 75). This may occur because the cyclopropyl Grignard is more nucleophilic than others previously coupled under iron catalysis.²²⁵ The electron deficient nature of **425**, and the presence of magnesium counterions, also meant that collapse of tetrahedral intermediate **428** did not occur until work-up. At this point residual Grignard reagent was consumed, avoiding the formation of a

biscyclopropyl alcohol. Other researchers have also reported alkyl ketone formation from amides and Grignard reagents.²²⁶⁻²²⁸



Scheme 75. Observed reaction in the first high throughput screen.

Low levels of coupled product (**427**) were observed in some reactions at up to 6% by HPLC area (**Chart 12**). Ligand **404** was found to give the highest level of desired product in combination with $FeCl_2$. Additionally, some *bis*-cyclopropyl substituted product **430** was formed, suggesting that cross-coupling was competent with a number of ligands. Ligand **410** gave the highest conversion to this *bis*-cyclopropyl ketone with both FeF_2 and $FeCl_2$; this NHC also gave relatively good conversion to the desired product with $FeCl_2$.

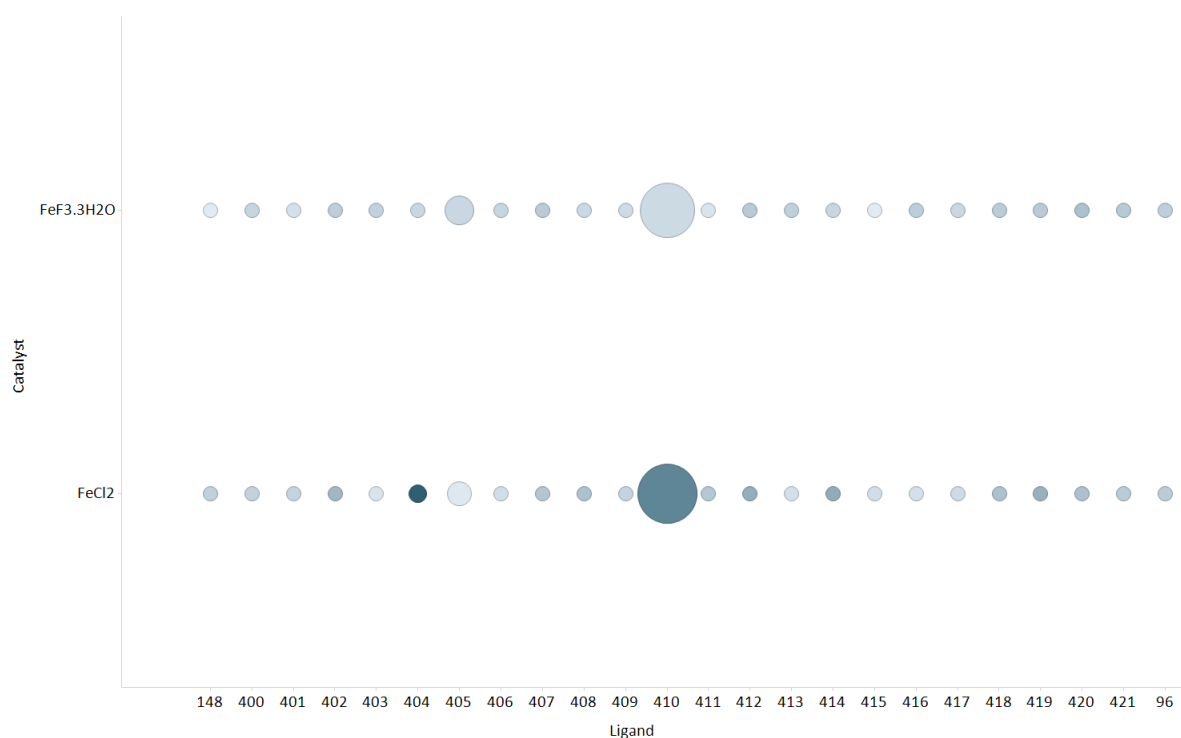


Chart 12. Chart to show results from reaction between **425** and **426**. Shade represents level of cyclopropyl ketone **427** (max = 6.4%), size represents level of *bis*-cyclopropyl ketone **430** (max = 20%).

Iron/NHC systems have been reported widely (*vide supra*); the σ -donor properties of these ligands are thought to lead to strong TM-NHC bonds. This may lead to a well-defined TM-NHC complex, which can stabilise the catalytic intermediates. NHCs such as SIPr, the saturated analogue of IPr **410** have previously been suggested to work synergistically with fluorides in $\text{FeF}_3 \cdot 3\text{H}_2\text{O}$ in a biaryl Kumada cross-coupling.^{111, 229} The fluoride counterion is proposed to reduce homocoupling, and the NHC ligand suggested to increase the rate of OA, and support the fluoride counterion in the suppression of homocoupling.

5.2.2.2. Screen 2 – Cross-Coupling of Cyclopropyl Grignard with 6-Chloroquinoline

In the earlier cross-coupling investigation, focussed upon *iso*-propylmagnesium chloride, heteroaryl chlorides were found to be more productive partners (**Chapter 3**). This is distinct from traditional cross-coupling protocols, where the reaction of heteroaryl halides often results in much lower conversion. Driven by these observations, along with the chemoselectivity problems discovered in the reaction with amide **424**, a chloroquinoline was chosen as a model substrate. 6-chloroquinoline **430** was selected as a challenging coupling partner; chlorine substitution on the pyridine ring is known to activate the C-Cl bond for cross-coupling reactions (**Figure 49**).¹⁷⁷

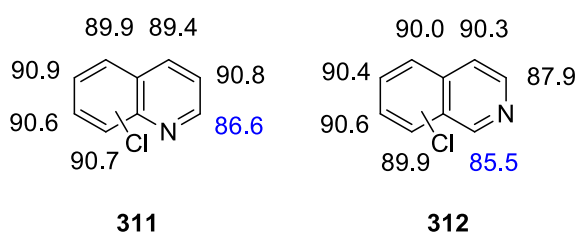
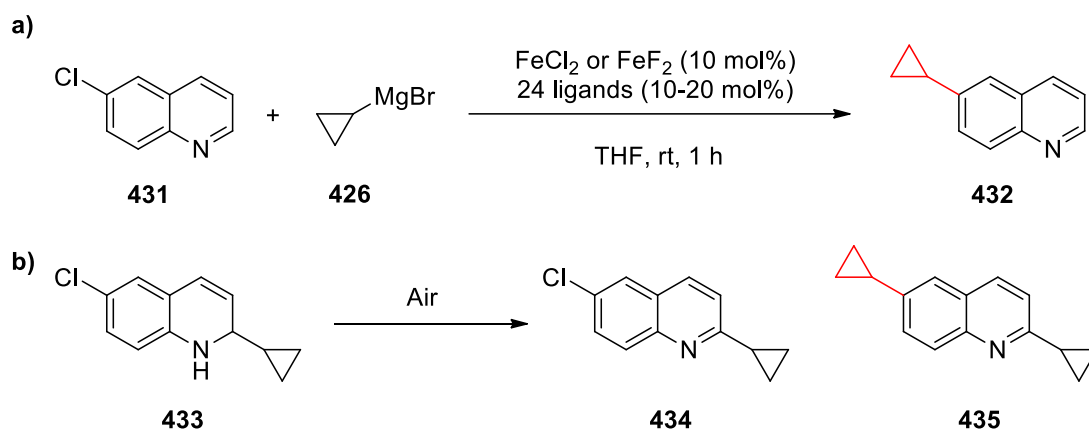


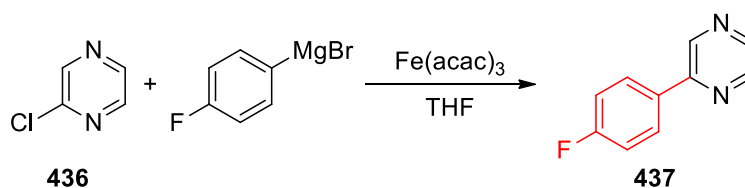
Figure 49. Houk and Merlic's BDEs of chloro-quinoline and -isoquinoline, preferred site of reaction highlighted (kcal mol⁻¹).

The reaction with 6-chloroquinoline **431** was repeated in an analogous manner to amide **425**. FeF₂ was used to replace FeF₃•3H₂O, following the poor reactivity observed in earlier screens. The nucleophilic nature of the cyclopropylmagnesium bromide led to the formation of a side product. This appeared to be an addition of a cyclopropyl group to the heteroaryl component of the quinoline ring giving dihydroquinoline **433** (observed by LCMS). This was found to oxidise readily to cyclopropyl-chloroquinoline **434**. Increased levels of adducts **433** and **434** were observed in reactions where FeF₂ was used as the pre-catalyst. Cross-coupled adduct **435** was also seen in several reactions.



Scheme 76. Proposed and observed reactions in the second high throughput screen.

The formation of adducts such as **434** has been proposed in earlier studies, especially with electron deficient substrates such as 2-chloropyridine **436**. This undesired reactivity has been tempered through the application of flow chemistry by Buono, fixing an intractable coupling with arylmagnesium bromides (**Scheme 77**).²³⁰ It is also notable that other authors coupling 2-chloroquinoline have blocked reactive positions, such as the 4-position, with a methyl group.²³¹



Scheme 77. Buono's flow investigation.

In this series of reactions **404** was found to give one of the highest conversions to desired product (**Chart 13**). This observation suggested that it produced a pre-catalyst with excellent properties for the cross-coupling of cyclopropylmagnesium bromide. **419** was also found to give very high reactivity, with slightly greater levels of the desired product formed in the reaction. Other ligands such as **410** and **414** gave moderate conversion. **420** was the only ligand capable of promoting cross-coupling in the presence of FeF_2 .

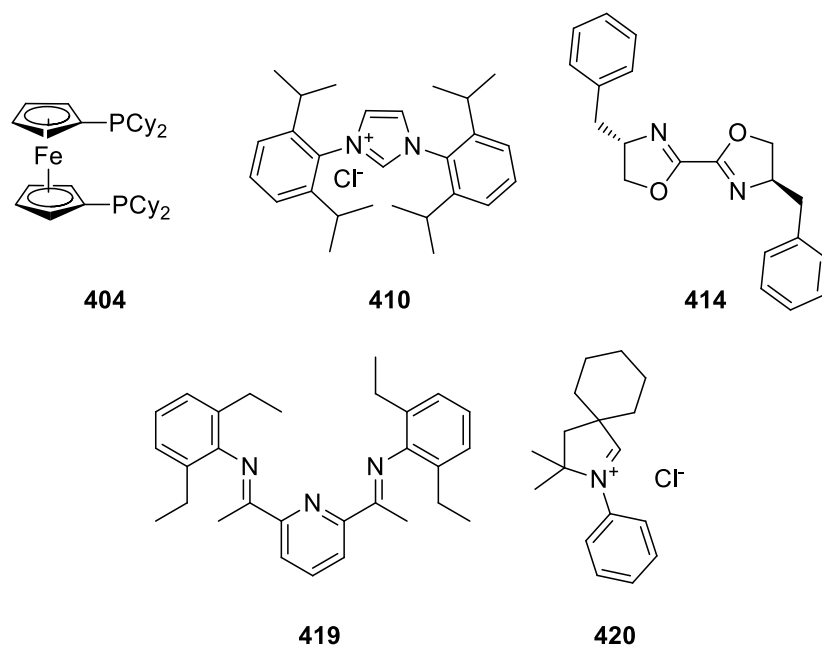


Figure 50. Key ligands in preliminary cyclopropyl screen.

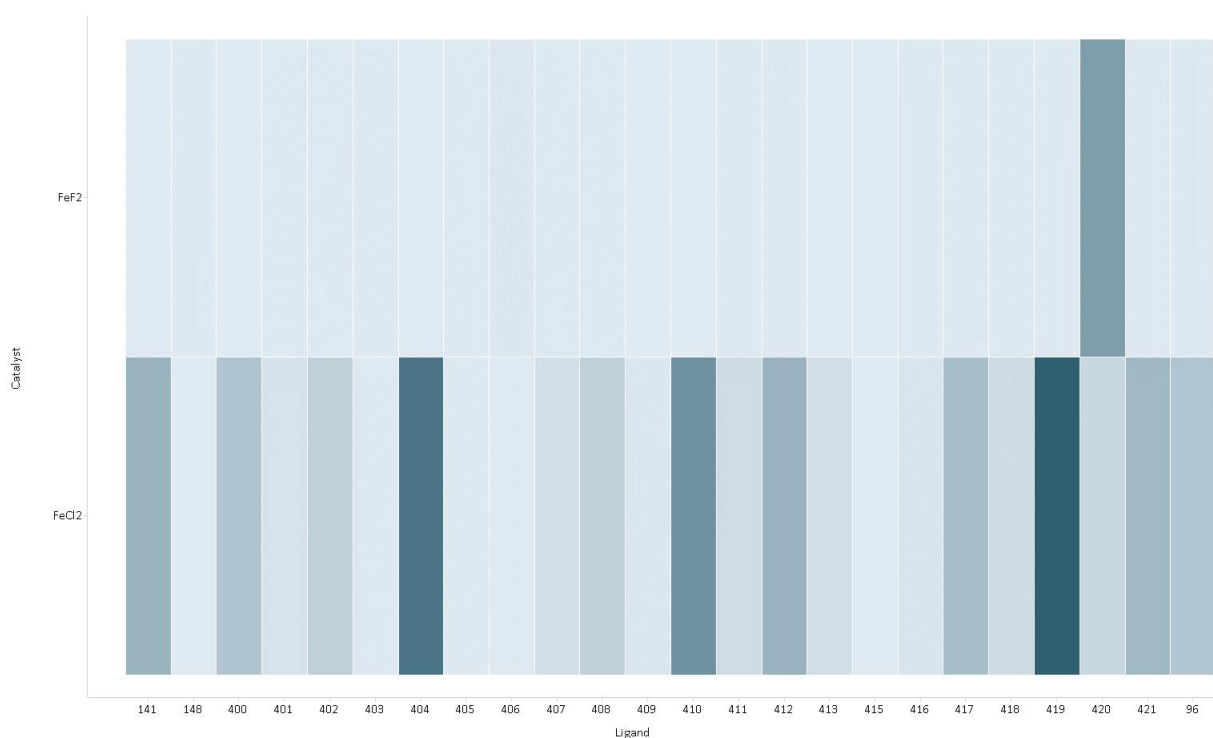


Chart 13. Results from Kumada screen 2. Shade represents conversion to desired product (max = 38%).

Although **419** gave the highest conversion, **404** was chosen to investigate further. This was due to the vast number of commercially available bisphosphine ligands, allowing rapid screening of numerous ligands in a smaller area of ligand space within a very short timeframe.

5.2.2.3. *Screen 3 – Focussed Ligand Screen for Cross-Coupling of Cyclopropyl Grignard with 6-Chloroquinoline*

The results from the previous screen suggested that wide bite-angle bisphosphines were efficient ligands to enable the cross-coupling between **431** and **426** (**Scheme 76**). To study their effect further, GSKs bisphosphine principal component analysis (PCA) model was used to select a series of readily available ligands. PCA is used widely in drug discovery and development to describe multivariate parameters using a 3-dimensional model. In this case, 29 descriptors were combined to create 3 principal components t_1 , t_2 and t_3 , plotted in **Chart 14**. This analysis is based upon the work of Fey, who calculated ligand knowledge bases (LKBs) for phosphorous,^{232, 233} nitrogen²³³ and carbon²³⁴ donor ligands. These axes describe 39%, 26% and 9% of the observed variability between ligands respectively, and can be used to select other ligands with similar or different properties, based upon their relative position in the plot.

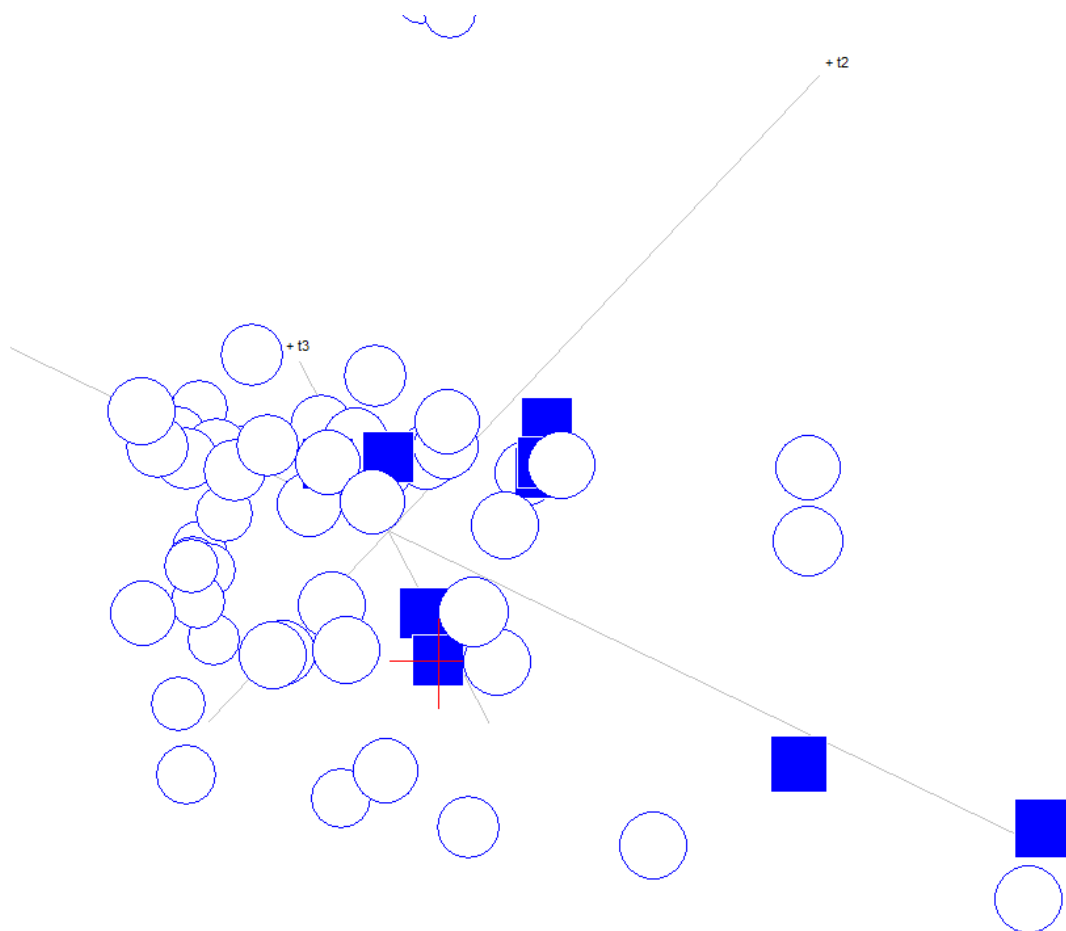


Chart 14. Ferrocene based ligand **404** highlighted by red cross.

The PCA model showed several systems which displayed similar characteristics to **404**. These are clustered around the previous ligand, and consist of mostly ferrocene-based ligands. A series of 12 ligands were selected based upon their likeness to **404**. The chosen ligands consisted of both ferrocene- and Xantphos-based ligands (**Figure 51**). These are known to have bite angles of between 100° (**438**) and 110° (**443**).²³⁵

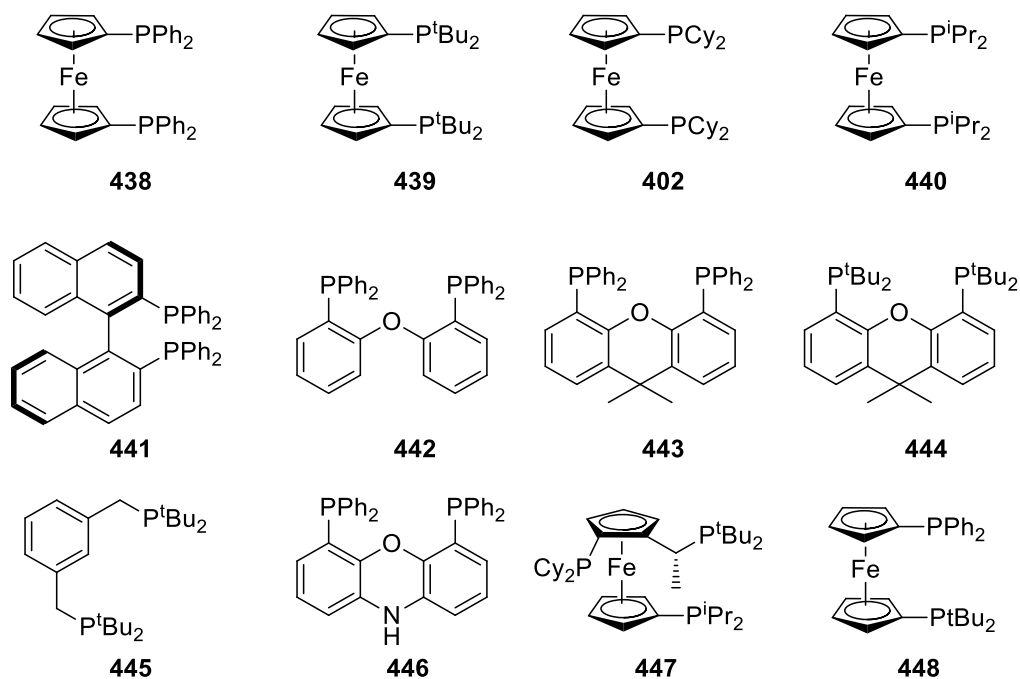


Figure 51. Ligands selected for second high throughput screen.

A large P-M-P angle should lead to a small Cl-M-Cl angle in the corresponding Alk-Fe-Ar complex. Upon OA and transmetalation this should give a small Ar-Fe-cyclopropyl angle, promoting RE.

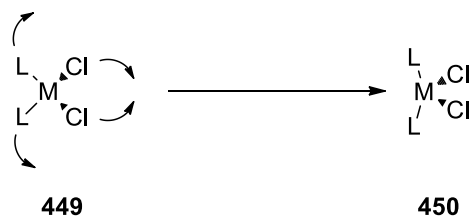
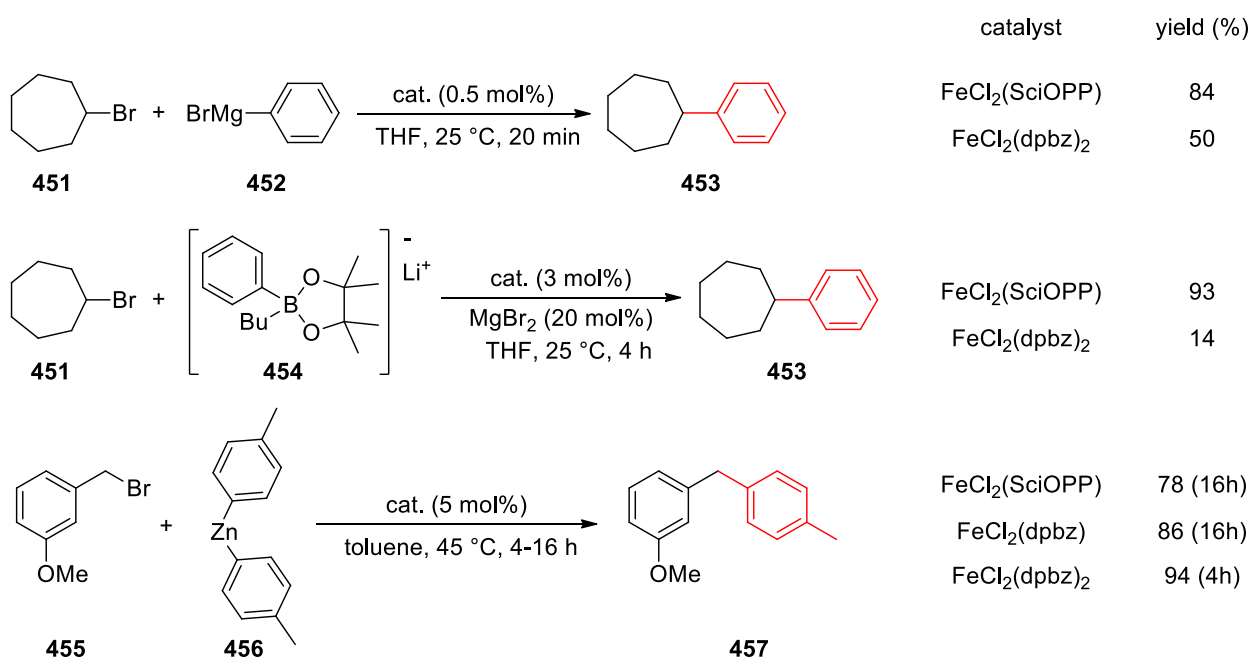


Figure 52. Sketch of the effect of ligand bite angle upon Cl-M-Cl bond angle.

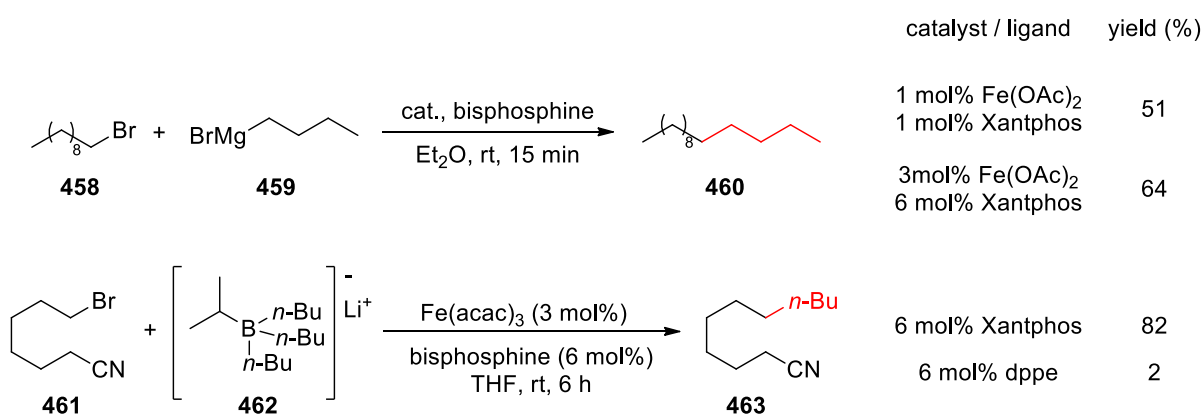
Interestingly, some bisphosphine ligands have been used for iron-catalysed cross-coupling reactions previously (**Scheme 78** and **Scheme 79**). Bedford and Nakamura have both reported the synthetic utility of ligands such as SciOPP (**422**), dpbz (**464**), dppe (**148**) and Xantphos (**443**) in specific cross-coupling reactions. Neidig recently reported a number of investigations related to

the intermediates formed in reactions where bisphosphine ligands have been shown to deliver significant improvements in reactivity.



Scheme 78. Some bisphosphines in iron-catalysed cross-coupling reactions, ligands shown in Figure 53.

Interestingly, Nakamura and Chai discussed the application of Fe(OAc)₂ and Fe(acac)₃ in combination with Xantphos **443**. Neidig studied this system further, and demonstrated significant differences in the bonding characteristics between the phenyl-bridged bisphosphines **422** and **464** and xanthene bridged Xantphos **443**. FeCl₂(Xantphos) was demonstrated to have reduced Fe-P bond covalency than the analogous FeCl₂(dpbz) and FeCl₂(SciOPP), possibly due to decreased π-character compared to the phenylene backbones.¹⁹⁸



Scheme 79. Xantphos based cross-coupling reactions, ligands shown in Figure 53.

The bisphosphine ligands studied by Neidig are shown in **Figure 53**. The observed reduction in Fe-P bond order discussed earlier may also be influenced by the increased P-Fe-P bond angle compared to both phenylene- and ethylene-bridged SciOPP, dpbz and dppe.

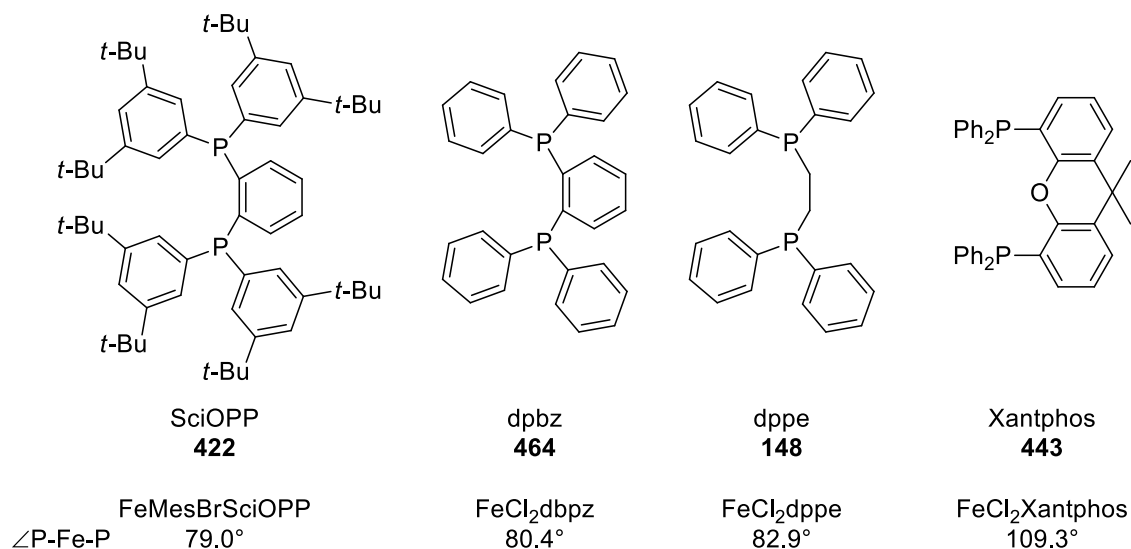


Figure 53. Some FeX₂(bisphosphine) complexes and their bite angles.

The screen of ligands from **Figure 51** demonstrated that ferrocene based ligands were not optimal in the cross-coupling reaction, and that Xantphos-based ligands gave much higher levels of desired product (**Chart 15**). Both Xantphos **443** and NiXantphos **446** gave similar levels of product (66 to 68%); *tert*-butyl-Xantphos **444** gave lower conversion than the original wide bite-angle bisphosphine **404** (32 vs. 37%).

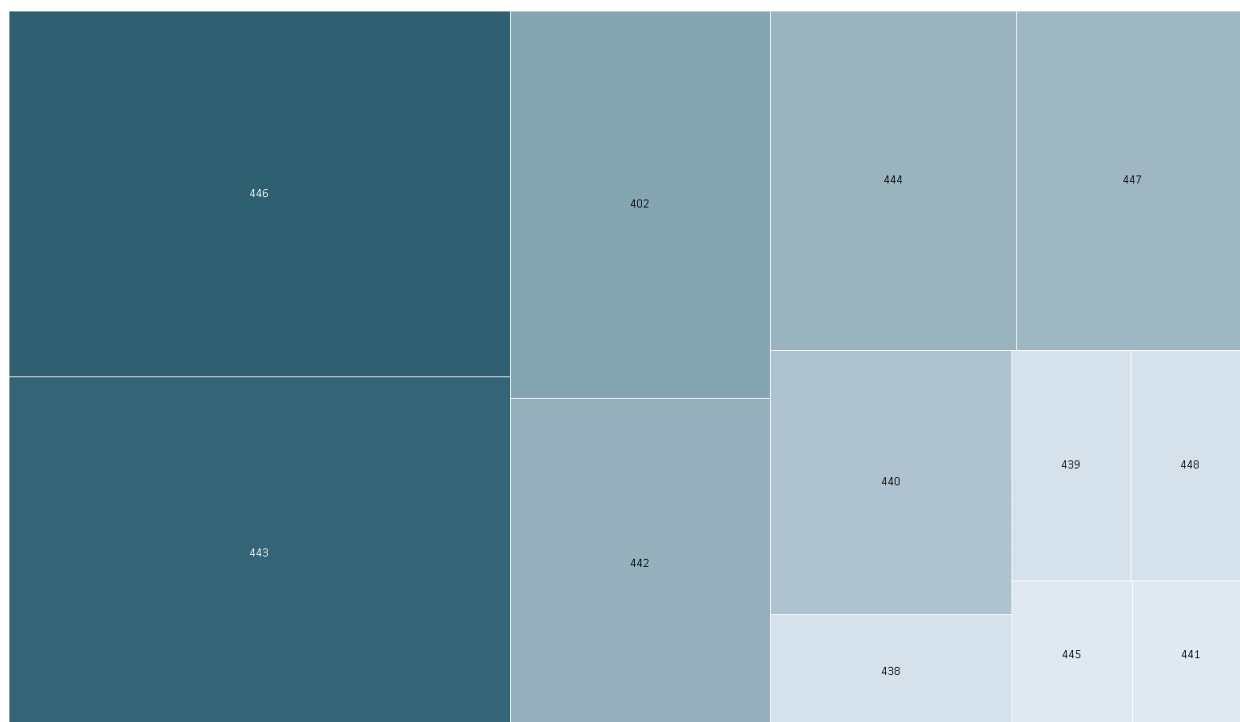
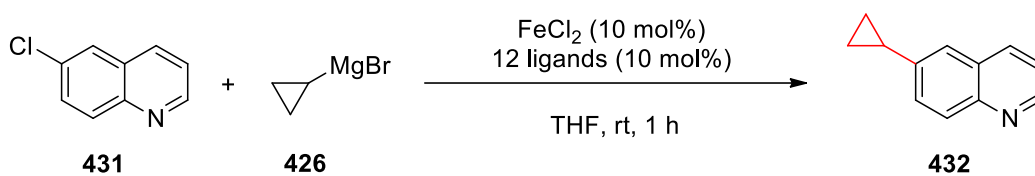
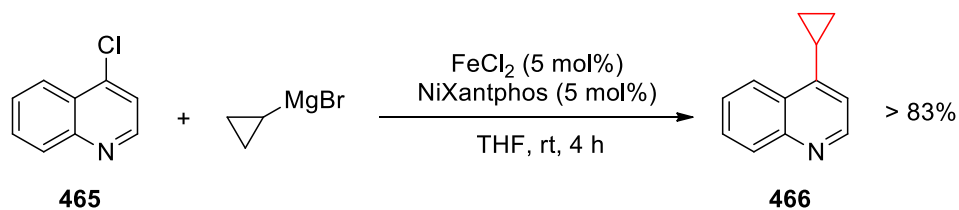


Chart 15. Results from wide bite-angle phosphine screen. Area/shade represents conversion (max = 69%).

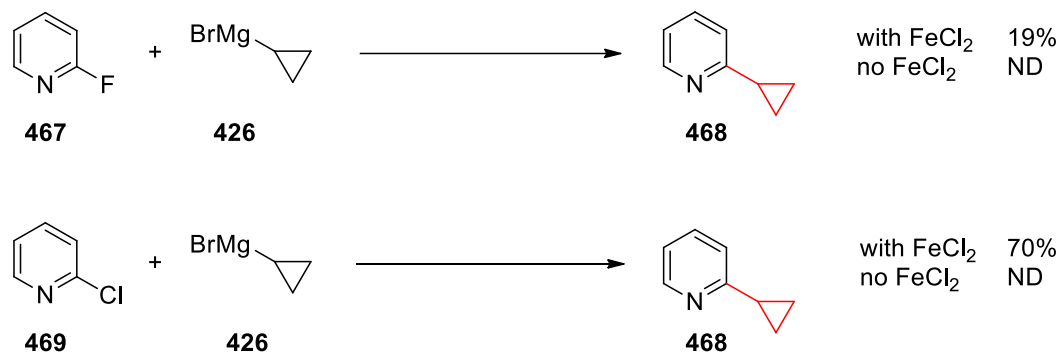
A more reactive substrate, 4-chloroquinoline **465**, was selected to repeat the scoping reactions, combined with NiXantphos. Quantitative conversion of 4-chloroquinoline **465** to 4-cyclopropylquinoline **466** was observed. This reflects the increased reactivity of the heterocyclic C-Cl bond *versus* the carbocyclic C-Cl bond.



Scheme 80. Reaction of 4-chloroquinoline with cyclopropylmagnesium bromide, LCMS conversion.

The improved conversion of 4-chloroquinoline raised a question – is this catalytic or is this $\text{S}_{\text{N}}\text{Ar}$? To test this hypothesis 2-fluoropyridine **467** and 2-chloropyridine **469** were tested with and without iron present. With 2-fluoropyridine, no product was observed without iron present, but

17% coupling was observed in the presence of FeCl₂. With 2-chloropyridine, 70% product was observed in the presence of iron. If S_NAr was the main pathway for the reaction higher conversion and/or a more rapid reaction would be expected with 2-fluoropyridine *versus* 2-chloropyridine.



Scheme 81. Testing S_NAr at fluoro- and chloro-pyridine, LCMS conversion. ND – not detected.

5.2.2.4. Screen 4 – Further Focussed Ligand Screen for Cross-Coupling of Cyclopropyl Grignard with 6-Chloroquinoline

Due to the success of Xantphos (**443**) based ligands in the previous screen, a further, more focussed screen was carried out (**Figure 54**). Ligands analogous to Xantphos were chosen initially, then others with wide bite angles or similar backbones were also selected. Many of these ligands were not part of the earlier PCA analysis. DIOP **476**, however, was included in the modelling (**Chart 16**).

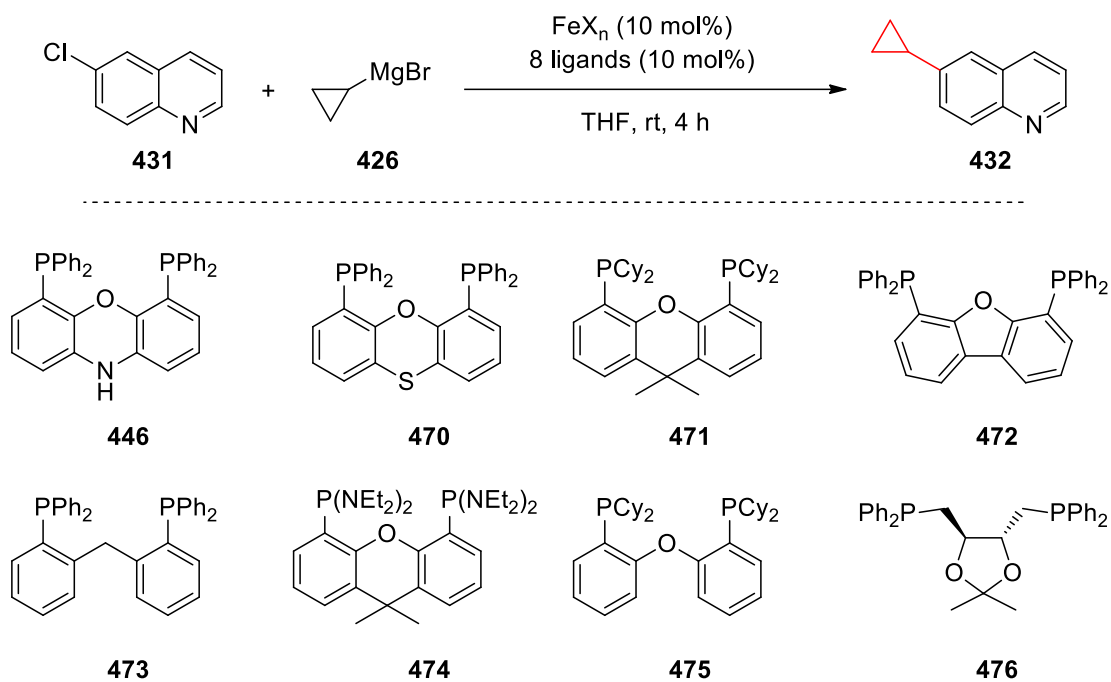


Figure 54. Further screen with some Xantphos based ligands.

The PCA model shows DIOP **476** to be much further from ferrocene **404** than most of the previously selected ligands (**Chart 16**).

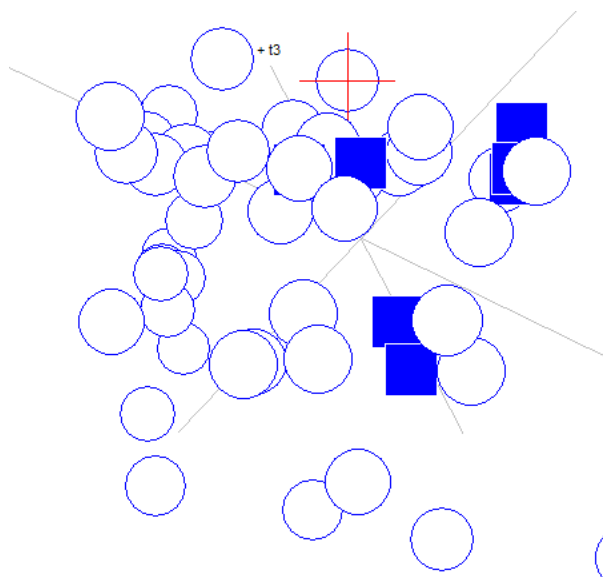


Chart 16. Bisphosphine PCA model, DIOP highlighted by red cross.

The screen used 8 ligands in combination with 4 iron sources, giving 32 reactions. FeCl_2 was investigated further due to its success in the earlier investigation. 3 other iron pre-catalysts were used: $\text{Fe}(\text{acac})_3$, $\text{Fe}(\text{dbm})_3$ and FeF_2 . Fe^{III} salts are generally used in the literature due to their low cost, ready availability and previous literature precedent. They were chosen for this screen as iron halides ($\text{FeCl}_2/\text{FeCl}_3$) are generally hygroscopic, leading to difficulty in handling them outside of a glove box.

Table 15. Iron pre-catalysts selected for the fourth high throughput screen.

Experiment	Iron Source
1	FeF_2
2	FeCl_2
3	$\text{Fe}(\text{dbm})_3$
4	$\text{Fe}(\text{acac})_3$

The results from this fourth screen showed that the Xantphos based ligands gave the highest conversion (**Chart 17**). This was repeated with all four pre-catalysts, with FeCl_2 displaying the greatest reactivity.

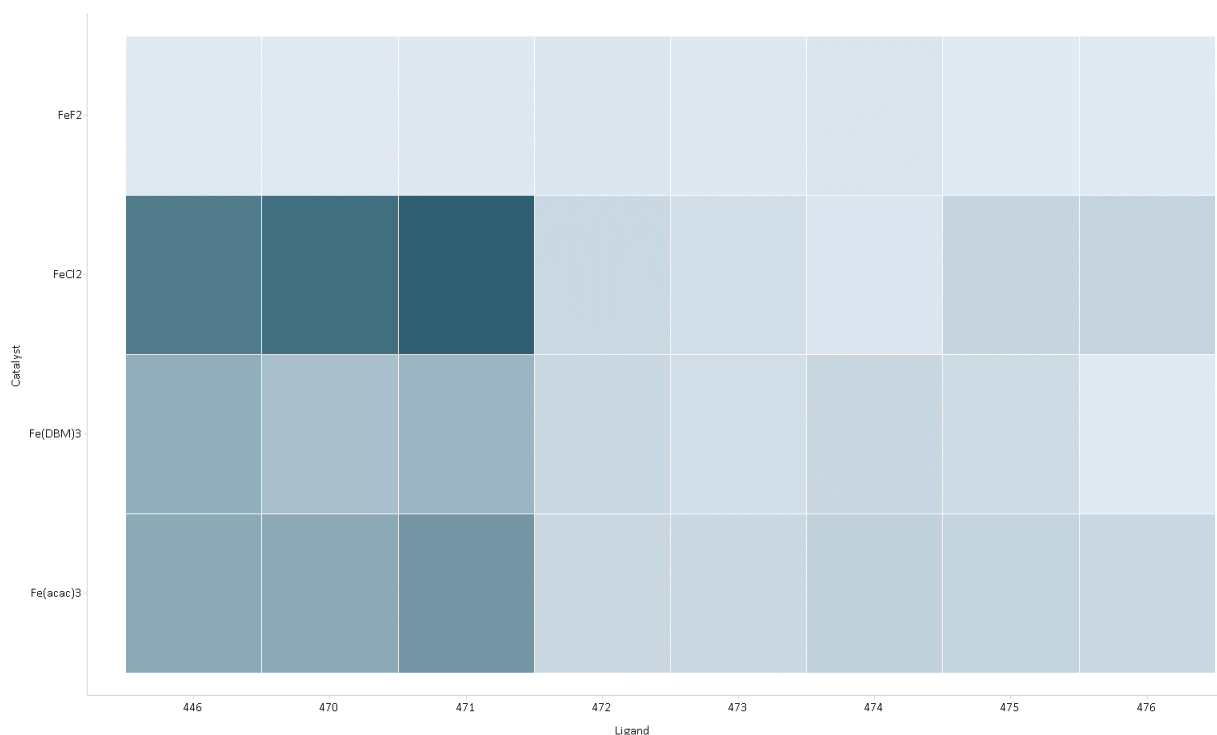


Chart 17. Heat map for third ligand screen, HPLC area (max = 80%).

The most productive ligands from the first three screens were found to be the Xantphos analogues **470** and **471** (72% and 80% respectively). These ligands were found to give 10-15% higher conversion than Xantphos itself (64%). However, their high cost and poor commercial availability precludes their use with a cheap, abundant metal such as iron. Xantphos costs around £16 per gram, around a third of the cost of ultra-dry trace metals FeCl₂ (£40/gram), or around twice the cost in £ per mole owing to the high molecular weight of Xantphos.

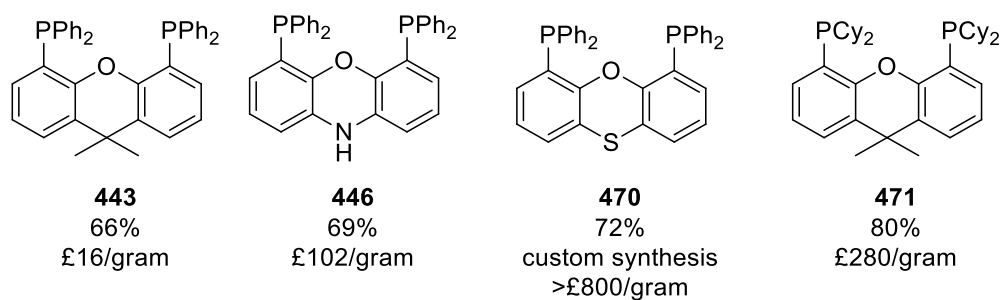


Figure 55. Price per gram (**443**, **446** and **471** – Sigma Aldrich, **470** – custom synthesis, AKOS GmbH).

5.2.2.5. Optimisation of Cyclopropyl Cross-Coupling using DoE

The reactions in the screens were all carried out with 10 mol% iron pre-catalyst and 10-20 mol% ligand. The polydentate ligands were used at a 1:1 catalyst:ligand ratio to avoid saturating the metal centre. This is a relatively high catalyst and ligand loading, especially when considering the molecular weight of the ligands (e.g. Xantphos, 578.6 g mol⁻¹) compared to the substrate (6-chloroquinoline, 163.6 g mol⁻¹).

DoE was chosen to optimise the reaction conditions following the early success with the challenging *iso*-propyl cross-coupling. The cyclopropylmagnesium bromide used in all the reactions was purchased as a 0.5 M solution in THF, and this forms the majority of the reaction volume. Therefore, it was not possible to study reaction concentration or temperature within the DoE. This led to the selection of only 4 factors as part of a fractional factorial investigation (2⁴⁻¹), giving 16 reactions and 4 centre-points.

Table 16. Factors and ranges for DoE investigation.

Entry	Factor	Range
1	Catalyst Loading	0.1 to 5 mol%
2	Ligand Loading	0.1 to 5 mol%
3	Grignard Loading	1 to 3 equiv.
4	Addition time	0 to 30 mins

The most significant factors for the cyclopropyl cross coupling were found to be catalyst, ligand and Grignard reagent loadings (**Table 17**). There were also two two-factor interactions between catalyst *and* ligand, and catalyst *and* Grignard, although the latter was shown to have less importance (p-value >0.05).

Table 17. ANOVA table for cyclopropyl DoE (abridged).

Entry	Source	p-value	Statistically Significant?
1	Model	0.0022	significant
2	A-Catalyst Loading	0.0006	significant
3	B-Ligand Loading	0.0556	not significant
4	C-Grignard Equivalents	0.1579	not significant
5	AB	0.0412	significant
5	AC	0.1314	not significant
6	Lack of Fit	0.0648	not significant

The two-factor interaction between catalyst and ligand loading (**Figure 56**) suggested that high catalyst loading was required to promote reactivity. This effect was more pronounced when combined with increased levels of Xantphos (red line) With lower catalyst loading (black line) a maximum of 20% conversion was observed.

Design-Expert® Software
Factor Coding: Actual
Product (%)
(adjusted for curvature)
● Design Points

X1 = A: Catalyst Loading
X2 = B: Ligand Loading

Actual Factors
C: Grignard Equivalents = 2
D: Addition Time = 15

■ B- 0.1
▲ B+ 5

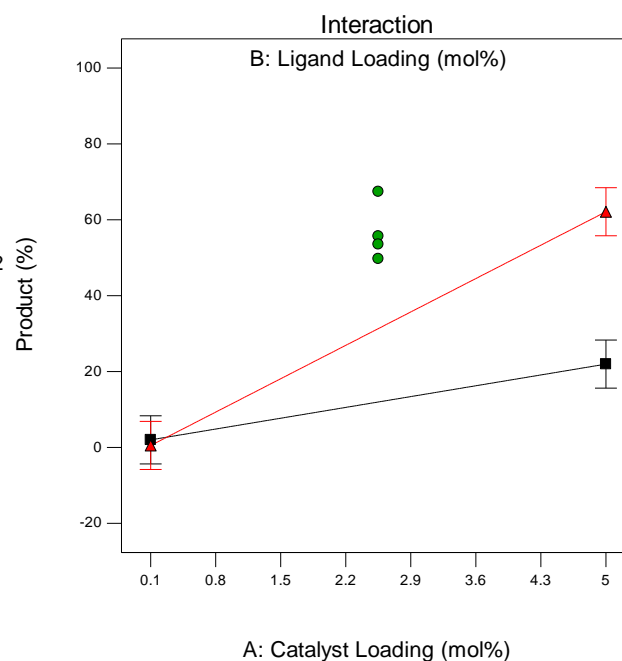


Figure 56. Interaction plot showing catalyst and ligand loading.

The two-factor interaction between catalyst loading and level of Grignard reagent also suggested that high catalyst loading was required to promote reactivity (**Figure 57**). This effect was again more pronounced when combined with increased levels of Xantphos (red line).

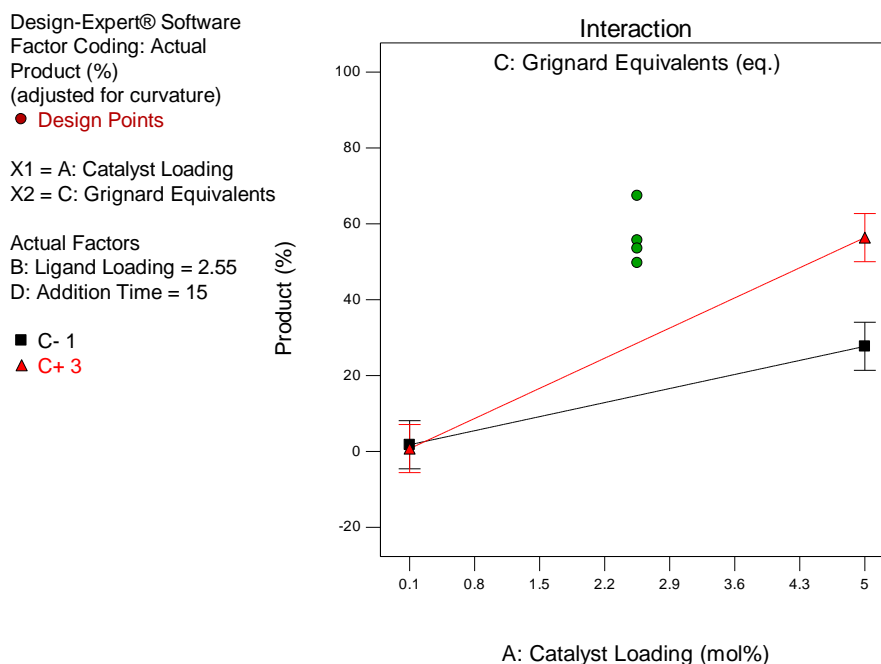


Figure 57. Interaction plot showing catalyst loading and equivalents of Grignard reagent.

The results from the first investigation displayed curvature toward the centre-point conditions. This was also observed throughout the *iso*-propyl DoE study. The fractional factorial design selected for the DoE cannot be used to model non-linear responses. 10 experiments were therefore added to the DoE investigation to understand the curvature in response to levels of Grignard reagent, catalyst and ligand. These were carried out on the faces of the 4-dimensional design space, giving a central composite design, analogous to the earlier investigation (**Chapter 3**).

The additional experiments led to the selection of a quadratic response surface, in combination with a square root transformation. The selected model showed that levels of Grignard reagent, catalyst and ligand continued to be the most important factors. The previously observed two-factor interactions were also demonstrated to be statistically significant.

Table 18. ANOVA table for cyclopropyl DoE (abridged).

Entry	Source	p-value	Statistically significant?
1	Model	< 0.0001	significant
2	AB	< 0.0002	significant
3	AC	< 0.0040	significant

The first two-factor interaction, between catalyst and ligand loading, was modelled well by the chosen quadratic response surface (**Figure 58**). Higher catalyst loading led to increased product formation. Beyond 4 mol% catalyst, however, conversion to desired product began to decrease. The product was replaced by undesirable side-products, suggesting that the catalyst may

influence their formation. The response to increased catalyst loading was more pronounced when more Xantphos was used. In fact, until around 4 mol% catalyst, the amount of ligand used had very little effect on the reaction.

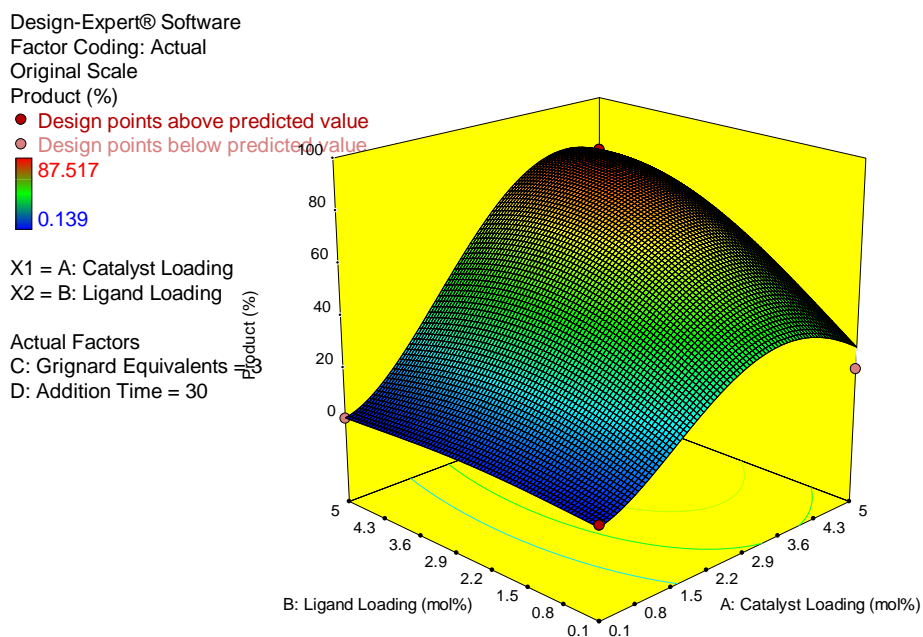


Figure 58. 3-Dimensional surface for the interaction between catalyst and ligand loading.

A similar response was observed when studying the two-factor interaction between catalyst loading and the equivalents of Grignard reagent used in the reaction (**Figure 59**). The reaction switched on at around 4 mol% FeCl_2 , and at this point increasing the amount of Grignard reagent from 1 eq. to 3 eq. gave a ~20% boost in conversion. Many early cross-coupling protocols have used an excess of Grignard reagent, often around 3-4 equivalents relative to (hetero)aryl halide.²⁵
²⁶ This is rather wasteful, especially considering the cost of cyclopropylmagnesium bromide, or the challenges associated with its synthesis.

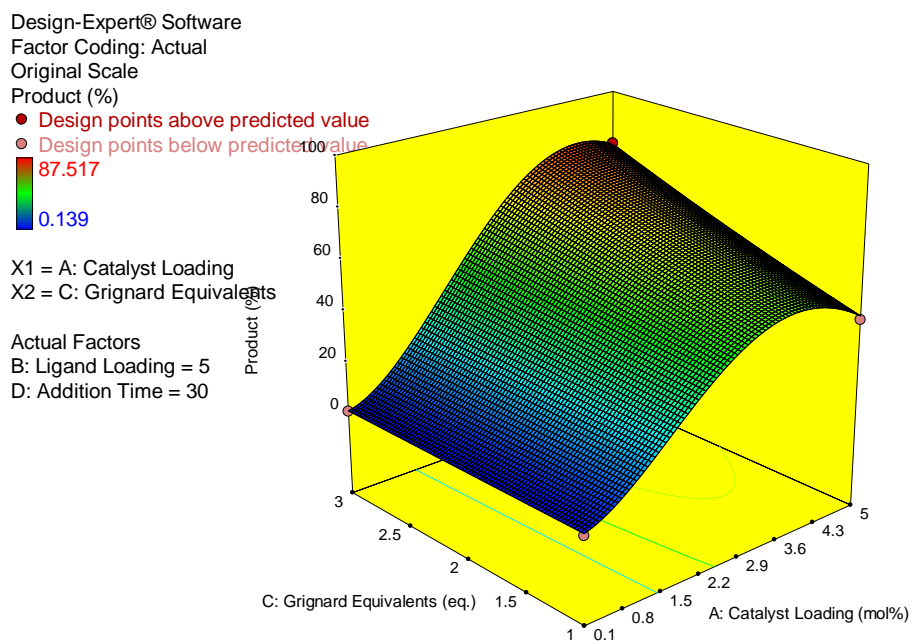
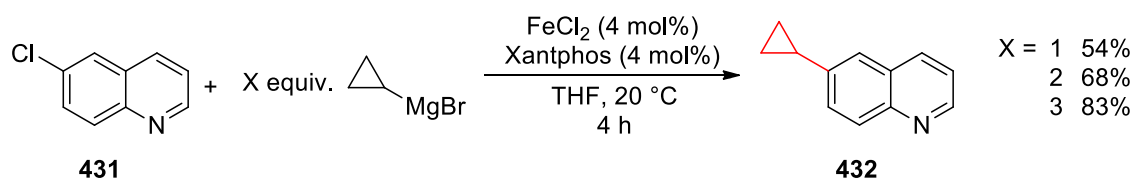


Figure 59. 3-Dimensional surface for the interaction between catalyst loading Grignard equivalents.

The predicted optimal conditions suggested that 83% conversion was achievable with 3 equivalents of Grignard reagent. However, significant challenges were observed in the purification of the reaction mixture. This is probably because the excess Grignard reagent combined with a lengthy reaction led to significant side-product formation. These impurities were difficult to remove using column chromatography.



Scheme 82. Predicted optimal conditions from DoE investigation.

The effect of temperature was not considered in the DoE due to the standard solution of Grignard reagent (0.5 M). The Grignard reagent was generally added as a single aliquot using a syringe or multi-channel pipette. Any handling of the solution would lead to an increase in temperature, and the addition of an unknown variable to the DoE. Temperature was shown to be a significant factor in the earlier *iso*-propyl cross-coupling (**Chapter 3**). It was studied after the DoE, using the predicted optimal conditions (**Scheme 82**).

In an attempt to improve the reaction selectivity a further study was carried out into the effect of temperature on the cross-coupling reaction. The large volume of THF added with the Grignard reagent meant that a reverse addition was required. The Grignard reagent was added to an Integrity 10 vial and pre-equilibrated at a range of temperatures between -20 and 40 °C (**Chart 18**). Initially, 10 °C intervals were used, but a flat region was observed between 10 and 20 °C. The reactions were then repeated between 0 and 30 °C at 5 °C intervals.

This study suggested that the optimal temperature was around 15 °C. Low temperatures led to the precipitation of a white solid from the reaction mixture, presumably cyclopropylmagnesium bromide, as the precipitate also formed on cooling the starting solution of Grignard reagent. This explains the poor conversion at low temperature. At high temperature, increased levels of adduct were observed, so less product was formed.

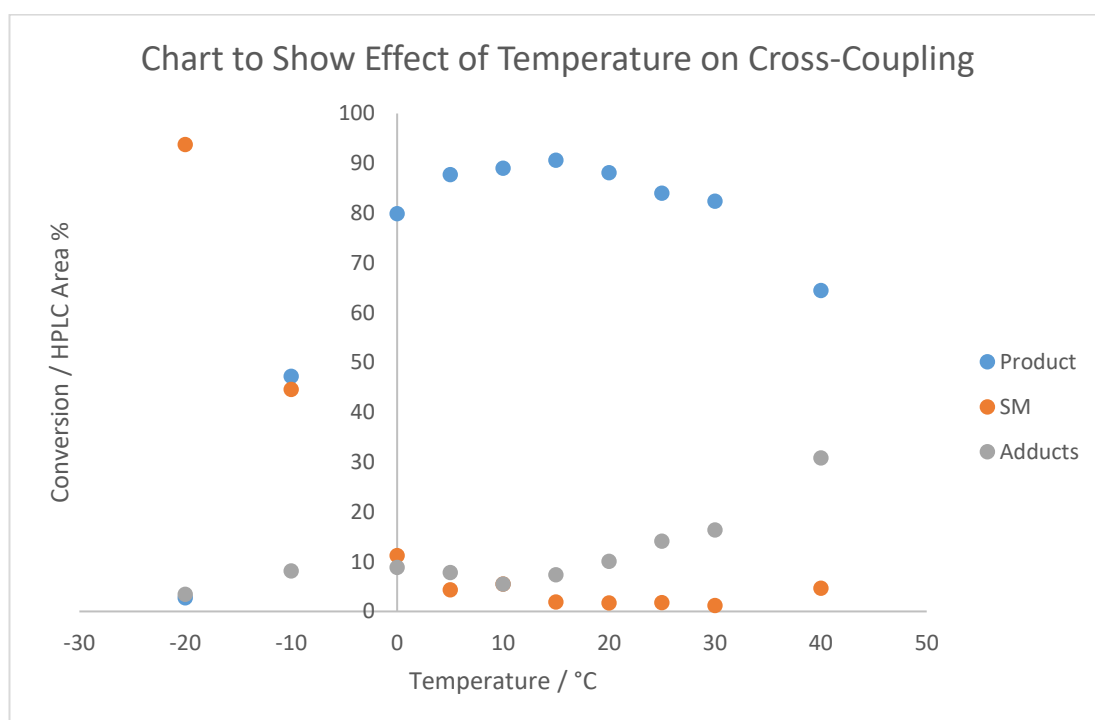
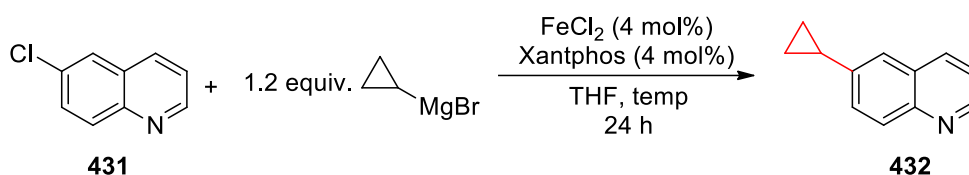
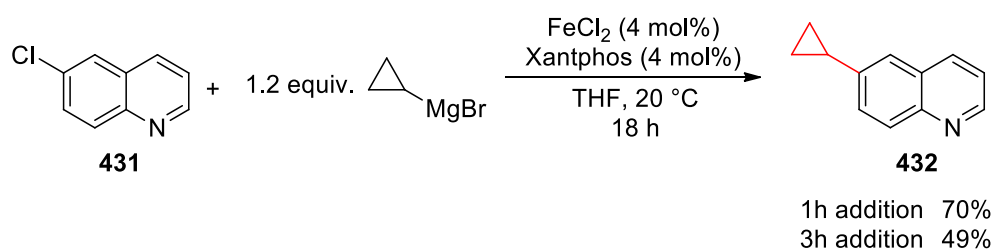


Chart 18. Plot of HPLC conversion *versus* temperature.

The use of 3 equivalents of Grignard reagent must promote the formation of the adduct from Grignard addition into the heteroaryl ring. Reducing the excess of cyclopropylmagnesium bromide may result in an improved product:side product ratio. Initially, controlled addition of the

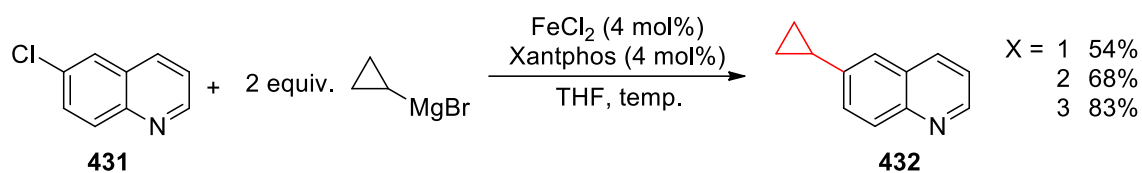
Grignard reagent was proposed to limit undesired reactivity. Unfortunately, this gave poor results. Adding 1.2 equivalents of Grignard reagent over 1 or 3 hours at 15 °C only gave an incomplete reaction, and increased levels of the side-products with the longer addition, possibly due to catalyst deactivation.



Scheme 83. Controlled addition investigation, HPLC conversion.

It has been noted that the reaction with cyclopropylmagnesium bromide is much slower than with *iso*-propylmagnesium bromide. In the earlier investigation, the reactions were found to be complete in <5 minutes. When coupling the cyclopropyl Grignard, reaction times of 16 hours were required to give complete conversion of the starting 6-chloroquinoline. This reduced rate may be related to the slow reduction of the FeCl₂ pre-catalyst, possibly because β -hydride elimination from Fe-cyclopropane is disfavoured. This is because β -hydride elimination requires a *syn* relationship of the TM and hydride, which is challenging due to the shape of the cyclopropane molecule. It would also lead to highly strained cyclopropene.

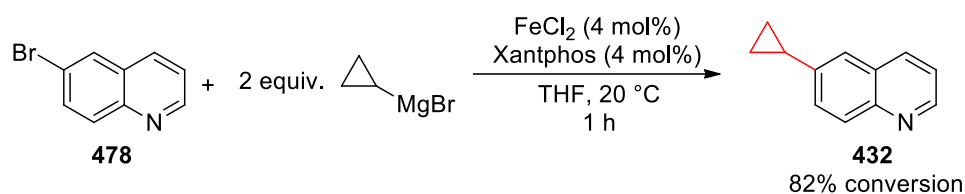
To increase the rate of reaction, either increased catalyst loading or increased temperature are required. The DoE suggested that increased catalyst loading only resulted in adduct formation, thus increased temperature was further investigated (**Figure 60**). Unfortunately, increased temperature with a shorter reaction time (*cf.* 24 hours, Chart 18), still led to significantly higher levels of side-products.



Entry	Temperature / °C	Time / h	Starting Material	Product	Adducts (combined)
1	20	1	60	38	2
2	40	1	40	55	4
3	60	1	32	56	12
4	20	4	21	74	5
5	40	4	11	80	10
6	60	4	8	68	24

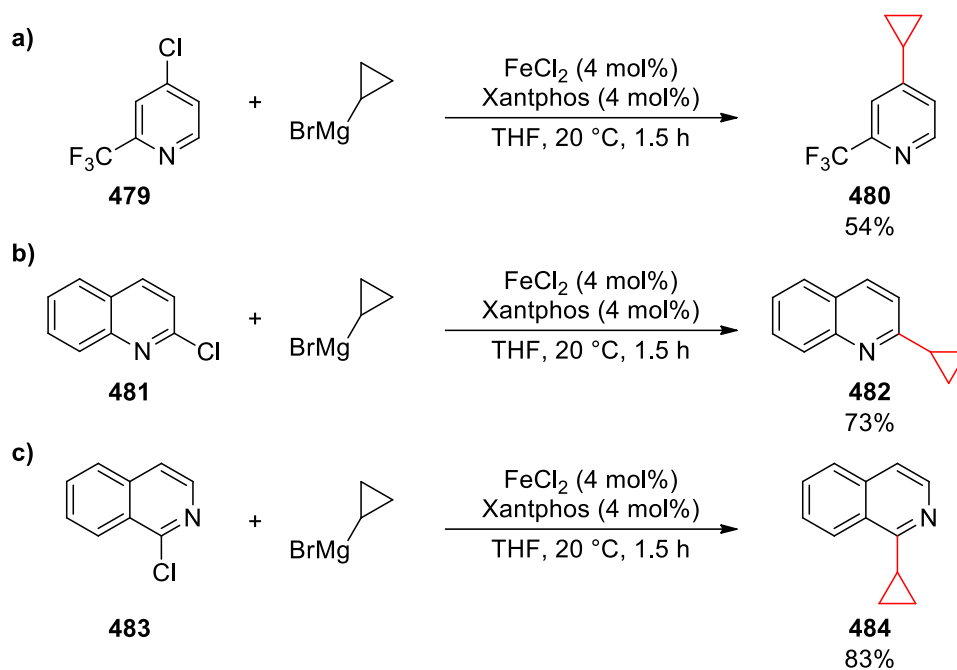
Figure 60. Further temperature investigation, HPLC conversion.

6-Bromoquinoline was tested in a final attempt to improve the conversion to 6-cyclopropyl quinoline (**Scheme 84**). Complete consumption of starting material was observed after 1 hour, but a high level of quinoline was observed by both LCMS and HPLC (10% by HPLC area).



Scheme 84. Coupling of 6-bromoquinoline under the optimised Kumada conditions, HPLC conversion.

Some further substrates were coupled, which were thought to be more reactive towards cross-coupling. They were a CF₃-substituted pyridine **479**, 1-chloroisoquinoline **481** and 2-chloroquinoline **483**. All gave very high conversion with HPLC/LCMS, and moderate isolated yields were obtained with the quinoline and isoquinoline substrates (**Scheme 85**). It may be possible to improve the isolated yield in these reactions by further optimising levels of Grignard reagent, addition time of Grignard reagent and reaction duration.



Scheme 85. Substrates coupled using optimised FeCl₂/Xantphos procedure, isolated yields.

It may be interesting to test dihalogenated heteroaryl chlorides such as those coupled by Malhotra in **Scheme 71**.¹⁷⁷ Many of these reactions were carried out in the presence of NMP in superstoichiometric amounts (>4:1 THF/NMP) – this could be replaced by Xantphos at a catalytic level. This may offer a significant advantage in the preparation of APIs, as Xantphos can be readily removed from the reaction mixture using extraction or chromatography.

5.3. Conclusion

Many of the iron-catalysed cross-coupling reactions described in the literature utilise NMP as a co-solvent, which is known to be reprotoxic, limiting its use in the manufacture of APIs. High throughput chemistry was used to search for an alternative additive, which could also be used in catalytic quantities, rather than the super-stoichiometric levels often used with NMP.

A series of high throughput screens were carried out, initially with an amide substituted chlorobenzene. Unfortunately, the chemoselectivity observed in the earlier *iso*-propyl cross-coupling was not maintained with cyclopropylmagnesium bromide. This may be related to the increased nucleophilic character of the cyclopropyl Grignard reagent.

A challenging heteroaryl chloride was then selected to further investigate the iron-catalysed cross-coupling of the cyclopropyl nucleophile. Application of the ligands selected for the earlier amide substrate led to the discovery of wide bite-angle bisphosphine ligand dcpf **404** as an efficient ligand for the promotion of this reaction. Following a more focussed second HTC screen, it was found that bisphosphines were not the most effective ligand; Xantphos and its analogue NiXantphos were found to give much higher conversion. A final screen of other Xantphos-like ligands showed that ThiXantphos and cyclohexyl-Xantphos gave higher productivity than both Xantphos and ThiXantphos. However, the requirement for custom synthesis, and their high associated cost, meant that the relatively cheap and simple Xantphos ligand was an attractive starting point for reaction optimisation.

DoE was used to investigate the effect of levels of catalyst, ligand and Grignard reagent, along with the addition time of Grignard reagent, upon the reaction. It was found that high levels of all factors led to the efficient conversion of starting material, although more catalyst and ligand tended to give increased side-product formation. The reaction was also found to be highly sensitive to temperature, with low temperature giving poor conversion, and high temperature also leading to more impurities.

As previously demonstrated, it was found that the Cl-substituted pyridyl ring was more reactive than a Cl-substituted aryl ring. A reaction with 1-chloroquinoline or 1-chloroisoquinoline gave much higher productivity and selectivity than 6-chloroquinoline. Further investigation is required in this respect to understand the substrate scope, and improve the reactivity of Cl-substituted aryl rings.

6. Concluding Remarks

In **Chapter 3** DoE was used to optimise the cross-coupling of *iso*-propylmagnesium chloride with aryl chlorides. These reactions were found to be highly selective for the desired *iso*-propyl isomer, over the unwanted *n*-propyl isomer. The reaction was found to be most productive for highly electron deficient substrates, leading to the efficient cross-coupling of heteroaryl chlorides. Electron rich substrates gave poor reactivity and selectivity; these differences in reactivity were investigated using DFT in **Chapter 4**. It may be possible to improve the reactivity of electron rich aromatics through the use of alternative (pseudo)halides. This could lead to a more general cross-coupling procedure. It would also be interesting to understand the chemoselectivity of these reactions in the presence of multiple reactive positions.

It was found that there was a correlation between a molecule's EA, and the experimental conversion to the coupled *iso*-propyl product. Electron poor substrates, with a high theoretical EA, gave the most productive (and selective) cross coupling reactions. This, combined with Hammett studies, suggested that OA may be the selectivity determining step. Unfortunately, the application of this methodology to a more complex heteroaryl chloride yielded a poor correlation. It would be interesting to further investigate the application of DFT as a triage method for iron-catalysed cross-coupling reactions. Could another simple molecular property be used to predict and understand reactivity?

In the final chapter, HTC was utilised to develop NMP free reaction conditions for the coupling of cyclopropylmagnesium bromide with heteroaryl chlorides. The reaction was optimised for 6-chloroquinoline, but issues with both reactivity and selectivity led to challenges with product isolation. The reaction was found to be very sensitive to catalyst loading and temperature; increasing both generally resulted in the formation of undesired side-products. However, the new cross-coupling procedure was found to be very efficient at forming heteroaryl-cyclopropyl (sp^2 - sp^3) bonds. The use of Xantphos in place of NMP could represent a step-change in the coupling of challenging nucleophiles under iron-catalysis. Future work should focus on the study of the reactions substrate scope, along with some reoptimisation for more challenging electrophiles, such as dihalogenated heteroaryl chlorides.

7. Experimental

7.1. General Information

All commercially available compounds were used as provided without further purification. Anhydrous solvents and Grignard reagents were purchased from Sigma Aldrich and used without further testing. Small scale (2 mmol) reactions were carried out using an Electrothermal Integrity 10 Reaction Station (STEM block). Larger scale reactions were carried out in round bottomed flasks. All experiments were carried out under an atmosphere of nitrogen unless otherwise stated. Normal phase purification was carried out using pre-packed silica columns on a Biotage Flash Purification system. Reverse phase purification was carried out using pre-packed C18 silica columns on a Teledyne Isco Combiflash Companion system.

NMR data was obtained using a Bruker AV400 instrument. Data analysis was carried out using MestReNova version 10.0.2-15465. Reference values for residual solvents were taken as $\delta = 7.27$ (CDCl₃) for ¹H NMR and $\delta = 77.16$ (CDCl₃) for ¹³C NMR.²³⁶ Multiplicities for coupled signals were reported as: s = singlet, d = doublet, t = triplet, q = quartet, sept = septet, m = multiplet. Coupling constants (*J*) are given in Hz and are uncorrected. GC and GC-MS were carried out on different instruments, and the methods are detailed below. HPLC and LCMS was carried out using walk up instruments, running a 5 minute gradient described below. High resolution mass spectrometry was carried out by Analytical Science at GSK. This was done using a Thermofinnigan Exactive or Waters Synapt (ASAP-TOF) instrument.

DoE investigations were prepared and analysed using Stat-Ease Design-Expert 7-10.²³⁷ DFT calculations were run with Gaussian 09²³⁸ and data was visualised in GaussView 5.0.²³⁹ Statistical analysis of computational results was carried out using SAS JMP 11/12.¹⁵⁴

7.2. HPLC and GC Methods

GCMS data of samples dissolved in ethyl acetate were acquired using the method detailed below:

Instrument	Thermo Electron PolarisQ Series GCMS			
Column	Agilent HP-5ms (30 m × 0.25 mm × 3.0 μm)			
Carrier Gas	Helium			
Gas Flow Rate	1 mL min ⁻¹			
Injection Split	Split (10:1)			
Oven Program	Ramp Rate / °C min ⁻¹	Final Temperature / °C	Hold Time / min	Elapsed Time / min
	-	40	1	1.00
	15	300	5	23.33
Temperatures / °C	Injector	Transfer	Oven	
	250	300	40	
Injection Volume	1.0 μL			

GC data of samples dissolved in ethyl acetate were acquired according to the following method:

Instrument	Agilent 6890 Series GC			
Column	Agilent DB5-HT (15 m × 0.25 mm × 0.10 μm)			
Carrier Gas	Helium			
Gas Pressure	1.7 bar			
Injection Split	Split (100:1)			
Oven Program	Ramp Rate / °C min ⁻¹	Final Temperature / °C	Hold Time / min	Elapsed Time / min
	-	50	0.5	0.50
	75	320	2.5	6.60
Temperatures / °C	Injector	Detector	Oven	
	275	320	275	
Injection Volume	1.0 μL			

HPLC data of samples dissolved in 1:1 acetonitrile/water were acquired according to the following method:

Instrument	Agilent HP1100 HPLC	
Column	Waters X-select CSH C18 column (XP) 2.5 µm particle size	
Solvent A	0.05% TFA in water	
Solvent B	0.05% TFA in acetonitrile	
Temperature	40 °C	
Flow Rate	1 mL min ⁻¹	
Gradient	Time / min	% B
	0.0	3
	3.7	95
	4.0	95
	4.1	3
	5.5	3
Injection Volume	0.5 µL	

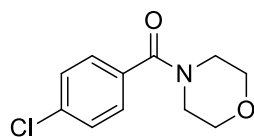
LCMS data of samples dissolved in 1:1 acetonitrile/water were acquired according to the following method:

Instrument	Agilent HP1100 HPLC Waters ZQ single quadrupole mass spectrometer	
Column	50 x 4.6mm, 3 μ m, Waters X-Bridge C18	
Solvent A	10 mM ammonium bicarbonate	
Solvent B	acetonitrile	
Temperature	40 °C	
Flow Rate	3 mL min ⁻¹	
Gradient	Time / min	% B
	0.0	1
	0.1	1
	4	97
	5	97
Injection Volume	5.0 μ L	

HRMS data of samples dissolved in 1:1 acetonitrile/water were acquired according to the following method:

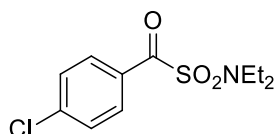
Instrument	Agilent HP1100 HPLC ThermoFinnigan Exactive mass spectrometer	
Column	5cm x 2.1mm, 3 μ m, Luna C18	
Solvent A	0.05% TFA in water	
Solvent B	0.05% TFA in acetonitrile	
Temperature	40 °C	
Flow Rate	1 mL min ⁻¹	
Gradient	Time / min	% B
	0.0	0
	8	95
	10	95
Injection Volume	2.0 μ L	

7.2.1. Preparation of Starting Materials/Ligands for the Iron-Catalysed Cross-Coupling Reactions



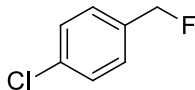
(4-chlorophenyl)(morpholino)methanone
270

Prepared according to literature procedure of Fox *et al.*¹¹⁴ Spectral data matched those reported.



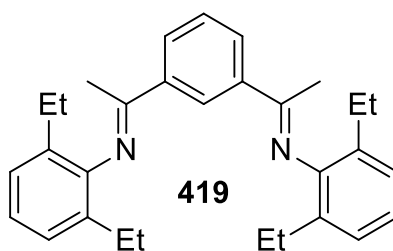
1-(4-chlorophenyl)-N,N-diethyl-1-oxomethanesulfonamide
274

Prepared according to literature procedure of Schneider *et al.*²⁴⁰ Spectral data matched those reported.²⁴¹

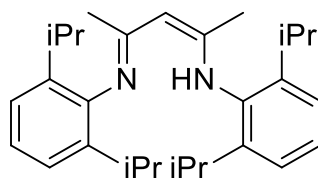


1-chloro-4-(fluoromethyl)benzene
283

Prepared according to literature procedure of Gouverneur *et al.*²⁴² Spectral data matched those reported.

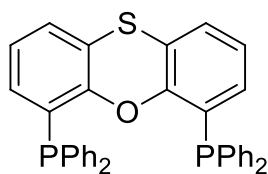


Provided by Jamie Docherty (Edinburgh University).



418

Prepared according to literature procedure of Webster *et al.*²¹⁸ Spectral data matched those reported.



470

Prepared according to literature procedure of Kramer *et al.*²⁴³ Spectral data matched those reported.

7.3. iso-Propyl DoE Optimisation Studies

7.3.1. Experimental Design 1

Procedure and results from analysis in **Section 3.2**.

For DoE 1 the procedure was:

1. Reactions carried out on a 0.2 g / 1.1 mmol scale in a STEM block tube on an Integrity 10 reaction station
2. A solution of $\text{Fe}(\text{acac})_3$ in THF was prepared at 10.1 mg mL^{-1} . The stock solution was used to prepare the reactions described in **Table 19/Table 20**
3. TMEDA or NMP was added as prescribed below
 - 3.1. TMEDA at a loading of 10 mol%
 - 3.2. NMP at $1/10^{\text{th}}$ total reaction volume
4. Reactions prepared at a total volume of:
 - 4.1. 60 volumes = 12 mL
 - 4.2. 40 volumes = 8 mL
 - 4.3. 20 volumes = 4 mL
5. Reactions run for 6 hours, then quenched with 1 M HCl (5 mL)
6. Reactions sampled for GC analysis
 - 6.1. 60 volumes: 250 μL into 1.5 mL ethyl acetate
 - 6.2. 40 volumes: 125 μL into 1.5 mL ethyl acetate
 - 6.3. 20 volumes: 50 μL into 1.5 mL ethyl acetate

Table 19. Reaction volumes for first experimental design.

Run	Temp	Cat / mg	Total vol / mL	THF (tot) / mL	THF (act) / mL	NMP / mL	Add time	Additive	Grignard / mL	Additive / mL
1	20	19.6	12	10.8	7.75	1.2	10	no	0.94	0.00
2	-20	0.4	12	12	10.87	0	10	no	0.94	0.00
3	20	0.4	4	4	2.87	0	0	no	0.94	0.00
4	0	10.0	8	8	5.91	0	5	no	0.94	0.00
5	0	10.0	8	8	5.91	0	5	yes	0.94	0.06
6	20	0.4	4	3.6	2.47	0.4	10	no	0.94	0.00
7	0	10.0	8	7.2	5.11	0.8	5	no	0.94	0.00
8	-20	0.4	4	4	2.87	0	0	yes	0.94	0.06
9	20	0.4	12	12	10.87	0	10	yes	0.94	0.06
10	-20	0.4	4	3.6	2.47	0.4	10	yes	0.94	0.06
11	20	19.6	4	3.6	0.55	0.4	10	yes	0.94	0.06
12	0	10.0	8	8	5.91	0	5	yes	0.94	0.06
13	20	0.4	12	10.8	9.67	1.2	0	yes	0.94	0.06
14	-20	19.6	12	10.8	7.75	1.2	10	yes	0.94	0.06
15	0	10.0	8	7.2	5.11	0.8	5	yes	0.94	0.06
16	0	10.0	8	7.2	5.11	0.8	5	no	0.94	0.00
17	0	10.0	8	8	5.91	0	5	no	0.94	0.00
18	0	10.0	8	8	5.91	0	5	yes	0.94	0.06
19	-20	0.4	12	10.8	9.67	1.2	0	no	0.94	0.00
20	20	19.6	4	3.6	0.55	0.4	0	yes	0.94	0.06
21	-20	19.6	4	3.6	0.55	0.4	0	no	0.94	0.00
22	20	19.6	12	12	8.95	0	0	no	0.94	0.00
23	-20	19.6	12	12	8.95	0	0	yes	0.94	0.06
24	-20	19.6	4	4	0.95	0	10	no	0.94	0.00

Table 20. Preliminary investigation, first experimental design.

		Factor 1	Factor 2	Factor 3	Factor 4	Factor 5	Factor 6
Std	Run	A:Temperature	B:Catalyst loading	C:Concentration	D:Addition time	E:nBuMgCl	F:Ligand
		degC	mol%	volumes	minutes		
16	1	20	5	60	10	no	NMP
13	2	-20	0.1	60	10	no	TMEDA
2	3	20	0.1	20	0	no	TMEDA
22	4	0	2.55	40	5	no	TMEDA
17	5	0	2.55	40	5	yes	TMEDA
10	6	20	0.1	20	10	no	NMP
24	7	0	2.55	40	5	no	NMP
1	8	-20	0.1	20	0	yes	TMEDA
14	9	20	0.1	60	10	yes	TMEDA
9	10	-20	0.1	20	10	yes	NMP
12	11	20	5	20	10	yes	TMEDA
23	12	0	2.55	40	5	yes	NMP
6	13	20	0.1	60	0	yes	NMP
15	14	-20	5	60	10	yes	NMP
19	15	0	2.55	40	5	yes	NMP
20	16	0	2.55	40	5	no	NMP
18	17	0	2.55	40	5	no	TMEDA
21	18	0	2.55	40	5	yes	TMEDA
5	19	-20	0.1	60	0	no	NMP
4	20	20	5	20	0	yes	NMP
3	21	-20	5	20	0	no	NMP
8	22	20	5	60	0	no	TMEDA
7	23	-20	5	60	0	yes	TMEDA
11	24	-20	5	20	10	no	TMEDA

Table 21. Results from first experimental design.

		Response 1	Response 2	Response 3	Response 4
Std	Run	SM	Product	Isomer	Biaryl
		Area%	Area%	Area%	Area%
16	1	3.8	88.1	1.5	6.5
13	2	95.2	3.5	0.0	1.3
2	3	82.3	14.3	0.1	3.4
22	4	67.7	23.7	0.7	7.9
17	5	62.8	27.5	0.8	9.0
10	6	68.5	28.9	0.3	2.3
24	7	0.1	93.8	1.0	5.1
1	8	80.6	14.0	0.1	5.4
14	9	75.6	18.4	0.1	5.8
9	10	88.5	11.2	0.0	0.3
12	11	62.9	27.9	0.5	8.8
23	12	1.2	91.2	1.5	6.2
6	13	96.5	3.3	0.1	0.1
15	14	1.5	92.1	0.7	5.7
19	15	0.1	92.4	1.2	6.4
20	16	0.2	92.6	1.2	6.1
18	17	67.9	23.5	0.7	7.9
21	18	62.0	28.0	0.8	9.2
5	19	94.5	5.4	0.0	0.1
4	20	9.0	75.2	5.4	10.4
3	21	0.6	89.5	2.6	7.4
8	22	73.5	21.9	0.9	3.6
7	23	53.1	35.0	1.1	10.8
11	24	72.8	20.7	0.5	5.9

Table 22. Analysis of variance: product.

Response	2	Product	
Transform:	Power	Lambda:	1.18
ANOVA for selected factorial model		Constant:	0
Analysis of variance table [Partial sum of squares - Type III]			
	p-value		
Source	Prob > F		
Model	< 0.0001	significant	
B-Catalyst loading	< 0.0001		
F-Ligand	< 0.0001		
BF	< 0.0001		
Curvature	< 0.0001	significant	
Residual			
Lack of Fit	0.0002	significant	

Table 23. Analysis of variance: isomer.

Response	3	Isomer	
Transform:	Natural log	Constant:	0.0539211
ANOVA for selected factorial model			
Analysis of variance table [Partial sum of squares - Type III]			
	p-value		
Source	Prob > F		
Model	29.4	significant	
A-Temperature	2.0		
B-Catalyst loading	22.4		
D-Addition time	0.8		
F-Ligand	1.0		
AB	0.8		
BD	1.1		
BF	1.0		
Curvature	5.1	significant	
Residual	1.6		
Lack of Fit	1.5	significant	

Table 24. Analysis of variance: biaryl.

Response	4	Biaryl
ANOVA for selected factorial model		
Analysis of variance table [Partial sum of squares - Type III]		
	p-value	
Source	Prob > F	
Model	< 0.0001	significant
B-Catalyst loading	< 0.0001	
E-nBuMgCl	0.0079	
F-Ligand	0.0418	
BF	0.0210	
EF	0.0093	
Curvature	0.0093	significant
Residual		
Lack of Fit	0.0056	significant
Pure Error	0.5	4
Cor Total	227.0	23

Design-Expert® Software
(Product)^{1.18}

▲ Error from replicates

Shapiro-Wilk test

W-value = 0.895

p-value = 0.135

A: Temperature

B: Catalyst loading

C: Concentration

D: Addition time

E: nBuMgCl

F: Ligand

■ Positive Effects

■ Negative Effects

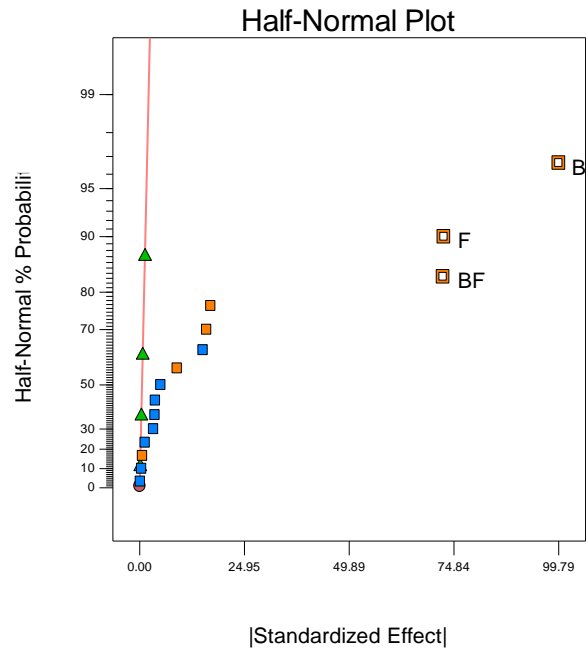


Chart 19. Half normal plot: product.

Design-Expert® Software
Ln(Isomer + 0.05)

▲ Error estimates

Shapiro-Wilk test

W-value = 0.950

p-value = 0.708

A: Temperature

B: Catalyst loading

C: Concentration

D: Addition time

E: nBuMgCl

F: Ligand

■ Positive Effects

■ Negative Effects

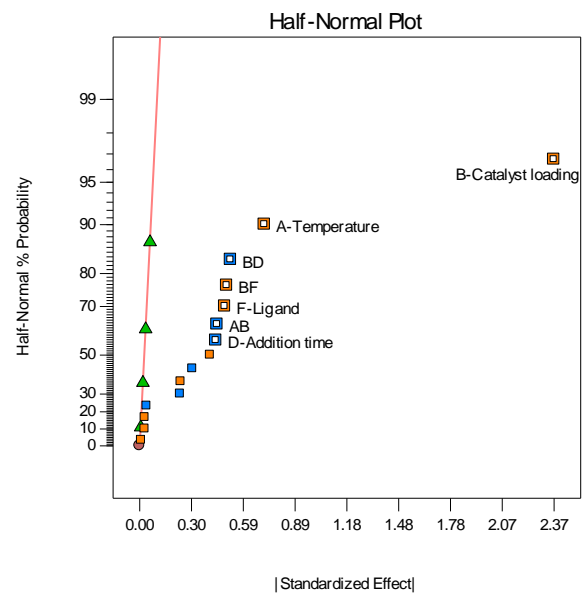


Chart 20. Half normal plot: isomer.

Design-Expert® Software
Biaryl

▲ Error from replicates

Shapiro-Wilk test

W-value = 0.927

p-value = 0.422

A: Temperature

B: Catalyst loading

C: Concentration

D: Addition time

E: nBuMgCl

F: Ligand

■ Positive Effects

■ Negative Effects

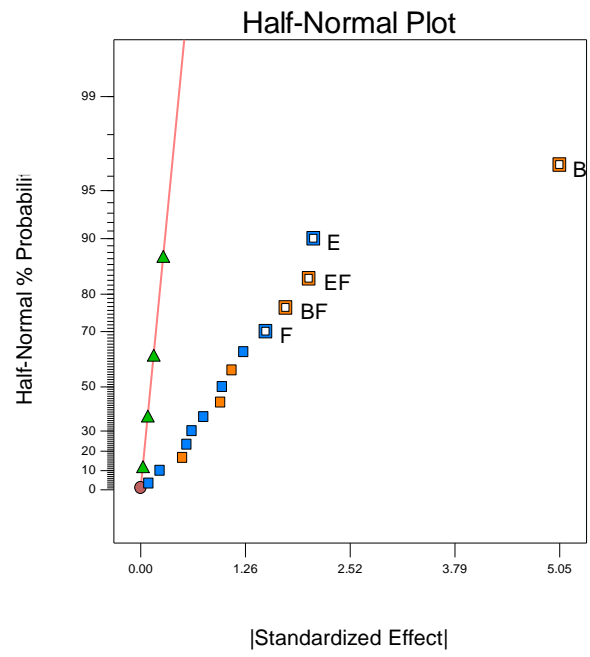


Chart 21. Half normal plot: biaryl.

7.3.2. Experimental Design 2

Procedure and results from analysis in **Section 3.2**.

For DoE 2 the procedure was:

1. Reactions carried out on a 0.2 g / 1.1 mmol scale in a STEM block tube on an Integrity 10 reaction station, in 40 volumes of solvent (8 mL, total)
2. A solution of $\text{Fe}(\text{acac})_3$ in THF was prepared at 20 mg mL⁻¹. The stock solution was used to prepare the reactions described in **Table 25/Table 26**
3. Reactions run for 6 hours, then quenched with 1 M HCl (5 mL)
4. Reactions sampled for GC analysis (250 μL into 1.25 mL ethyl acetate)

Table 25. Volumes for second experimental design.

Run	Cat / mg	NMP / mL	THF / mL
1	0.4	0.03	6.84
2	19.8	0.84	5.07
3	19.8	0.84	5.07
4	0.4	0.03	6.84
5	39.1	0.11	4.83
6	19.8	0.84	5.07
7	39.1	0.11	4.83
8	0.4	0.00	6.87
9	39.1	3.20	1.73
10	19.8	0.84	5.07
11	0.4	0.00	6.87
12	39.1	3.20	1.73

Table 26. Second experimental design.

		Factor 1	Factor 2	Factor 3	Factor 4
Std	Run	A:Temperature	B:Addition Time	C:Ligand	D:Catalyst Loading
		degC	Minutes	Cat. Equiv	mol%
7	1	-20	30	300	0.1
11	2	10	15	155	5.05
10	3	10	15	155	5.05
6	4	40	0	300	0.1
3	5	-20	30	10	10
9	6	10	15	155	5.05
2	7	40	0	10	10
1	8	-20	0	10	0.1
8	9	40	30	300	10
12	10	10	15	155	5.05
4	11	40	30	10	0.1
5	12	-20	0	300	10

Table 27. Results from second experimental design.

		Response 1	Response 2	Response 3	Response 4
Std	Run	Starting Material	Product	Isomer	Biaryl
7	1	84.6	12.9	0.0	2.5
11	2	3.9	90.3	1.0	4.8
10	3	3.4	91.5	0.9	4.2
6	4	87.1	11.4	0.0	1.6
3	5	32.3	64.0	0.5	3.2
9	6	2.7	91.5	1.0	4.8
2	7	56.0	36.0	1.2	6.8
1	8	86.4	9.4	0.0	4.2
8	9	16.1	73.8	2.0	8.1
12	10	5.9	88.7	0.9	4.5
4	11	91.4	7.3	0.0	1.3
5	12	0.4	88.7	1.2	9.8

Table 28. Analysis of variance: product.

Response	2	Product
ANOVA for selected factorial model		
Analysis of variance table [Partial sum of squares - Type III]		
	p-value	
Source	Prob > F	
Model	< 0.0001	significant
A-Temperature	0.0032	
C-Ligand	0.0005	
D-Catalyst Loading	< 0.0001	
AD	0.0066	
CD	0.0015	
Curvature	< 0.0001	significant
Residual		
Lack of Fit	0.0364	significant
Pure Error	5	3
Cor Total	15002	11

Table 29. Analysis of variance: isomer.

Response	3	Isomer
ANOVA for selected factorial model		
Analysis of variance table [Partial sum of squares - Type III]		
	p-value	
Source	Prob > F	
Model	< 0.0001	significant
A-Temperature	0.0004	
C-Ligand	0.0006	
D-Catalyst Loading	< 0.0001	
AD	0.0004	
CD	0.0006	
Curvature	0.0004	significant
Residual		
Lack of Fit	0.6716	not significant
Pure Error	0.016	3
Cor Total	4.410	11

Table 30. Analysis of variance: biaryl.

Response	4	Biaryl
ANOVA for selected factorial model		
Analysis of variance table [Partial sum of squares - Type III]		
	p-value	
Source	Prob > F	
Model	0.0008	significant
B-Addition Time	0.0118	
C-Ligand	0.0179	
D-Catalyst Loading	0.0002	
BC	0.0266	
CD	0.0040	
Curvature	0.8209	not significant
Residual		
Lack of Fit	0.0370	significant
Pure Error	0.24	3
Cor Total	69.90	11

Design-Expert® Software
Product

- ▲ Error from replicates
- A: Temperature
- B: Addition Time
- C: Ligand
- D: Catalyst Loading
- Positive Effects
- Negative Effects

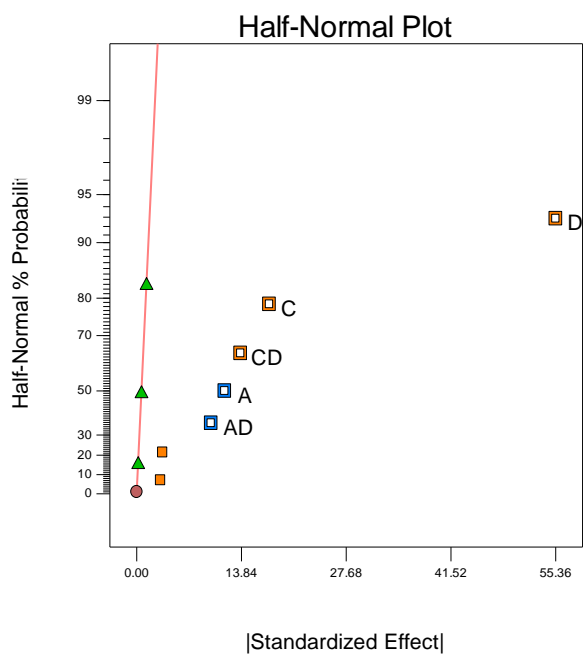


Chart 22. Half normal plot: product.

Design-Expert® Software
Isomer

- ▲ Error from replicates
- A: Temperature
- B: Addition Time
- C: Ligand
- D: Catalyst Loading
- Positive Effects
- Negative Effects

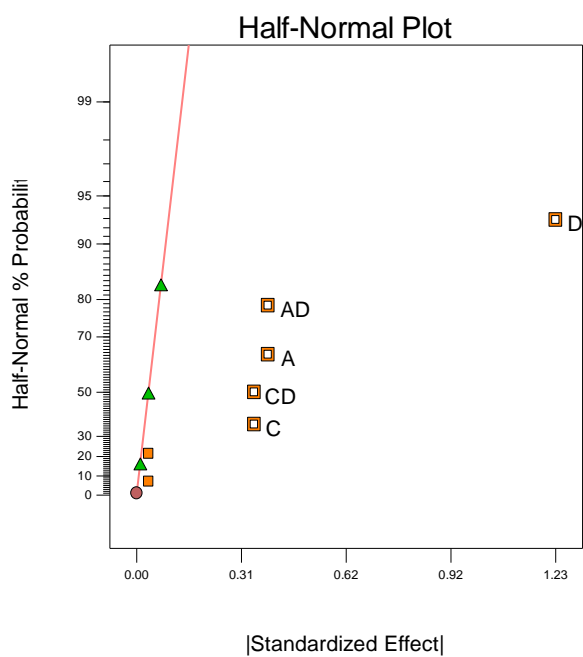


Chart 23. Half normal plot: isomer.

Design-Expert® Software
Biaryl

- ▲ Error from replicates
- A: Temperature
- B: Addition Time
- C: Ligand
- D: Catalyst Loading
- Positive Effects
- Negative Effects

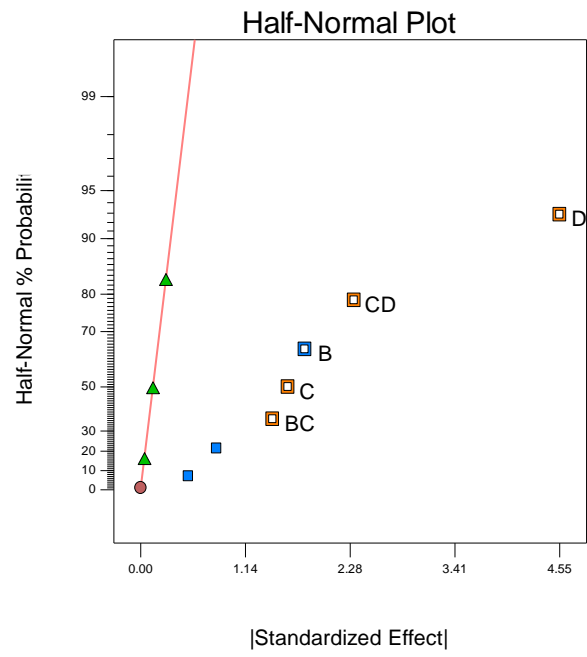


Chart 24. Half normal plot: biaryl.

7.3.3. Experimental Design 2: Augmented

Procedure and results from analysis in **Section 3.2**.

For DoE 2 the procedure was:

1. Reactions carried out on a 0.2 g / 1.1 mmol scale in a STEM block tube on an Integrity 10 reaction station, in 40 volumes of solvent (8 mL, total)
2. A solution of Fe(acac)₃ in THF was prepared at 20 mg mL⁻¹. The stock solution was used to prepare the reactions described in **Table 31/****Table 32**
3. Reactions run for 6 hours, then quenched with 1 M HCl (5 mL)
4. Reactions sampled for GC analysis (250 μL into 1.25 mL ethyl acetate)

Table 31. Volumes for augmented experimental design.

Run	Cat / mg	NMP / mL	THF / mL
13	0.84	5.07	0.84
14	0.02	6.86	0.02
15	0.84	5.07	0.84
16	0.84	5.07	0.84
17	1.66	3.28	1.66
18	1.62	4.29	1.62
19	0.84	5.07	0.84
20	0.84	5.07	0.84
21	0.84	5.07	0.84
22	0.05	5.85	0.05

Table 32. Augmented second experimental design.

			Factor 1	Factor 2	Factor 3	Factor 4
Std	Run	Block	A:Temperature	B:Addition Time	C:Ligand	D:Catalyst Loading
			degC	Minutes	Cat. Equiv	mol%
7	1	Block 1	-20	30	300	0.1
11	2	Block 1	10	15	155	5.05
10	3	Block 1	10	15	155	5.05
6	4	Block 1	40	0	300	0.1
3	5	Block 1	-20	30	10	10
9	6	Block 1	10	15	155	5.05
2	7	Block 1	40	0	10	10
1	8	Block 1	-20	0	10	0.1
8	9	Block 1	40	30	300	10
12	10	Block 1	10	15	155	5.05
4	11	Block 1	40	30	10	0.1
5	12	Block 1	-20	0	300	10
15	13	Block 2	10	0	155	5.05
19	14	Block 2	10	15	155	0.1
21	15	Block 2	10	15	155	5.05
22	16	Block 2	10	15	155	5.05
20	17	Block 2	10	15	155	10
18	18	Block 2	10	15	300	5.05
16	19	Block 2	10	30	155	5.05
14	20	Block 2	40	15	155	5.05
13	21	Block 2	-20	15	155	5.05
17	22	Block 2	10	15	10	5.05

Table 33. Results from augmented second experimental design.

		Response 1	Response 2	Response 3	Response 4
Std	Run	Starting Material	Product	Isomer	Biaryl
7	1	84.55	12.90	0.00	2.55
11	2	3.88	90.31	0.97	4.84
10	3	3.42	91.47	0.86	4.25
6	4	87.06	11.39	0.00	1.56
3	5	32.25	63.97	0.53	3.24
9	6	2.67	91.51	1.03	4.80
2	7	56.02	35.98	1.24	6.76
1	8	86.41	9.37	0.00	4.22
8	9	16.14	73.78	2.00	8.08
12	10	5.93	88.68	0.91	4.48
4	11	91.38	7.30	0.00	1.31
5	12	0.40	88.68	1.16	9.76
15	13	0.18	88.13	4.11	7.57
19	14	66.03	26.52	0.35	7.09
21	15	7.87	87.42	0.79	3.93
22	16	8.48	86.97	0.68	3.87
20	17	0.02	90.63	1.61	7.73
18	18	2.33	90.02	1.04	6.61
16	19	6.86	88.78	0.74	3.62
14	20	12.07	77.29	2.50	8.13
13	21	8.55	86.54	0.44	4.47
17	22	64.19	30.29	0.85	4.67

Table 34. Analysis of variance: product.

Response	2	Product	
Transform:	Logit	Lower bound:	0
ANOVA for Response Surface Reduced Quadratic Model		Upper bound:	100
Analysis of variance table [Partial sum of squares - Type III]			
	p-value		
Source	Prob > F		
Block			
Model	< 0.0001	significant	
A-Temperature	0.0340		
C-Ligand	0.0002		
D-Catalyst Loading	< 0.0001		
CD	0.0885		
C^2	< 0.0001		
D^2	< 0.0001		
Residual			
Lack of Fit	0.0095	significant	
Pure Error	0.07	4	
Cor Total	65.18	21	

Table 35. Analysis of variance: isomer.

Response	3	Isomer	
Transform:	Base 10 log	Constant:	0.0411459
ANOVA for Response Surface Reduced Linear Model			
Analysis of variance table [Partial sum of squares - Type III]			
	p-value		
Source	Prob > F		
Block			
Model	< 0.0001	significant	
D-Catalyst Loading	< 0.0001		
Residual			
Lack of Fit	0.0002	significant	
Pure Error	0.005	4	
Cor Total	7.552	21	

Table 36. Analysis of variance: biaryl.

Response	4	Biaryl
ANOVA for Response Surface Reduced 2FI Model		
Analysis of variance table [Partial sum of squares - Type III]		
	p-value	
Source	Prob > F	
Block		
Model	0.0012	significant
B-Addition Time	0.0288	
C-Ligand	0.0897	
D-Catalyst Loading	0.0009	
CD	0.0392	
Residual		
Lack of Fit	0.0010	significant
Pure Error	0.24	4
Cor Total	106.33	21

7.3.4. Confirmation of DoE Results

Table 37. Table to show confirmation of temperature selection, and introduce the use of higher purity Fe(acac)₃.

Temperature / °C	Addition Time / min	Iron / purity	Starting Material	Product	Isomer	Biaryl
			Area %			
(-20)	30	97%	25.4	70.2	0	4.4
20	30	97%	20.4	73.7	0	5.9
(-20)	0	97%	0	94.2	1.6	4.1
20	0	97%	0	88.0	5.1	7.0
(-20)	30	99.9%	1.6	84.4	4.8	9.2
20	30	99.9%	5.7	85.6	1.6	7.2
(-20)	0	99.9%	0.3	92.4	1.5	5.8
20	0	99.9%	0.1	89.6	4.8	5.4
(-20)	30	99.9%, 7.5 mol%	5.0	87.0	0.3	7.7
20	30	99.9%, 7.5 mol%	21.9	71.6	1.0	5.5
(-20)	0	99.9%, 7.5 mol%	0.2	93.5	1.3	5.0
20	0	99.9%, 7.5 mol%	0.0	89.8	4.5	5.7

7.3.5. Reproducibility Experiments

General Procedure following the DoE Optimisation:

iso-Propylmagnesium chloride (2 M in THF, 1.7 mL, 3.4 mmol) was added to a solution of (hetero)aryl chloride (2 mmol) and Fe(acac)₃ (53 mg, 0.15 mmol, 7.5 mol%) in THF (7.2 mL) and NMP (2.9 mL) at -20 °C. The mixture was stirred for 30 minutes then quenched with 1 M HCl (5 mL). The pH of heteroaryl halide solutions was adjusted using Na₂CO₃. The reaction mixture was sampled for GC/GCMS or HPLC/LCMS analysis.

Table 38. *para*-Substituted aryl chlorides.

Substrate	Hydrodehalogenated	Starting material	Product	Isomer	Biaryl	Other
4-Me	37.8	54.0	6.7	ND	1.6	ND
	37.7	54.0	6.4	ND	1.8	ND
4-CO ₂ Me	14.6	4.7	80.3	0.4	ND	ND
	14.6	4.3	80.5	0.6	ND	ND
4-CN	31.4	ND	68.6	ND	ND	ND
	33.9	1.6	64.5	ND	ND	ND
4-OMe	31.0	66.3	2.7	ND	ND	ND
	32.8	64.2	3.1	ND	ND	ND
4-F	0.8	ND	68.7	0.6	30.0	ND
	8.7	ND	65.9	0.5	24.9	ND
4-OCF ₃	34.9	1.9	52.5	1.8	8.9	ND
	35.9	0.6	54.6	1.9	7.1	ND
4-Cl	11.6	ND	70.9	1.3	ND	16.1
	11.0	ND	70.7	2.2	ND	16.1
4-CF ₂ H	21.8	5.1	61.5	2.1	9.5	ND

Table 39. *meta*-Substituted aryl chlorides.

Substrate	Hydrodehalogenated	Starting material	Product	Isomer	Biaryl	Other
3-CF₃	ND	ND	96.5	0.3	3.2	ND
	ND	ND	95.3	0.8	3.9	ND
3-CO₂Me	10.0	ND	87.9	ND	2.1	ND
	10.6	ND	87.1	ND	2.3	ND
3-CN	21.7	22.8	53.6	ND	1.8	ND
	27.5	20.5	49.5	ND	2.5	ND
3-OMe	44.6	29.4	23.5	1.3	8.4	ND
	50.9	23.9	23.6	0.8	5.8	ND
3-F	31.8	ND	58.7	0.7	8.8	ND
	32.5	ND	58.0	0.6	8.8	ND
3-OCF₃	37.0	16.6	40.1	ND	6.4	ND
	36.7	16.6	40.3	ND	6.4	ND
3-Cl	14.2	0.2	63.7	1.7	ND	20.1
	14.1	0.2	63.7	1.8	ND	20.2

7.4. Isolated iso-Propyl Substrates

Procedure and results from analysis in **Section 3.2**.

General Procedure following the DoE Optimisation:

Method A (preparation of 1-*iso*-propyl-4-(trifluoromethyl)benzene **268a**): *iso*-Propylmagnesium chloride (2 M in THF, 28.2 mL, 56.5 mmol) was added to a solution of 1-chloro-4-(trifluoromethyl)benzene (6 g, 33.2 mmol) and Fe(acac)₃ (0.88 g, 2.49 mmol, 7.5 mol%) in THF (159 mL) and NMP (48 mL) at -20 °C. The mixture was stirred for 30 minutes then quenched with a pH 2 buffer solution (240 mL, 0.125 M H₂SO₄ + 0.375 M Na₂SO₄). This mixture was further diluted with water (400 mL) and loaded onto a 120 g Biotage KP-C18-HS reverse phase column. The mixture was first eluted with water (1.2 L) then diethyl ether (300 mL). The diethyl ether fraction was concentrated in vacuo to afford the crude material as a yellow oil. This was further purified by distillation (66-68 °C, 45 mbar) to give 1-*iso*-propyl-4-(trifluoromethyl)benzene **268a** as a clear colourless oil (2.8 g, 45%).

¹H NMR (400 MHz, CDCl₃): δ 7.55 (d, J = 8.1 Hz, 2H), 7.34 (d, J = 8.1 Hz, 2H), 2.97 (sept, J = 6.8 Hz, ¹H), 1.27 (d, J = 6.9 Hz, 6H). ¹³C NMR (101 MHz, CDCl₃): δ 153.0, 128.3 (q, J = 32.2 Hz), 125.4 (q, J = 3.7 Hz), 124.6 (q, J = 271.6 Hz), 34.3, 23.9. ¹⁹F NMR (377 MHz, CDCl₃): δ -67.6. IR: ν = 2966, 1619, 1323, 1118, 1069, 606. MS (EI): m/z 188.0. HRMS (ASAP-TOF): calculated 180.0813, actual 180.0800.

Preparation of methyl 4-*iso*-propylbenzoate **189a**. Clear colourless oil (1.41 g, 22%).

¹H NMR (400 MHz, CDCl₃): δ 7.96 (d, J = 8.3 Hz, 2H), 7.29 (d, J = 8.1 Hz, 2H), 3.90 (s, 3H), 2.96 (sept, J = 6.9 Hz, 1H), 1.27 (d, J = 7.0 Hz, 6H). ¹³C NMR (101 MHz, CDCl₃): δ 167.3, 154.4, 129.9, 127.9, 126.6, 126.6, 52.1, 34.4, 23.8. IR: ν = 2961, 1719, 1273, 1109, 773, 706. MS (EI): m/z 179.0 HRMS (ESI+): calculated 179.1067, actual 179.1068.

Method B (preparation of tert-butyl 2-*iso*-propylnicotinate **292**): *iso*-Propylmagnesium chloride (2 M in THF, 1.9 mL, 3.77 mmol) was added to a solution of tert-butyl 2-chloronicotinate (473 mg, 2.2 mmol) and Fe(acac)₃ (58.7 mg, 0.17 mmol, 7.5 mol%) in THF (7.6 mL) and NMP (3.2 mL) at -20 °C. The mixture was stirred for 30 minutes then quenched with 1 M HCl (5 mL) and neutralized with 5 M sodium hydroxide (2 mL). The resulting mixture was diluted with water (10 mL) and ethyl acetate (15 mL). The phases were separated and the organic phase was washed with brine (5 x 10 mL). The organic phase was dried over magnesium sulfate and concentrated in vacuo. The resulting residue was dry loaded onto a pre-packed normal phase column and purified by flash

chromatography (25% diethyl ether in hexane). This gave tert-butyl 2-*iso*-propylnicotinate as a yellow oil (0.34 g, 69%).

^1H NMR (400 MHz, CDCl_3): δ 8.64 (dd, $J = 4.7, 1.8$ Hz, 1H), 7.92 (d, $J = 7.8$ Hz, 1H), 7.13 (d, $J = 7.8$ Hz, 1H), 3.75 (sept, $J = 6.8$ Hz, 1H), 1.60 (s, 9H), 1.30 (d, $J = 6.8$ Hz, 6H). ^{13}C NMR (101 MHz, CDCl_3): δ 166.4, 165.8, 150.6, 136.9, 127.0, 119.9, 81.2, 31.8, 27.7, 21.8. IR: $\nu = 2966, 1721, 1255, 1132, 1069, 783$. (EI): m/z 222.0. HRMS (ESI+): calculated 222.1489, actual 222.1491.

Preparation of ethyl 2-*iso*-propylnicotinate **293**. Yellow oil (0.29 g, 69%).

^1H NMR (400 MHz, CDCl_3): δ 8.68 (dd, $J=4.77, 1.83$ Hz, 1 H), 8.03 (dd, $J=7.83, 1.96$ Hz, 1 H), 7.17 (dd, $J=7.82, 4.89$ Hz, 1 H), 4.39 (q, $J=7.09$ Hz, 2 H), 3.83 (spt, $J=6.72$ Hz, 1 H), 1.41 (t, $J=7.09$ Hz, 3 H), 1.31 (d, $J=6.85$ Hz, 6 H). ^{13}C NMR (101 MHz, CDCl_3): δ 167.3, 167.1, 151.6, 137.8, 125.7, 120.5, 61.4, 32.3, 22.3, 14.2. IR: $\nu = 2977, 1716, 1132, 1071$. MS (EI): m/z 194.1 HRMS (ESI+): calculated 194.1176, actual 194.1175.

Method C (preparation of 3-*iso*-propyl-6-phenylpyridazine **296**): *iso*-Propylmagnesium chloride (2 M in THF, 17.8 mL, 35.7 mmol) was added to a solution of 3-chloro-6-phenylpyridazine (4 g, 21.0 mmol) and $\text{Fe}(\text{acac})_3$ (0.56 g, 1.57 mmol, 7.5 mol%) in THF (75 mL) and NMP (18 mL) at -20 °C. The mixture was stirred for 30 minutes then quenched with 0.5 M citric acid (100 mL) and neutralised with 0.5 M sodium carbonate (100 mL). The organic phase was separated, and the aqueous phase was extracted using diethyl ether (2 x 100 mL). The combined organics were dried over sodium sulfate and concentrated in vacuo. The resulting residue was dry loaded onto a pre-packed normal phase column and purified by flash chromatography (0-20% EtOAc in heptane). This gave 3-*iso*-propyl-6-phenylpyridazine as a yellow solid (3.1 g, 75%).

^1H NMR (400 MHz, CDCl_3): δ 8.09 (d, $J = 8.1$ Hz, 2H), 7.79 (d, $J = 8.8$ Hz, 1H), 7.56 – 7.44 (m, 3H), 7.41 (d, $J = 8.8$ Hz, 1H), 3.36 (sept, $J = 7.0$ Hz, 1H), 1.42 (d, $J = 7.0$ Hz, 6H). ^{13}C NMR (101 MHz, CDCl_3): δ 166.9, 157.5, 136.7, 129.8, 129.1, 127.0, 125.0, 124.2, 34.8, 22.5. IR: $\nu = 3048, 2957, 1422, 750, 693$. MS (EI): m/z 197.2. HRMS (ESI+): calculated 199.1230, actual 199.1221. MP: 61-62 °C.

Preparation of (4-*iso*-propylphenyl)(morpholino)methanone **270a**. Clear colourless oil (0.94 g, 46%)

^1H NMR (400 MHz, CDCl_3): δ 7.34 (d, $J = 8.2$ Hz, 2H), 7.26 (d, $J = 8.1$ Hz, 2H), 3.73 (br. s, 6H), 3.50 (br. s, 2H), 2.93 (sept, $J = 6.9$ Hz, 1H), 1.25 (d, $J = 6.9$ Hz, 6H). ^{13}C NMR (101 MHz, CDCl_3): δ 170.6, 150.9, 132.7, 127.3, 126.6, 66.9, 48.2, 42.6, 34.0, 23.8. IR: $\nu = 2960, 2856, 1629, 1422, 1277, 1010, 837$. MS (EI): m/z 232.2. HRMS (ESI+): calculated 234.1478, actual 234.1489.

Preparation of 2-(4-*iso*-propylphenyl)pyridine **271a**. Clear colorless oil (1.0 g, 48%).

^1H NMR (400 MHz, CDCl_3): δ 8.67 (d, J = 4.7 Hz, 1H), 7.92 (d, J = 8.3 Hz, 2H), 7.77 – 7.66 (m, 2H), 7.33 (d, J = 8.2 Hz, 2H), 7.19 (dd, J = 6.2, 4.9 Hz, 1H), 2.97 (sept, J = 6.8 Hz, 1H), 1.29 (d, J = 6.9 Hz, 6H). ^{13}C NMR (101 MHz, CDCl_3): δ 157.7, 150.0, 149.7, 137.2, 136.7, 127.0, 127.0, 121.9, 120.4, 34.1, 24.1. IR: ν = 2959, 2869, 1587, 1466, 1435, 779. MS (EI): m/z 197.1 HRMS (ESI+): calculated 198.1277, actual 198.1273.

Preparation of 1-*iso*-propylisoquinoline **295**. Red oil (2.96 g, 71%).

^1H NMR (400 MHz, CDCl_3) δ 8.49 (d, J = 5.7 Hz, 1H), 8.23 (d, J = 8.4 Hz, 1H), 7.81 (d, J = 8.0 Hz, 1H), 7.65 (t, J = 6.9 Hz, 1H), 7.58 (t, J = 7.0 Hz, 1H), 7.49 (d, J = 5.7 Hz, 1H), 3.95 (sept, 6.7 Hz, 1H), 1.45 (d, J = 6.8 Hz, 6H). ^{13}C NMR (101 MHz, CDCl_3): δ 166.4, 142.1, 136.5, 129.7, 127.7, 127.0, 126.4, 124.9, 119.1, 31.1, 22.4. IR: ν = 3050, 2963, 1561, 820, 744, 680. MS (ESI+): m/z 172.2 HRMS (ESI+): calculated 172.1121, actual 172.1115.

Preparation of 6-*iso*-propylpicolinonitrile **294**. Yellow oil (0.64 g, 61%).

^1H NMR (400 MHz, CDCl_3): δ 7.73 (t, J = 7.8 Hz, 1H), 7.51 (dd, J = 7.6, 1.0 Hz, 1H), 7.39 (dd, J = 8.0, 1.0 Hz, 1H), 3.10 (sept, J = 6.9 Hz, 1H), 1.30 (d, J = 7.0 Hz, 6H). ^{13}C NMR (101 MHz, CDCl_3): δ 169.6, 137.3, 133.3, 126.0, 124.5, 117.8, 36.5, 22.4. IR: ν = 2968, 2236, 1588, 1445, 811, 733. MS (EI): m/z 146.0. HRMS (ESI+): calculated 147.0917, actual 147.0913.

Method D (preparation of 2-*iso*-propylpyridine **291**): *iso*-Propylmagnesium chloride (2 M in THF, 17.8 mL, 35.7 mmol) was added to a solution of 2-chloropyridine (2 g, 1.67 mL, 17.6 mmol) and $\text{Fe}(\text{acac})_3$ (0.47 g, 1.32 mmol, 7.5 mol%) in THF (63 mL) and NMP (25 mL) at -20 °C. The mixture was stirred for 30 minutes then quenched with 0.5 M citric acid (25 mL) and neutralised with 0.5 M sodium carbonate (25 mL). The organic phase was separated, and the aqueous phase was extracted using tert-butyl methyl ether (3 x 100 mL). The combined organics were dried over sodium sulfate and concentrated in vacuo. The resulting residue was dry loaded onto a pre-packed C18 (reverse phase) column and purified by flash chromatography [5-70% (acetonitrile + ammonia) in (water + sodium bicarbonate)]. This gave 2-*iso*-propylpyridine as a clear colorless oil (1.2 g, 56%).

^1H NMR (400 MHz, CDCl_3) δ 8.53 (d, J = 4.2 Hz, 1H), 7.60 (t, J = 7.6 Hz, 1H), 7.16 (d, J = 7.9 Hz, 1H), 7.09 (dd, J = 7.6, 4.8 Hz, 1H), 3.06 (sept, J = 6.9 Hz, 1H), 1.30 (d, J = 6.9 Hz, 6H). ^{13}C NMR (101 MHz, CDCl_3) δ 167.4, 149.1, 136.5, 121.1, 120.7, 36.5, 22.7. IR: ν = 2964, 1591, 1475, 1433, 731. MS (EI): 122.1. HRMS (ESI+): calculated 122.0964, actual 122.0968.

Preparation of 3-*iso*-propylpyridine **290**. Orange oil (0.5 g, 47%).

^1H NMR (400 MHz, CDCl_3): δ 8.49 (s, 1H), 8.43 (d, $J = 4.9$ Hz, 1H), 7.54 (d, $J = 7.9$ Hz, 1H), 7.22 (dd, $J = 7.7, 4.9$ Hz, 1H), 2.94 (sept, $J = 7.0$ Hz, 1H), 1.27 (dd, $J = 6.9, 1.0$ Hz, 6H). ^{13}C NMR (101 MHz, CDCl_3): δ 148.8, 147.4, 143.9, 133.9, 123.5, 31.9, 23.8. IR: $\nu = 2962, 1422, 713$. MS (EI): 122.1. HRMS (ESI+): calculated 122.0964, actual 122.0968.

Preparation of 2-methoxy-6-*iso*-propylpyridine **223a**. Clear colorless oil (1.7 g, 79%).

^1H NMR (400 MHz, CDCl_3): δ 7.47 (dd, $J = 8.2, 7.3$ Hz, 1H), 6.71 (d, $J = 7.3$ Hz, 1H), 6.53 (d, $J = 8.1$ Hz, 1H), 3.92 (s, 3H), 2.94 (sept, $J = 6.9$ Hz, 1H), 1.27 (d, $J = 6.9$ Hz, 6H). ^{13}C NMR (101 MHz, CDCl_3): δ 165.4, 163.6, 138.9, 113.0, 107.4, 53.5, 36.0, 22.5. IR: $\nu = 2964, 1578, 1286, 1029, 799, 732$. MS (ESI+): 152.1. HRMS (ESI+): calculated 152.1070, actual 152.1065.

Method E (preparation of 6-chloro-2-*iso*-propylquinoline **297**): iso-Propylmagnesium chloride (2 M in THF, 7.6 mL, 15.2 mmol) was added to a solution of 2,6-dichloroquinoline (2.5 g, 12.6 mmol) and $\text{Fe}(\text{acac})_3$ (0.33 g, 0.95 mmol, 7.5 mol%) in THF (48 mL) and NMP (18 mL) at -20 °C. The mixture was stirred for 30 minutes then quenched with 0.5 M citric acid (25 mL) and neutralised with 0.5 M sodium carbonate (25 mL). The organic phase was separated, and the aqueous phase was extracted using tert-butyl methyl ether (3 x 100 mL). The combined organics were dried over sodium sulfate and concentrated in vacuo. The resulting residue was dry loaded onto a pre-packed C18 (reverse phase) column and purified by flash chromatography [5-70% (acetonitrile + ammonia) in (water + sodium bicarbonate)]. This gave 6-chloro-2-*iso*-propylquinoline as a yellow oil (1.9 g, 73%).

^1H NMR (400 MHz, CDCl_3) δ 7.98 (dd, $J = 8.8, 4.3$ Hz, 2H), 7.74 (d, $J = 2.3$ Hz, 1H), 7.60 (dd, $J = 9.0, 2.4$ Hz, 1H), 7.35 (d, $J = 8.6$ Hz, 1H), 3.24 (sept, $J = 6.9$ Hz, 1H), 1.39 (d, $J = 6.9$ Hz, 6H). ^{13}C NMR (101 MHz, CDCl_3) δ 168.1, 146.3, 135.6, 131.4, 130.8, 130.2, 127.6, 126.2, 120.3, 37.4, 22.6. IR: $\nu = 2964, 1597, 1490, 1071, 830$. MS (ESI+): 206.2. HRMS (ESI+): calculated 206.0731, actual 206.0728.

7.5. Additive Screening for iso-Propyl Cross-Coupling

Procedure and results from analysis in **Section 5.2.1**.

General Procedure:

Reaction carried out on a 2 mmol scale, with 1.7 equiv. Grignard reagent. Additive added in 2 quantities – 15 and 1500 mol%.

1. Solvent, additive and aryl chloride added to pre-dried nitrogen flushed stem-block tube
2. Iron catalyst added as a 20 mg mL⁻¹ solution in solvent
3. Reaction mixture stirred in integrity 10, whilst cooling to -20 °C over 30 minutes
4. Grignard reagent added rapidly in 1 aliquot
5. Reaction mixture stirred for 30 minutes
6. Reaction mixture quenched with 1M HCl
7. Reaction mixture sampled for GC analysis

Table 40. Results from additive screen for *iso*-propyl cross-coupling.

Additive	SM	Product	Isomer	Biaryl	Solvent	Additive mol%
Propylene carbonate	22	66	0	11	THF	1500
	48	35	5	12	THF	15
	57	39	0	4	2-MeTHF	1500
	67	20	6	7	2-MeTHF	15
Pyridine	45	55	0	0	THF	1500
	54	38	0	8	THF	15
	72	28	0	0	2-MeTHF	1500
	88	10	0	2	2-MeTHF	15
Pyridine/propylene carbonate (1:1)	1	94	1	4	THF	1500
	14	80	1	4	2-MeTHF	1500
DMEU	0	91	1	8	THF	1500
	54	33	0	12	THF	15
	0	91	1	8	2-MeTHF	1500
	70	21	0	9	2-MeTHF	15
N-methylpyrrolidinone	0	95	1	4	THF	1500
	43	41	0	16	THF	15
	0	97	0	3	2-MeTHF	1500
	56	32	1	12	2-MeTHF	15
N-methylmorpholine	57	34	0	10	THF	1500
	57	30	0	12	THF	15
	85	13	0	2	2-MeTHF	1500
	70	21	0	8	2-MeTHF	15
N-octylpyrrolidinone	0	94	0	6	THF	1500
	48	37	0	15	THF	15
	0	94	0	6	2-MeTHF	1500
	74	19	0	7	2-MeTHF	15
	63	31	0	5	THF	1500
	51	40	0	9	THF	15
	66	26	1	7	2-MeTHF	1500
	71	22	0	7	2-MeTHF	15
Isoquinoline	96	4	0	0	THF	1500
	44	45	2	9	THF	15
	98	2	0	0	2-MeTHF	1500
	84	13	0	3	2-MeTHF	15
HMTA	39	45	1	15	THF	1500
	59	29	0	12	THF	15
	42	45	0	12	2-MeTHF	1500
	70	21	0	8	2-MeTHF	15

Dimethoxyethane	96	4	0	1	THF	1500
	57	33	0	9	THF	15
	100	0	0	0	2-MeTHF	1500
	78	17	0	5	2-MeTHF	15
Tert-butyl methyl ether	55	31	1	13	THF	1500
	61	28	0	11	THF	15
	63	26	1	11	2-MeTHF	1500
	74	19	0	7	2-MeTHF	15
D-glucosamine	64	25	0	10	THF	15
	78	16	0	6	2-MeTHF	15
Sarcosine	35	47	1	17	THF	15
	73	19	1	7	2-MeTHF	15
N,N-dimethylglycine	69	22	0	9	THF	15
	64	25	1	10	2-MeTHF	15
N,N-dimethylglycine ethyl ester	59	29	0	13	THF	15
	61	27	0	12	2-MeTHF	15

7.5.1. DoE Experiments for iso-Propyl Additives

Procedure and results from analysis in **Section 5.2.1**.

General experimental:

Reaction carried out on a 2 mmol scale, with 1.7 equiv. Grignard reagent. Additive added in 2 quantities – 15 and 1500 mol%. Propylene carbonate used with THF, DMEU used with 2-methyl THF.

1. Solvent, additive and aryl chloride added to pre-dried nitrogen flushed stem-block tube
2. Iron catalyst added as a 20 mg mL⁻¹ solution in solvent
3. Reaction mixture stirred in integrity 10, whilst cooling to -20 °C over 30 minutes
4. Grignard reagent added rapidly in 1 aliquot
5. Reaction mixture stirred for 30 minutes
6. Reaction mixture quenched with 1M HCl
7. Reaction mixture sampled for GC analysis (50 µL into 1 mL ethyl acetate)

Table 41. DoE structure for *iso*-propyl additive DoE.

Expt.	Run	Temp.	Cat. Mol%	Ligand eq.	Grignard eq.	Time	Conc.
13	1	-20	2.5	300	2	0	20
16	2	20	10	300	2	0	20
26	3	20	2.5	10	2	30	60
18	4	20	2.5	10	1	30	20
21	5	-20	2.5	300	1	30	20
11	6	-20	10	10	2	0	20
25	7	-20	2.5	10	2	30	20
22	8	20	2.5	300	1	30	60
20	9	20	10	10	1	30	60
1	10	-20	2.5	10	1	0	20
17	11	-20	2.5	10	1	30	60
15	12	-20	10	300	2	0	60
10	13	20	2.5	10	2	0	20
32	14	20	10	300	2	30	60
3	15	-20	10	10	1	0	60
7	16	-20	10	300	1	0	20
8	17	20	10	300	1	0	60
5	18	-20	2.5	300	1	0	60
28	19	20	10	10	2	30	20
4	20	20	10	10	1	0	20
19	21	-20	10	10	1	30	20
6	22	20	2.5	300	1	0	20
2	23	20	2.5	10	1	0	60
35	24	0	6.25	155	1.5	15	40
14	25	20	2.5	300	2	0	60
27	26	-20	10	10	2	30	60
30	27	20	2.5	300	2	30	20
24	28	20	10	300	1	30	20
9	29	-20	2.5	10	2	0	60
31	30	-20	10	300	2	30	20
12	31	20	10	10	2	0	60
23	32	-20	10	300	1	30	60
34	33	0	6.25	155	1.5	15	40
33	34	0	6.25	155	1.5	15	40
29	35	-20	2.5	300	2	30	60
36	36	0	6.25	155	1.5	15	40

Table 42. Results from propylene carbonate DoE.

	Hydrodehalogenated	Starting Material	Product	Biaryl
1	50	12	34	4
2	41	50	8	2
3	50	18	26	6
4	25	66	6	2
5	22	74	4	1
6	59	16	19	5
7	22	74	2	1
8	18	76	5	1
9	18	75	6	1
10	30	52	13	5
11	24	59	13	4
12	45	24	25	6
13	54	19	21	6
14	24	69	6	1
15	33	46	16	5
16	28	60	10	3
17	26	65	7	2
18	27	56	13	5
19	26	65	8	2
20	30	57	10	4
21	28	66	6	1
22	34	55	8	3
23	31	49	15	5
24	31	60	8	1
25	41	47	10	2
26	28	60	10	3
27	36	48	13	3
28	26	69	5	1
29	53	11	28	8
30	35	39	24	3
31	42	33	19	5
32	21	68	10	1
33	33	52	12	2
34	39	41	16	4
35	28	57	13	2
36	36	45	15	3

Table 43. Results from DMEU DoE

	Hydrodehalogenated	Starting Material	Product	Biaryl
1	25	8	59	9
2	38	0	59	3
3	23	74	2	0
4	28	71	1	0
5	19	11	63	7
6	69	2	23	5
7	36	60	4	0
8	24	18	49	9
9	27	57	13	3
10	33	52	11	4
11	21	73	5	2
12	26	0	70	4
13	63	16	17	4
14	20	0	79	1
15	34	45	17	4
16	28	53	18	1
17	20	32	40	9
18	18	25	55	3
19	50	21	26	3
20	38	53	7	2
21	33	45	20	2
22	23	13	52	12
23	26	29	38	7
24	27	0	65	7
25	38	0	60	2
26	55	15	27	3
27	25	6	62	6
28	28	0	68	3
29	39	39	16	6
30	27	59	13	0
31	57	26	15	3
32	15	35	48	2
33	26	0	69	5
34	26	2	67	6
35	22	22	50	7
36	29	0	63	8

7.6. HTC Screens for Cyclopropyl Coupling

Ligands from **Section 5.2.2**.

Table 44. Ligands and their associated numbers (screen 1 and 2).

Entry	Ligand	Number
1	1,10-phenanthroline	400
2	di-tertbutyl(methyl)phosphonium tetrafluoroborate	401
3	N,N,N',N'',N''-pentamethyldiethylenetriamine	402
4	Bis(2-diphenylphosphinoethyl)phenylphosphine	403
5	1,1'-Bis(dicyclohexylphosphino)ferrocene	404
6	Bis[(2-diphenylphosphino)ethyl]ammonium chloride	405
7	2,2':6',2''-Terpyridine	406
8	(S,S)-(+)-N,N'-Bis(3,5-di-tert-butylsalicylidene)-1,2-cyclohexanediamine	407
9	2,6-Bis(di-tert-butylphosphinomethyl)pyridine	408
10	Tris(pentafluorophenyl)phosphine	409
11	1,3-Bis-(2,6-diisopropylphenyl)imidazolium chloride	410
12	1,3-Diisopropylimidazolium tetrafluoroborate	411
13	(S,S)-DACH-phenyl Trost ligand	412
14	2,6-Bis[(4S)-(-)-isopropyl-2-oxazolin-2-yl]pyridine	413
15	Ethylenebis(diphenylphosphine)	148
16	2,2'-Bis[(4S)-4-benzyl-2-oxazoline]	414
17	Triphenyl phosphite	415
18	1,1,1-Tris(diphenylphosphinomethyl)ethane	416
19	2,2'-Bipyridyl	417
20	NACNAC (isopropyl)	418
21	pyridine diimine (ethyl)	419
22	N,N,N',N'-Tetramethylethylenediamine	96
23	Cyclohexyl-CAAC	420
24	(R,R)-DACH-pyridyl Trost ligand	421

Table 45. Ligands and their associated numbers (screen 3).

Entry	Ligand	Number
1	1,1'-BIS(DIPHENYLPHOSPHINO)FERROCENE	438
2	1,3-BIS(DI-T-BUTYLPHOSPHINOMETHYL)BENZENE	445
3	1,1'-BIS(DICYCLOHEXYLPHOSPHINO)FERROCENE	402
4	1,1'-BIS(DIISOPROPYLPHOSPHINO)FERROCENE	440
5	1,1'-BIS(DI-TERT-BUTYLPHOSPHINO)FERROCENE	439
6	(R)-(+)-2,2'-BIS(DIPHENYLPHOSPHINO)-1,1'-BINAPHTHYL	441
7	(Oxydi-2,1-phenylene)bis(diphenylphosphine)	442
8	9,10A-DIHYDRO-9,9-DIMETHYL-4,5-BIS(DIPHENYLPHOSPHINO)-8AH-XANTHENE	443
9	9,9-Dimethyl-4,5-bis(di-tert-butylphosphino)xanthene	444
10	4,6-BIS(DIPHENYLPHOSPHINO)PHENOXAZINE	446
11	(2R)-1-[(1R)-1-[BIS(1,1-DIMETHYLETHYL)PHOSPHINO]ETHYL]-2-(DICYCLOHEXYLPHOSPHINO)FERROCENE	447
12	1-Diphenylphosphino-1'-(di-tert-butylphosphino)ferrocene	448

Table 46. Ligands and their associated numbers (screen 4).

Entry	Ligand	Number
1	4,6-Bis(diphenylphosphino)-10H-phenoxazine, 4,6-Bis(diphenylphosphino)phenoxazine	446
2	Phosphine, 4,6-phenoxathiindiybis[diphenyl- (9Cl)]	470
3	4,5-Bis(dicyclohexylphosphino)-9,9-dimethyl-9H-xanthene	471
4	4,6-Bis(diphenylphosphino)dibenzofuran	472
5	Bis[2-(4-methyldiphenylphosphino)phenyl]methane	473
6	P,P'-(9,9-Dimethyl-9H-xanthene-4,5-diyl)bis[N,N,N',N'-tetraethylphosphonous diamide]	474
7	Bis(dicyclohexylphosphinophenyl) ether	475
8	(-)-2,3-O-Isopropylidene-2,3-dihydroxy-1,4-bis(diphenylphosphino)butane	476

7.6.1. Screen 1 – Cyclopropylmagnesium Bromide + (4-chlorophenyl)(morpholino)methanone

Procedure and results from **Section 5.2.2.1**.

For high throughput screen 1 the procedure was:

1. Catalyst (10 mol%), solid ligands and aryl chloride weighed into a vial (50 mg, 0.24 mmol scale)
2. Solids purged in a glove bag with nitrogen overnight
3. Liquid ligands added using Gilson pipette
4. 2-methylTHF added using multi-channel pipette (0.5 mL)
5. Mixture stirred for 30 minutes
6. Grignard reagent added rapidly in 1 aliquot using a multichannel pipette (cyclopropylmagnesium bromide, 1.0M in 2-methyl THF)
7. Reaction mixture stirred for 1 hour
8. Reaction mixture quenched with pH 2 buffer (0.25 mL, 0.125 M H₂SO₄, 0.375 M Na₂SO₄)
9. Reaction mixture stirred for 15 minutes, then sampled for HPLC/LCMS (20 μL into 1 mL MeCN/water)

NOTE: Monodentate ligands used at 20 mol% loading, multidentate ligands used at 10 mol% loading.

Table 47. Results from high throughput screen.

Entry	Catalyst	Ligand	Dehalogenated	Starting Material	Coupled	Cyclopropyl Ketone	Dicyclopropyl
1	FeCl ₂	187	1.1	22.5	1.3	74.8	0.3
2	FeCl ₂	401	0.9	78.3	1.2	19.6	0.0
3	FeCl ₂	402	1.5	22.0	2.4	73.6	0.5
4	FeCl ₂	403	0.2	25.5	0.5	73.8	0.0
5	FeCl ₂	404	1.5	18.8	6.4	71.5	1.7
6	FeCl ₂	405	1.8	22.6	0.3	70.8	4.4
7	FeCl ₂	406	0.6	20.4	0.8	77.9	0.2
8	FeCl ₂	407	1.7	29.4	1.8	67.1	0.0
9	FeCl ₂	408	1.4	22.8	2.0	73.4	0.5
10	FeCl ₂	409	0.0	26.6	1.2	71.9	0.2
11	FeCl ₂	410	1.4	17.0	4.7	56.5	20.4
12	FeCl ₂	411	1.4	71.1	1.7	25.9	0.0
13	FeCl ₂	412	1.5	30.2	2.9	65.1	0.3
14	FeCl ₂	413	0.8	22.3	1.3	75.3	0.3
15	FeCl ₂	148	0.2	21.8	0.6	77.4	0.0
16	FeCl ₂	414	0.5	22.6	2.9	73.5	0.4
17	FeCl ₂	415	0.0	55.7	0.7	43.6	0.0
18	FeCl ₂	416	0.5	22.0	0.7	76.8	0.0
19	FeCl ₂	417	0.6	22.5	0.9	76.0	0.0
20	FeCl ₂	418	1.5	24.6	2.0	71.5	0.4
21	FeCl ₂	419	2.0	25.3	1.5	71.2	0.0
22	FeCl ₂	96	1.9	22.5	2.7	72.5	0.4
23	FeCl ₂	420	1.5	27.7	2.0	68.5	0.3
24	FeCl ₂	421	1.3	20.3	1.6	76.6	0.3
25	FeF ₃ •3H ₂ O	187	0.0	17.0	1.2	81.9	0.0
26	FeF ₃ •3H ₂ O	401	0.0	40.0	0.6	59.4	0.0
27	FeF ₃ •3H ₂ O	402	0.0	17.4	1.5	81.1	0.0
28	FeF ₃ •3H ₂ O	403	0.0	19.4	1.3	79.3	0.0
29	FeF ₃ •3H ₂ O	404	0.0	20.4	1.0	78.6	0.0
30	FeF ₃ •3H ₂ O	405	0.0	20.3	1.0	72.0	6.6
31	FeF ₃ •3H ₂ O	406	0.0	16.5	1.1	82.4	0.0
32	FeF ₃ •3H ₂ O	407	0.0	25.6	1.6	72.8	0.0
33	FeF ₃ •3H ₂ O	408	0.0	21.5	1.0	77.5	0.0
34	FeF ₃ •3H ₂ O	409	0.0	19.0	0.9	80.1	0.0

35	FeF ₃ •3H ₂ O	410	0.0	17.0	0.9	63.6	18.4
36	FeF ₃ •3H ₂ O	411	0.0	32.4	0.5	67.1	0.0
37	FeF ₃ •3H ₂ O	412	0.0	20.6	1.6	77.8	0.0
38	FeF ₃ •3H ₂ O	413	0.5	19.4	0.2	79.9	0.0
39	FeF ₃ •3H ₂ O	148	0.0	17.9	1.4	80.7	0.0
40	FeF ₃ •3H ₂ O	414	0.0	15.5	1.1	83.5	0.0
41	FeF ₃ •3H ₂ O	415	0.0	26.5	0.2	73.3	0.0
42	FeF ₃ •3H ₂ O	416	0.0	18.3	1.4	80.3	0.0
43	FeF ₃ •3H ₂ O	417	0.0	19.1	1.0	79.9	0.0
44	FeF ₃ •3H ₂ O	418	0.0	19.7	1.6	78.8	0.0
45	FeF ₃ •3H ₂ O	419	0.0	21.3	1.4	77.3	0.0
46	FeF ₃ •3H ₂ O	96	0.0	20.0	1.6	78.3	0.0
47	FeF ₃ •3H ₂ O	420	0.3	22.8	2.0	74.5	0.4
48	FeF ₃ •3H ₂ O	421	0.0	18.3	1.7	80.1	0.0

7.6.2. Screen 2 - Cyclopropylmagnesium Bromide + 6-Chloroquinoline (2 catalysts, 24 ligands)

Procedure and results from **Section 5.2.2.2**.

For high throughput screen 2 the procedure was:

1. Catalyst (10 mol%), solid ligands and aryl chloride weighed into a vial (25 mg, 0.15 mmol scale)
2. Solids purged in a glove bag with nitrogen overnight
3. Liquid ligands added using Gilson pipette
4. THF added using multi-channel pipette (0.2 mL)
5. Mixture stirred for 20 minutes
6. Grignard reagent added rapidly in 1 aliquot using a multichannel pipette (2 equiv., cyclopropylmagnesium bromide, 0.5 M in THF)
7. Reaction mixture stirred for 1 hour
8. Reaction mixture quenched with pH 2 buffer (0.1 mL, 0.125 M H₂SO₄, 0.375 M Na₂SO₄)
9. Reaction mixture stirred for 15 minutes, then sampled for HPLC/LCMS (10 μ L into 0.5 mL MeCN/water)

NOTE: Monodentate ligands used at 20 mol% loading, multidentate ligands used at 10 mol% loading.

Table 48. Results from high throughput screen.

Entry	Catalyst	Ligand	Starting Material	Product	Adduct 1	Adduct 2	Adduct 3
1	FeCl ₂	187	84.9	10.3	4.4	0.2	0.1
2	FeCl ₂	401	95.6	2.1	1.8	0.1	0.4
3	FeCl ₂	402	89.6	7.0	2.6	0.3	0.5
4	FeCl ₂	403	93.9	0.2	3.0	0.0	3.0
5	FeCl ₂	404	64.1	31.9	3.4	0.2	0.4
6	FeCl ₂	405	94.2	0.4	2.5	2.1	0.8
7	FeCl ₂	406	94.2	0.2	5.2	0.2	0.2
8	FeCl ₂	407	91.1	3.1	4.7	0.5	0.7
9	FeCl ₂	408	87.4	6.7	5.0	0.4	0.5
10	FeCl ₂	409	98.2	0.9	0.9	0.0	0.0
11	FeCl ₂	410	71.1	24.0	3.6	0.6	0.7
12	FeCl ₂	411	93.6	3.9	2.3	0.2	0.0
13	FeCl ₂	412	79.8	14.9	4.4	0.3	0.5
14	FeCl ₂	413	91.2	3.1	5.0	0.4	0.3
15	FeCl ₂	148	92.0	0.1	6.3	1.1	0.5
16	FeCl ₂	414	77.4	14.8	7.6	0.1	0.0
17	FeCl ₂	415	97.8	0.1	2.0	0.1	0.0
18	FeCl ₂	416	92.6	1.3	5.9	0.2	0.0
19	FeCl ₂	417	82.0	11.8	5.2	0.5	0.5
20	FeCl ₂	418	90.1	3.9	4.4	0.6	1.0
21	FeCl ₂	419	57.3	37.6	4.2	0.7	0.2
22	FeCl ₂	96	85.7	9.8	3.8	0.4	0.3
23	FeCl ₂	420	88.4	5.0	5.7	0.5	0.4
24	FeCl ₂	421	82.5	13.3	3.8	0.4	0.1
25	FeF ₂	187	92.4	0.1	6.6	0.0	1.0
26	FeF ₂	401	92.5	0.3	6.0	0.0	1.3
27	FeF ₂	402	95.0	0.2	3.1	0.0	1.7
28	FeF ₂	403	87.8	0.3	10.5	0.0	1.3
29	FeF ₂	404	94.0	0.1	6.0	0.0	0.0
30	FeF ₂	405	95.7	0.2	2.2	1.0	1.0
31	FeF ₂	406	94.3	0.7	3.7	0.2	1.1
32	FeF ₂	407	95.6	0.2	2.7	0.0	1.5
33	FeF ₂	408	94.7	0.2	3.1	0.0	2.1
34	FeF ₂	409	96.2	0.0	2.1	0.0	1.6

35	FeF ₂	410	96.0	0.1	3.2	0.0	0.6
36	FeF ₂	411	93.9	0.2	4.2	0.0	1.7
37	FeF ₂	412	93.8	0.3	3.8	0.0	2.1
38	FeF ₂	413	94.8	0.1	4.5	0.0	0.6
39	FeF ₂	148	94.1	0.2	4.0	0.2	1.5
40	FeF ₂	414	93.8	0.0	3.3	0.0	2.9
41	FeF ₂	415	97.7	0.1	1.4	0.0	0.8
42	FeF ₂	416	94.1	0.2	5.3	0.0	0.4
43	FeF ₂	417	93.9	0.2	3.8	0.0	2.1
44	FeF ₂	418	94.9	0.2	3.5	0.0	1.4
45	FeF ₂	419	94.8	0.2	4.0	0.0	1.0
46	FeF ₂	96	94.8	0.2	3.5	0.0	1.5
47	FeF ₂	420	75.7	20.6	3.6	0.1	0.0
48	FeF ₂	421	95.3	0.2	3.9	0.0	0.6

7.6.3. Screen 3 – Cyclopropylmagnesium Bromide + 6-Chloroquinoline (1 catalyst, 12 ligands)

Procedure and results from **Section 5.2.2.3**.

For high throughput screen 3 the procedure was:

1. Catalyst (10 mol%), ligands (10 mol%) and aryl chloride weighed into a vial (25 mg, 0.15 mmol scale)
2. Solids purged in a glove bag with nitrogen overnight
3. THF added using multi-channel pipette (0.2 mL)
4. Mixture stirred for 20 minutes
5. Grignard reagent added rapidly in 1 aliquot using a multichannel pipette (2 equiv., cyclopropylmagnesium bromide, 0.5 M in THF)
6. Reaction mixture stirred for 1 hour
7. Reaction mixture quenched with pH 2 buffer (0.1 mL, 0.125 M H₂SO₄, 0.375 M Na₂SO₄)
8. pH neutralised with 0.5 M Na₂CO₃ (0.1 mL)
9. Reaction mixture stirred for 15 minutes, then sampled for HPLC/LCMS (10 µL into 0.5 mL MeCN/water)

Table 49. Results from third high throughput screen.

Entry	Ligand	Starting Material	Product	Adduct 1	Adduct 2	Adduct 3
1	438	82.0	10.4	5.4	0.9	1.2
2	445	86.5	6.8	4.9	0.7	1.2
3	402	57.6	37.8	3.7	0.5	0.4
4	440	71.3	23.9	3.3	0.5	0.9
5	439	84.7	10.3	3.6	0.4	1.0
6	441	87.2	6.5	4.5	0.6	1.2
7	442	60.9	32.3	4.7	0.7	1.5
8	443	30.7	66.4	2.5	0.2	0.3
9	444	64.9	31.4	3.0	0.3	0.4
10	446	28.5	68.7	2.2	0.2	0.5
11	447	65.6	29.5	3.5	0.2	1.2
12	448	85.5	10.2	3.0	0.4	1.0

7.6.4. Screen 4 – Cyclopropylmagnesium Bromide + 6-Chloroquinoline (4 catalyst, 8 ligands)

Procedure and results from **Section 5.2.2.4**.

For high throughput screen 4 the procedure was:

1. Catalyst (10 mol%), ligands (10 mol%) and aryl chloride weighed into a vial (25 mg, 0.15 mmol scale)
2. Solids purged in a glove bag with nitrogen overnight
3. THF added using multi-channel pipette (0.2 mL)
4. Mixture stirred for 20 minutes
5. Grignard reagent added rapidly in 1 aliquot using a multichannel pipette (2 equiv., cyclopropylmagnesium bromide, 0.5 M in THF)
6. Reaction mixture stirred for 1 hour
7. Reaction mixture quenched with pH 2 buffer (0.1 mL, 0.125 M H₂SO₄, 0.375 M Na₂SO₄)
8. pH neutralised with 0.5 M Na₂CO₃ (0.1 mL)
9. Reaction mixture stirred for 15 minutes, then sampled for HPLC/LCMS (10 µL into 0.5 mL MeCN/water)

Table 50. Results from fourth high throughput screen.

Entry	Catalyst	Ligand	SM	Product	Adduct 1	Adduct 2	Adduct 3
1	FeCl ₂	446	24.3	64.1	5.5	2.7	3.3
2	FeCl ₂	470	16.8	71.7	6.0	2.1	3.4
3	FeCl ₂	471	10.7	80.2	5.0	1.6	2.6
4	FeCl ₂	473	70.6	9.5	8.5	3.3	8.0
5	FeCl ₂	472	73.3	6.8	9.4	3.2	7.2
6	FeCl ₂	474	78.5	2.1	6.6	1.8	10.9
7	FeCl ₂	475	69.2	11.6	9.4	3.3	6.5
8	FeCl ₂	476	68.7	12.3	8.4	2.1	8.5
9	FeF ₂	446	81.0	0.1	6.2	0.1	12.6
10	FeF ₂	470	78.1	0.0	7.6	0.1	14.2
11	FeF ₂	471	79.7	0.7	7.2	0.3	12.1
12	FeF ₂	473	78.0	1.7	7.1	0.1	13.1
13	FeF ₂	472	78.8	0.4	7.3	0.2	13.4
14	FeF ₂	474	79.4	2.3	6.4	1.0	11.0
15	FeF ₂	475	78.1	0.3	7.6	0.2	13.9
16	FeF ₂	476	77.5	0.0	7.2	0.0	15.3
17	Fe(acac) ₃	446	56.9	37.7	1.6	3.7	0.0
18	Fe(acac) ₃	470	55.5	37.7	3.7	1.7	1.4
19	Fe(acac) ₃	471	45.1	49.2	2.9	1.6	1.1
20	Fe(acac) ₃	473	81.1	9.6	4.7	2.1	2.4
21	Fe(acac) ₃	472	81.5	10.1	4.4	2.0	2.0
22	Fe(acac) ₃	474	77.3	14.5	4.5	2.1	1.6
23	Fe(acac) ₃	475	79.5	12.9	4.3	1.6	1.7
24	Fe(acac) ₃	476	80.7	10.2	4.3	2.0	2.8
25	Fe(DBM) ₃	446	60.2	35.0	1.8	1.0	2.0
26	Fe(DBM) ₃	470	68.2	25.0	4.0	0.8	2.0
27	Fe(DBM) ₃	471	62.2	30.7	4.0	0.8	2.3
28	Fe(DBM) ₃	473	80.8	9.9	4.4	1.2	3.7
29	Fe(DBM) ₃	472	84.4	6.7	5.3	1.2	2.3
30	Fe(DBM) ₃	474	81.6	10.6	4.0	1.1	2.7
31	Fe(DBM) ₃	475	82.4	8.3	4.5	1.4	3.3
32	Fe(DBM) ₃	476	98.3	0.1	1.2	0.2	0.2

7.7. DoE and Temperature Studies for Cyclopropyl Coupling

7.7.1. DoE Investigation

Procedure and results from **Section 5.2.2.5**.

For the experimental design the procedure was:

1. Catalyst, ligands and heteroaryl chloride weighed into an integrity 10 tube (0.36g, 2.2 mmol scale)
2. Tubes vacuum purged with nitrogen 3 times
3. Solids dissolved in THF (2 mL)
4. Grignard reagent added rapidly in 1 aliquot (cyclopropylmagnesium bromide, 0.5 M in THF)
5. Reaction mixture stirred for 4 hours
6. Reaction mixture quenched with pH 2 buffer (2 mL, 0.125 M H₂SO₄, 0.375 M Na₂SO₄)
7. Reaction neutralised with 0.5 M Na₂CO₃ (2 mL)
8. Reaction mixture allowed to separate, then sampled for HPLC/LCMS (20 µL into 0.5 mL MeCN/water)

Table 51. DX7 parameters from full cyclopropyl DoE investigation.

			Factor 1	Factor 2	Factor 3	Factor 4
Std	Block	Run	A:Catalyst Loading	B:Ligand Loading	C:Grignard Equivalents	D:Addition Time
			mol%	mol%	eq.	mins
19	Block 1	1	2.55	2.55	2	15
13	Block 1	2	0.1	0.1	3	30
4	Block 1	3	5	5	1	30
20	Block 1	4	2.55	2.55	2	15
2	Block 1	5	5	0.1	1	0
16	Block 1	6	5	5	3	30
1	Block 1	7	0.1	0.1	1	30
18	Block 1	8	2.55	2.55	2	15
15	Block 1	9	0.1	5	3	0
9	Block 1	10	0.1	0.1	1	0
5	Block 1	11	0.1	0.1	3	0
12	Block 1	12	5	5	1	0
14	Block 1	13	5	0.1	3	0
7	Block 1	14	0.1	5	3	30
11	Block 1	15	0.1	5	1	30
17	Block 1	16	2.55	2.55	2	15
10	Block 1	17	5	0.1	1	30
3	Block 1	18	0.1	5	1	0
8	Block 1	19	5	5	3	0
6	Block 1	20	5	0.1	3	30
25	Block 2	21	2.55	2.55	1	15
27	Block 2	22	2.55	2.55	2	0
30	Block 2	23	2.55	2.55	2	15
21	Block 2	24	0.1	2.55	2	15
28	Block 2	25	2.55	2.55	2	30
24	Block 2	26	2.55	5	2	15
23	Block 2	27	2.55	0.1	2	15
29	Block 2	28	2.55	2.55	2	15
22	Block 2	29	5	2.55	2	15
26	Block 2	30	2.55	2.55	3	15

Table 52. Results from full cyclopropyl DoE investigation.

Experiment	SM	Product	Adduct 1	Adduct 2	Adduct 3
1	26.8	66.7	5.5	0.5	0.5
2	83.9	1.8	13.9	0.4	0.0
3	52.5	41.4	3.9	1.2	1.1
4	43.8	49.2	5.9	0.5	0.5
5	72.3	21.4	4.9	1.0	0.4
6	13.9	78.6	6.9	0.2	0.4
7	91.6	2.8	5.1	0.5	0.0
8	40.0	52.9	5.9	0.6	0.5
9	87.5	0.6	11.6	0.3	0.0
10	90.6	3.2	5.6	0.6	0.0
11	88.1	0.1	11.6	0.2	0.0
12	54.5	37.2	4.2	1.9	2.2
13	53.9	37.6	7.4	0.7	0.4
14	89.8	0.5	9.4	0.3	0.0
15	95.4	0.3	3.8	0.4	0.0
16	38.3	55.1	5.6	0.6	0.4
17	85.7	7.9	4.6	1.3	0.5
18	94.5	0.7	4.3	0.6	0.0
19	7.5	87.5	4.2	0.3	0.5
20	70.9	20.1	8.9	0.0	0.0
21	57.4	36.3	3.9	1.2	1.1
22	26.8	66.7	5.1	0.6	0.8
23	37.0	56.4	5.4	0.6	0.6
24	91.1	1.0	7.5	0.4	0.0
25	52.3	40.1	5.8	1.2	0.6
26	27.1	66.4	5.4	0.6	0.5
27	78.4	13.8	6.2	1.2	0.4
28	56.8	35.5	5.9	1.4	0.4
29	42.7	50.0	5.5	0.9	1.0
30	30.6	61.9	6.4	0.6	0.5

Design-Expert® Software
Product

▲ Error estimates

Shapiro-Wilk test

W-value = 0.913

p-value = 0.299

A: Catalyst Loading

B: Ligand Loading

C: Grignard Equivalents

D: Addition Time

■ Positive Effects

■ Negative Effects

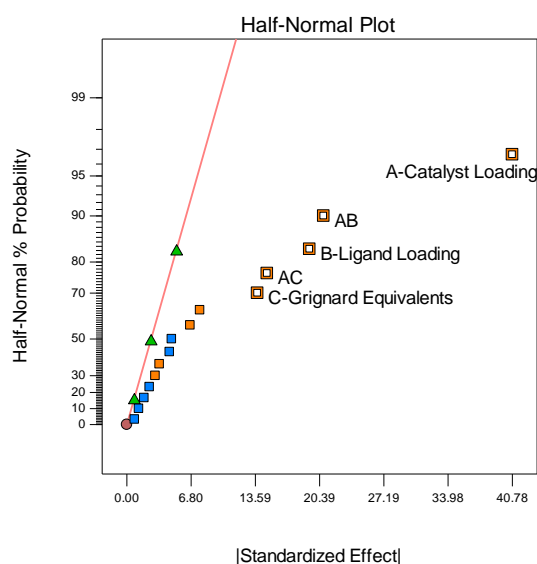


Chart 25. Half-normal plot for first cyclopropyl DoE investigation.

Table 53. ANOVA table for first cyclopropyl DoE investigation.

ANOVA for selected factorial model						
Analysis of variance table [Partial sum of squares - Type III]						
Source	Sum of Squares	df	Mean Square	F Value	p-value Prob > F	
Model	11525.59	5	2305.12	33.47	< 0.0001	significant
A-Catalyst Loading	6651.63	1	6651.63	96.58	< 0.0001	
B-Ligand Loading	1495.18	1	1495.18	21.71	0.0004	
C-Grignard Equivalents	763.97	1	763.97	11.09	0.0054	
AB	1733.68	1	1733.68	25.17	0.0002	
AC	881.14	1	881.14	12.79	0.0034	
Curvature	3908.72	1	3908.72	56.75	< 0.0001	
Residual	895.32	13	68.87			
Lack of Fit	721.00	10	72.10	1.24	0.4812	not significant
Pure Error	174.32	3	58.11			
Cor Total	16329.64	19				

Design-Expert® Software
Factor Coding: Actual
Product (%)
(adjusted for curvature)
● Design Points

X1 = A: Catalyst Loading
X2 = B: Ligand Loading

Actual Factors
C: Grignard Equivalents = 2
D: Addition Time = 15

■ B- 0.1
▲ B+ 5

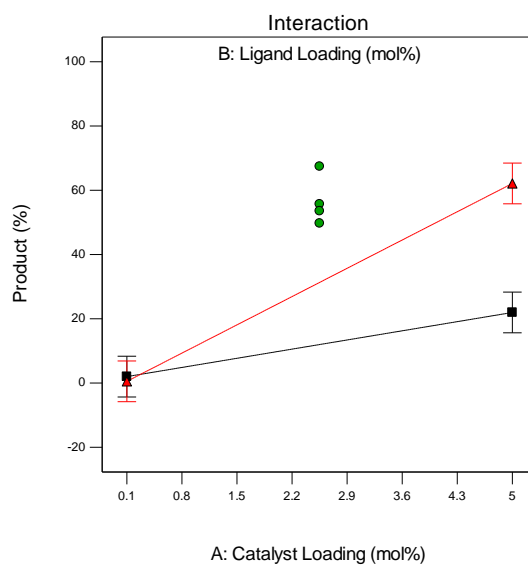


Chart 26. Interaction diagram for first DoE investigation.

Design-Expert® Software
Factor Coding: Actual
Product (%)
(adjusted for curvature)
● Design Points

X1 = A: Catalyst Loading
X2 = C: Grignard Equivalents

Actual Factors
B: Ligand Loading = 2.55
D: Addition Time = 15

■ C- 1
▲ C+ 3

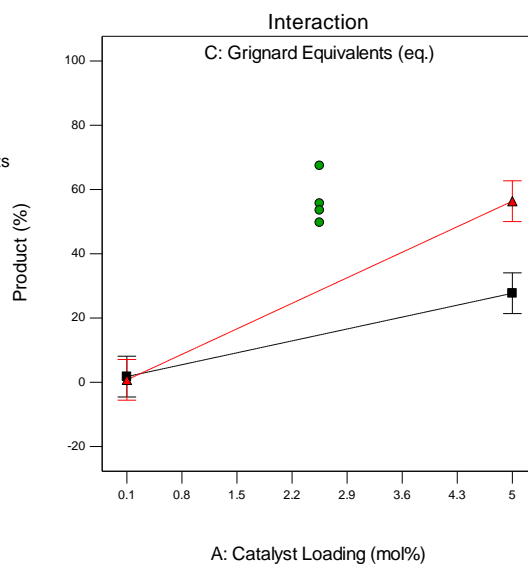


Chart 27. Interaction diagram for first DoE investigation.

Table 54. Model summary for second DoE investigation.

Summary (detailed tables shown below)					
	Sequential	Lack of Fit	Adjusted	Predicted	
Source	p-value	p-value	R-Squared	R-Squared	
Linear	0.0002	0.0211	0.5242	0.4057	
2FI	0.4661	0.0192	0.5220	0.2786	
Quadratic	< 0.0001	0.3465	0.9153	0.7952	Suggested
Cubic	0.1170	0.8790	0.9577	0.8001	Aliased

Table 55. ANOVA table for second DoE investigation.

Response	1	Product	
Transform:	Square Root	Constant:	0.23

ANOVA for Response Surface Reduced Quadratic model						
Analysis of variance table [Partial sum of squares - Type III]						
	Sum of		Mean	F	p-value	
Source	Squares	df	Square	Value	Prob > F	
Block	21.76	1	21.76			
Model	214.46	7	30.64	47.37	< 0.0001	significant
A-Catalyst Loading	116.74	1	116.74	180.50	< 0.0001	
B-Ligand Loading	12.30	1	12.30	19.02	0.0003	
C-Grignard Equivalents	4.64	1	4.64	7.17	0.0141	
AB	13.76	1	13.76	21.27	0.0002	
AC	6.74	1	6.74	10.43	0.0040	
A ²	25.86	1	25.86	39.99	< 0.0001	
B ²	3.23	1	3.23	5.00	0.0364	
Residual	13.58	21	0.65			
Lack of Fit	11.64	17	0.68	1.41	0.4023	not significant
Pure Error	1.94	4	0.48			
Cor Total	249.80	29				

Design-Expert® Software
Factor Coding: Actual
Original Scale
Product (%)

● Design points above predicted value
● Design points below predicted value
87.517
0.139

X1 = A: Catalyst Loading
X2 = B: Ligand Loading

Actual Factors
C: Grignard Equivalents =
D: Addition Time = 30

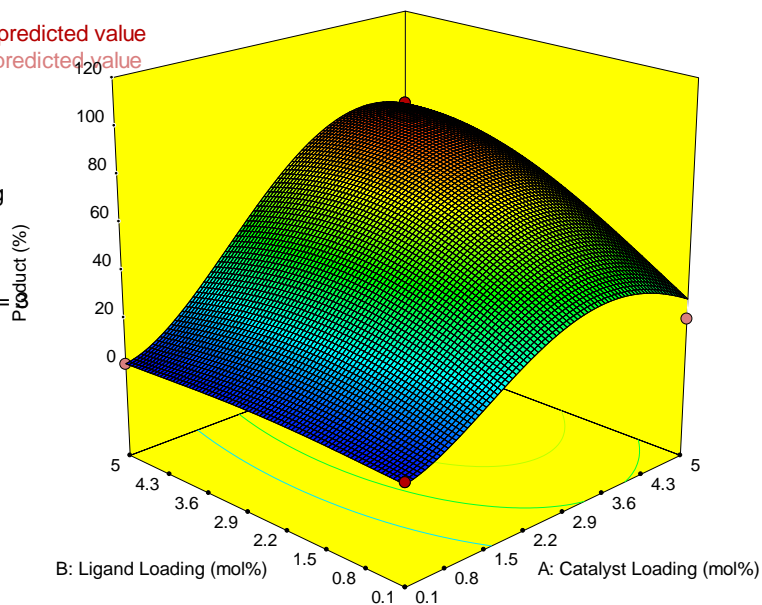


Chart 28. Quadratic response surface for second DoE investigation.

Design-Expert® Software
Factor Coding: Actual
Original Scale
Product (%)

● Design points above predicted value
● Design points below predicted value
87.517
0.139

X1 = A: Catalyst Loading
X2 = C: Grignard Equivalents

Actual Factors
B: Ligand Loading = 5
D: Addition Time = 30

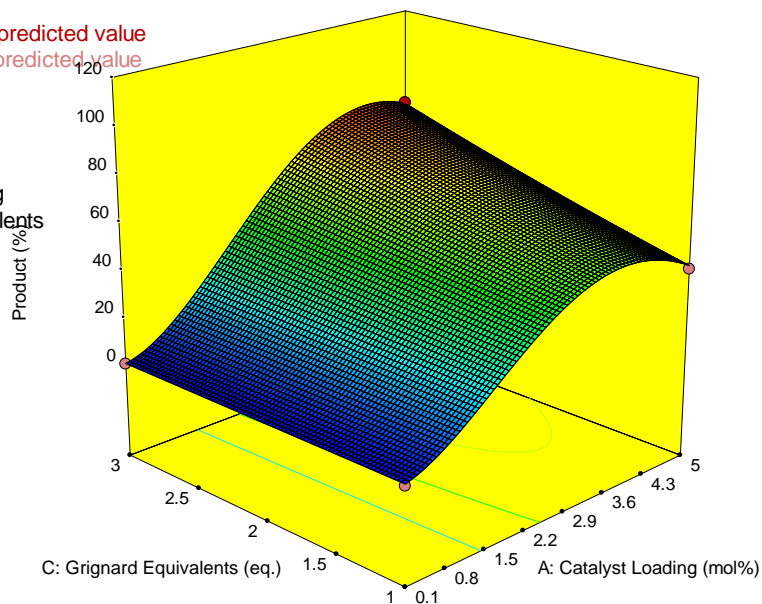


Chart 29. Quadratic response surface for second DoE investigation.

7.7.2. Low Temperature Investigation

Procedure and results from **Section 5.2.2.5**.

For the temperature investigation the procedure was:

1. Grignard reagent pre-equilibrated at the desired reaction temperature
2. Standard solution of catalyst, ligands and heteroaryl chloride prepared (2.2 mmol in 2 mL)
3. Starting material added rapidly in 1 aliquot
4. Reaction mixture stirred for 24 hours
5. Reaction mixture quenched with pH 2 buffer (2 mL, 0.125 M H₂SO₄, 0.375 M Na₂SO₄)
6. Reaction neutralised with 0.5 M Na₂CO₃ (2 mL)
7. Reaction mixture allowed to separate, then sampled for HPLC/LCMS (20 µL into 0.5 mL MeCN/water)

Table 56. Results from temperature study.

T	Product	SM	Adducts
-20	3	94	3
-10	47	45	8
0	80	11	9
5	88	4	8
10	89	5	6
15	91	2	7
20	88	2	10
25	84	2	14
30	82	1	16
40	64	5	31

7.7.3. Elevated Temperature Investigation

Procedure and results from **Section 5.2.2.5**.

For the temperature investigation the procedure was:

1. Catalyst (4 mol%), ligand (4 mol%) and heteroaryl chloride prepared (2.2 mmol)
2. THF added, and reaction mixture equilibrated at the desired temperature
3. Grignard reagent added rapidly in 1 aliquot
4. Reaction mixture stirred for 1 hour and sampled for HPLC
5. Reaction mixture stirred for 3 hours
6. Reaction mixture quenched with pH 2 buffer (2 mL, 0.125 M H₂SO₄, 0.375 M Na₂SO₄)
7. Reaction neutralised with 0.5 M Na₂CO₃ (2 mL)
8. Reaction mixture allowed to separate, then sampled for HPLC/LCMS (20 µL into 0.5 mL MeCN/water)

Table 57. Results from second temperature investigation.

Temperature	Time	Starting Material	Product	Adducts
20	1h	60	38	2
40	1h	40	55	4
60	1h	32	56	12
20	4h	21	74	5
40	4h	11	80	10
60	4h	8	68	24

7.7.4. Controlled Addition Investigation

Procedure and results from **Section 5.2.2.5**.

For the controlled addition investigation the procedure was:

1. Starting material (3 g, 18.3 mmol), catalyst and ligand added to an Easymax reactor
2. THF added (14.4 mL), and reaction mixture equilibrated at 15 °C
3. Grignard reagent added over the prescribed time (cyclopropylmagnesium bromide, 1.2 equivalents, 0.5 M in THF)
4. Reaction mixture stirred for 18 hours
5. Reaction mixture quenched with pH 2 buffer (10 mL, 0.125 M H₂SO₄, 0.375 M Na₂SO₄)
6. Reaction neutralised with 0.5 M Na₂CO₃ (10 mL)
7. Reaction mixture allowed to separate, then sampled for HPLC/LCMS (20 µL into 0.5 mL MeCN/water)

Table 58.

Entry	Addition time	Starting Material	Product	Adducts
1	1 h	25.3	70.3	4.3
2	3 h	46.0	48.5	5.4

7.7.5. 6-Haloquinoline Test Reactions

Procedure and results from **Section 5.2.2.5**.

For the haloquinoline investigation the procedure was:

1. Starting material (2.2 mmol), catalyst and ligand added to an Easymax reactor
2. THF added (2 mL), and reaction mixture equilibrated at 15 °C
3. Grignard reagent added over the prescribed time (cyclopropylmagnesium bromide, 1.2 equivalents, 0.5 M in THF)
4. Reaction mixture stirred for 1 hour
5. Reaction mixture sampled for HPLC/LCMS (20 μ L into 0.5 mL MeCN/water)

	Quinoline	Starting Material	Product	Adducts
6-chloroquinoline	0.4	60.3	37.2	2.1
6-bromoquinoline	12.5	0.1	85.7	1.8

NOTE: No reaction with 6-fluoroquinoline.

7.8. Isolated Cyclopropyl Substrates

Procedure and results from **Section 5.2.2.5**. General procedure:

Preparation of 2-cyclopropylquinoline **482**: Iron(II) chloride (11.15 mg, 0.088 mmol) and (9,9-dimethyl-9H-xanthene-4,5-diyl)bis(diphenylphosphane) (50.9 mg, 0.088 mmol) was weighed into an Integrity 10 tube followed by 2-chloroquinoline (360 mg, 2.2 mmol). The tube was vacuum purged with nitrogen 3 times. Tetrahydrofuran (THF) (2 mL) was then added. The mixture was stirred for 30 minutes. Cyclopropylmagnesium bromide (8.80 mL, 4.40 mmol) was then added. The reaction was stirred for 1h 50 minutes then quenched with pH 2 buffer (0.125 M H₂SO₄, 0.375 M Na₂SO₄) (2 mL) and neutralised with 0.5 M Na₂CO₃ (2 mL). Aqueous phase extracted twice with ethyl acetate (10 mL). Combined organics dried with brine (20 mL) then sodium sulfate and concentrated *in vacuo*. Purified using column chromatography (1-10% ethyl acetate in heptane). This gave 2-cyclopropylquinoline **482** as an orange low melting solid (270 mg, 73%).

¹H NMR (400 MHz, CDCl₃): δ 7.97 (app. dd, J = 11.8, 8.5 Hz, 2H), 7.73 (d, J = 8.2 Hz, 1H), 7.64 (t, J = 7.0 Hz, 1H), 7.42 (t, J = 7.0 Hz, 1H), 7.16 (d, J = 8.5 Hz, 1H), 2.28 – 2.20 (m, 1H), 1.18 – 1.13 (m, 2H), 1.13 – 1.06 (m, 2H). ¹³C NMR (101 MHz, CDCl₃): δ 163.4, 148.0, 135.8, 129.3, 128.7, 127.5, 126.8, 125.2, 119.4, 18.1, 10.3. IR: ν = 2998, 2866, 1597, 1503, 825. MS (ESI⁺): m/z 170.0. HRMS (ESI⁺): calculated 170.0964, actual 170.0963.

Preparation of 4-cyclopropyl-2-(trifluoromethyl)pyridine **480**. Clear colourless oil (220 mg, 53%).

¹H NMR (400 MHz, CDCl₃): δ 8.52 (d, J = 5.1 Hz, 1H), 7.32 (d, J = 1.7 Hz, 1H), 7.12 (dd, J = 5.1, 1.7 Hz, 1H), 2.01 – 1.90 (m, 1H), 1.24 – 1.12 (m, 2H), 0.90 – 0.82 (m, 2H). ¹³C NMR (101 MHz, CDCl₃): δ 156.0, 149.6, 148.1 (q, J = 34.1 Hz), 123.2, 121.7 (q, J = 274.2 Hz), 117.5 (q, J = 2.7 Hz), 15.3, 11.2. ¹⁹F NMR (101 MHz, CDCl₃): δ -68.1. IR: ν = 3018, 1612, 1328, 1135, 917. MS (ESI⁺): m/z 188.0. HRMS (ESI⁺): calculated 188.0682, actual 188.0679.

Preparation of 1-cyclopropylisoquinoline **484**. Pale yellow waxy low melting solid (310 mg, 83%).

¹H NMR (400 MHz, CDCl₃): δ 8.40 (d, J = 8.4 Hz, 1H), 8.36 (d, J = 5.7 Hz, 1H), 7.78 (d, J = 7.8 Hz, 1H), 7.62 (dddd, J = 22.6, 8.3, 6.8, 1.4 Hz, 2H), 7.42 (d, J = 5.7 Hz, 1H), 2.79 – 2.68 (m, 1H), 1.33 – 1.19 (m, 2H), 1.19 – 1.06 (m, 2H). ¹³C NMR (101 MHz, CDCl₃): δ 161.9, 141.9, 136.0, 129.7, 127.8, 127.3, 126.9, 125.1, 118.4, 13.5, 9.4. IR: ν = 3053, 3008, 1561, 1409. MS (ESI⁺): m/z 170.0. HRMS (ESI⁺): calculated 170.0964, actual 170.0957.

7.9. Computational Chemistry Data

7.9.1. Results from Method Screen

Results from **Section 0**.

Table 59. Results from B3LYP investigation.

Substrate	B3LYP/6-31G(d)		B3LYP/6-311++G(d,p)	
	gas phase		acetonitrile	
	GS / a.u.	RA / a.u.	GS / a.u.	RA / a.u.
3-CF ₃	-1028.88	-1028.86	-1029.09	-1028.99
3-CH ₃	-731.16	-731.11	-731.19	-731.30
3-Cl	-1151.44	-1151.40	-1151.46	Cl disc.
3-CN	-784.09	-784.09	-784.11	-731.23
3-CO ₂ CH ₃	-919.72	-919.72	-919.76	-919.84
3-F	-791.08	-791.03	-791.11	Cl disc.
3-OCF ₃	-1104.10	Cl disc.	-1104.14	-1104.20
3-OCH ₃	-806.37	Cl disc.	-806.40	-806.44
4-CF ₃	-1028.88	Cl disc.	-1028.92	Cl disc.
4-CH ₃	-731.16	Cl disc.	-731.19	-731.23
4-CHF ₂	-929.63	-929.59	-929.67	-1660.97
4-Cl	-1151.44	-1151.40	-1151.46	-1151.51
4-CN	-784.09	-784.08	-784.11	-784.20
4-CO ₂ CH ₃	-919.70	-919.72	-844.53	-844.62
4-COMOR	-1091.79	-1091.79	-1091.84	-1091.92
4-F	-791.08	-791.03	-791.11	-791.16
4-OCF ₃	-1104.10	Cl disc.	-1104.14	-1104.20
4-OCH ₃	-806.36	-806.31	-806.39	-806.44
4-OCHF ₂	-1004.85	Cl disc.	-1004.89	-1004.95
4-Py	-938.94	-938.94	-938.98	-939.05
4-SO ₂ NEt ₂	-1453.01	-1453.01	-1453.06	-1453.14
4-CH ₂ F	-830.39	Cl disc.	-830.43	F disc.
4-SCH ₃	-1129.34	Cl disc.		Cl disc.
4-H	-691.84	-691.79	-691.87	-691.91

Table 60. Key for computational data.

KEY:
imaginary frequency
dissociation
good

Table 61. Results from M06-2X investigation.

	GS / a.u.	RA / a.u.	ΔE / a.u.	(-) ΔE / eV	(%)- <i>i</i> -Pr	\log_{10} (%)- <i>i</i> -Pr
3-CF ₃	-1028.85	-1028.92	-6.15E-02	1.67	96.5	1.98
3-CH ₃	-731.11	-731.15	-3.50E-02	0.95	6.4	0.81
3-Cl	-1151.40	-1151.45	-4.56E-02	1.24	63.7	1.80
3-CN	-784.04	-784.12	-7.62E-02	2.07	53.6	1.73
3-CO ₂ CH ₃	-919.67	-919.75	-7.70E-02	2.09	87.9	1.94
3-F	-791.04	-791.09	-4.28E-02	1.17	58.7	1.77
3-OCF ₃	-1104.07	-1104.12	-4.71E-02	1.28	40.1	1.60
3-OCH ₃	-806.32	-806.35	-3.60E-02	0.98	23.5	1.37
4-CF ₃	-1028.86	-1028.91	-5.93E-02	1.61	89.8	1.95
4-CH ₃	-731.11	-731.15	-3.51E-02	0.96	6.7	0.83
4-CHF ₂	-929.60	-929.65	-5.49E-02	1.49	64.5	1.81
4-Cl	-1151.40	-1151.45	-4.61E-02	1.25	70.9	1.85
4-CN	-784.04	-784.12	-7.34E-02	2.00	68.6	1.84
4-CO ₂ CH ₃	-844.44	-844.52	-8.18E-02	2.23	80.3	1.90
4-COMOR	-1091.72	-1091.79	-7.05E-02	1.92	84.3	1.93
4-F	-791.04	-791.09	-4.45E-02	1.21	68.7	1.84
4-OCF ₃	-1104.07	-1104.12	-4.78E-02	1.30	52.5	1.72
4-OCH ₃	-806.32	-806.35	-3.73E-02	1.01	2.7	0.43
4-OCHF ₂	-1004.82	-1004.87	-4.70E-02	1.28	59.9	1.78
4-Py	-938.87	-938.93	-6.87E-02	1.87	75.5	1.88
4-SO ₂ NEt ₂	-1452.93	-1453.00	-7.05E-02	1.92	69.8	1.84
4-CH ₂ F	-830.35	F disc.			12.6	1.10
4-SCH ₃	-1129.29	-1129.33			56.5	1.75
4-H	-691.80	-691.84				

Table 62. LUMO energies at M06-2X level.

Substrate	M062X/6-311++G(d,p)	
	tetrahydrofuran	
	E(LUMO) / a.u.	E(LUMO+1) / a.u.
3-CF ₃	-0.1946	-0.0890
3-CH ₃	-0.0078	0.0037
3-Cl	-0.0069	-0.0050
3-CN	-0.0385	-0.0116
3-CO ₂ CH ₃	-0.0350	-0.0027
3-F	-0.0055	0.0008
3-OCF ₃	-0.0836	-0.0065
3-OCH ₃	-0.0111	0.0020
4-CF ₃	-0.0184	-0.0979
4-CH ₃	-0.0077	0.0024
4-CHF ₂	-0.0145	-0.0052
4-Cl	-0.0731	-0.0051
4-CN	-0.0369	-0.0123
4-CO ₂ CH ₃	-0.0411	-0.0032
4-COMOR	-0.0185	-0.0058
4-F	-0.0065	-0.0012
4-OCF ₃	-0.0083	-0.0068
4-OCH ₃	-0.0014	0.0012
4-OCHF ₂	-0.0081	-0.0010
4-Py	-0.0295	-0.0085
4-SO ₂ NEt ₂	-0.0266	-0.0128
4-CH ₂ F	-0.0103	-0.0020
4-SCH ₃	-0.0013	-0.0010
4-H	0.0043	0.0031

Table 63. Energies for predictive calculations.

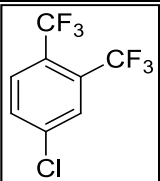
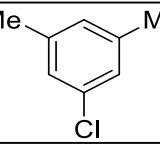
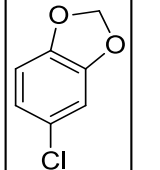
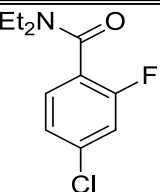
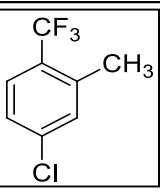
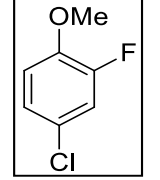
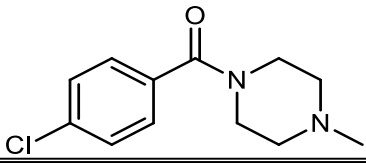
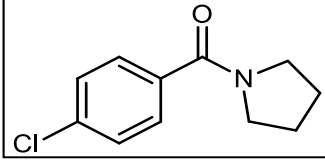
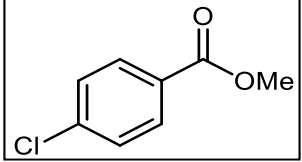
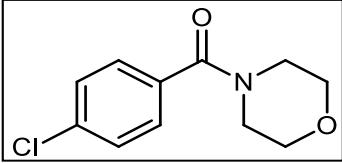
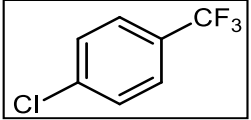
Substrate	M062X/6-311++G(d,p)				Experimental	
	tetrahydrofuran				GC Conversion	
	GS / a.u.	RA / a.u.	ΔE / a.u.	$(-)\Delta E$ / eV	(%)- <i>i</i> -Pr	$\log_{10}(\%)-i$ -Pr
	-1365.90	-1365.98	-0.0803	2.18	100	2.00
	-770.42	-770.45	-0.0308	0.84	6	0.78
	-880.33	-880.37	-0.0407	1.11	18	1.26
	-1116.94	-1117.01	-0.0642	1.75	69	1.84
	-1068.16	-1068.22	-0.0576	1.57	78	1.89
	-905.55	-905.59	-0.0434	1.18	12	1.08

Table 64. LUMO energies from Fox's primary alkylation¹¹⁴

Substrate	M062X/6-311++G(d,p)				Experimental	
	tetrahydrofuran				GC Conversion	
	GS / a.u.	RA / a.u.	ΔE / a.u.	(-) ΔE / eV	(%)- <i>i</i> -Pr	\log_{10} (%)- <i>i</i> -Pr
	-1111.21	-1111.14	-0.06851384	1.86	99	2.00
	-1016.57	-1016.51	-0.06306621	1.72	96	1.98
	-844.518	-844.437	-0.08181643	2.23	99	2.00
	-1091.79	-1091.72	-0.07053126	1.92	93	1.97
	-1028.91	-1028.86	-0.05927295	1.61	97	1.99

7.9.2. Sample Input File

```
%chk=4CF3.chk
```

```
%nprocshared=4
```

```
%mem=8GB
```

```
#p UM062X/6-311++G(d,p) opt=tight freq scf=tight  
int=grid=ultrafine scrf=(cpcm,solvent=tetrahydrofuran)
```

```
4CF3 at M062X/6-311++G(d,p) with THF tighttightultrafine
```

```
-1 2
```

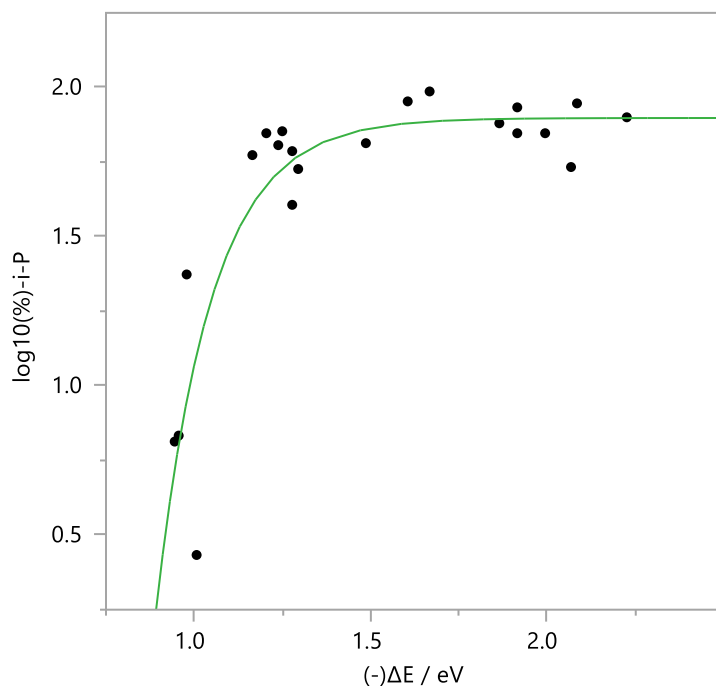
C	-1.31435400	1.21379500	-0.01126000
C	0.07423600	1.20970500	-0.02728400
C	0.76092300	-0.00000300	-0.03790100
C	0.07423500	-1.20970900	-0.02728400
C	-1.31435700	-1.21379700	-0.01126100
C	-1.99022600	-0.00000100	-0.00282400
H	-1.86513400	2.14509000	-0.00762500
H	0.61599600	2.14730200	-0.03852200
H	0.61599200	-2.14730700	-0.03852300
H	-1.86513700	-2.14509100	-0.00762600
Cl	-3.73292600	0.00000200	0.01458000
C	2.25988200	-0.00000100	-0.00045500
F	2.78280400	-1.07962600	-0.60021000
F	2.72950400	0.00004500	1.26205800
F	2.78280200	1.07958500	-0.60028700

7.9.3. JMP Analysis of Computational Results

7.9.3.1. Analysis of electron affinity data

Model	AICc	BIC	SSE	MSE	RMSE	R-Square
Exponential 3P	1.5388855	3.2169753	0.8024591	0.0445811	0.2111423	0.7809273

Plot



Parameter Estimates

Parameter	Estimate	Std Error	Lower 95%	Upper 95%
Asymptote	1.8977373	0.0717644	1.7570818	2.0383929
Scale	-482.2702	956.01654	-2356.028	1391.4878
Growth Rate	-6.366387	2.0689556	-10.42147	-2.311309

Correlation of Estimates

	Asymptote	Scale	Growth Rate
Asymptote	1.0000	0.6026	0.6313
Scale	0.6026	1.0000	0.9980
Growth Rate	0.6313	0.9980	1.0000

Covariance of Estimates

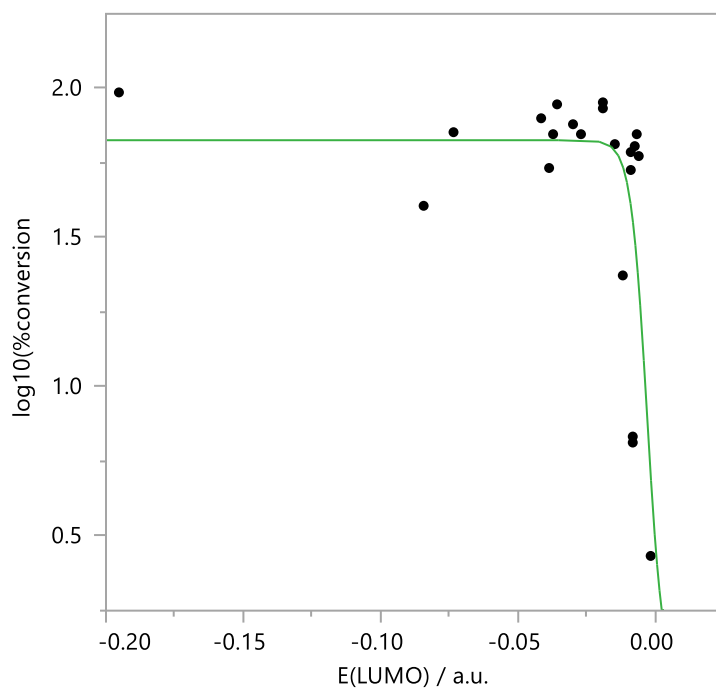
	Asymptote	Scale	Growth Rate
Asymptote	0.0052	41.3432	0.0937
Scale	41.3432	913968	1974.03
Growth Rate	0.0937	1974.03	4.2806

7.9.3.2. Analysis of LUMO data

Model Comparison

Model	AICc	BIC	SSE	MSE	RMSE	R-Square
Logistic 3P	20.077734	21.755824	1.9400775	0.1077821	0.3283018	0.4703556

Plot



Parameter Estimates

Parameter	Estimate	Std Error	Lower 95%	Upper 95%
Growth Rate	-340.0151	154.48336	-642.7969	-37.23328
Inflection Point	-0.002866	0.001641	-0.006082	0.0003506
Asymptote	1.8264767	0.0967555	1.6368394	2.0161139

Correlation of Estimates

	Growth Rate	Inflection Point	Asymptote
Growth Rate	1.0000	0.6075	0.3394
Inflection Point	0.6075	1.0000	-0.1755
Asymptote	0.3394	-0.1755	1.0000

Covariance of Estimates

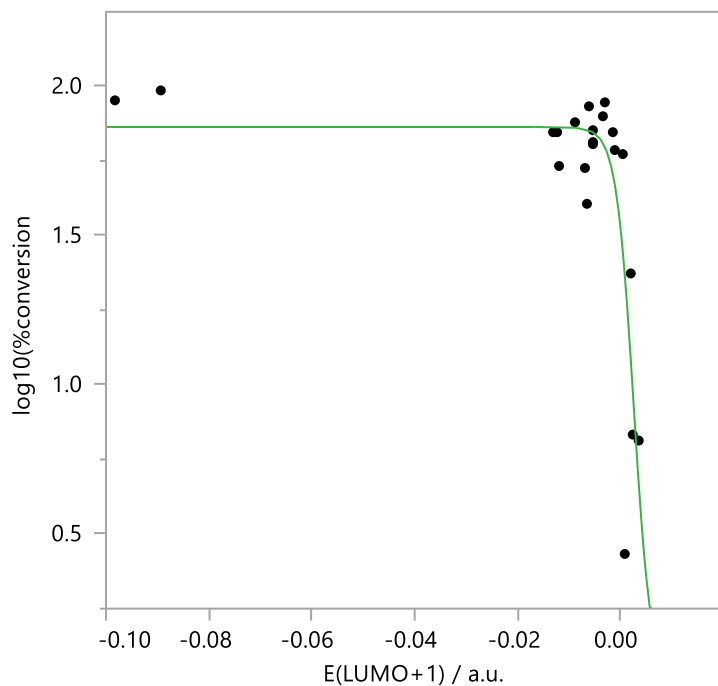
	Growth Rate	Inflection Point	Asymptote
Growth Rate	23865.1	0.1540	5.0723
Inflection Point	0.1540	0.0000	-0.0000
Asymptote	5.0723	-0.0000	0.0094

7.9.3.3. Analysis of LUMO+1 data

Model Comparison

Model	AICc	BIC	SSE	MSE	RMSE	R-Square
Logistic 3P	10.523558	12.201648	1.2309265	0.0683848	0.2615049	0.663955

Plot



Parameter Estimates

Parameter	Estimate	Std Error	Lower 95%	Upper 95%
Growth Rate	-590.1202	227.46504	-1035.944	-144.2969
Inflection Point	0.002557	0.0005263	0.0015254	0.0035885
Asymptote	1.864096	0.0788405	1.7095715	2.0186205

Correlation of Estimates

	Growth Rate	Inflection Point	Asymptote
Growth Rate	1.0000	0.3060	0.4631
Inflection Point	0.3060	1.0000	-0.2175
Asymptote	0.4631	-0.2175	1.0000

Covariance of Estimates

	Growth Rate	Inflection Point	Asymptote
Growth Rate	51740.3	0.0366	8.3045
Inflection Point	0.0366	0.0000	-0.0000
Asymptote	8.3045	-0.0000	0.0062

7.9.4. Bond Dissociation Energy Calculations

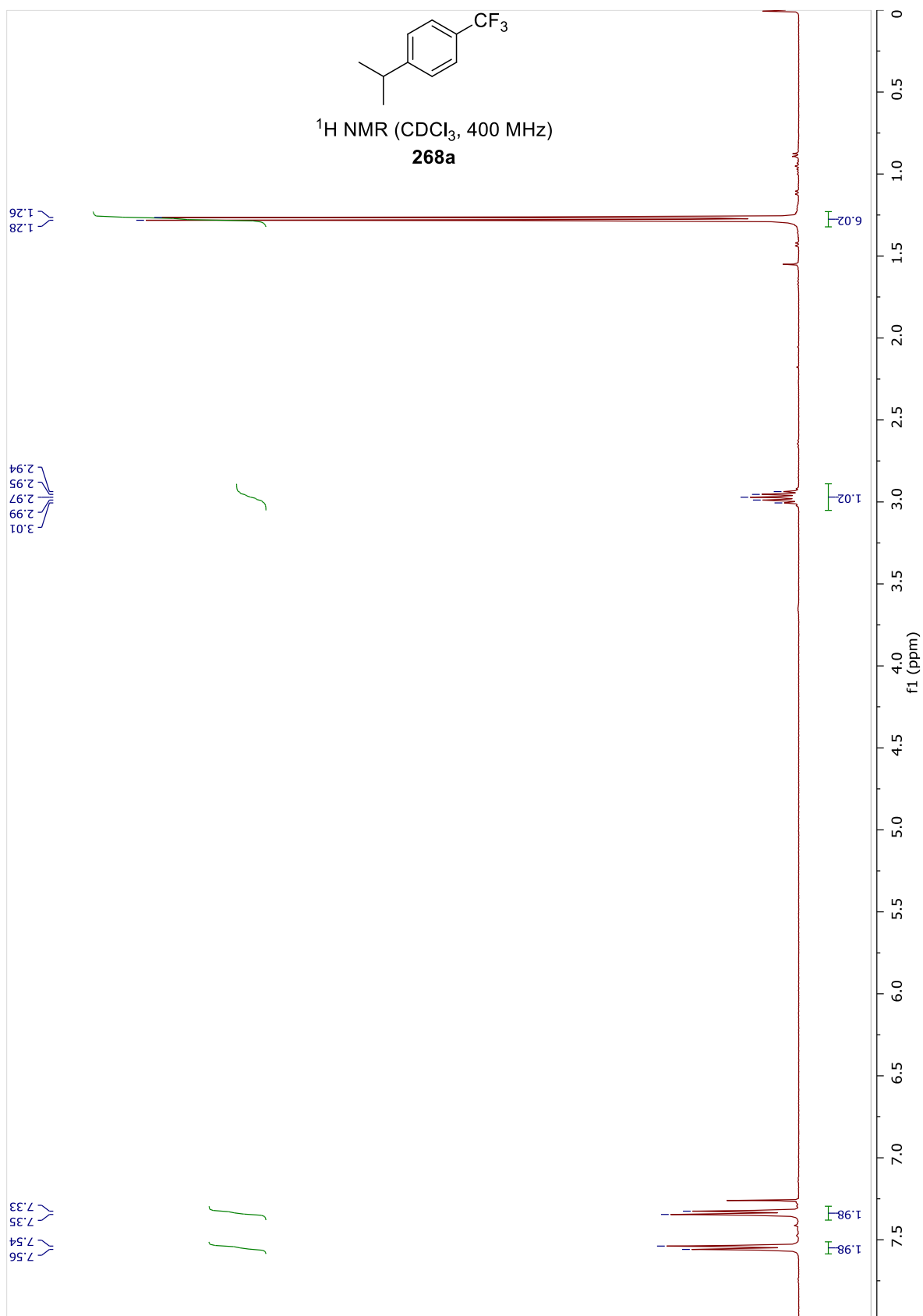
Results from **Section 4.2.1.1**.

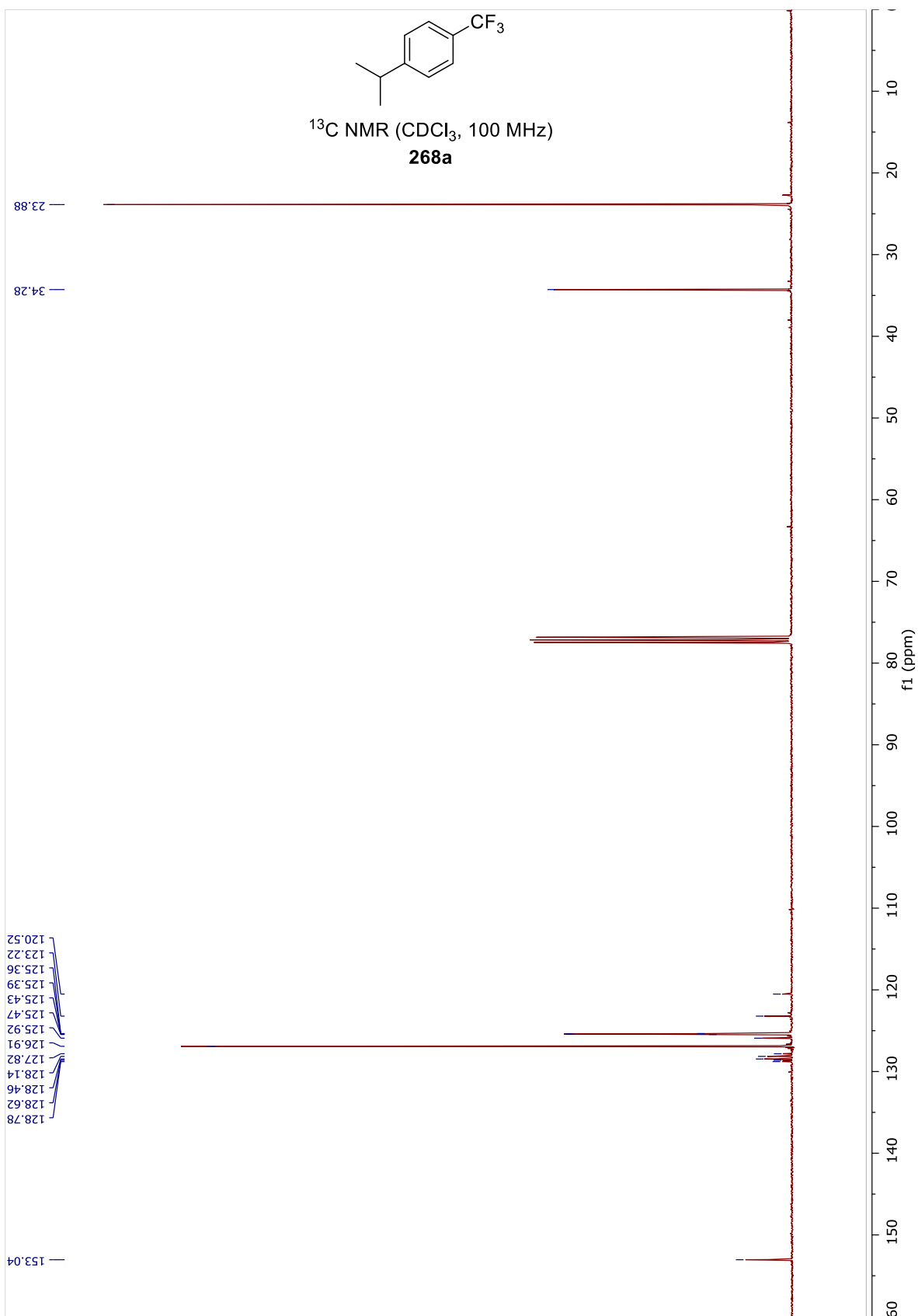
Bond dissociation energy calculated as described by Houk.¹³⁶

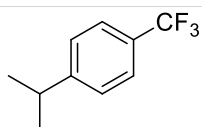
Table 65. Results from BDE calculations.

	GS / a.u.	RA / a.u.	BDE / a.u.	BDE / kcal mol ⁻¹
3-CF₃	-1028.88	-568.60	0.1465	92.3
3-CH₃	-731.16	-270.88	0.1474	92.9
3-Cl	-1151.44	-691.16	0.1460	92.0
3-CN	-784.09	-323.80	0.1459	91.9
3-CO₂CH₃	-919.72	-459.44	0.1468	92.5
3-F	-791.08	-330.79	0.1465	92.3
3-OCF₃	-1104.10	-643.82	0.1462	92.1
3-OCH₃	-806.37	-346.08	0.1471	92.7
4-CF₃	-1028.88	-568.60	0.1469	92.5
4-CH₃	-731.16	-270.88	0.1480	93.2
4-CHF₂	-830.39	-370.10	0.1476	93.0
4-Cl	-1151.44	-691.16	0.1473	92.8
4-CN	-784.09	-323.80	0.1466	92.3
4-CO₂MOR	-1166.96	-706.68	0.1473	92.8
4-F	-791.08	-330.79	0.1476	93.0
4-OCF₃	-1104.10	-643.82	0.1470	92.6
4-OCH₃	-806.36	-346.08	0.1479	93.1
4-OCHF₂	-1004.85	-544.57	0.1476	93.0
4-Py	-938.94	-478.66	0.1481	93.3
4-SO₂NEt₂	-1453.01	-992.73	0.1468	92.5
4-CH₂F	-929.63	-469.35	0.1472	92.8
4-SCH₃	-1129.34	-669.06	0.1473	92.8

7.10. Copies of NMR Spectra



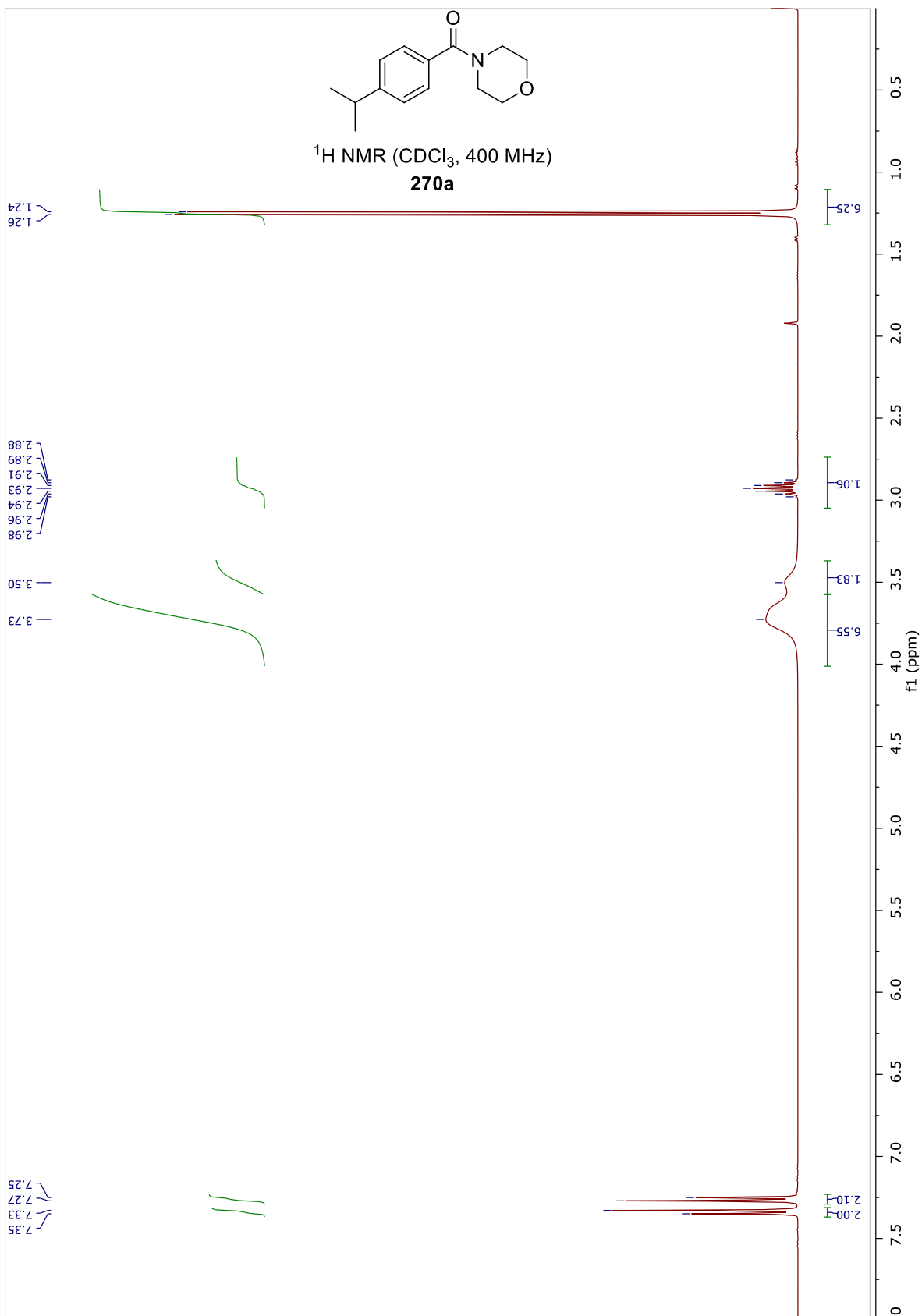


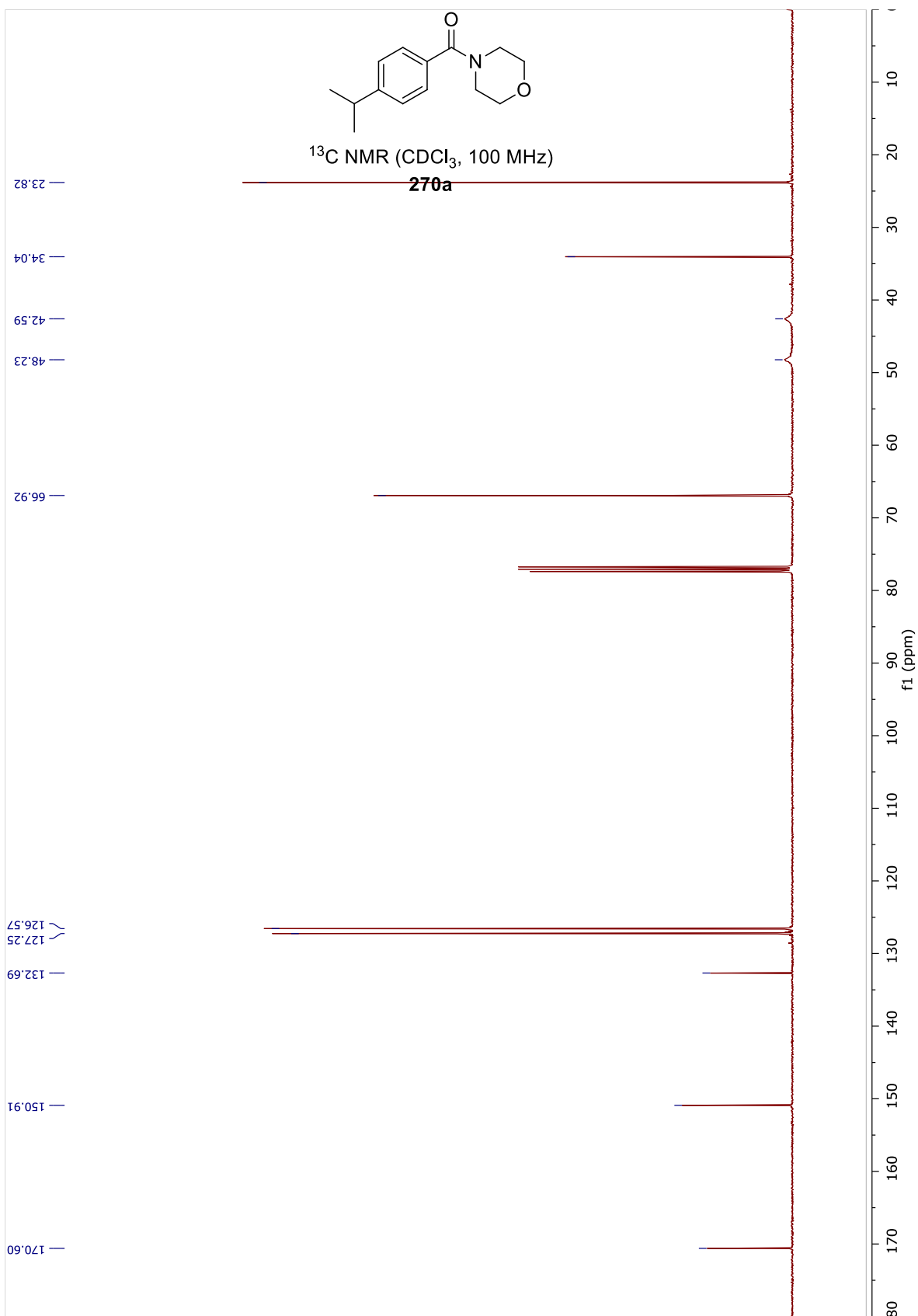


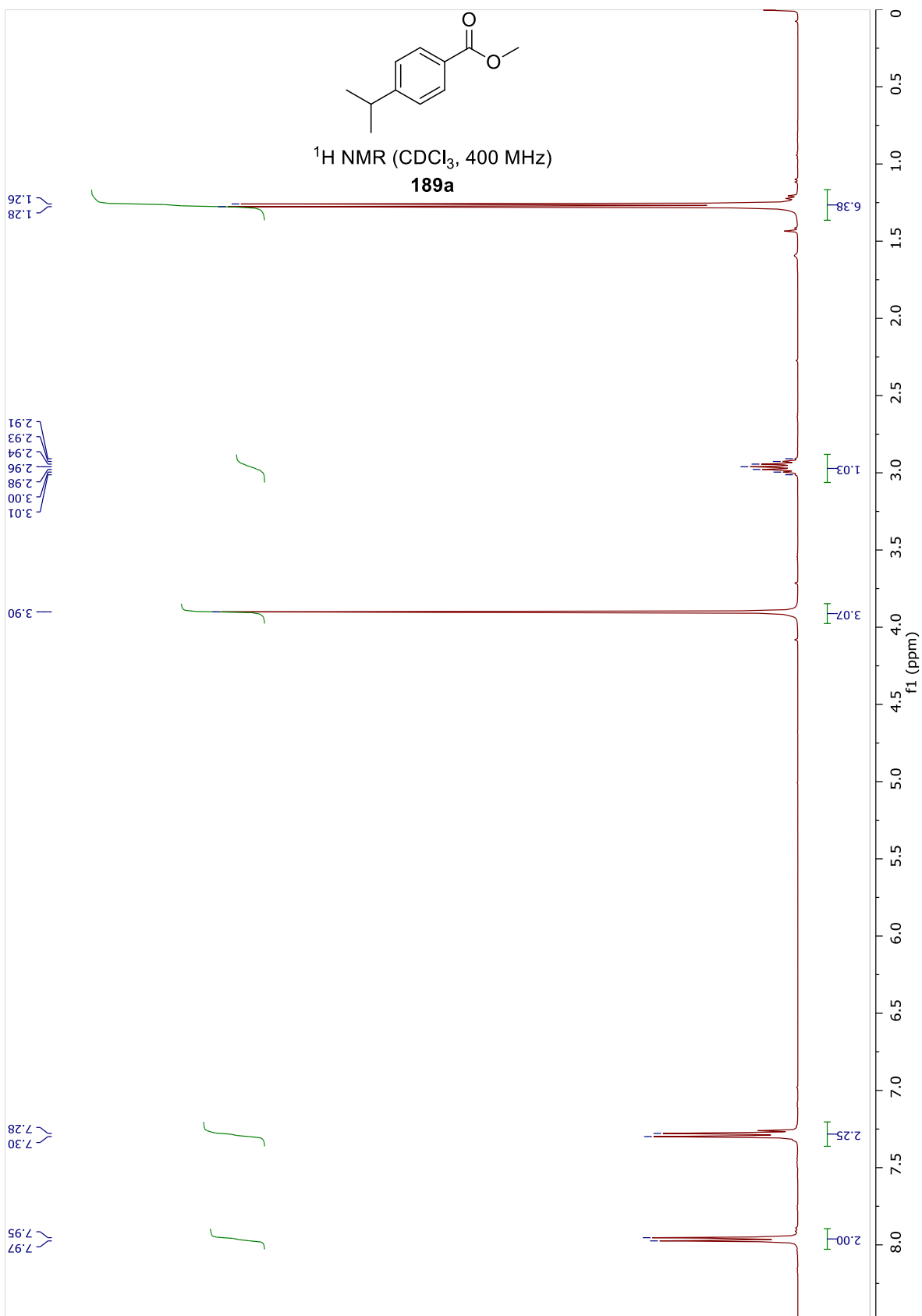
^{19}F NMR (CDCl_3 , 377 MHz)
268a

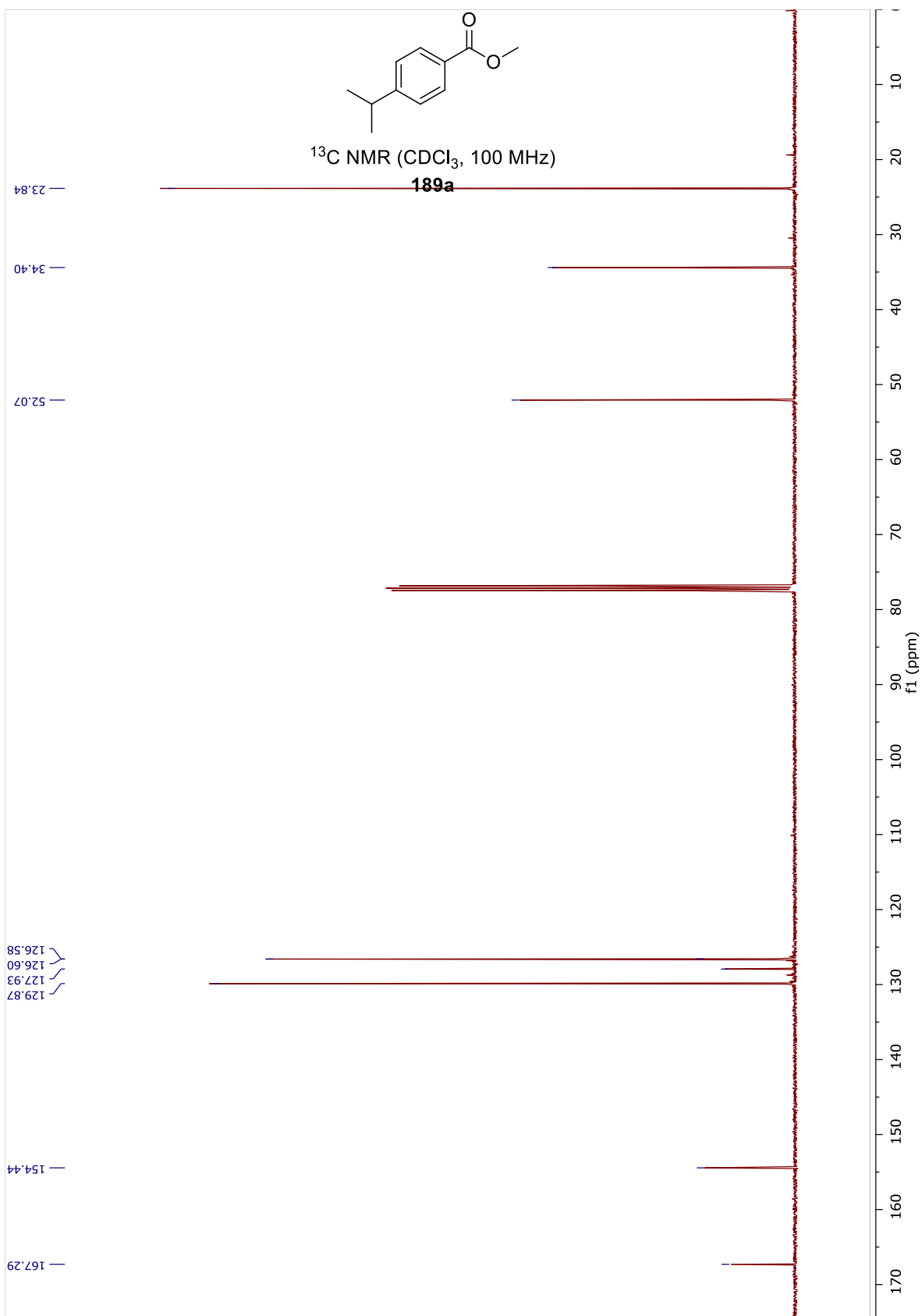
09.29-

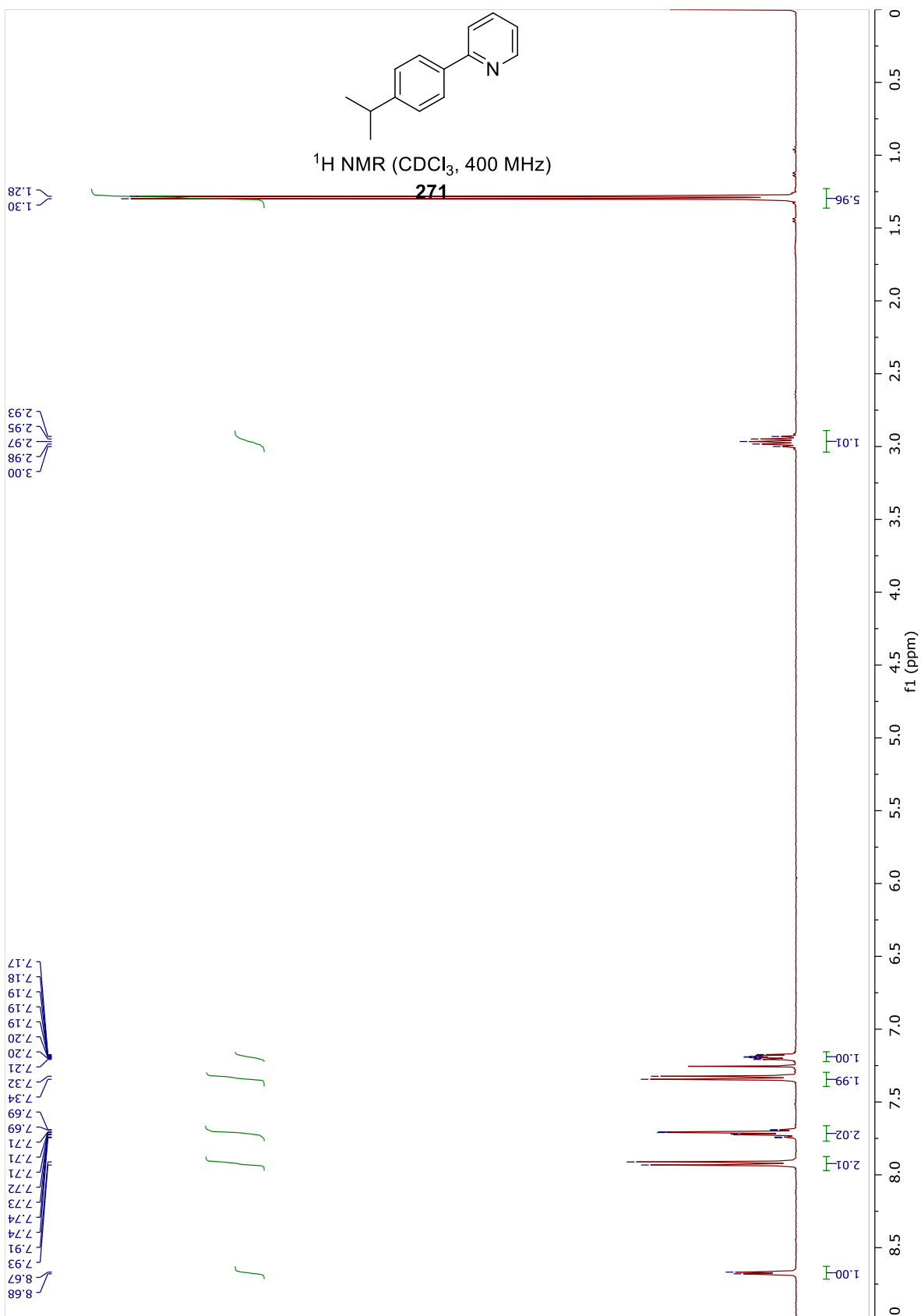
-290
-270
-250
-230
-210
-190
-170
-150
-130
-110
-90
-70
-50
-30
-10
10
30
50
70
90
f1 (ppm)

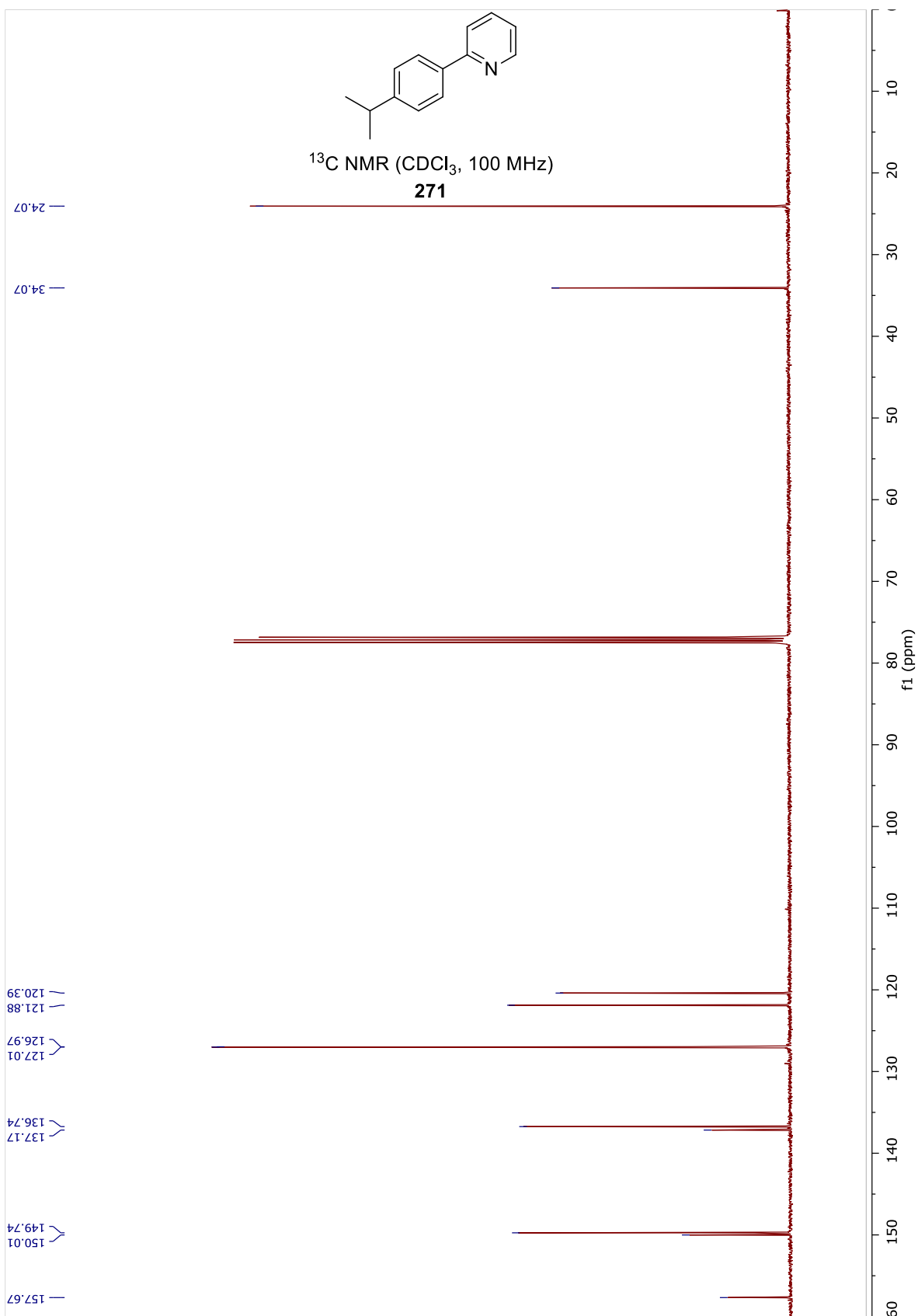


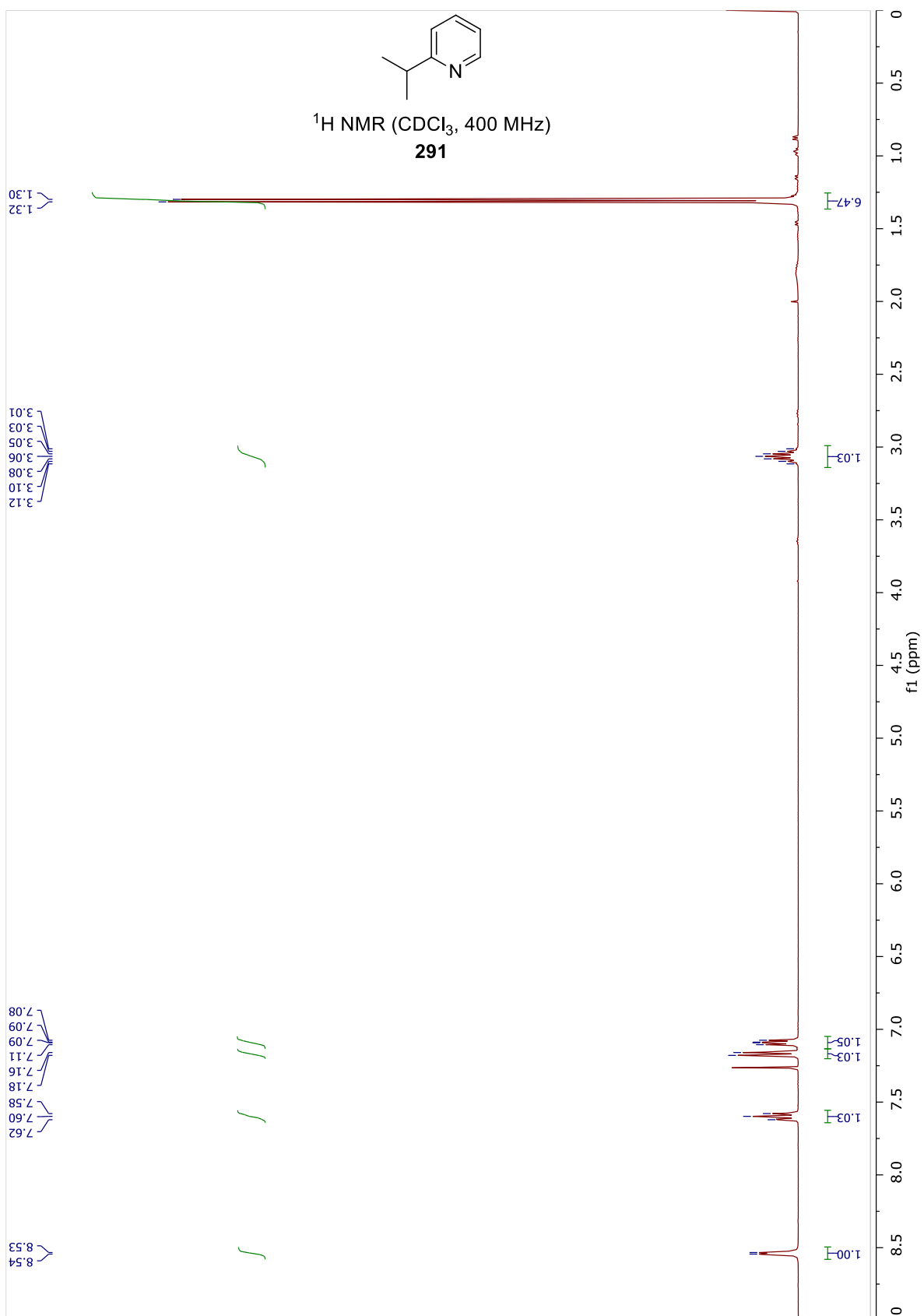


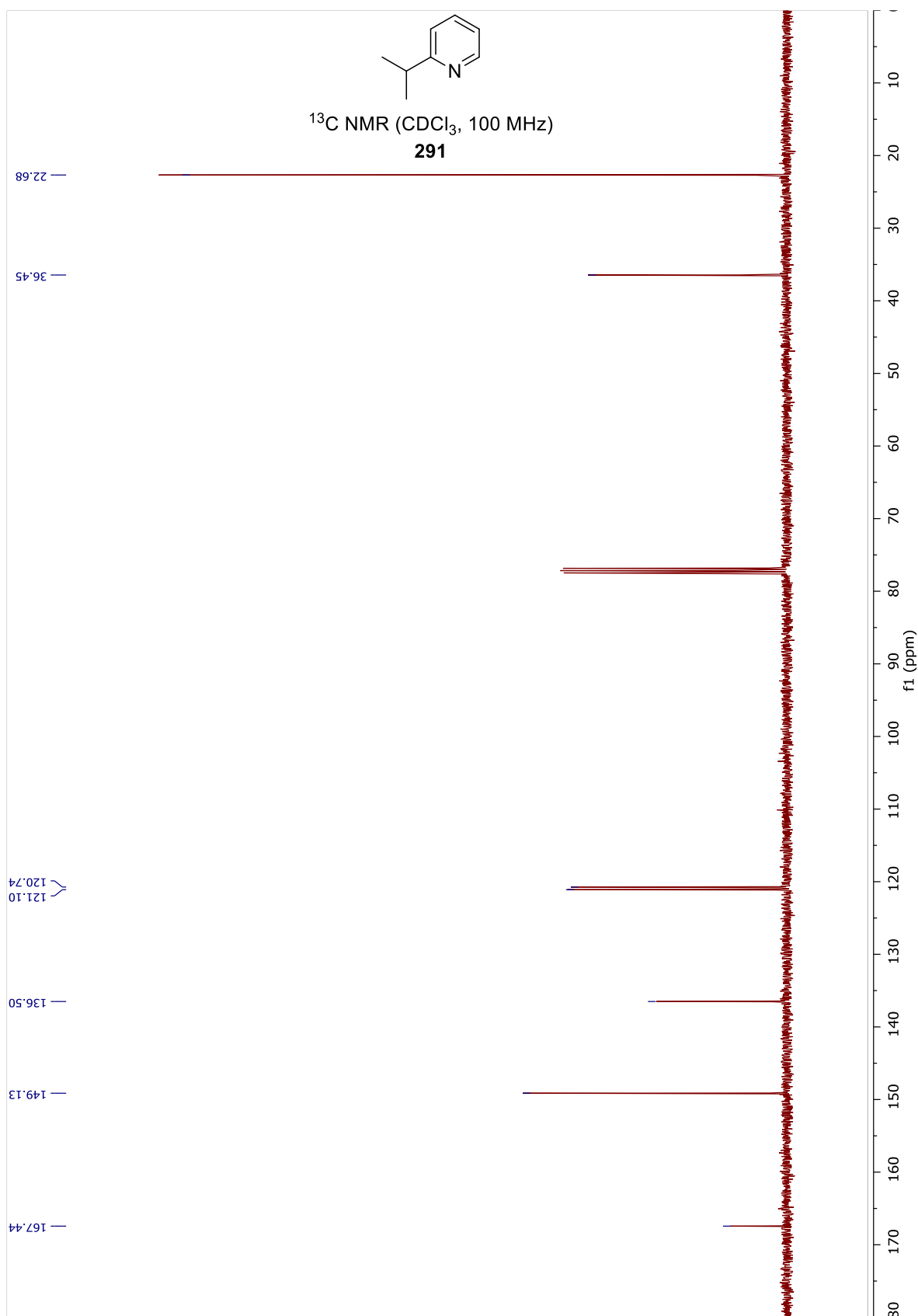


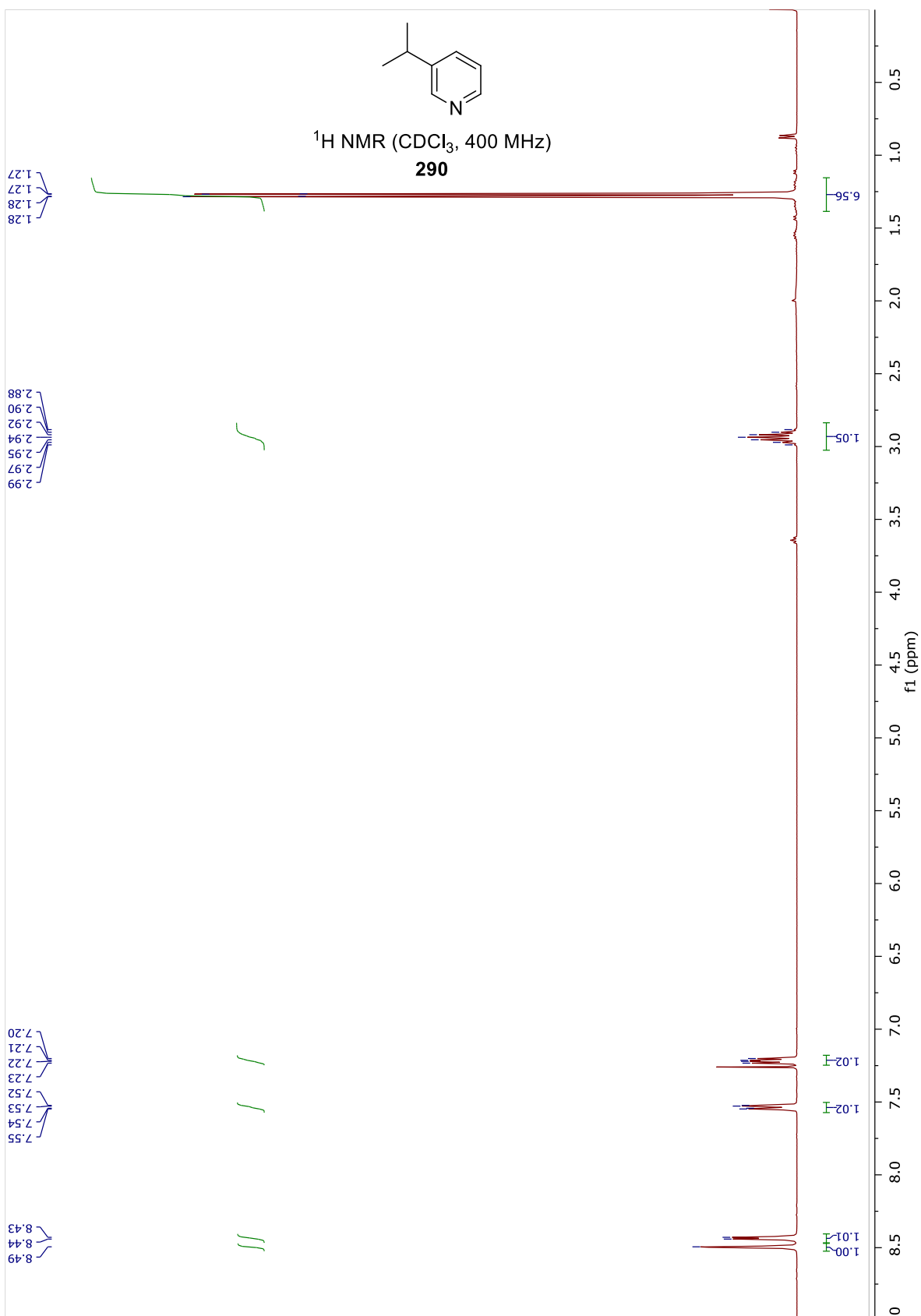


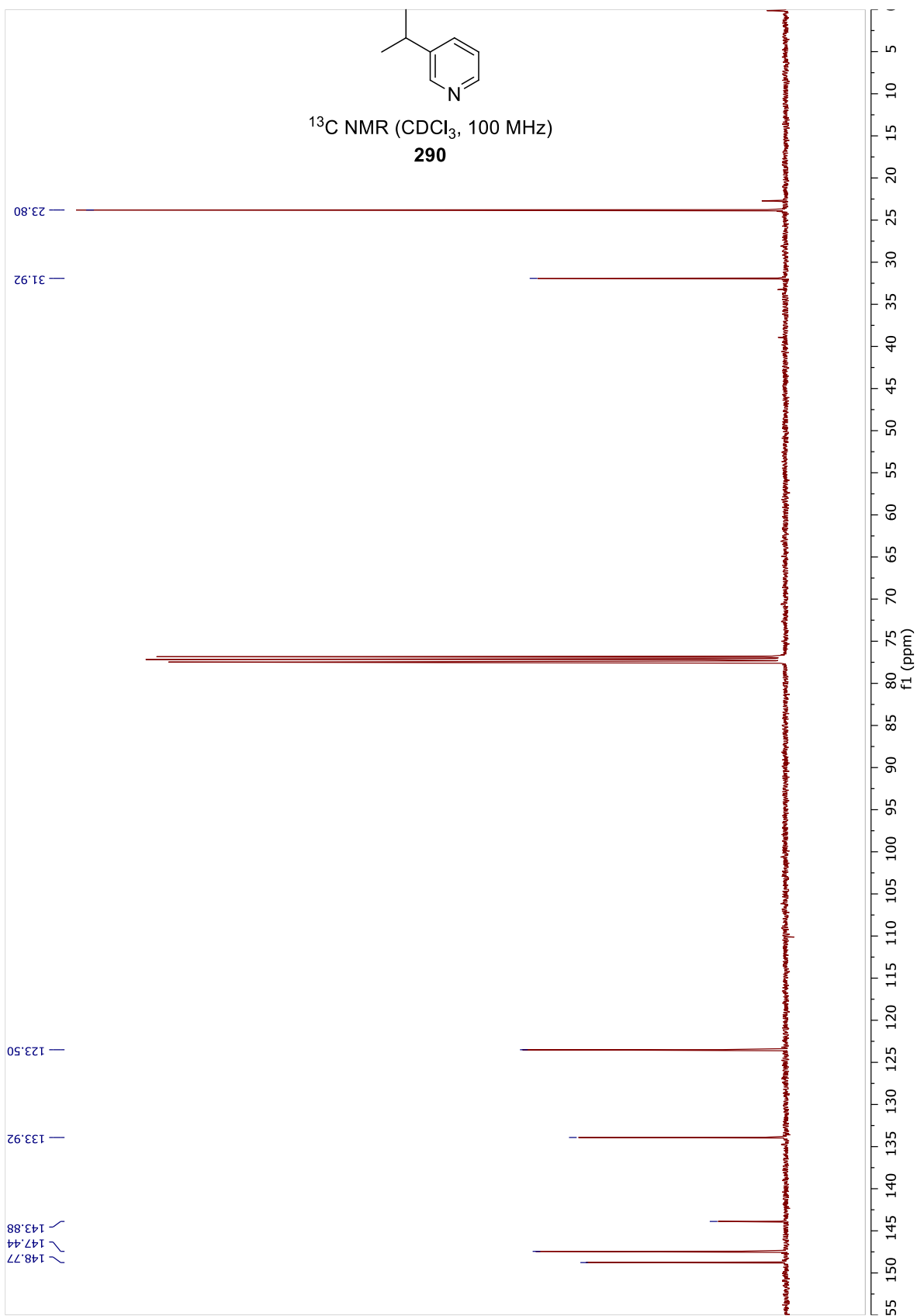


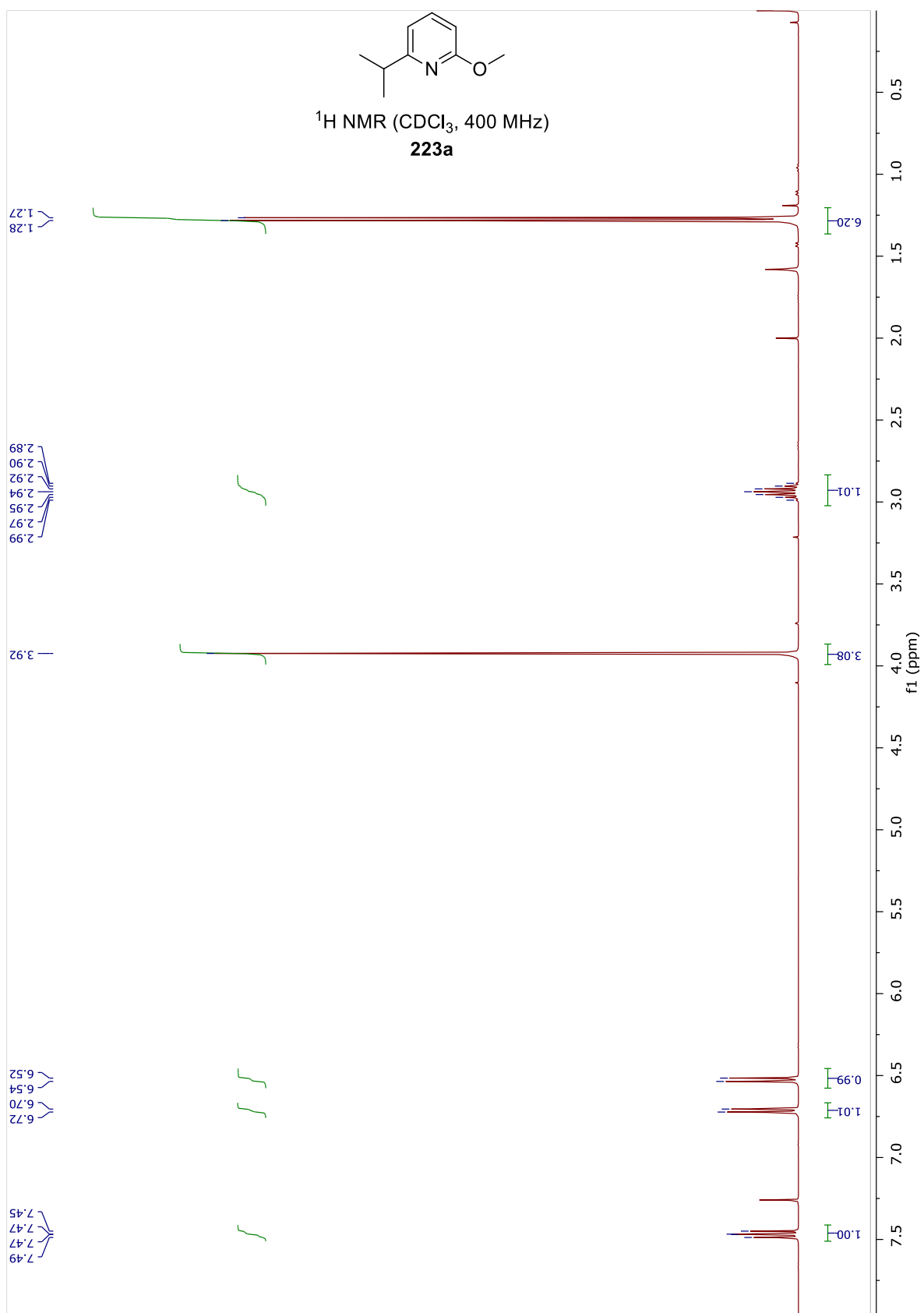


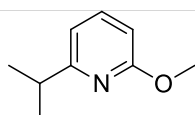




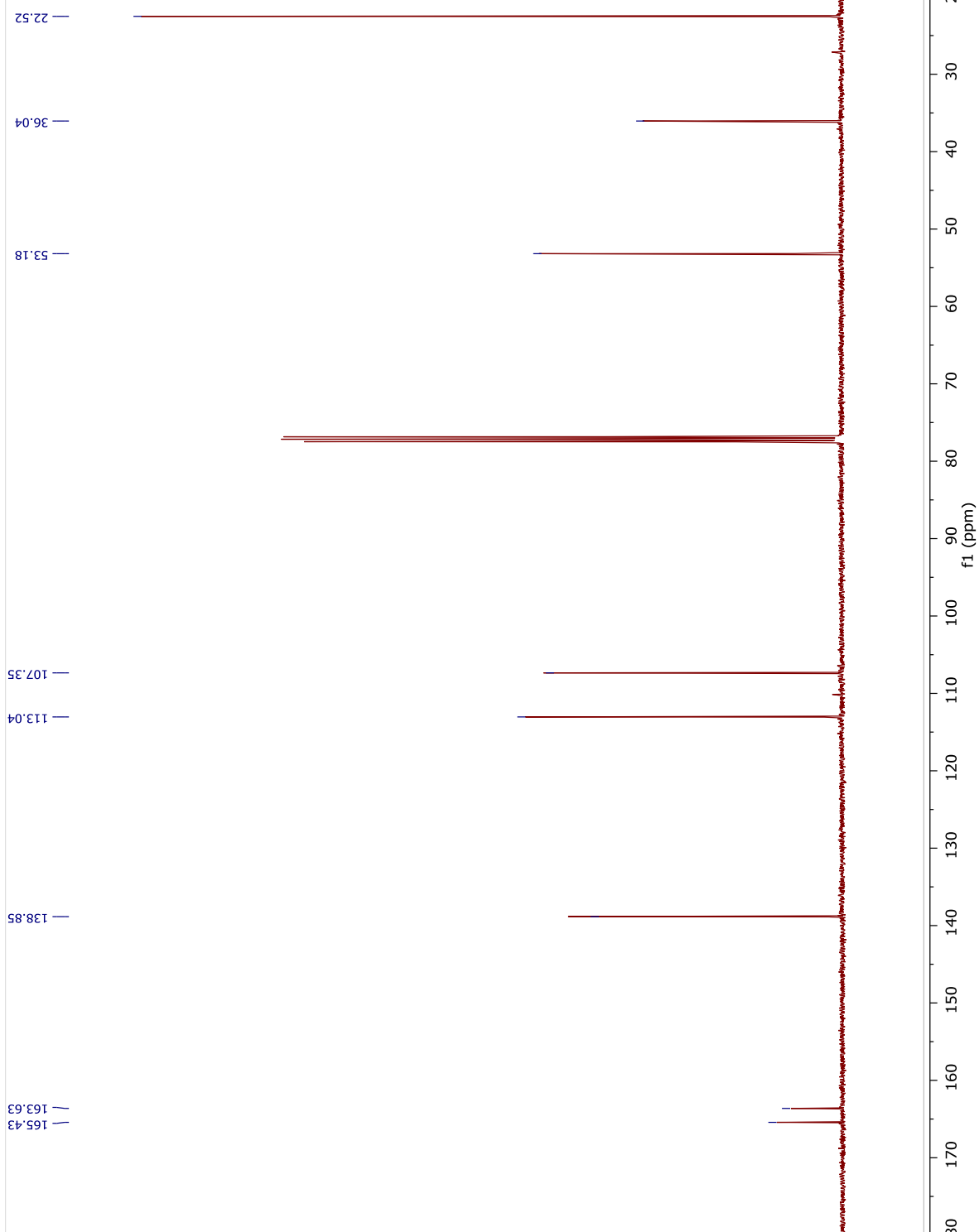


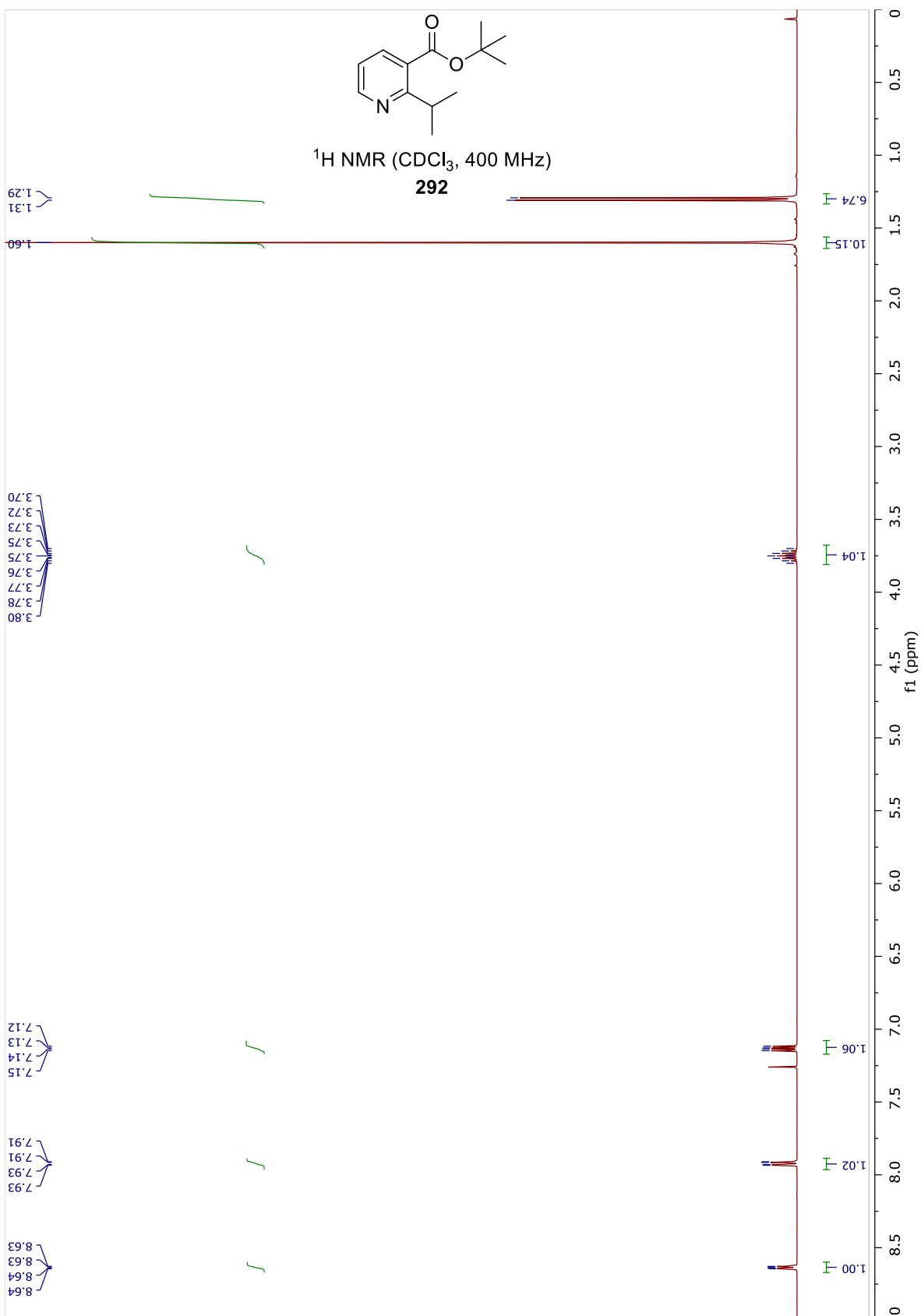


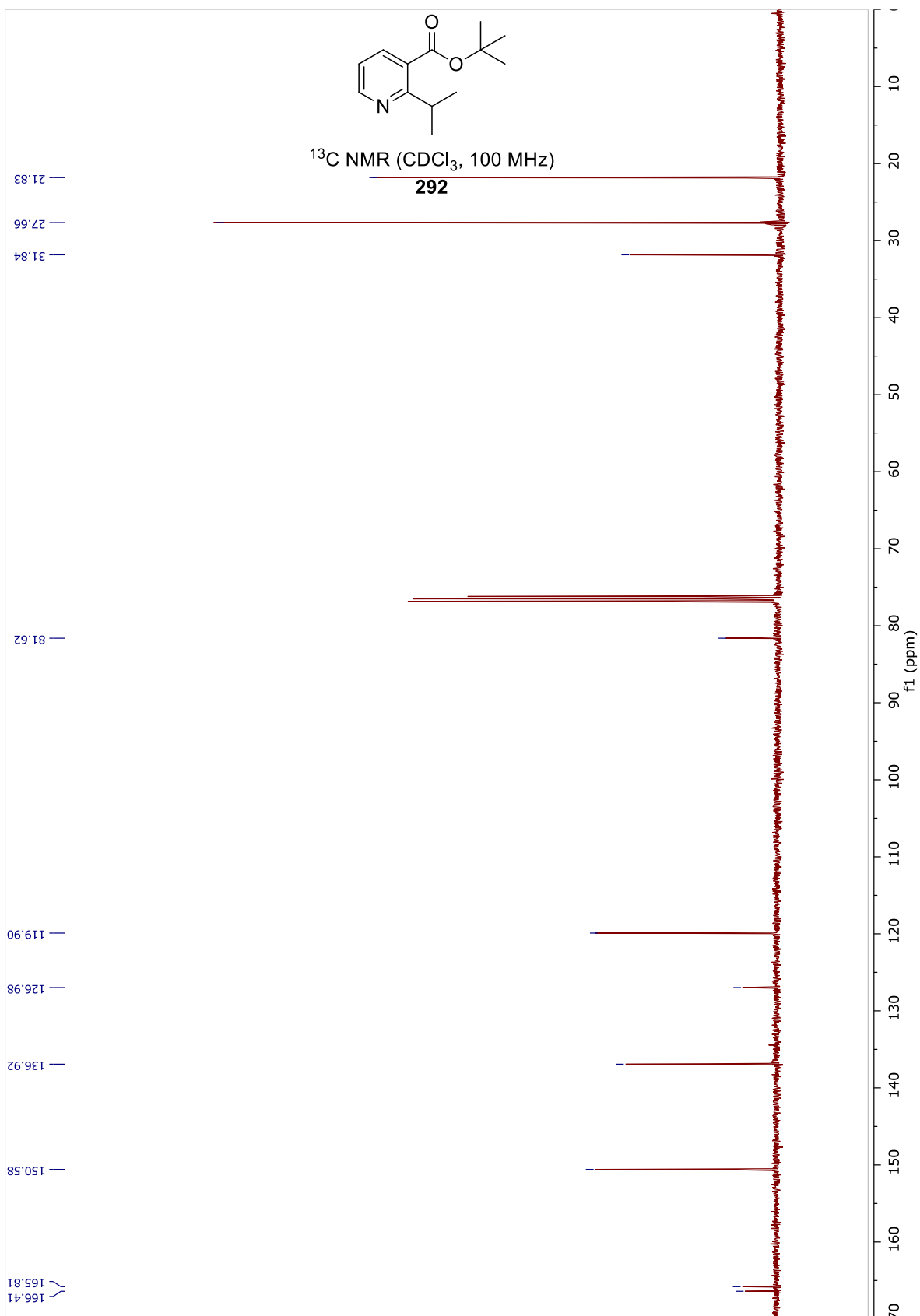


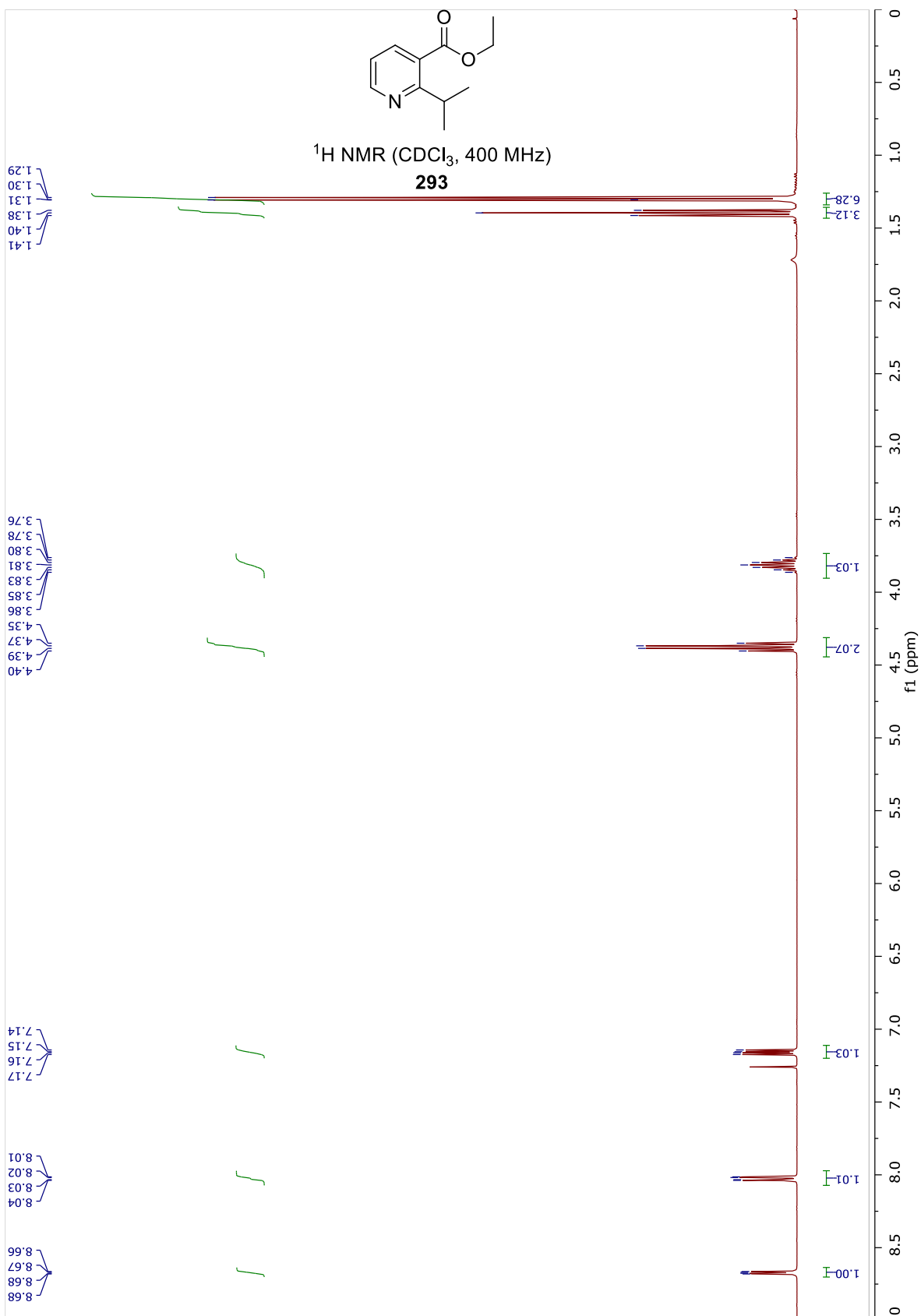


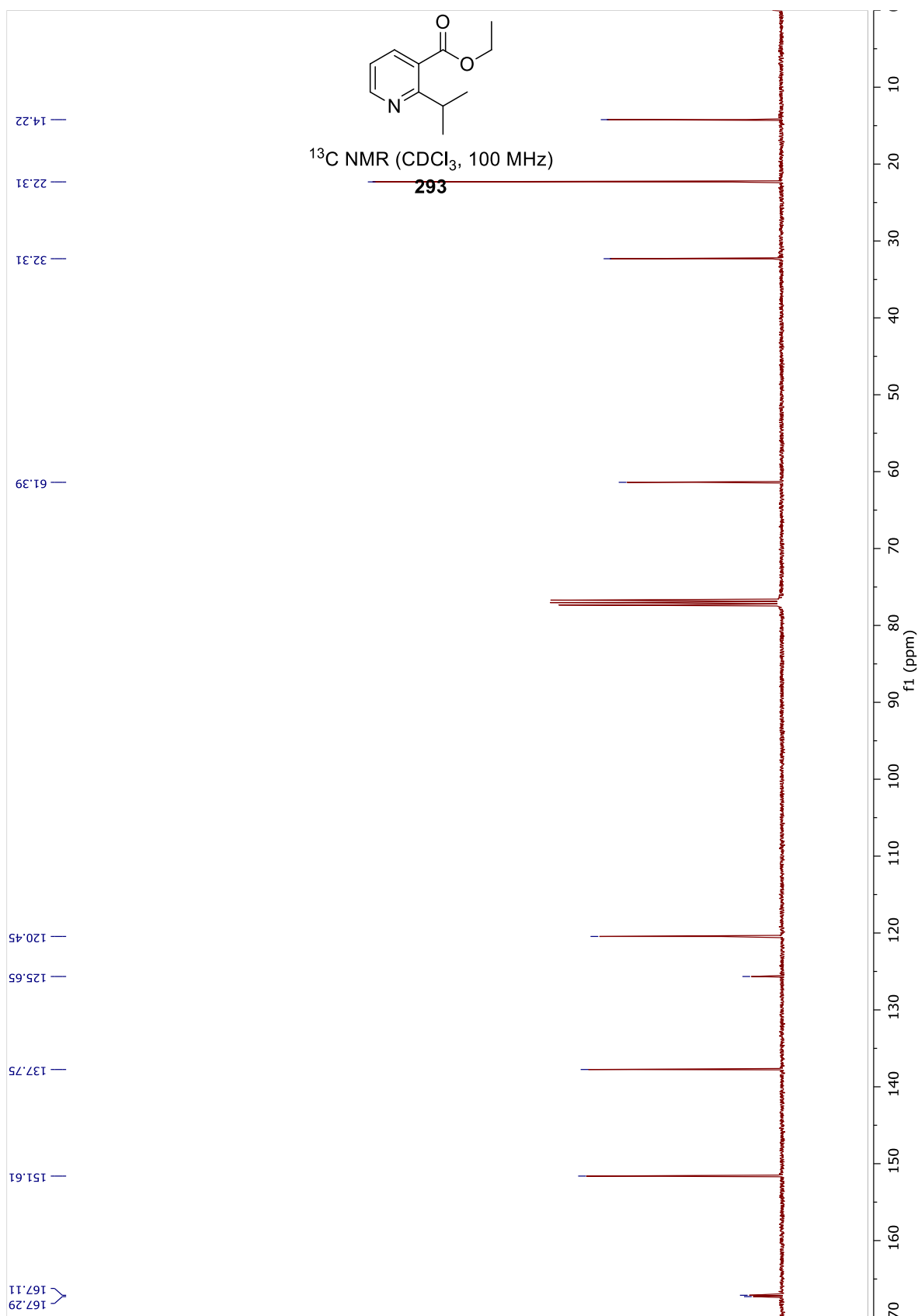
^{13}C NMR (CDCl_3 , 100 MHz)
223a

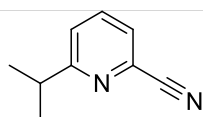




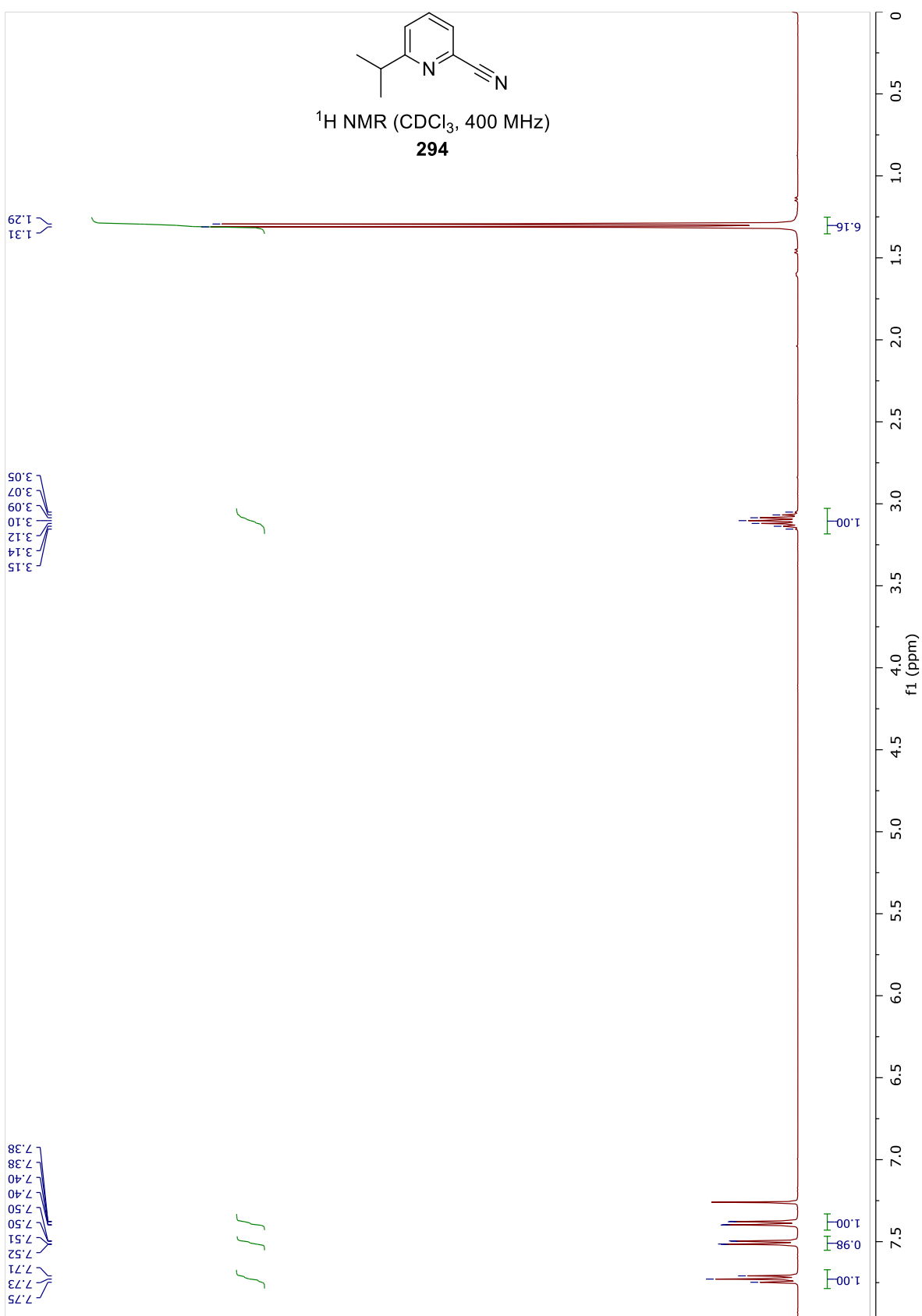


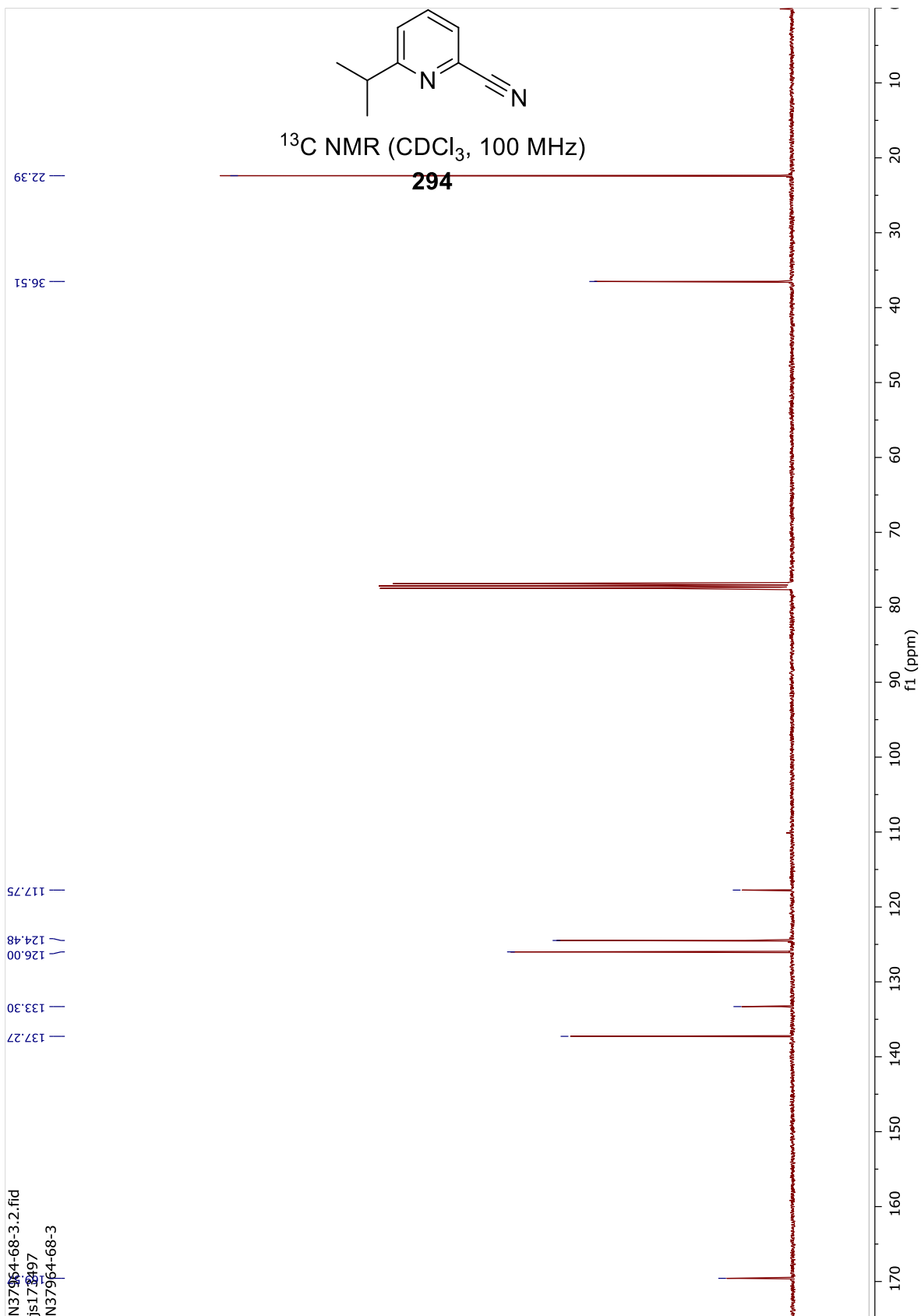


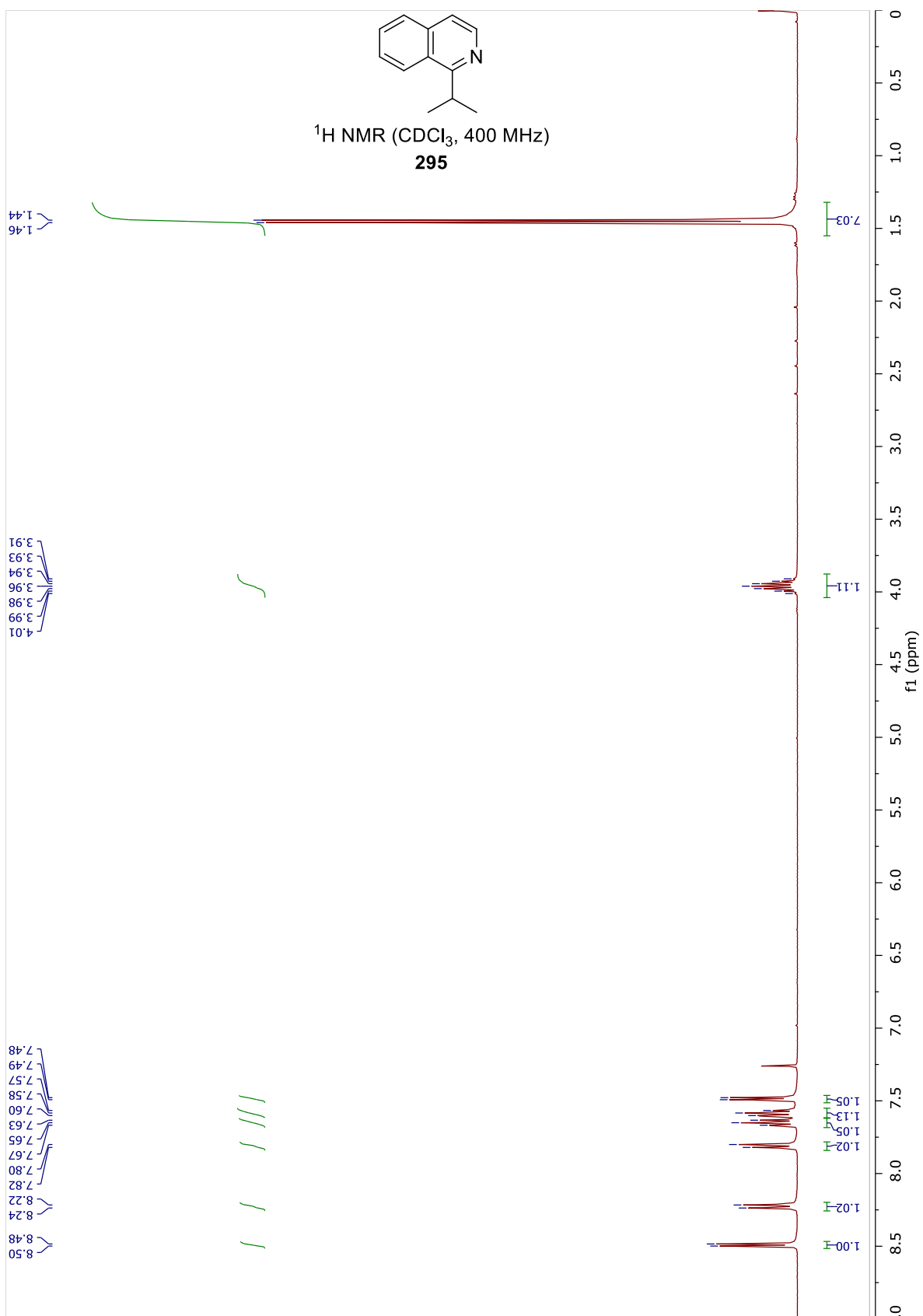


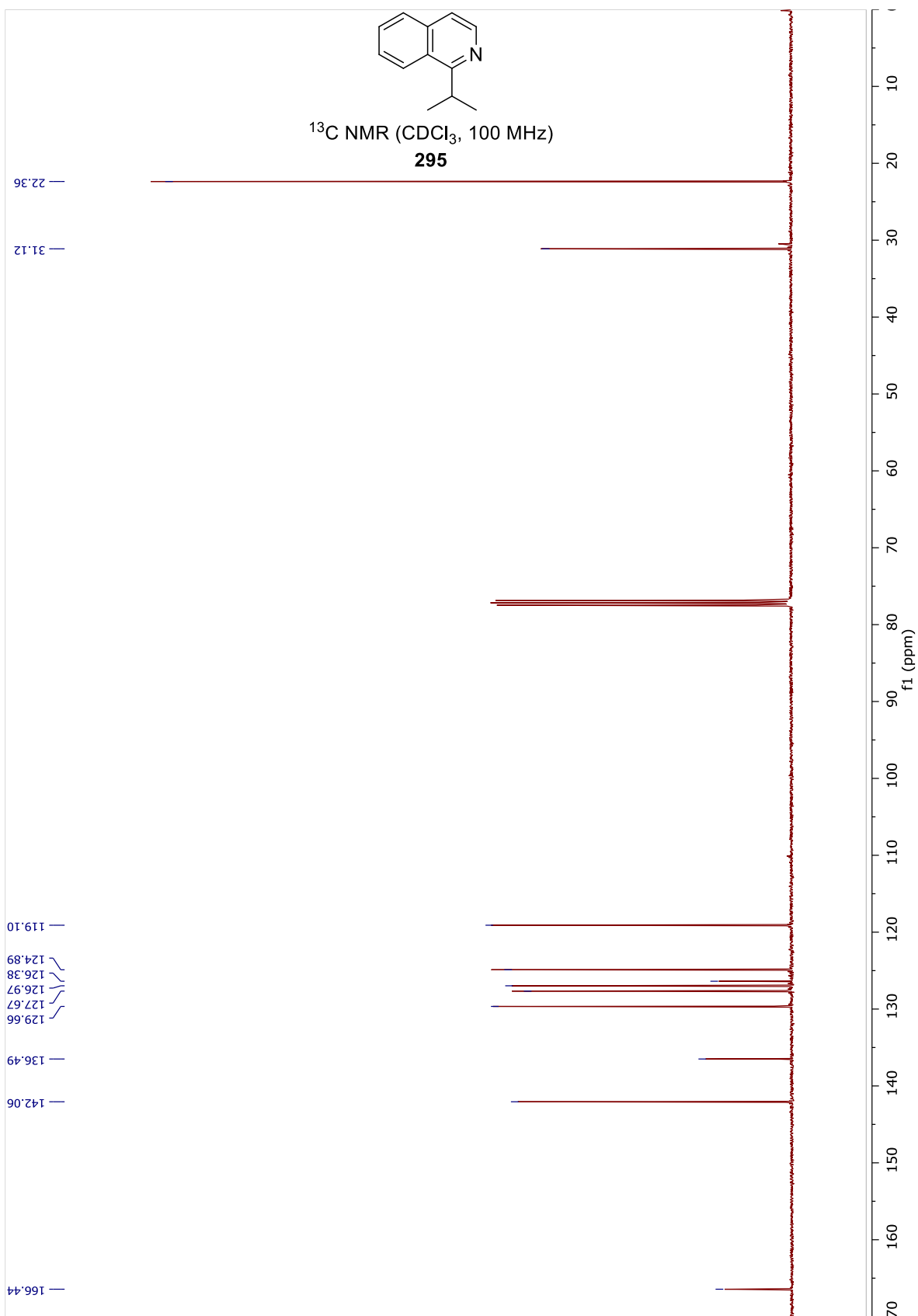


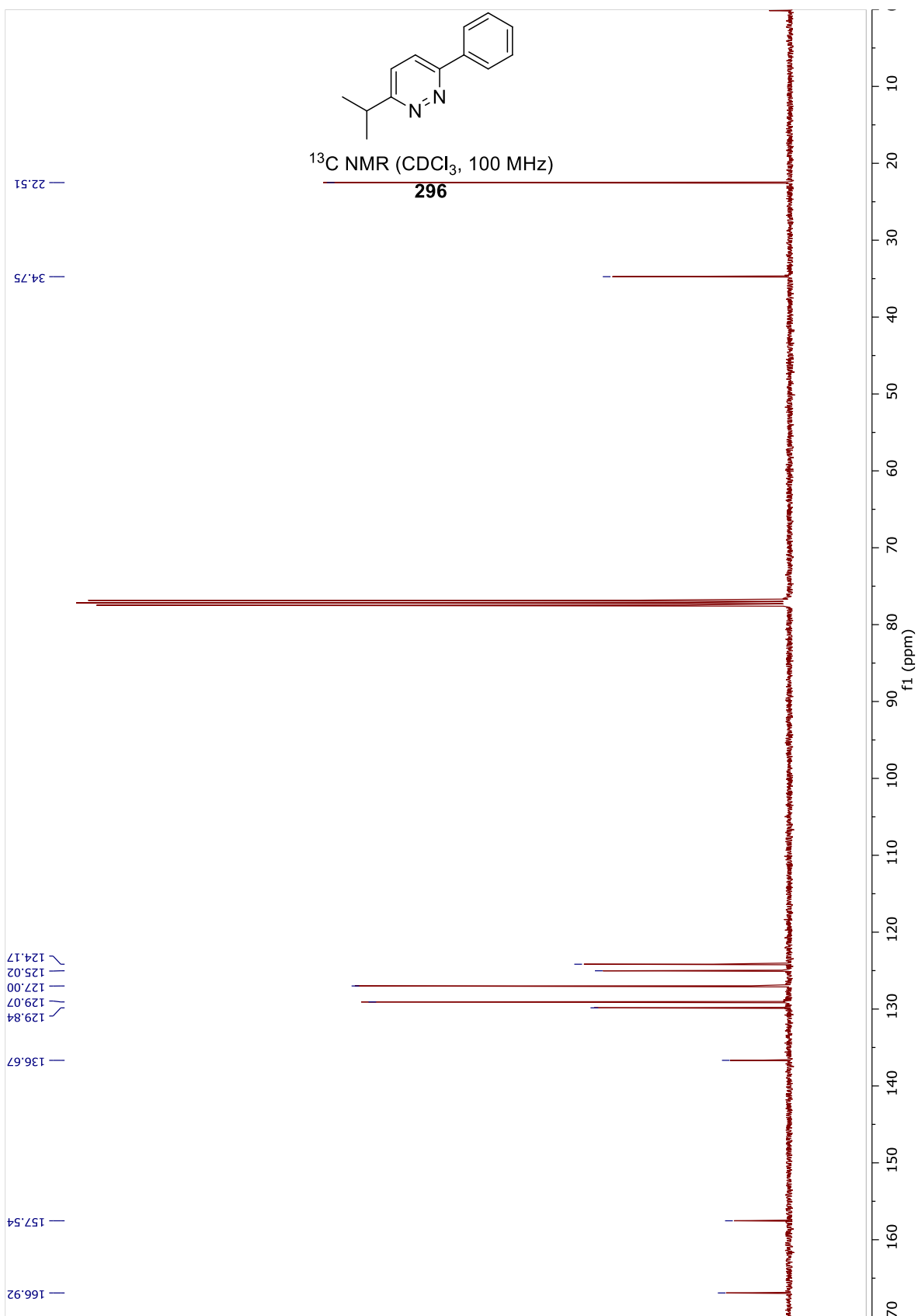
¹H NMR (CDCl₃, 400 MHz)
294

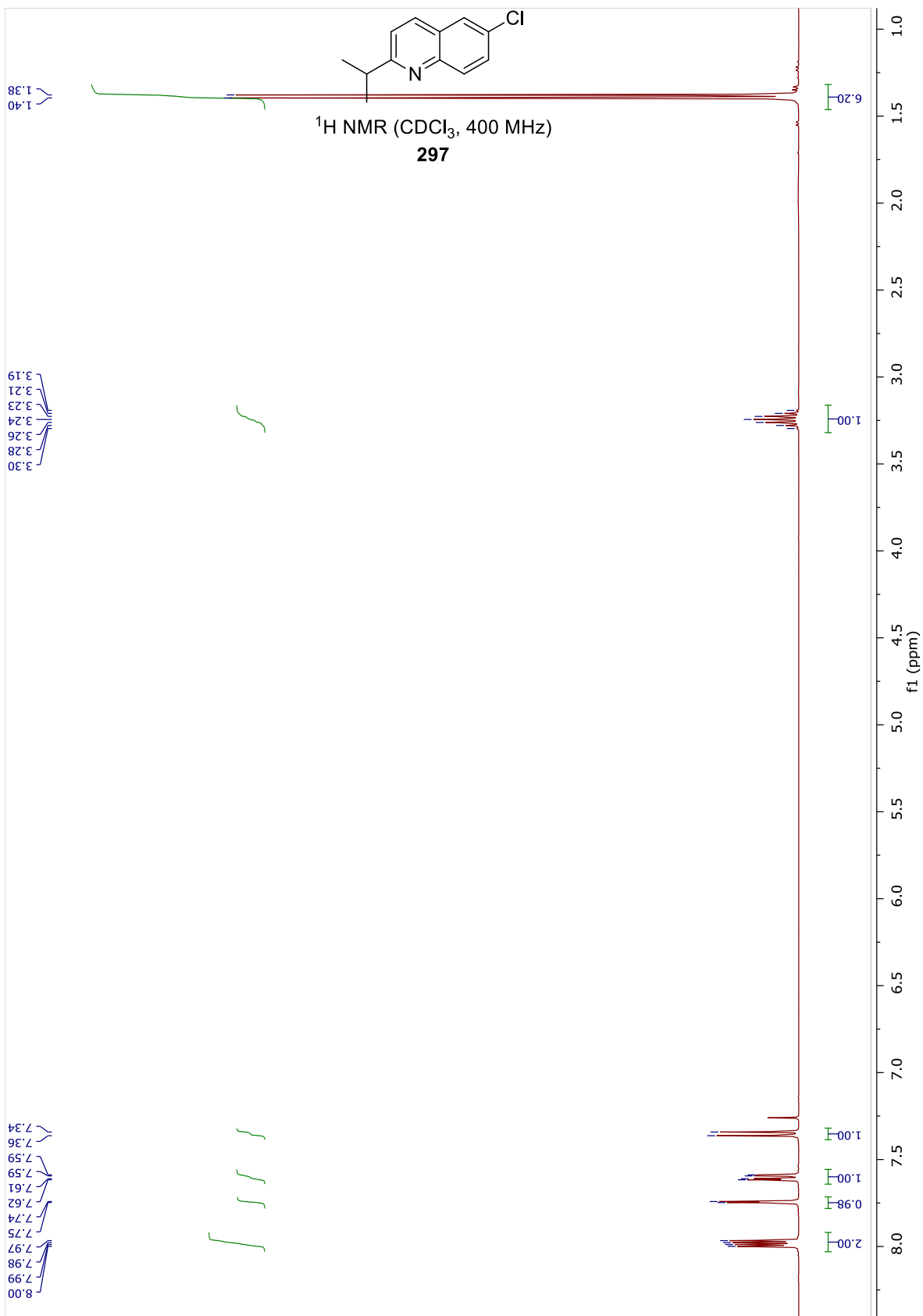


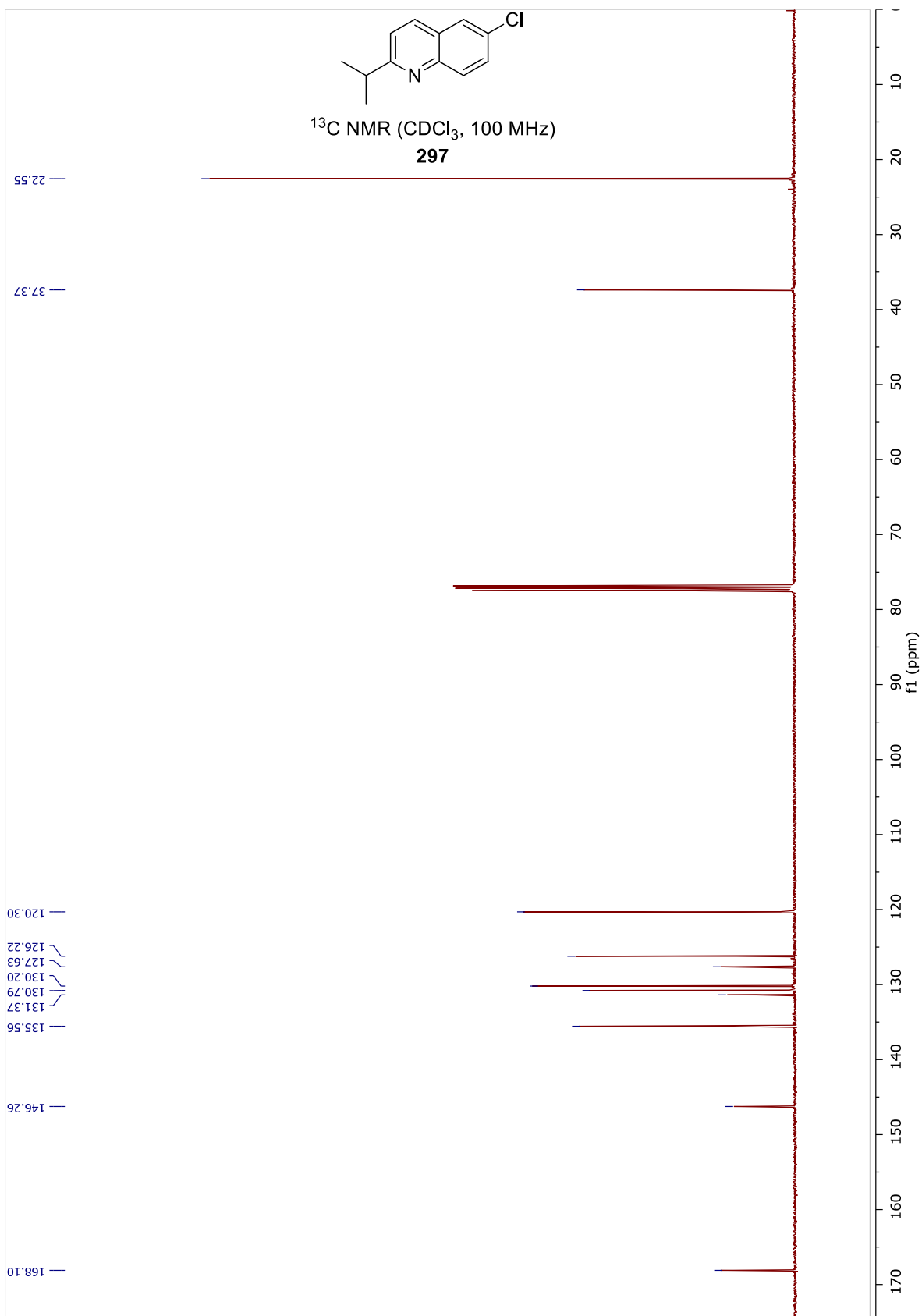


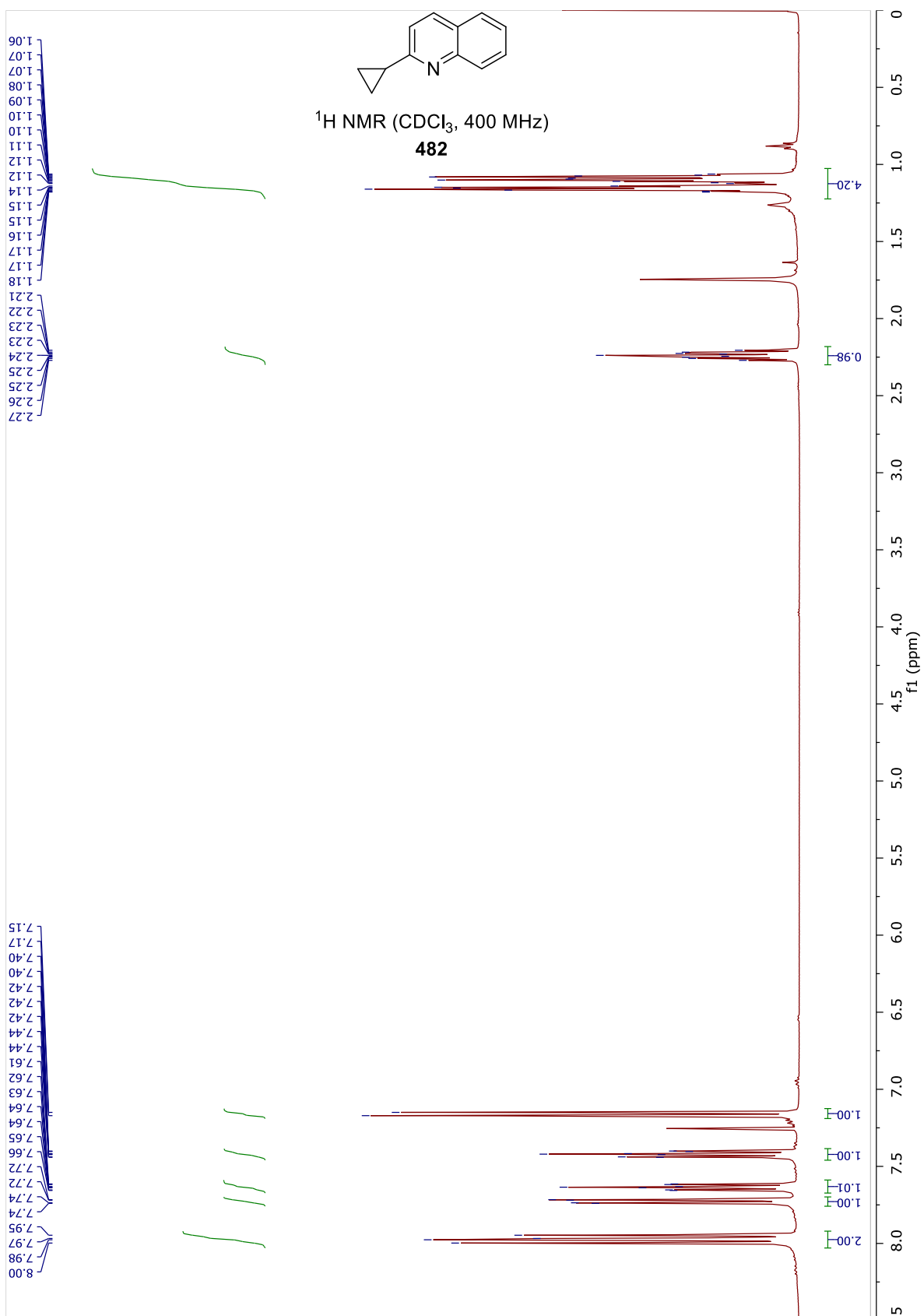


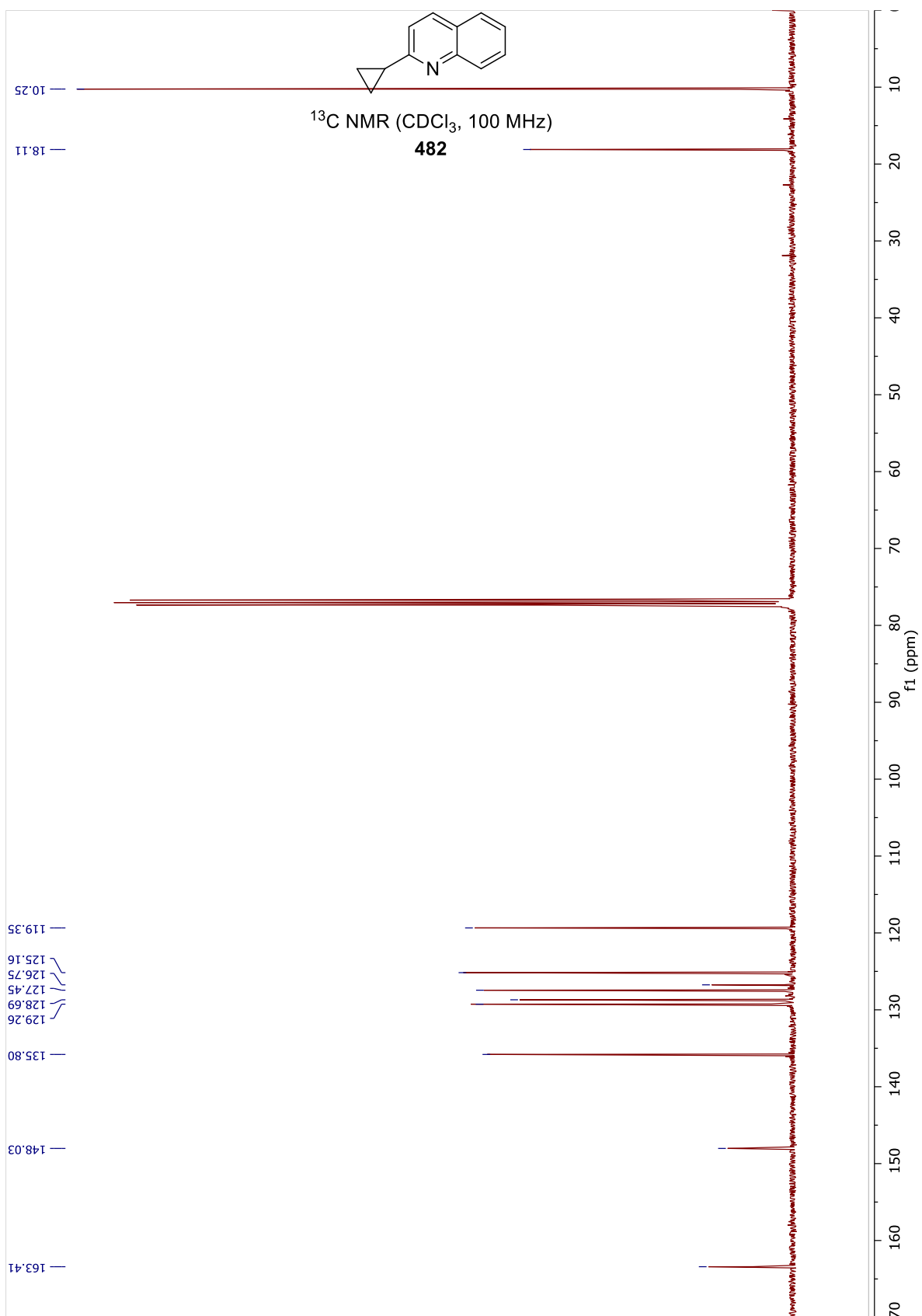


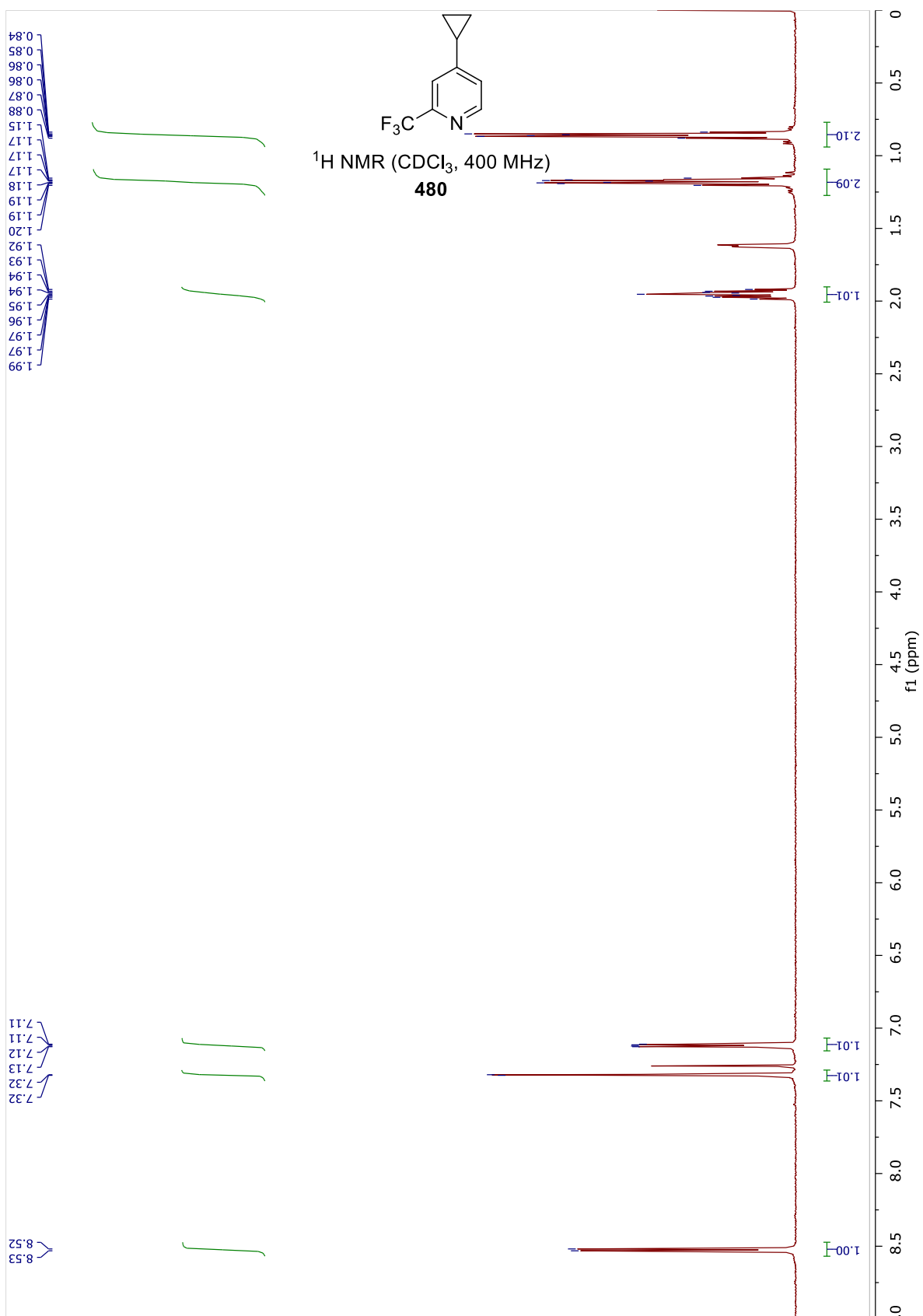


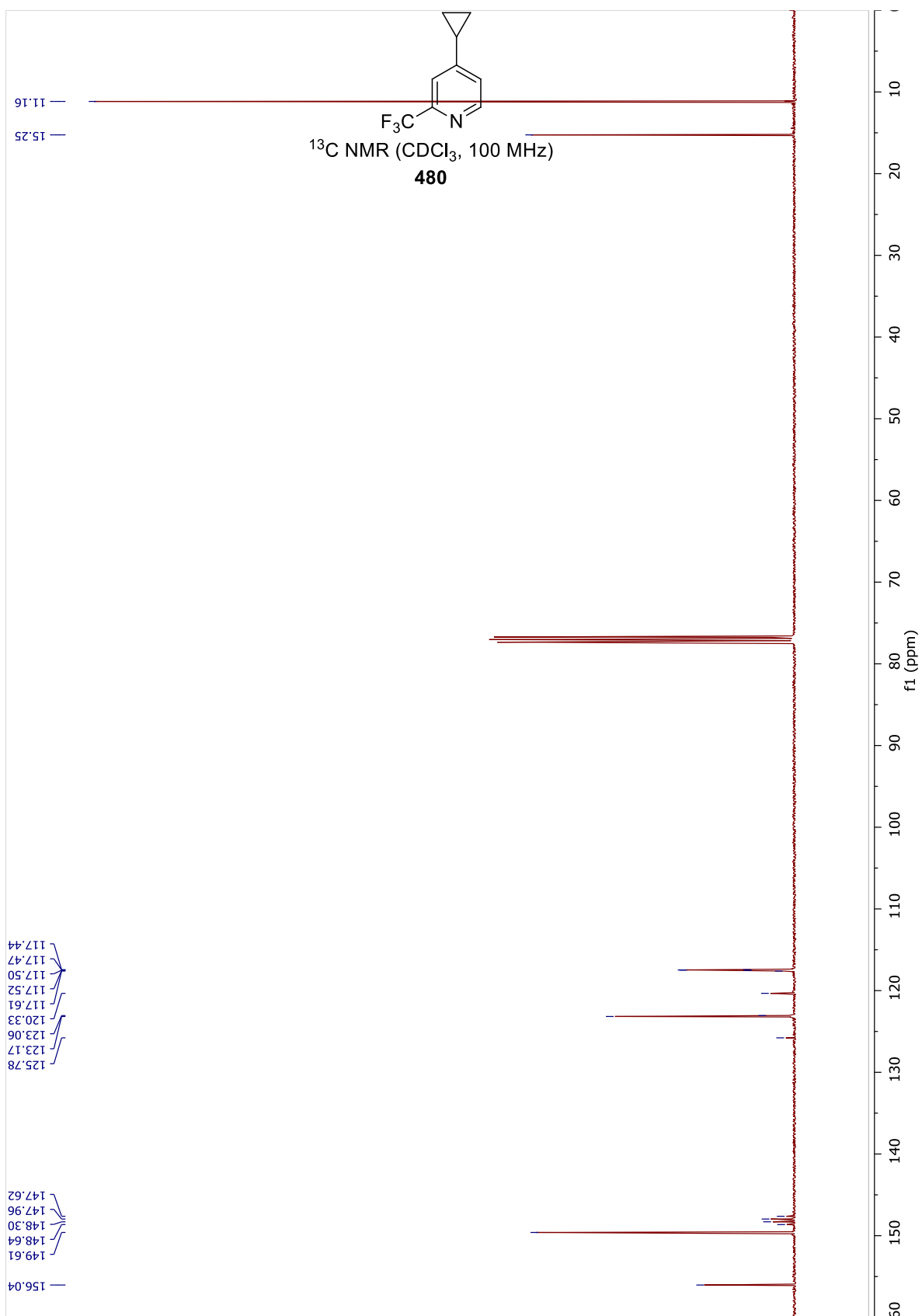


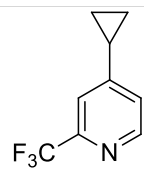






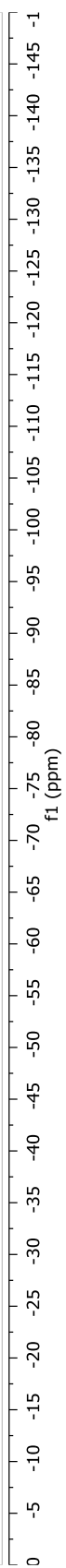


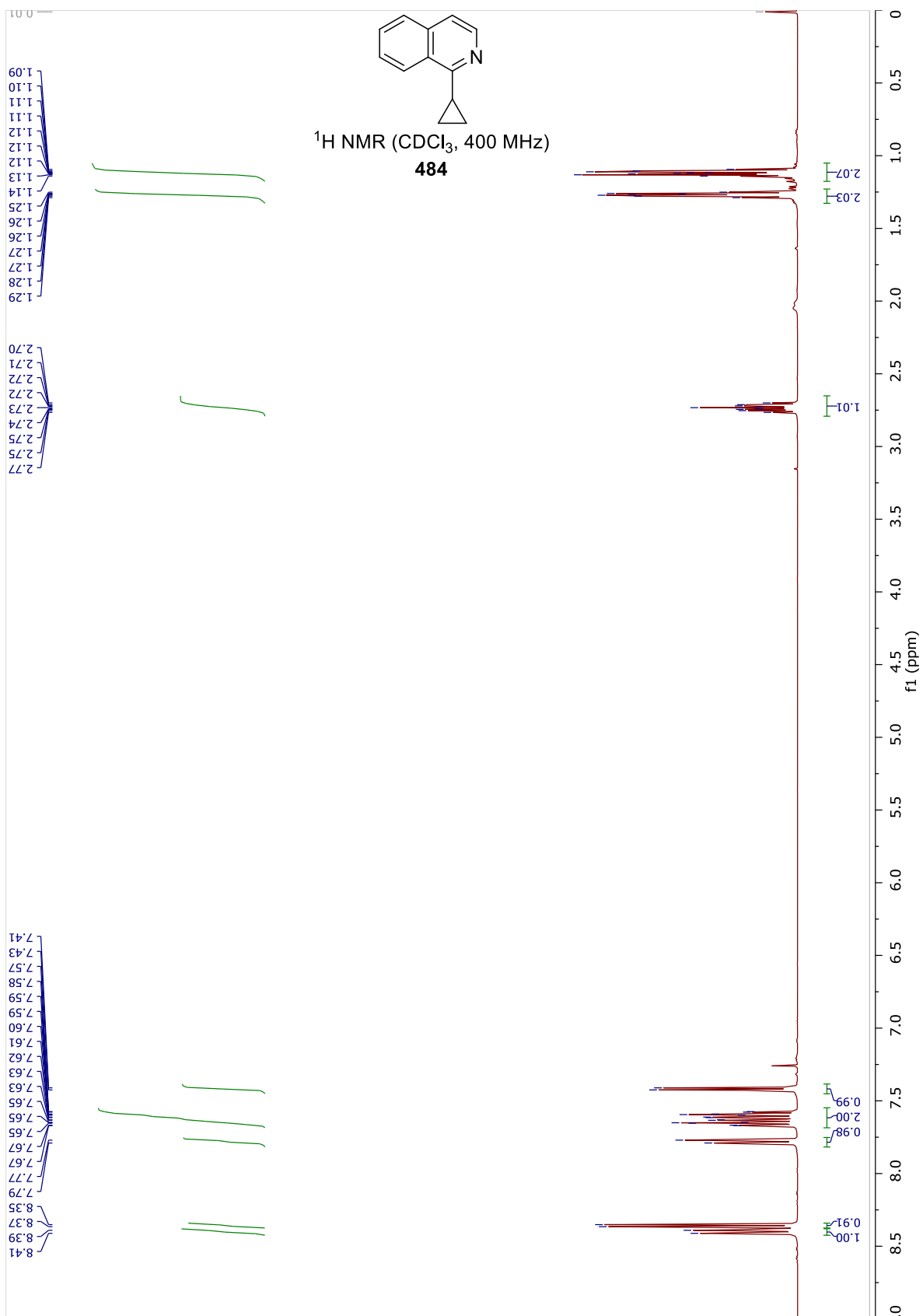


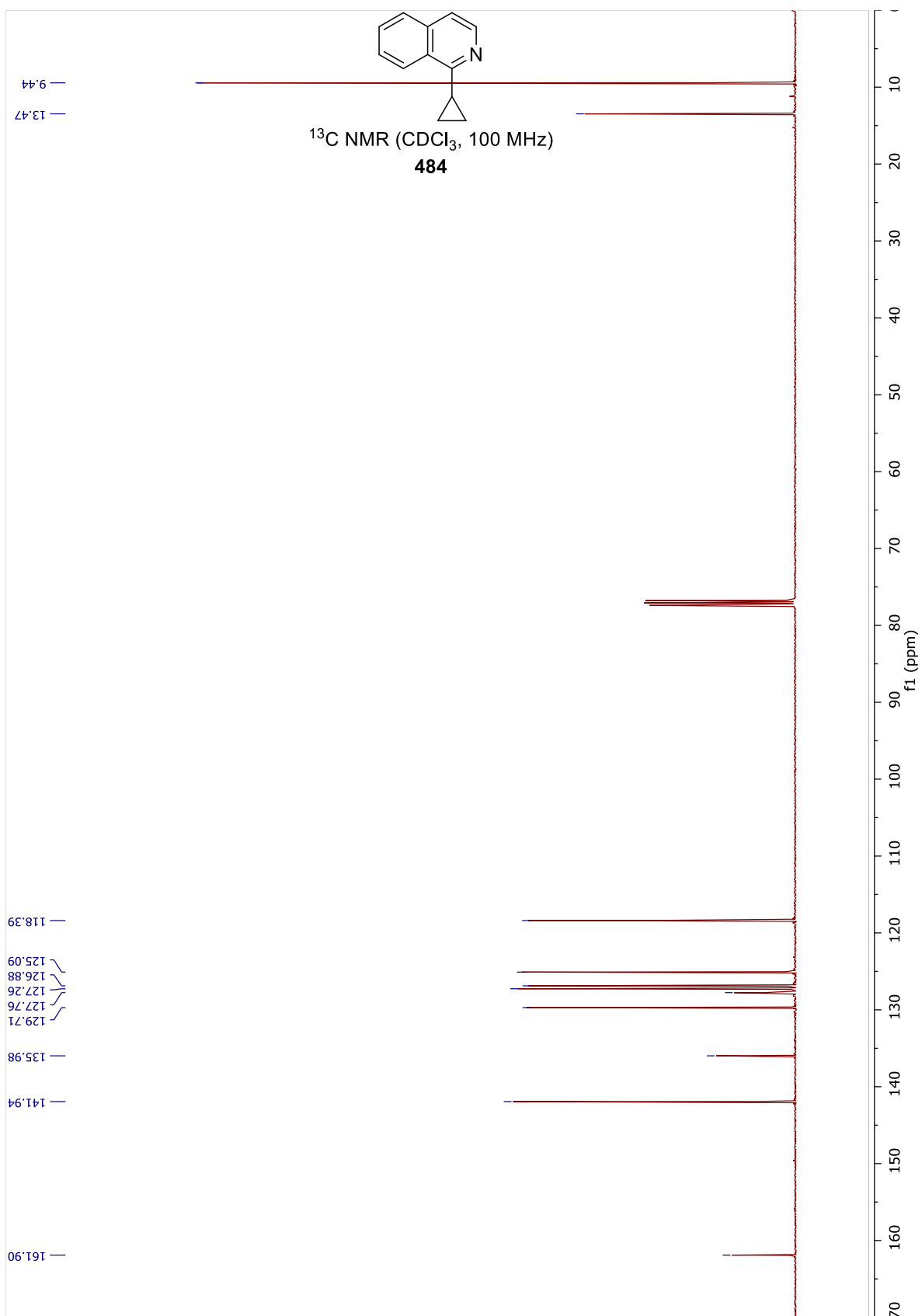


^{19}F NMR (CDCl_3 , 377 MHz)
480

01'89-







8. References

1. C. C. C. Johansson Seechurn, M. O. Kitching, T. J. Colacot and V. Snieckus, *Angew. Chem. Int. Ed.*, 2012, **51**, 5062-5085.
2. C. Glaser, *Ber. Dtsch. Chem. Ges.*, 1869, **2**, 422-424.
3. F. Bohlmann, H. Schönowsky, E. Inhoffen and G. Grau, *Chem. Ber.*, 1964, **97**, 794-800.
4. F. Ullmann and J. Bielecki, *Ber. Dtsch. Chem. Ges.*, 1901, **34**, 2174-2185.
5. H. Meerwein, E. Büchner and K. van Emster, *J. Prakt. Chem.*, 1939, **152**, 237-266.
6. M. S. Kharasch and E. K. Fields, *J. Am. Chem. Soc.*, 1941, **63**, 2316-2320.
7. J. K. Kochi, *J. Am. Chem. Soc.*, 1955, **77**, 5090-5092.
8. M. S. Kharasch and C. F. Fuchs, *J. Am. Chem. Soc.*, 1943, **65**, 504-507.
9. G. Trinquier and R. Hoffmann, *Organometallics*, 1984, **3**, 370-380.
10. C. Le Berre, P. Serp, P. Kalck and G. P. Torrence, in *Ullmann's Encyclopedia of Industrial Chemistry*, Wiley-VCH Verlag GmbH & Co. KGaA, 2000.
11. G. J. Sunley and D. J. Watson, *Catal. Today*, 2000, **58**, 293-307.
12. C. Amatore, A. Jutand and G. Le Duc, *Chem. Eur. J.*, 2011, **17**, 2492-2503.
13. A. A. Thomas and S. E. Denmark, *Science*, 2016, **352**, 329-332.
14. A. A. Thomas, H. Wang, A. F. Zahrt and S. E. Denmark, *J. Am. Chem. Soc.*, 2017, **139**, 3805-3821.
15. R. J. P. Corriu and J. P. Masse, *J. Chem. Soc., Chem. Commun.*, 1972, **1972**, 144a.
16. K. Tamao, K. Sumitani and M. Kumada, *J. Am. Chem. Soc.*, 1972, **94**, 4374-4376.
17. K. Tamao, K. Sumitani, Y. Kiso, M. Zembayashi, A. Fujioka, S. Kodama, I. Nakajima, A. Minato and M. Kumada, *B. Chem. Soc. Jpn.*, 1976, **49**, 1958-1969.
18. M. Uchino, A. Yamamoto and S. Ikeda, *J. Organomet. Chem.*, 1970, **24**, C63-C64.
19. M. Hidai, T. Kashiwagi, T. Ikeuchi and Y. Uchida, *J. Organomet. Chem.*, 1971, **30**, 279-282.
20. G. W. Parshall, *J. Am. Chem. Soc.*, 1974, **96**, 2360-2366.
21. J. Breitenfeld, M. D. Wodrich and X. Hu, *Organometallics*, 2014, **33**, 5708-5715.
22. J. Breitenfeld, J. Ruiz, M. D. Wodrich and X. Hu, *J. Am. Chem. Soc.*, 2013, **135**, 12004-12012.
23. D. N. Primer, I. Karakaya, J. C. Tellis and G. A. Molander, *J. Am. Chem. Soc.*, 2015, **137**, 2195-2198.
24. J. A. Terrett, J. D. Cuthbertson, V. W. Shurtleff and D. W. C. MacMillan, *Nature*, 2015, **524**, 330-334.
25. C. Bolm, J. Legros, J. Le Paih and L. Zani, *Chem. Rev.*, 2004, **104**, 6217-6254.
26. I. Bauer and H.-J. Knölker, *Chem. Rev.*, 2015, **115**, 3170-3387.
27. V. G. P. Mottez, *C. R. Acad. Sci.*, 1944, **218**, 557-559.
28. M. Tamura and J. Kochi, *Synthesis*, 1971, **1971**, 303-305.
29. R. S. Smith and J. K. Kochi, *J. Org. Chem.*, 1976, **41**, 502-509.
30. C. L. Kwan and J. K. Kochi, *J. Am. Chem. Soc.*, 1976, **98**, 4903-4912.

31. J. Kleimark, A. Hedström, P.-F. Larsson, C. Johansson and P.-O. Norrby, *ChemCatChem*, 2009, **1**, 152-161.
32. C. J. Adams, R. B. Bedford, E. Carter, N. J. Gower, M. F. Haddow, J. N. Harvey, M. Huwe, M. A. Cartes, S. M. Mansell, C. Mendoza, D. M. Murphy, E. C. Neeve and J. Nunn, *J. Am. Chem. Soc.*, 2012, **134**, 10333-10336.
33. G. Cahiez and S. Marquais, *Tetrahedron Lett.*, 1996, **37**, 1773-1776.
34. G. Cahiez and H. Avedissian, *Synthesis*, 1998, **1998**, 1199-1205.
35. A. Fürstner, A. Leitner, M. Mendez and H. Krause, *J. Am. Chem. Soc.*, 2002, **124**, 13856-13863.
36. L. E. Aleandri, B. Bogdanovic, P. Bons, C. Duerr, A. Gaidies, T. Hartwig, S. C. Hockett, M. Lagarden, U. Wilczok and R. A. Brand, *Chem. Mater.*, 1995, **7**, 1153-1170.
37. B. Bogdanović and M. Schwickardi, *Angew. Chem. Int. Ed.*, 2000, **39**, 4610-4612.
38. A. Fürstner and A. Leitner, *Angew. Chem. Int. Ed.*, 2002, **41**, 609-612.
39. Y. Li, H.-Y. Hu, J.-P. Ye, H.-K. Fun, H.-W. Hu and J.-H. Xu, *J. Org. Chem.*, 2004, **69**, 2332-2339.
40. A. Fürstner, R. Martin, H. Krause, G. Seidel, R. Goddard and C. W. Lehmann, *J. Am. Chem. Soc.*, 2008, **130**, 8773-8787.
41. L. E. Aleandri, B. Bogdanovic, P. Bons, C. Duerr, A. Gaidies, T. Hartwig, S. C. Hockett, M. Lagarden, U. Wilczok and R. A. Brand, *Chem. Mater.*, 1995, **7**, 1153-1170.
42. R. B. Bedford, *Acc. Chem. Res.*, 2015, **48**, 1485-1493.
43. B. Scheiper, M. Bonnekessel, H. Krause and A. Fürstner, *J. Org. Chem.*, 2004, **69**, 3943-3949.
44. M. H. Al-Afyouni, K. L. Fillman, W. W. Brennessel and M. L. Neidig, *J. Am. Chem. Soc.*, 2014, **136**, 15457-15460.
45. S. B. Muñoz III, S. L. Daifuku, W. W. Brennessel and M. L. Neidig, *J. Am. Chem. Soc.*, 2016, **138**, 7492-7495.
46. M. Nakamura, K. Matsuo, S. Ito and E. Nakamura, *J. Am. Chem. Soc.*, 2004, **126**, 3686-3687.
47. D. Noda, Y. Sunada, T. Hatakeyama, M. Nakamura and H. Nagashima, *J. Am. Chem. Soc.*, 2009, **131**, 6078-6079.
48. R. B. Bedford, P. B. Brenner, E. Carter, P. M. Cogswell, M. F. Haddow, J. N. Harvey, D. M. Murphy, J. Nunn and C. H. Woodall, *Angew. Chem. Int. Ed.*, 2014, **53**, 1804-1808.
49. R. B. Bedford, M. Betham, D. W. Bruce, S. A. Davis, R. M. Frost and M. Hird, *Chem. Commun.*, 2006, **0**, 1398-1400.
50. T. Hatakeyama, Y.-i. Fujiwara, Y. Okada, T. Itoh, T. Hashimoto, S. Kawamura, K. Ogata, H. Takaya and M. Nakamura, *Chem. Lett.*, 2011, **40**, 1030-1032.
51. S. L. Daifuku, M. H. Al-Afyouni, B. E. R. Snyder, J. L. Kneebone and M. L. Neidig, *J. Am. Chem. Soc.*, 2014, **136**, 9132-9143.
52. A. Hedström, U. Bollmann, J. Bravidor and P.-O. Norrby, *Chem. Eur. J.*, 2011, **17**, 11991-11993.
53. J. Kleimark, P.-F. Larsson, P. Emamy, A. Hedström and P.-O. Norrby, *Adv. Synth. Catal.*, 2012, **354**, 448-456.
54. A. Hedström, E. Lindstedt and P.-O. Norrby, *J. Organomet. Chem.*, 2013, **748**, 51-55.
55. M. C. Perry, A. N. Gillett and T. C. Law, *Tetrahedron Lett.*, 2012, **53**, 4436-4439.
56. J. Legros and B. Figadere, *Nat. Prod. Rep.*, 2015, **32**, 1541-1555.
57. A. A. Camacho-Davila, *Synth. Commun.*, 2008, **38**, 3823-3833.

58. R. N. Shakhmaev, A. S. Sunagatullina and V. V. Zorin, *Russ. J. Org. Chem.*, 2014, **50**, 322-331.
59. L. K. Ottesen, F. Ek and R. Olsson, *Org. Lett.*, 2006, **8**, 1771-1773.
60. C. Risatti, K. J. Natalie, Z. Shi and D. A. Conlon, *Org. Process Res. Dev.*, 2013, **17**, 257-264.
61. A. Fürstner and A. Leitner, *Angew. Chem. Int. Ed.*, 2003, **42**, 308-311.
62. B. Scheiper, F. Glorius, A. Leitner and A. Fürstner, *Proc. Natl. Acad. Sci. U.S.A.*, 2004, **101**, 11960-11965.
63. S. M. Andersen, M. Bollmark, R. Berg, C. Fredriksson, S. Karlsson, C. Liljeholm and H. Sörensen, *Org. Process Res. Dev.*, 2014, **18**, 952-959.
64. P. Anastas and J. Warner, *Green Chemistry: Theory and Practice*, Oxford Univ Press, 1998.
65. T. A. C. Society, 12 Principles of Green Chemistry, <https://www.acs.org/content/acs/en/greenchemistry/what-is-green-chemistry/principles/12-principles-of-green-chemistry.html>, (accessed 26/10/2017, 2017).
66. ICH, ICH Harmonised Tripartite Guideline: Pharmaceutical Development Q8 (R2), http://www.ich.org/fileadmin/Public_Web_Site/ICH_Products/Guidelines/Quality/Q8_R1/Step4/Q8_R2_Guideline.pdf, (accessed 03/12/2017, 2017).
67. M. Baumann and I. R. Baxendale, *Beilstein J. Org. Chem.*, 2013, **9**, 2265-2319.
68. T. Minami, M. Iwamoto, H. Ohtsu, H. Ohishi, R. Tanaka and A. Yoshitake, *Planta Med.*, 2002, **68**, 742-745.
69. M. Rueping and B. J. Nachtsheim, *Beilstein J. Org. Chem.*, 2010, **6**, 6.
70. D. L. Reger and E. C. Culbertson, *Inorg. Chem.*, 1977, **16**, 3104-3107.
71. R. Jana, T. P. Pathak and M. S. Sigman, *Chem. Rev.*, 2011, **111**, 1417-1492.
72. C. Valente, S. Çalimsiz, K. H. Hoi, D. Mallik, M. Sayah and M. G. Organ, *Angew. Chem. Int. Ed.*, 2012, **51**, 3314-3332.
73. N. Miyaura and A. Suzuki, *Chem. Commun.*, 1979, **0**, 866-867.
74. N. Miyaura, K. Yamada and A. Suzuki, *Tetrahedron Lett.*, 1979, **20**, 3437-3440.
75. N. Miyaura and A. Suzuki, *Chem. Rev.*, 1995, **95**, 2457-2483.
76. Z. Qureshi, C. Toker and M. Lautens, *Synthesis*, 2017, **49**, 1-16.
77. A. Rudolph and M. Lautens, *Angew. Chem. Int. Ed.*, 2009, **48**, 2656-2670.
78. Z. Sobol, M. E. Engel, E. Rubitski, W. W. Ku, J. Aubrecht and R. H. Schiestl, *Mutat. Res. Genet. Toxicol. Environ. Mutagen.*, 2007, **633**, 80-94.
79. G. K. Surya Prakash, P. Yan, B. Török, I. Bucsi, M. Tanaka and G. A. Olah, *Catal. Lett.*, 2003, **85**, 1-6.
80. O. V. Shutkina, O. A. Ponomareva and I. I. Ivanova, *Neftekhimiya.*, 2013, **53**, 20-26.
81. E. Peyroux, F. Berthiol, H. Doucet and M. Santelli, *Eur. J. Org. Chem.*, 2004, **2004**, 1075-1082.
82. T. Bach and S. Heuser, *Angew. Chem. Int. Ed.*, 2001, **40**, 3184-3185.
83. C. Dai and G. C. Fu, *J. Am. Chem. Soc.*, 2001, **123**, 2719-2724.
84. G. Bastug and S. P. Nolan, *Organometallics*, 2014, **33**, 1253-1258.
85. K. Tamao, Y. Kiso, K. Sumitani and M. Kumada, *J. Am. Chem. Soc.*, 1972, **94**, 9268-9269.
86. D. L. Reger, D. G. Garza and L. Lebioda, *Organometallics*, 1991, **10**, 902-906.
87. D. L. Reger, D. G. Garza and L. Lebioda, *Organometallics*, 1992, **11**, 4285-4292.

88. T. Hayashi, M. Konishi, Y. Kobori, M. Kumada, T. Higuchi and K. Hirotsu, *J. Am. Chem. Soc.*, 1984, **106**, 158-163.
89. S. D. Dreher, P. G. Dormer, D. L. Sandrock and G. A. Molander, *J. Am. Chem. Soc.*, 2008, **130**, 9257-9259.
90. A. van den Hoogenband, J. H. M. Lange, J. W. Terpstra, M. Koch, G. M. Visser, M. Visser, T. J. Korstanje and J. T. B. H. Jastrzebski, *Tetrahedron Lett.*, 2008, **49**, 4122-4124.
91. S. D. Walker, T. E. Barder, J. R. Martinelli and S. L. Buchwald, *Angew. Chem. Int. Ed.*, 2004, **43**, 1871-1876.
92. F. R. Hartley, *Chem. Rev.*, 1973, **73**, 163-189.
93. C. Han and S. L. Buchwald, *J. Am. Chem. Soc.*, 2009, **131**, 7532-7533.
94. Y. Yang, K. Niedermann, C. Han and S. L. Buchwald, *Org. Lett.*, 2014, **16**, 4638-4641.
95. S. Calimsiz and M. G. Organ, *Chem. Commun.*, 2011, **47**, 5181-5183.
96. M. G. Organ, S. Avola, I. Dubovyk, N. Hadei, E. A. B. Kantchev, C. J. O'Brien and C. Valente, *Chem. Eur. J.*, 2006, **12**, 4749-4755.
97. M. G. Organ, G. A. Chass, D.-C. Fang, A. C. Hopkinson and C. Valente, *Synthesis*, 2008, **2008**, 2776-2797.
98. G. A. Chass, C. J. O'Brien, N. Hadei, E. A. B. Kantchev, W.-H. Mu, D.-C. Fang, A. C. Hopkinson, I. G. Csizmadia and M. G. Organ, *Chem. Eur. J.*, 2009, **15**, 4281-4288.
99. J. Nasielski, N. Hadei, G. Achonduh, E. A. B. Kantchev, C. J. O'Brien, A. Lough and M. G. Organ, *Chem. Eur. J.*, 2010, **16**, 10844-10853.
100. C. Li, T. Chen, B. Li, G. Xiao and W. Tang, *Angew. Chem. Int. Ed.*, 2015, **54**, 3792-3796.
101. C. Vila, M. Giannerini, V. Hornillos, M. Fananas-Mastral and B. L. Feringa, *Chem. Sci.*, 2014, **5**, 1361-1367.
102. C. E. Garrett and K. Prasad, *Adv. Synth. Catal.*, 2004, **346**, 889-900.
103. P. Chirik and R. Morris, *Acc. Chem. Res.*, 2015, **48**, 2495-2495.
104. B. D. Sherry and A. Fürstner, *Acc. Chem. Res.*, 2008, **41**, 1500-1511.
105. M. Tamura and J. K. Kochi, *J. Am. Chem. Soc.*, 1971, **93**, 1487-1489.
106. S. M. Neumann and J. K. Kochi, *J. Org. Chem.*, 1975, **40**, 599-606.
107. R. B. Bedford, D. W. Bruce, R. M. Frost, J. W. Goodby and M. Hird, *Chem. Commun.*, 2004, **0**, 2822-2823.
108. W. M. Czaplik, M. Mayer and A. Jacobi von Wangelin, *Angew. Chem. Int. Ed.*, 2009, **48**, 607-610.
109. A. L. Silberstein, S. D. Ramgren and N. K. Garg, *Org. Lett.*, 2012, **14**, 3796-3799.
110. T. Agrawal and S. P. Cook, *Org. Lett.*, 2012, **15**, 96-99.
111. T. Hatakeyama, S. Hashimoto, K. Ishizuka and M. Nakamura, *J. Am. Chem. Soc.*, 2009, **131**, 11949-11963.
112. X. Chen, Z.-J. Quan and X.-C. Wang, *Appl. Organomet. Chem.*, 2015, **29**, 296-300.
113. R. Agata, T. Iwamoto, N. Nakagawa, K. Isozaki, T. Hatakeyama, H. Takaya and M. Nakamura, *Synthesis*, 2015, **47**, 1733-1740.
114. P. J. Rushworth, D. G. Hulcoop and D. J. Fox, *J. Org. Chem.*, 2013, **78**, 9517-9521.
115. R. Leardi, *Anal. Chim. Acta*, 2009, **652**, 161-172.

116. H. Tye, *Drug Discov. Today*, 2004, **9**, 485-491.
117. W. M. Czaplik, S. Grupe, M. Mayer and A. J. v. Wangelin, *Chem. Commun.*, 2010, **46**, 6350-6352.
118. R. B. Bedford, M. Nakamura, N. J. Gower, M. F. Haddow, M. A. Hall, M. Huwe, T. Hashimoto and R. A. Okopie, *Tetrahedron Lett.*, 2009, **50**, 6110-6111.
119. I. Thome, A. Nijs and C. Bolm, *Chem. Soc. Rev.*, 2012, **41**, 979-987.
120. S. L. Buchwald and C. Bolm, *Angew. Chem. Int. Ed.*, 2009, **48**, 5586-5587.
121. G. Lefevre and A. Jutand, *Chem. - Eur. J.*, 2014, **20**, 4796-4805.
122. S. Gülak and A. Jacobi von Wangelin, *Angew. Chem. Int. Ed.*, 2012, **51**, 1357-1361.
123. *US Pat.*, WO2015192981A1, 2015.
124. *US Pat.*, WO2015187905A1, 2015.
125. *US Pat.*, WO2015057626A1, 2015.
126. *US Pat.*, WO2016012474A1, 2016.
127. E. Colacino, H. Benakki, F. Guenoun, J. Martinez and F. Lamaty, *Synth. Commun.*, 2009, **39**, 1583-1591.
128. C. Hansch, A. Leo and R. W. Taft, *Chem. Rev.*, 1991, **91**, 165-195.
129. C. Cassani, G. Bergonzini and C.-J. Wallentin, *ACS Catal.*, 2016, **6**, 1640-1648.
130. T. Parchomyk and K. Koszinowski, *Synthesis*, 2017, **49**, 3269-3280.
131. S. H. Carpenter and M. L. Neidig, *Isr. J. Chem.*, 2017, DOI: 10.1002/ijch.201700036.
132. V. P. W. Böhm and W. A. Herrmann, *Chem. Eur. J.*, 2001, **7**, 4191-4197.
133. C. Amatore and F. Pfluger, *Organometallics*, 1990, **9**, 2276-2282.
134. C. Y. Legault, Y. Garcia, C. A. Merlic and K. N. Houk, *J. Am. Chem. Soc.*, 2007, **129**, 12664-12665.
135. P. C. J. Kamer, P. W. N. M. van Leeuwen and J. N. H. Reek, *Acc. Chem. Res.*, 2001, **34**, 895-904.
136. Y. Garcia, F. Schoenebeck, C. Y. Legault, C. A. Merlic and K. N. Houk, *J. Am. Chem. Soc.*, 2009, **131**, 6632-6639.
137. Q. Xiu-Juan, F. Yong, L. Lei and G. Qing-Xiang, *Chin. J. Chem.*, 2005, **23**, 194-199.
138. A. Hedström, Z. Izakian, I. Vreto, C.-J. Wallentin and P.-O. Norrby, *Chem. Eur. J.*, 2015, **21**, 5946-5953.
139. C.-G. Zhan, J. A. Nichols and D. A. Dixon, *J. Phys. Chem. A*, 2003, **107**, 4184-4195.
140. M. F. Semmelhack, G. R. Clark, R. Farina and M. Saeman, *J. Am. Chem. Soc.*, 1979, **101**, 217-218.
141. F. M. Bickelhaupt and T. Ziegler, *Organometallics*, 1995, **14**, 2288-2296.
142. G. T. de Jong, A. Kovács and F. M. Bickelhaupt, *The Journal of Physical Chemistry A*, 2006, **110**, 7943-7951.
143. G. T. de Jong, R. Visser and F. M. Bickelhaupt, *Journal of Organometallic Chemistry*, 2006, **691**, 4341-4349.
144. A. S. Lobach and V. V. Strelets, *Russ. Chem. Bull.*, 2001, **50**, 1593-1595.
145. P. Politzer and F. Abu-Awwad, *Theor. Chem. Acc.*, 1998, **99**, 83-87.

146. S. Hamel, P. Duffy, M. E. Casida and D. R. Salahub, *J. Electron. Spectrosc. Relat. Phenom.*, 2002, **123**, 345-363.
147. A. L. Speelman and J. G. Gillmore, *J. Phys. Chem. A*, 2008, **112**, 5684-5690.
148. D. D. Méndez-Hernández, J. G. Gillmore, L. A. Montano, D. Gust, T. A. Moore, A. L. Moore and V. Mujica, *J. Phys. Org. Chem.*, 2015, **28**, 320-328.
149. E. J. Lynch, A. L. Speelman, B. A. Curry, C. S. Murillo and J. G. Gillmore, *J. Org. Chem.*, 2012, **77**, 6423-6430.
150. Y. Zhao and D. G. Truhlar, *Chem. Phys. Lett.*, 2011, **502**, 1-13.
151. Y. Zhao and D. G. Truhlar, *The Journal of Chemical Physics*, 2006, **125**, 194101.
152. Y. Zhao and D. G. Truhlar, *Theor. Chem. Acc.*, 2008, **120**, 215-241.
153. V. B. Oyeyemi, J. A. Keith, M. Pavone and E. A. Carter, *The Journal of Physical Chemistry Letters*, 2012, **3**, 289-293.
154. JMP 12[®], SAS Institute Inc., Cary, NC, USA, www.jmp.com, 1989-2017.
155. P. Canonne, G. B. Foscolos and G. Lemay, *Tetrahedron Lett.*, 1980, **21**, 155-158.
156. G. Cahiez and S. Marquais, *Pure Appl. Chem.*, 1996, **68**, 53-60.
157. R. Bedford, University of Strathclyde, Glasgow, 2014.
158. C. L. Rollinson and R. C. White, *Inorg. Chem.*, 1962, **1**, 281-285.
159. J. H. Bright, R. S. Drago, D. M. Hart and S. K. Madan, *Inorg. Chem.*, 1965, **4**, 18-20.
160. S. K. Madan and J. A. Sturr, *J. Inorg. Nucl. Chem.*, 1967, **29**, 1669-1683.
161. R. Siefker Joseph, *Proc. Indiana Acad. Sci.*, 1971, **80**, 155-158.
162. K. Ding, F. Zannat, J. C. Morris, W. W. Brennessel and P. L. Holland, *Journal of Organometallic Chemistry*, 2009, **694**, 4204-4208.
163. U. B. Jürgen Angerer, Claire Chambers, Qasim Chaudhry, Gisela Degen, Thomas Platzek, Suresh Chandra Rastogi, Vera Rogiers, Christophe Rousselle, Tore Sanner, Jacqueline van Engelen, Maria Pilar Vinardell, Rosemary Waring, Ian R. White, *Opinion on N-methyl-2-pyrrolidinone (NMP)*, European Commission, Online, 2011.
164. J. N. Sanderson, A. P. Dominey and J. M. Percy, *Adv. Synth. Catal.*, 2017, **359**, 1007-1017.
165. T. L. Mako and J. A. Byers, *Inorg. Chem. Front.*, 2016, **3**, 766-790.
166. R. S. Smith and J. K. Kochi, *J. Org. Chem.*, 1976, **41**, 502-509.
167. T. Parchomyk and K. Koszinowski, *Chem. Eur. J.*, 2016, **22**, 15609-15613.
168. T. Parchomyk and K. Koszinowski, *Chem. Eur. J.*, 2017, **23**, 3213-3219.
169. N. A. Meanwell, *J. Med. Chem.*, 2011, **54**, 2529-2591.
170. T. T. Talele, *J. Med. Chem.*, 2016, **59**, 8712-8756.
171. H. Lebel, J.-F. Marcoux, C. Molinaro and A. B. Charette, *Chem. Rev.*, 2003, **103**, 977-1050.
172. *US Pat.*, EP320136A2, 1989.
173. *US Pat.*, WO2010092339A1, 2010.
174. P. A. Cox, A. G. Leach, A. D. Campbell and G. C. Lloyd-Jones, *J. Am. Chem. Soc.*, 2016, **138**, 9145-9157.
175. D. J. Wallace and C.-y. Chen, *Tetrahedron Lett.*, 2002, **43**, 6987-6990.
176. *CN Pat.*, CN101440100A, 2009.

177. S. Malhotra, P. S. Seng, S. G. Koenig, A. J. Deese and K. A. Ford, *Org. Lett.*, 2013, **15**, 3698-3701.
178. *US Pat.*, WO2011163518A1, 2011.
179. *US Pat.*, WO2012086735A1, 2012.
180. *US Pat.*, WO2012171506A1, 2012.
181. *US Pat.*, US9067933B2, 2015.
182. *US Pat.*, WO2017009804A1, 2017.
183. *US Pat.*, WO2017069270A1, 2017.
184. R. K. Henderson, C. Jimenez-Gonzalez, D. J. C. Constable, S. R. Alston, G. G. A. Inglis, G. Fisher, J. Sherwood, S. P. Binks and A. D. Curzons, *Green Chem.*, 2011, **13**, 854-862.
185. ECHA, 1-butylpyrrolidin-2-one, <https://echa.europa.eu/registration-dossier/-/registered-dossier/10579/1>, (accessed 02/12/2017, 2017).
186. O. M. Kuzmina, A. K. Steib, J. T. Markiewicz, D. Flubacher and P. Knochel, *Angew. Chem. Int. Ed.*, 2013, **52**, 4945-4949.
187. G. A. Molander, B. J. Rahn, D. C. Shubert and S. E. Bonde, *Tetrahedron Lett.*, 1983, **24**, 5449-5452.
188. O. M. Kuzmina, A. K. Steib, D. Flubacher and P. Knochel, *Org. Lett.*, 2012, **14**, 4818-4821.
189. R. Frlan, M. Sova, S. Gobec, G. Stavber and Z. Časar, *J. Org. Chem.*, 2015, **80**, 7803-7809.
190. M. Sova, R. Frlan, S. Gobec, G. Stavber and Z. Časar, *Applied Organometallic Chemistry*, 2015, **29**, 528-535.
191. K. D. Collins, T. Gensch and F. Glorius, *Nat. Chem.*, 2014, **6**, 859-871.
192. E. C. Hansen, D. J. Pedro, A. C. Wotal, N. J. Gower, J. D. Nelson, S. Caron and D. J. Weix, *Nat. Chem.*, 2016, **8**, 1126-1130.
193. T. Cernak, N. J. Gesmundo, K. Dykstra, Y. Yu, Z. Wu, Z.-C. Shi, P. Vachal, D. Sperbeck, S. He, B. A. Murphy, L. Sonatore, S. Williams, M. Madeira, A. Verras, M. Reiter, C. H. Lee, J. Cuff, E. C. Sherer, J. Kuethe, S. Goble, N. Perrotto, S. Pinto, D.-M. Shen, R. Nargund, J. Balkovec, R. J. DeVita and S. D. Dreher, *J. Med. Chem.*, 2017, **60**, 3594-3605.
194. J. R. Schmink, A. Bellomo and S. Berritt, *Aldrichimica Acta*, 2013, **46**, 71-80, 10 pp.
195. S. D. Dreher, P. G. Dormer, D. L. Sandrock and G. A. Molander, *J. Am. Chem. Soc.*, 2008, **130**, 9257-9259.
196. B. Butschke, K. L. Fillman, T. Bendikov, L. J. W. Shimon, Y. Diskin-Posner, G. Leituss, S. I. Gorelsky, M. L. Neidig and D. Milstein, *Inorg. Chem.*, 2015, **54**, 4909-4926.
197. T. M. Baker, T. L. Mako, A. Vasilopoulos, B. Li, J. A. Byers and M. L. Neidig, *Organometallics*, 2016, **35**, 3692-3700.
198. J. L. Kneebone, V. E. Fleischauer, S. L. Daifuku, A. A. Shaps, J. M. Bailey, T. E. Iannuzzi and M. L. Neidig, *Inorg. Chem.*, 2016, **55**, 272-282.
199. N. Uchiyama, E. Shirakawa, R. Nishikawa and T. Hayashi, *Chem. Commun.*, 2011, **47**, 11671-11673.
200. F. Vallée, J. J. Mousseau and A. B. Charette, *J. Am. Chem. Soc.*, 2010, **132**, 1514-1516.
201. K. Kamata, A. Suzuki, Y. Nakai and H. Nakazawa, *Organometallics*, 2012, **31**, 3825-3828.

202. A. M. Tondreau, C. C. H. Atienza, J. M. Darmon, C. Milsman, H. M. Hoyt, K. J. Weller, S. A. Nye, K. M. Lewis, J. Boyer, J. G. P. Delis, E. Lobkovsky and P. J. Chirik, *Organometallics*, 2012, **31**, 4886-4893.
203. W.-Y. Wu, J.-C. Wang and F.-Y. Tsai, *Green Chem.*, 2009, **11**, 326-329.
204. S. Luo, D.-G. Yu, R.-Y. Zhu, X. Wang, L. Wang and Z.-J. Shi, *Chem. Commun.*, 2013, **49**, 7794-7796.
205. S. E. Denmark and A. J. Cresswell, *J. Org. Chem.*, 2013, **78**, 12593-12628.
206. M. P. Sibi and G. Petrovic, *Tetrahedron: Asymmetry*, 2003, **14**, 2879-2882.
207. J. Jankowska, J. Paradowska, B. Rakiel and J. Mlynarski, *J. Org. Chem.*, 2007, **72**, 2228-2231.
208. M. Redlich and M. M. Hossain, *Tetrahedron Lett.*, 2004, **45**, 8987-8990.
209. H. Jacobsen, A. Correa, A. Poater, C. Costabile and L. Cavallo, *Coord. Chem. Rev.*, 2009, **253**, 687-703.
210. M. J. Ingleson and R. A. Layfield, *Chem. Commun.*, 2012, **48**, 3579-3589.
211. M. Melaimi, R. Jazzar, M. Soleilhavoup and G. Bertrand, *Angew. Chem. Int. Ed.*, 2017, **56**, 10046-10068.
212. T. Hatakeyama, T. Hashimoto, Y. Kondo, Y. Fujiwara, H. Seike, H. Takaya, Y. Tamada, T. Ono and M. Nakamura, *J. Am. Chem. Soc.*, 2010, **132**, 10674-10676.
213. T. Hatakeyama, Y. Okada, Y. Yoshimoto and M. Nakamura, *Angew. Chem. Int. Ed.*, 2011, **50**, 10973-10976.
214. A. Petuker, K. Merz, C. Merten and U.-P. Apfel, *Inorg. Chem.*, 2016, **55**, 1183-1191.
215. T. Komuro, T. Matsuo, H. Kawaguchi and K. Tatsumi, *Inorg. Chem.*, 2003, **42**, 5340-5347.
216. C. Gunanathan and D. Milstein, *Chem. Rev.*, 2014, **114**, 12024-12087.
217. A. K. King, K. J. Gallagher, M. F. Mahon and R. L. Webster, *Chem. Eur. J.*, 2017, **23**, 9039-9043.
218. N. T. Coles, M. F. Mahon and R. L. Webster, *Organometallics*, 2017, **36**, 2262-2268.
219. C. H. Schuster, T. Diao, I. Pappas and P. J. Chirik, *ACS Catal.*, 2016, **6**, 2632-2636.
220. G. W. Margulieux, M. J. Bezdek, Z. R. Turner and P. J. Chirik, *J. Am. Chem. Soc.*, 2017, **139**, 6110-6113.
221. M. V. Joannou, M. J. Bezdek, K. Al-Bahily, I. Korobkov and P. J. Chirik, *Organometallics*, 2017, **36**, 4215-4223.
222. V. Vallet, U. Wahlgren and I. Grenthe, *J. Am. Chem. Soc.*, 2003, **125**, 14941-14950.
223. A. Skinner Henry, *Pure Appl. Chem.*, 1985, **57**, 79-88.
224. M. A. V. Ribeiro da Silva, M. J. S. Monte and J. Huinink, *J. Chem. Thermodyn.*, 1996, **28**, 413-419.
225. J. F. Garst, F. Ungvary, R. Batlaw and K. E. Lawrence, *J. Am. Chem. Soc.*, 1991, **113**, 6697-6698.
226. G. A. Olah, G. K. Surya Prakash and M. Arvanaghi, *Synthesis*, 1984, **1984**, 228-230.
227. H. Kurata, P. R. Gentry, M. Kokubo, H. P. Cho, T. M. Bridges, C. M. Niswender, F. W. Byers, M. R. Wood, J. S. Daniels, P. J. Conn and C. W. Lindsley, *Bioorganic & Medicinal Chemistry Letters*, 2015, **25**, 690-694.
228. A. Gomtsyan, R. G. Schmidt, E. K. Bayburt, G. A. Gfesser, E. A. Voight, J. F. Daanen, D. L. Schmidt, M. D. Cowart, H. Liu, R. J. Altenbach, M. E. Kort, B. Clapham, P. B. Cox, A. Shrestha, R. Henry, D. N. Whittern, R. M. Reilly, P. S. Puttfarcken, J.-D. Brederson, P. Song, B. Li, S. M. Huang, H. A. McDonald, T. R. Neelands, S. P. McGaraughty, D. M. Gauvin, S. K. Joshi, P. N.

- Banfor, J. A. Segreti, M. Shebley, C. R. Faltynek, M. J. Dart and P. R. Kym, *J. Med. Chem.*, 2016, **59**, 4926-4947.
229. T. Hatakeyama and M. Nakamura, *J. Am. Chem. Soc.*, 2007, **129**, 9844-9845.
230. F. G. Buono, Y. Zhang, Z. Tan, A. Brusoe, B.-S. Yang, J. C. Lorenz, R. Giovannini, J. J. Song, N. K. Yee and C. H. Senanayake, *Eur. J. Org. Chem.*, 2016, **2016**, 2599-2602.
231. G. A. Price, A. Hassan, N. Chandrasoma, A. R. Bogdan, S. W. Djuric and M. G. Organ, *Angew. Chem. Int. Ed.*, 2017, **56**, 13347-13350.
232. J. Jover, N. Fey, J. N. Harvey, G. C. Lloyd-Jones, A. G. Orpen, G. J. J. Owen-Smith, P. Murray, D. R. J. Hose, R. Osborne and M. Purdie, *Organometallics*, 2012, **31**, 5302-5306.
233. N. Fey, J. N. Harvey, G. C. Lloyd-Jones, P. Murray, A. G. Orpen, R. Osborne and M. Purdie, *Organometallics*, 2008, **27**, 1372-1383.
234. N. Fey, M. F. Haddow, J. N. Harvey, C. L. McMullin and A. G. Orpen, *Dalton Transactions*, 2009, **2009**, 8183-8196.
235. P. W. N. M. van Leeuwen, P. C. J. Kamer, J. N. H. Reek and P. Dierkes, *Chem. Rev.*, 2000, **100**, 2741-2770.
236. G. R. Fulmer, A. J. M. Miller, N. H. Sherden, H. E. Gottlieb, A. Nudelman, B. M. Stoltz, J. E. Bercaw and K. I. Goldberg, *Organometallics*, 2010, **29**, 2176-2179.
237. Design-Expert® Software, version 10, Stat-Ease, Inc., Minneapolis, MN 55413, USA, www.statease.com,
238. Gaussian 09, Gaussian, Inc., Wallingford, CT, USA, 2009.
239. GaussView 5, Semichem, Inc., Shawnee Mission, KS, USA, 2009.
240. T. Hanke, F. Rörsch, T. M. Thieme, N. Ferreiros, G. Schneider, G. Geisslinger, E. Proschak, S. Grösch and M. Schubert-Zsilavec, *Biorg. Med. Chem.*, 2013, **21**, 7874-7883.
241. J. L. García Ruano, A. Parra, F. Yuste and V. M. Mastranzo, *Synthesis*, 2008, **2008**, 311-319.
242. G. Blessley, P. Holden, M. Walker, J. M. Brown and V. Gouverneur, *Org. Lett.*, 2012, **14**, 2754-2757.
243. L. Shaw, D. M. U. K. Somisara, R. C. How, N. J. Westwood, P. C. A. Bruijninx, B. M. Weckhuysen and P. C. J. Kamer, *Catalysis Science & Technology*, 2017, **7**, 619-626.